UCONN LIBRARY

University of Connecticut
OpenCommons@UConn

Doctoral Dissertations | University of Connecticut Graduate School

8-7-2015

Dynamic and Contact Analysis of a Special Percussive Drill for Planetary Subsurface Exploration

Luis J. Vila
University of Connecticut - Storrs, luisvila@engr.uconn.edu

Follow this and additional works at: https://opencommons.uconn.edu/dissertations

Recommended Citation
Vila, Luis J., "Dynamic and Contact Analysis of a Special Percussive Drill for Planetary Subsurface Exploration" (2015). *Doctoral Dissertations*. 861.
https://opencommons.uconn.edu/dissertations/861

ABSTRACT

Dynamic and Contact Analysis of a Special Percussive Drill for Planetary Subsurface Exploration

Luis J. Vila, Ph.D.

University of Connecticut, 2015

Planetary drilling is a vital task in the challenge for space exploration. Drilling and planetary soil/rock sample acquisition provides information about history of past events, minerals and chemical composition of the soil/rock of the planetary body, available resources for future manned missions and the mechanical behavior of the planetary soil/rock. Several types of drilling devices have been proposed for lunar, Mars, and planetary subsurface exploration. However, these devices have limitations (e.g. heavy equipment and need for large axial force) that need to be addressed in order to be feasible for extraterrestrial bodies' exploration. A special type of ultrasonic percussive drill have been proposed by Honeybee Spacecraft Mechanisms Corporation and NASA Jet Propulsion Laboratory (JPL) to address the limitations of current drilling devices.

In this study, the mechanical system of the ultrasonic percussive drill and its interaction with the supporting medium is studied. The percussive mechanism consists of an ultrasonic horn, a free mass, and the drill rod. Special attention is given to the impact between the free mass and the drill rod, including the effects of structural damping, the supporting medium of the rod, plastic deformation in the contact area, and repeated impacts of the free mass on the drill rod.

A general methodology to analyze the impact of the free mass on the drill rod, analogous to the longitudinal impact of a mass on a rod, is developed. The methodology

involves uncoupling the nonlinear problem by determining the response of each body independently under the contact force to find the local indentation, then using Hertz force-indentation relation to find the contact force. This method is applied using mode superposition method and finite element technique for various support conditions of the rod (e.g. rigid, elastic, free, viscoelastic). Additionally, a model to account for drill rod penetration into the supporting medium due to impact of the free mass is also presented. It was found that for an undamped rod, the support condition of the rod does not affect the contact force if the contact ends before the arrival of the reflected wave to the point of contact. It was also observed that the contact force due to impact, for a given support condition, increases with increasing damping of the rod. Moreover, a modified Hertz equation is introduced to include plastic deformation on the rod due to impact of the free mass. The study was performed for identical repetitive impacts and it was found that the largest plastic deformation occurs in the first impact, with additional plastic deformation decreasing with the increasing number of impacts.

The dynamic response of the overall percussive drill was investigated with a finite element model, including the interaction of the free mass with the ultrasonic horn and the drill rod. A numerical example indicated that the dynamic response of the ultrasonic drill is directly affected by the supporting medium. It was found that system with fixed support experienced a higher frequency of oscillation of the free mass and higher impact force compared to the system with the elastic support and the model accounting for penetration into the supporting medium.

Dynamic and Contact Analysis of a Special Percussive Drill for Planetary Subsurface Exploration

Luis J. Vila

B.S., Civil Engineering, University of Puerto Rico, Mayaguez, Puerto Rico, 2010

M.S., Structural Engineering, University of Connecticut, Storrs, CT, USA, 2014

A Dissertation

Submitted in Partial Fulfillment of the

Requirements for the Degree of

Doctor of Philosophy

at the

University of Connecticut

2015

Copyright by

Luis J. Vila

2015

APPROVAL PAGE

Doctor of Philosophy Dissertation

Dynamic and Contact Analysis of a Special Percussive Drill for Planetary Subsurface Exploration

Presented by

Luis J. Vila

Major Advisor _____

Ramesh B. Malla

Associate Advisor _____

Jeong-Ho Kim

Associate Advisor _____

Shinae Jang

University of Connecticut

2015

ACKNOWLEDGEMENT

I would like to express my deepest gratitude and appreciation to my major advisor, Dr. Ramesh B. Malla, for his invaluable advice, mentorship, guidance, and encouragement during the last several years. This dissertation would not have been possible without his constant support, motivation, and availability to help me throughout the duration of my Ph.D. program.

I am grateful to my associate advisors, Dr. Jeong-Ho Kim and Dr. Shinae Jang, for serving on my dissertation advisory committee as Associate Advisors. I would also like to acknowledge the financial support from University of Connecticut Graduate School Multicultural Scholarship Program (MSP), U.S. Department of Education Graduate Assistance in Areas of National Need (GAANN), Connecticut Space Grant Consortium, and the Department of Civil and Environmental Engineering at the University of Connecticut. In addition I would like to thank Dr. Kris Zacny, from Honeybee Robotics Spacecraft Mechanisms Corporation, Pasadena, CA for providing information on the ultrasonic percussive drill.

I am especially grateful to my parents for supporting me through all these years. I am indebted to my wife, Katy, for always being there when I needed it the most. Moreover, I would like to express my gratitude to the two persons that gave me the first opportunity to do research and encouraged me to pursue a Ph.D. degree, Dr. Lee Aggison Jr. and Dr. Ruth Washington. I would also like to thank my cousin, Abdiel, for his constant support since before starting graduate school. Finally, I would like to thank my friends and fellow graduate students that have accompanied me during this journey and in one way or another helped to make this possible.

ABSTRACT

Dynamic and Contact Analysis of a Special Percussive Drill for Planetary Subsurface Exploration

Luis J. Vila, Ph.D.

University of Connecticut, 2015

Planetary drilling is a vital task in the challenge for space exploration. Drilling and planetary soil/rock sample acquisition provides information about history of past events, minerals and chemical composition of the soil/rock of the planetary body, available resources for future manned missions and the mechanical behavior of the planetary soil/rock. Several types of drilling devices have been proposed for lunar, Mars, and planetary subsurface exploration. However, these devices have limitations (e.g. heavy equipment and need for large axial force) that need to be addressed in order to be feasible for extraterrestrial bodies' exploration. A special type of ultrasonic percussive drill have been proposed by Honeybee Spacecraft Mechanisms Corporation and NASA Jet Propulsion Laboratory (JPL) to address the limitations of current drilling devices.

In this study, the mechanical system of the ultrasonic percussive drill and its interaction with the supporting medium is studied. The percussive mechanism consists of an ultrasonic horn, a free mass, and the drill rod. Special attention is given to the impact between the free mass and the drill rod, including the effects of structural damping, the supporting medium of the rod, plastic deformation in the contact area, and repeated impacts of the free mass on the drill rod.

A general methodology to analyze the impact of the free mass on the drill rod, analogous to the longitudinal impact of a mass on a rod, is developed. The methodology

involves uncoupling the nonlinear problem by determining the response of each body independently under the contact force to find the local indentation, then using Hertz force-indentation relation to find the contact force. This method is applied using mode superposition method and finite element technique for various support conditions of the rod (e.g. rigid, elastic, free, viscoelastic). Additionally, a model to account for drill rod penetration into the supporting medium due to impact of the free mass is also presented. It was found that for an undamped rod, the support condition of the rod does not affect the contact force if the contact ends before the arrival of the reflected wave to the point of contact. It was also observed that the contact force due to impact, for a given support condition, increases with increasing damping of the rod. Moreover, a modified Hertz equation is introduced to include plastic deformation on the rod due to impact of the free mass. The study was performed for identical repetitive impacts and it was found that the largest plastic deformation occurs in the first impact, with additional plastic deformation decreasing with the increasing number of impacts.

The dynamic response of the overall percussive drill was investigated with a finite element model, including the interaction of the free mass with the ultrasonic horn and the drill rod. A numerical example indicated that the dynamic response of the ultrasonic drill is directly affected by the supporting medium. It was found that system with fixed support experienced a higher frequency of oscillation of the free mass and higher impact force compared to the system with the elastic support and the model accounting for penetration into the supporting medium.

Table of Contents

List of Tables

List of Figures

Chapter 1

Introduction

A study of lunar regolith and soil/rock samples of other planetary bodies (i.e. Mars, asteroids) is vital towards promoting human understanding of the moon, Mars and outer space environment, and ultimately facilitate the human colonization. However, the task of obtaining a regolith/ soil sample is a great challenge given the radically different conditions on these planetary bodies compared to that of Earth (ASCE task committee 1992; Heiken et al. 1991; Malla et al. 1995; Malla and Chaudhuri 2008). Regolith (soil) samples obtained from previous lunar missions, such as those obtained using self-recording penetrometer (SPR) in Apollo 15 and 16 missions, have provided some useful information on properties of the regolith (Mitchell and Houston 1974). However, more information is needed in order to fully understand the mechanical properties of the lunar soil. Existing drilling techniques are limited by the need for large axial forces and holding torques, high power consumption, and inability to duty cycle at a high power efficiency (Bao et al. 2003). Additionally, current drilling devices for planetary exploration are not suitable for deep drilling applications. To address these challenges, a percussive ultrasonic/sonic driller/corer (USDC) was developed by Honeybee Robotics Spacecraft Mechanism Corp. and NASA Jet Propulsion Laboratory (JPL) (Bar-Cohen et al. 2001).

The USDC mechanism consists of an ultrasonic horn that is vibrated by a piezoelectric actuator. The ultrasonic horn drives a free-mass, which hits the drill bit (rod), creating a stress wave that propagates through the rod. During operation the free mass oscillates between the horn and drill bit creating multiple impacts (Bar-Cohen et al. 2001). While the

percussive mechanism is effective for drilling hard-brittle materials, it is not as effective in soft materials, in which rotary drilling provides a better efficiency. A percussive augmenter for a commercial rotary drill was developed to combine the advantages of both, rotary and percussive drilling (Badescu et al. 2012). Based on this concept the Auto-Gopher was designed to combine rotary and percussive drilling in a compact device suitable for space applications (Bar-Cohen et al. 2012). In the Auto-Gopher device that is developed by Honeybee Robotics Spacecraft Mechanisms Corporation and NASA Jet Propulsion Laboratory, the rotation is provided by an electromagnetic motor, while the percussive impacts are provided by the ultrasonic actuator of the USDC. A thorough understanding of the behavior and performance of this special type of drill can help designers and scientists to create an optimum design and overcome the challenges in current drilling techniques.

1.1 Literature Review

Ultrasonic drills have been shown to be a promising tool for subsurface exploration in planetary bodies (Sherrit et al. 1999). A novel ultrasonic percussive drill consisting of an ultrasonic actuator (piezoelectric stack) and a rotary actuator (electromagnetic motor) has been proposed by Honeybee Robotics Spacecraft Mechanisms Corporation and NASA Jet Propulsion Laboratory (JPL). The percussive mechanism consists of an ultrasonic horn that drives a free mass between the horn tip and the drill rod. Several studies have been conducted investigating the performance of this special percussive drilling device. Sherrit et al. (1999) studied the very early stages of the ultrasonic percussive drill for planetary applications and found that the inclusion of a free mass between the horn and the drill bit increased the low frequency energy transfer and reduced the dependence of the drilling

rates on the drill stem length. Bar-Cohen et al. (2001) modeled the interaction between the free mass and the drill rod and determined the stress in the rod by finite element analysis. Furthermore, Bao et al. (2003) found the force at the drill rod/rock interface and penetration rate for hard, medium, and soft rocks. The previous analytical studies on ultrasonic percussive drills have been performed with the assumption that the supporting medium is rock, therefore the drill rod can be regarded as clamped at the bottom end. However, the ultrasonic percussive drill can be used for applications other than planetary exploration (e.g. construction, geology, military, and hiking) (Bar-Cohen et al. 2001; Bar-Cohen and Sherrit 2007), in which supporting media other than rock will be present. In such cases the assumption of a clamped/fixed rod at the bottom end is no longer valid. Therefore, studying and understanding the behavior and performance of ultrasonic percussive drills supported on a variety of media is of practical importance.

The impact of the free mass on the drill rod is analogous to the longitudinal impact of a striker on a rod. The impact of elastic bodies has been extensively studied in engineering mechanics over time, e.g. longitudinal impact of rods (Hu and Eberhard 2003; King and Bourgeois 1993; Goldsmith 1960; St. Venant and Flamant 1889; Take et al. 1999; Volterra and Zachmanoglou 1965; YuFeng and DeChao 1998) and transverse impact on beams and strings (Cox 1849; Lo 1980; Malla and Gionet 2013; Timoshenko 1913; Valkering 1994; Wilcox and Dankowicz 2009; Yongqiang and Lili 2011). Devices that utilize longitudinal impact to generate stress waves (also known as the Hopkinson bar) have been used for different applications such as pile driving (Raj 2008) and soil testing in geotechnical engineering (Das 2006) and percussive drilling in the mining (Kaliski 1989) and aerospace industry (Badescu et al. 2012; Malla et al. 2010a,2010b, 2012; Shrestha et al. 2011). An

important parameter in the impact phenomena is the force exerted on the rod (or beam) by the striker (hammer). The longitudinal impact of a rigid striker on an elastic uniform cantilever rod was studied by St. Venant and Flamant (1889) by applying the theory of wave propagation. The impact of the free mass on the drill rod was also analyzed using an energy method developed by Cox (1849) (Vila and Malla 2014a). Hertz (1881) developed a normal force relation for two spheres in contact. Normal and tangential force relations for contact problems involving spheres including plastic deformation were developed by Vu-Quoc et al. (2000; 2001). The nonlinear impact of a particle on an undamped rod was studied by Xing and Zhu (1998), in which the effects of the boundary conditions on the wave propagation are analyzed.

1.2 Objectives

In this work, the main focus is modeling the interaction between the different components of the ultrasonic percussive drill. Special attention is given to the interaction between the free mass and the drill rod. The objective of this work is to study the overall dynamic response of a special ultrasonic percussive drill, the contact phenomena between its different components, and its interaction with the supporting medium. The following is addressed in this study:

(i) Development of a simplified and practical analytical model to track the position of each component (i.e. ultrasonic horn, free mass, and drill rod) of the ultrasonic drill during operation.

(ii) Perform an in depth analysis of the contact between the free mass and the drill rod. The contact force (for various contact theories) and the dynamic response

of the rod due to impact will be determined for different boundary conditions to account for a rod supported on different media.

(iii) Analyze the repetitive impact between the free mass and the drill bit considering the stress/strain history of the rod.

(iv) Modeling of drill rod penetration into the supporting medium.

(v) Verify the model by comparing to experimental data and a commercially available finite element package.

1.3 Organization of the Dissertation

This dissertation is organized in eight chapters. The introduction, literature review, and objectives of the research are presented in Chapter 1. In Chapter 2 a simplified model of the percussive drill mechanism is presented. Methods such as conservation of momentum, impulse momentum principle, and particle motion analysis are used to model the system. Chapter 3 presents a detailed methodology to analyze the longitudinal impact of a spherical striker on a rod. Hertz theory of contact coupled with the structural vibration of the rod due to impact is presented.

In Chapter 4, the methodology developed in Chapter 3 is used to investigate the effect of a fixed, an elastic, and a free support condition of the rod on the contact force due to impact of the striker. Chapter 5 implements the methodology for the impact analysis for a rod with viscous and viscoelastic support. Additionally, a model to simulate penetration of the rod into the supporting medium is presented.

Chapter 6 introduces a modified Hertz theory to include the effect of plastic deformation of the rod on the contact force. In this chapter the effect of identical repetitive impacts on the contact force and the coefficient of restitution is also presented. In Chapter 7 a finite element model of the percussive mechanism is presented. In this chapter the interaction between the different components of the percussive drill including the contact period for the impact between the free mass and the horn, and the contact between the free mass and the drill rod is presented. The effect of the support condition of the rod on the dynamic response of the overall drill rod is discussed. Chapter 8 presents a summary of the work performed in this study, including final conclusions and recommendations for future work.

Chapter 2

Interaction between the Components of the Ultrasonic Percussive Drill: Simplified Model

In this chapter the impact between the free mass and the drill bit is analyzed using solid body collision analysis. The impulse and the energy transferred to the drill bit by the free mass are obtained using impulse momentum principle and determining the change in kinetic energy due to impact, respectively. Finally the contact force and duration of impact is determined by the wave propagation method and an energy balance method (Cox method).

2.1 Solid Body Collision Analysis

The ultrasonic percussive mechanism (Fig. 2.1) is composed of an ultrasonic horn, a free mass, and a drill rod. The operation of the ultrasonic percussive system begins with the excitation of the ultrasonic horn by imparting high frequency voltage to the piezoelectric stack. The ultrasonic horn vibrates harmonically with a frequency of about 22.5 kHz and amplitude, B_0, of around 10 μm (Bao et al. 2003). For convenience, the horn position function is selected so that the horn tip is able to move up and down from its initial position (t = 0). The position and the velocity of the horn tip are given by:

$$u_h = B_0 \sin(\varpi t + \beta) \tag{2.1}$$

$$v_h = B_0 \omega \cdot cos(\varpi t + \beta) \tag{2.2}$$

where u_0 is the amplitude of vibration, ϖ is the vibration frequency, and β is the phase angle. The excitation imparted to the horn causes it to impact the free mass. The velocity, v'_{fm}, of the free mass after impact with the ultrasonic horn is obtained by applying conservation of momentum principle, thus:

$$m_h v_h + m_{fm} v_{fm} = m_h v'_h + m_{fm} v'_{fm} \tag{2.3}$$

where m is the mass, v is the velocity immediately before impact, v' is the velocity immediately after impact, and the subscripts h and fm correspond to horn and free-mass, respectively. By definition the coefficient of restitution e is given by:

$$e = \frac{v'_{fm} - v'_h}{v_h - v_{fm}} \tag{2.4}$$

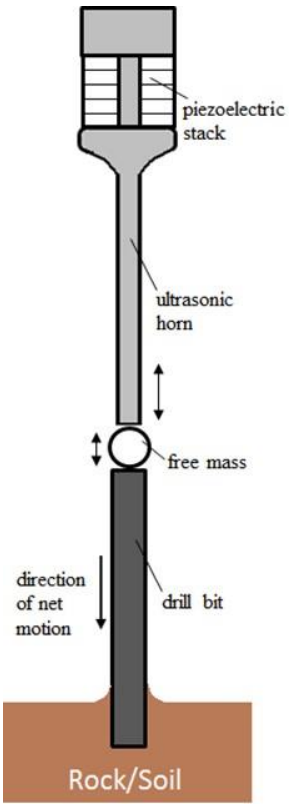

Fig. 2.1: Interaction between vibrating ultrasonic horn, free mass, and drill bit.

Using Eqns. (2.3) and (2.4) the velocity, v'_{fm}, of the free mass after impact is given by:

$$v'_{fm} = \frac{m_{fm}v_{fm} + m_h v_h + m_h e(v_h - v_{fm})}{m_h + m_{fm}} \tag{2.5}$$

Since the ultrasonic horn is controlled by the piezoelectric actuator, and its mass is much greater than that of the free mass, it is assumed that its motion is not affected by the impact of the free mass (i.e. $v'_h = v_h$). Considering particle motion, the position/displacement, u_{fm}, of the free mass is given by:

$$u_{fm} = u_0 + v_{fm} \cdot t + \frac{1}{2}at^2 \tag{2.6}$$

where t is the time, u_0 is the initial position of the mass, v_{fm} is the velocity of the free mass, and a is the acceleration. For vertical motion, the acceleration, a, is given by the gravitational acceleration, g.

2.1.1 Free Mass/Drill rod interaction

After being struck by the horn, the free mass will move toward the drill rod with velocity v'_{fm}, and hit the drill rod, thus creating percussive hammering mechanism. Due to this impact, the rod will experience axial vibration. Since the focus of this chapter is to present a practical methodology to analyze the interaction between the various components of the percussive mechanism, the drill rod is modeled as a single degree of freedom (SDOF) system as shown in Fig. 2.2. To approximate the continuous rod as a SDOF system, the mass and stiffness of the rod are obtained using the generalized properties (Clough and Penzien 1975). Assuming a linear mode shape (see Fig. 2.18c), the stiffness, k, of the SDOF system is given by $k = EA/L$; where E is the Young's modulus, A is the cross-sectional area, and L is the length of the rod. The mass of the drill rod is given by an effective mass, $m_{r,eff}$,

equal to one third of the total mass of the rod (i.e. $m_{r,eff} = m_r/3$). This can be seen in Eqn. (17) from the derivation presented in Section 4. The equation of motion of the drill rod as a SDOF system is then given by:

$$m_{r,eff}\ddot{u}_r + C\dot{u}_r + ku_r = 0 \tag{2.7}$$

where u_r is the displacement of the rod, $C = 2m_{r,eff}\,\omega_n\xi$ is the damping coefficient and ξ is the damping ratio. The frequency of the equivalent SDOF system ($\omega_n = \sqrt{k/m_{r,eff}} = 22{,}106\,rad/sec$) is observed to be reasonably close (within 11 percent) to that of the actual continuous drill rod ($\omega = (\pi/2L) * \sqrt{E/\rho} = 20{,}048\,rad/sec$; where ρ is the density of the rod material).

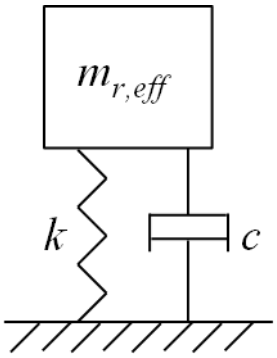

Figure 2.2: Equivalent SDOF system for the drill rod.

The dynamic response of the drill rod due to impact of the free mass is obtained by using the velocity of the rod after impact and the position of the rod after impact as initial conditions for free vibration. The free vibration response of the drill rod after impact with the free mass is given by (Clough and Penzien 1975; Vila and Malla 2013):

$$u_r(t) = e^{-\xi\omega_n t}\left[\frac{v_{r_i} + u_{r_i}\xi\omega}{\omega_D}\sin(\omega_D t) + u_{r_i}\cos(\omega_D t)\right] \tag{2.8}$$

where $c = \sqrt{E/\rho}$, E is the material Young's modulus, ρ is the mass density, and $v_{r,i}$ and $u_{r,i}$ are the velocity and the position of the drill rod immediately after impact i, respectively. The interaction of the free mass with the drill rod is taken similar to that of the horn and the free mass. Using conservation of momentum and introducing the coefficient of restitution, the velocity of the drill rod and the free mass after impact is given by:

$$v_r' = \frac{m_r v_r + m_{fm} v_{fm} + m_{fm} e(v_{fm} - v_r)}{m_r + m_{fm}} \tag{2.9}$$

$$v_{fm}' = \frac{m_r v_r + m_{fm} v_{fm} + m_r e(v_r - v_{fm})}{m_r + m_{fm}} \tag{2.10}$$

where e is the coefficient of restitution, the m is the mass, v is the velocity before impact, v' is the velocity after impact, and the subscripts r and fm corresponds to drill rod and free-mass, respectively.

2.2 Impulse and Energy Transferred to the Drill Rod

For the simple collision model, the impulse imparted to the drill rod by the free-mass is calculated by applying the linear impulse-momentum law (Eqn. (2.11)) (Goldsmith 1960).

$$\Delta m_r v_r = m_r v_r' - m_r v_r = \int_{t_1}^{t_2} F \cdot dt \tag{2.11}$$

where $F*dt$ is the impulse exerted by external forces. Fig. 2.3 shows the forces acting on the free mass and drill rod during contact (neglecting the weight of the drill rod and free mass). Applying Eqn. (2.11) to the system in Fig. 2.3, the impulse exerted by the free-mass on the drill rod is given by:

$$\int F \cdot dt = m_r (v_r' - v_r) \tag{2.12}$$

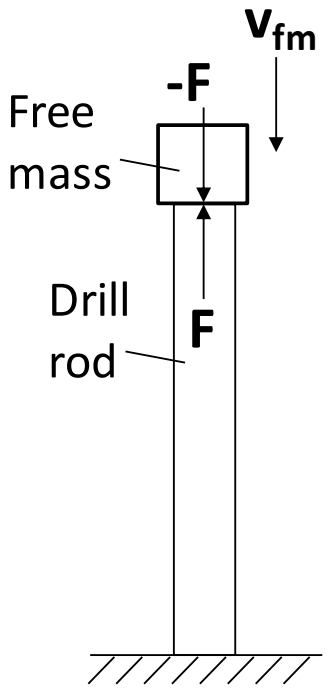

Fig. 2.3: Forces on free-mass and drill rod during contact.

Another important parameter to determine is the energy transferred by the free mass to the drill rod due to impact. To determine this energy transfer, the change in kinetic energy, ΔT, in the rod due to impact of the free mass is calculated. Therefore, the energy, U, transferred to the rod during impact is calculated by:

$$U = \Delta T = \frac{1}{2} m_r (v_r'^2 - v_r^2) \tag{2.13}$$

where m, is the mass, v, is the velocity before impact, v', is the velocity after impact, and the subscript r refers to rod.

A computer code was developed to simulate the interaction between the ultrasonic horn, free mass and the drill rod during operation. Table 2.1 shows the set of representative material properties and dimensions used for the simulation. Structural damping in the drill rod is considered to be equal to 10 percent of the critical damping. Since the special drill is intended for planetary exploration the gravitational acceleration was considered

according to the gravitational acceleration of Mars, thus g is taken as equal to 3.77 m/s^2. The position of each component through time for a coefficient of restitution equal to one (i.e. perfectly elastic impact) for an undamped rod is shown in Fig. 2.4. Although a coefficient of restitution of one may differ from reality, it will be used as a baseline to compare the effects and importance of accounting for energy loss. It is observed that the drill rod remains static until the first impact of the free mass. After this first impact the rod undergoes free vibration and the free mass oscillates between the drill rod and the ultrasonic horn. A total of 26 impacts were observed over the 11.1 msec. duration of the simulation with an average impact frequency of 3700 Hz.

Table 2.1: Properties of the free mass and the drill rod.

Property	Value	Unit
Horn Vib. Freq., f	22.5	kHz
Horn Vib. Amp.	10	μm
m_{fm} (steel)	0.067	kg
L (rod)	0.4	m
ω_n (rod)	22,106	rad/sec
m_r	0.89	kg

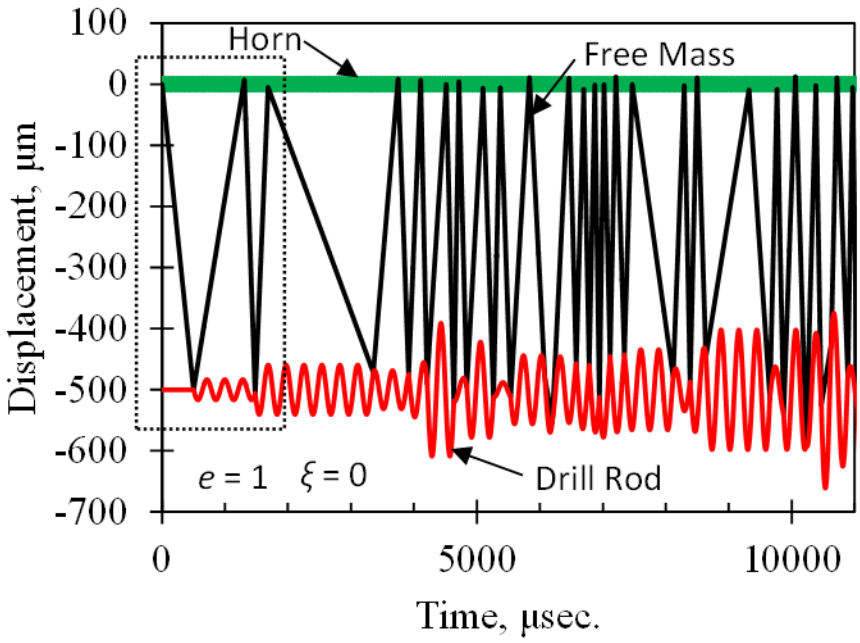

Fig. 2.4: Position of ultrasonic horn, free mass and drill rod as a function of time for e = 1 and $\xi = 0$. (undamped)

Figure 2.5 shows an inset (shown in the dotted squared on Fig. 2.4) of Fig. 2.4. It is observed that the ultrasonic horn experiences several cycles for each oscillation cycle of the free mass. This is consistent with the purpose of including a free mass, which is to convert the high frequency oscillation of the ultrasonic horn into lower frequency impacts on the drill rod (Sherrit et al. 1999). The impulse imparted to the drill rod by the free mass at each impact (with e = 1) is shown in Fig. 2.6 as a function of time. It is observed that the maximum impulse imparted on the drill bit is 0.95 N-sec. Figure 2.7 shows the energy transferred to the drill rod as a function of the oscillation frequency of the free mass. It is observed that the frequency of oscillation of the free mass ranges between 400 Hz. and 6000 Hz. with an average energy of 0.35 J.

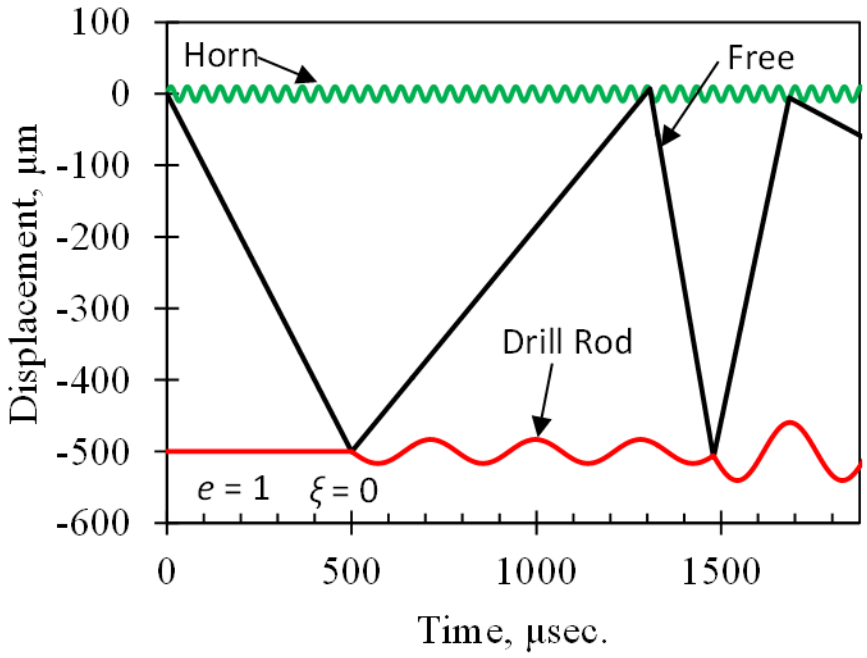

Fig. 2.5: Inset of Fig. 2.4 showing the position of ultrasonic horn, free mass and drill rod as a function of time for $e = 1$ and $\xi = 0$. (undamped)

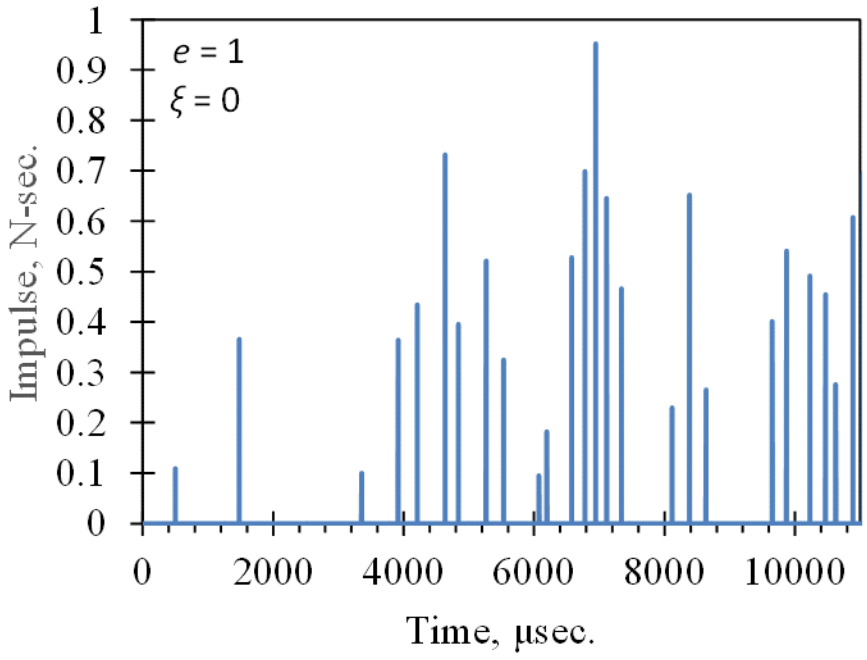

Fig. 2.6: Impulse imparted to the drill rod due to impact of the free mass for $e = 1$ and $\xi = 0$. (undamped)

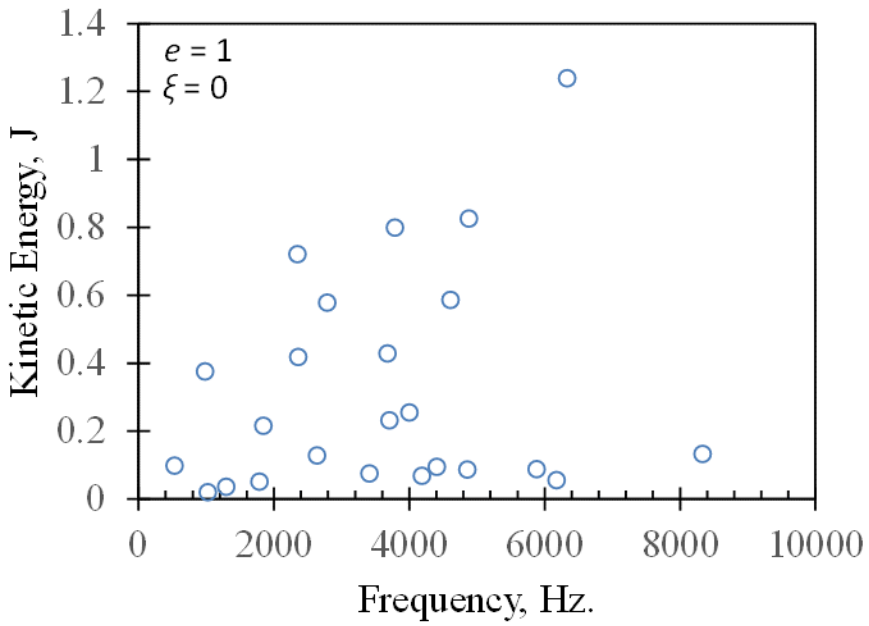

Fig. 2.7: Energy transferred to the drill rod by the free mass as a function of the frequency of oscillation of the free mass for $e = 1$ and $\xi = 0$. (undamped)

During impact there are several causes for loss of energy (e.g. plastic deformation, wave propagation, sound). To include the effects of such energy losses the operation of the ultrasonic percussive drill was simulated for different values of the coefficient of restitution ranging from 0.2 to 0.8. The position of the free mass, the ultrasonic horn and the drill rod for a coefficient of restitution equal to 0.8, 0.6, 0.4, and 0.2 is shown in Figs. 2.8 to 2.11, respectively. It is observed that the number of impacts decreases with decreasing coefficient of restitution. This is attributed to the fact that more energy loss during impact (i.e. smaller coefficient of restitution) causes the rebound velocity of the free mass to be smaller. Figure 2.12 shows the number of impacts, average kinetic energy and average impulse transferred to the drill rod by the free mass as a function of the coefficient of restitution for the undamped case. It is observed that the kinetic energy and impulse transferred to the drill rod increase with the coefficient of restitution. The number of

impacts, in general, seem to follow the same trend. However, the number of impacts for a coefficient of restitution equal to 0.6 is higher than that for a coefficient of restitution of 0.8. Nevertheless, the kinetic energy and impulse transferred during impact for a coefficient of restitution equal to 0.6 is smaller compared to the case for a coefficient of restitution equal to 0.8.

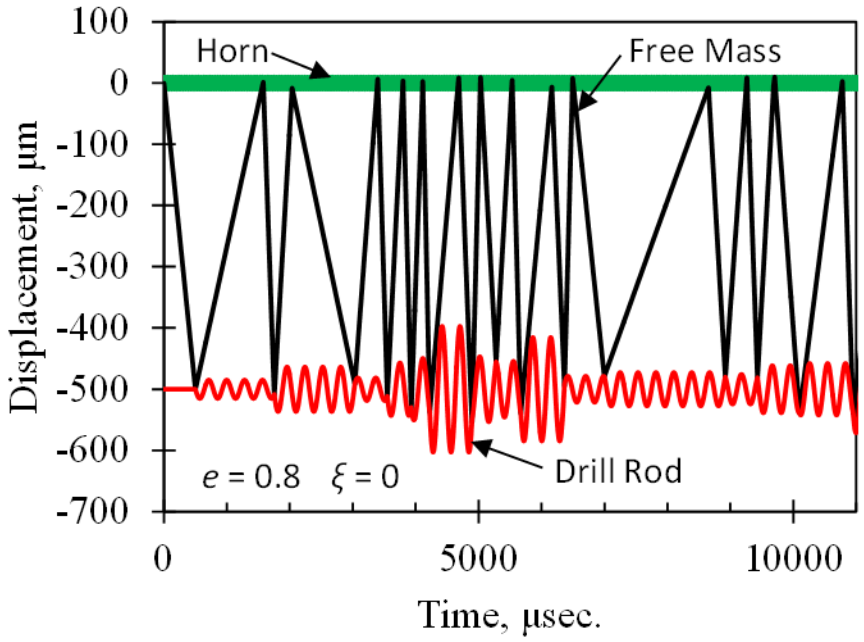

Fig. 2.8: Position of ultrasonic horn, free mass and drill rod as a function of time for $e = 0.8$ and $\xi = 0$. (undamped)

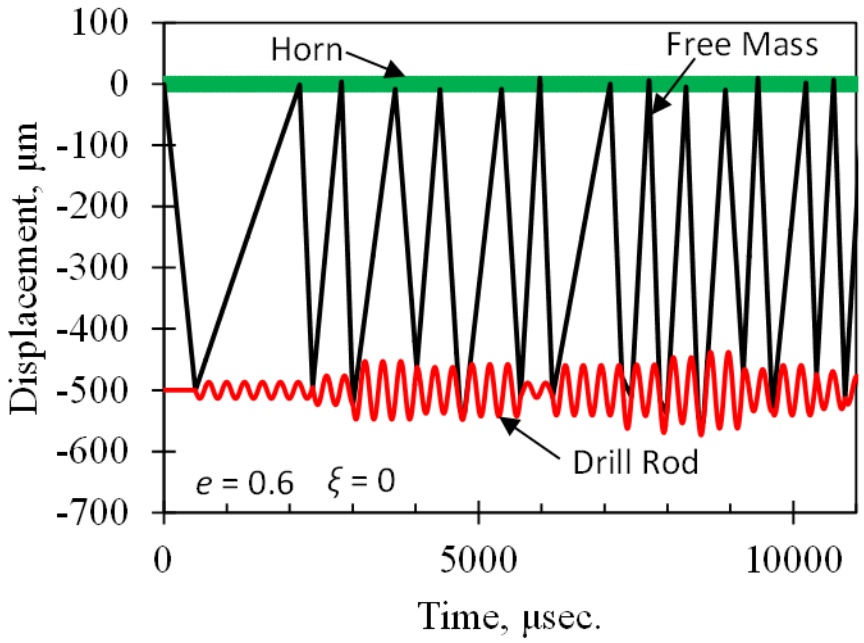

Fig. 2.9: Position of ultrasonic horn, free mass and drill rod as a function of time for $e = 0.6$ and $\xi = 0$. (undamped)

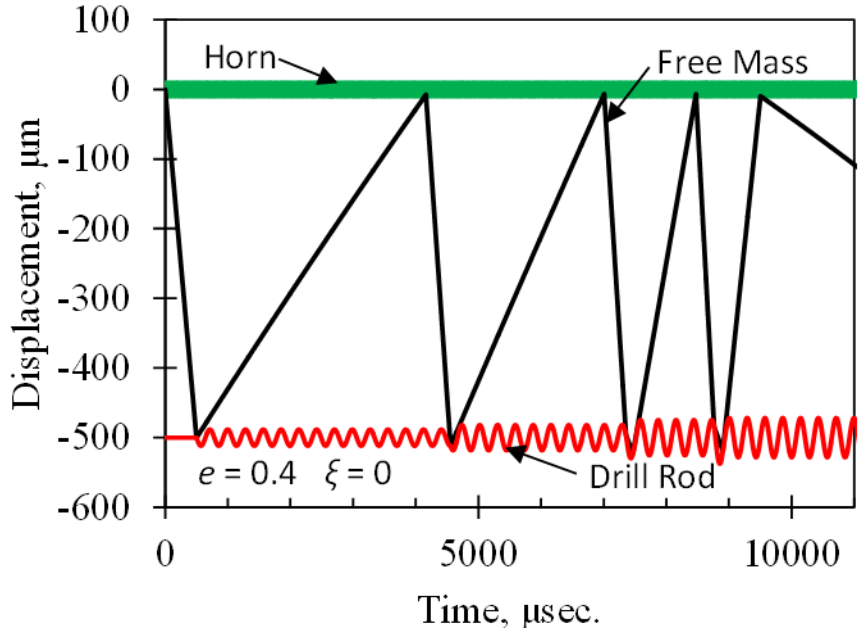

Fig. 2.10: Position of ultrasonic horn, free mass and drill rod as a function of time for $e = 0.4$ and $\xi = 0$. (undamped)

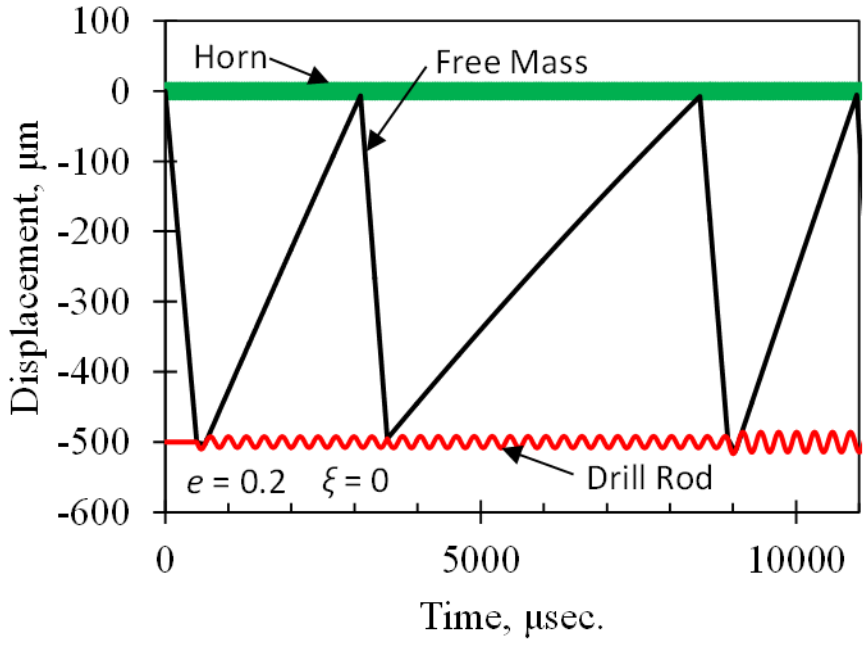

Fig. 2.11: Position of ultrasonic horn, free mass and drill rod as a function of time for $e = 0.2$ and $\xi = 0$. (undamped)

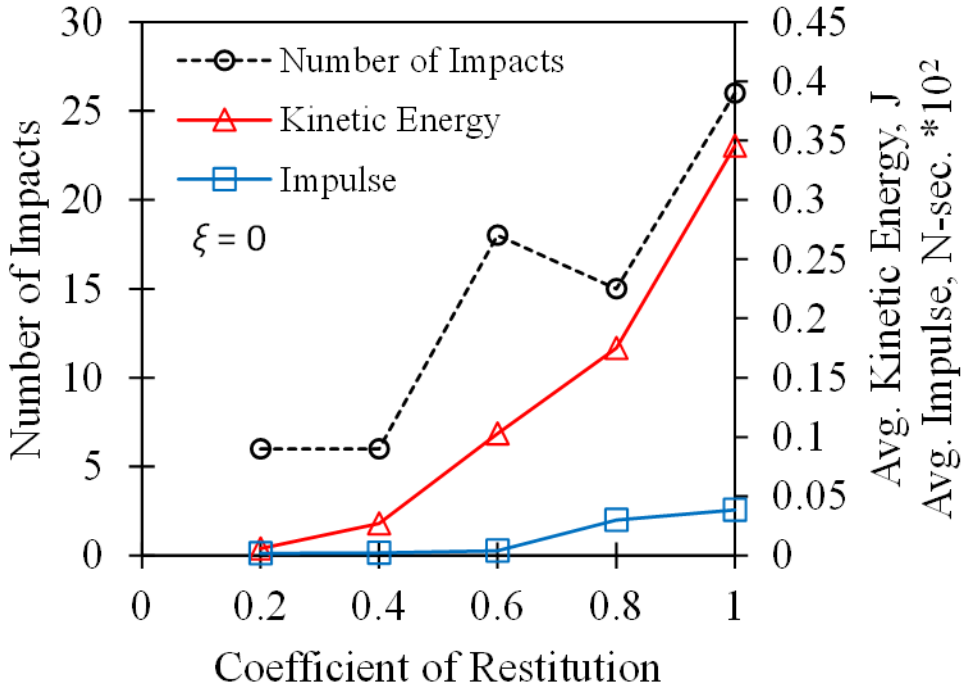

Fig. 2.12: Number of impacts, average kinetic energy transferred and average impulse obtained from the simulation ($t = 11.1$ msec.) for different coefficients of restitution. (undamped)

The position of the free mass, the ultrasonic horn and the drill rod for a coefficient of restitution equal to 1, 0.6 and 0.2 for an underdamped rod ($\xi = 0.1$) is shown in Figs. 2.13, 2.14 and 2.15, respectively. Similar to the undamped case, it is observed that the number of impacts decreases with the coefficient of restitution. In this case, however, the increasing time period between impacts (as the coefficient of restitution decreases) allows the oscillations of the drill rod to damp out (see e.g. Fig. 2.15).

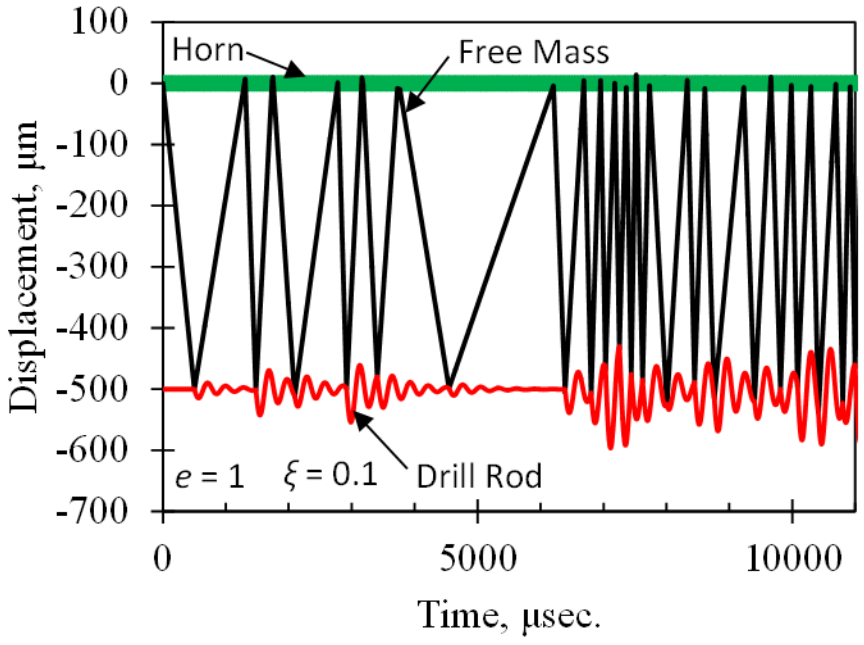

Fig. 2.13: Position of ultrasonic horn, free mass and drill rod as a function of time for $e = 1$ and $\xi = 0.1$. (damped)

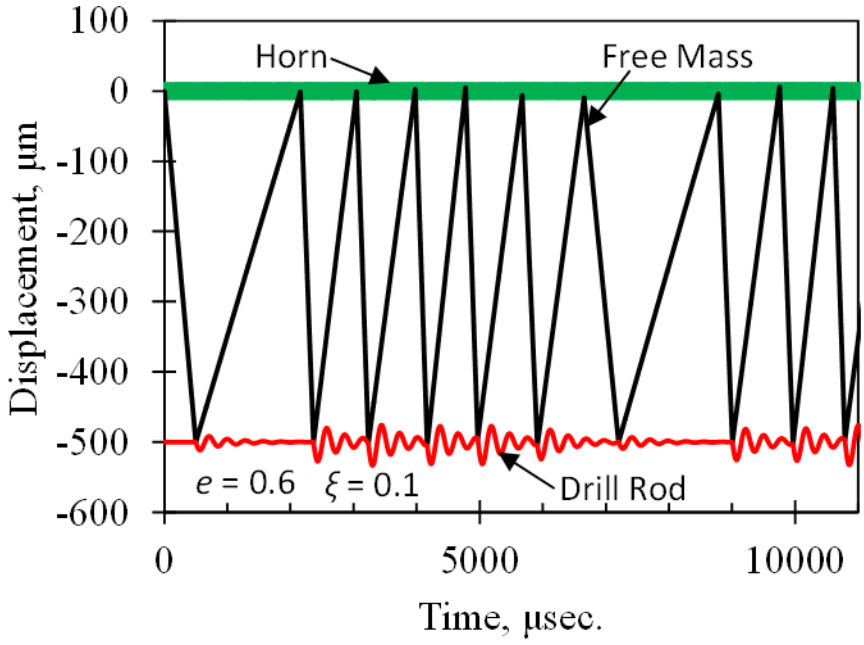

Fig. 2.14: Position of ultrasonic horn, free mass and drill rod as a function of time for $e = 0.6$ and $\xi = 0.1$. (damped)

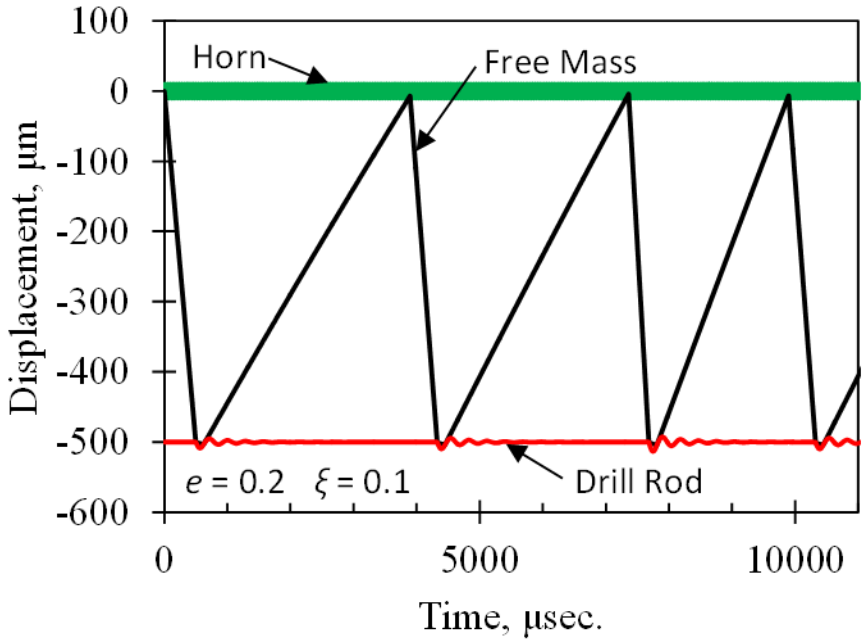

Fig. 2.15: Position of ultrasonic horn, free mass and drill rod as a function of time for $e = 0.2$ and $\xi = 0.1$. (damped)

Figure 2.16 shows the number of impacts, average kinetic energy and average impulse transferred to the drill rod by the free mass as a function of the coefficient of restitution for the underdamped case. Similar to the undamped case, the kinetic energy and impulse transferred to the drill rod increase with the coefficient of restitution. The number of impacts is also observed to increase with the coefficient of restitution in all but the case of a coefficient of restitution equal to 0.2 and 0.4, where a higher number of impacts is observed for e = 0.2. However, as it was the case for the undamped system, even though a higher number of impacts occur for e = 0.2, less kinetic energy and impulse is transferred to the drill rod.

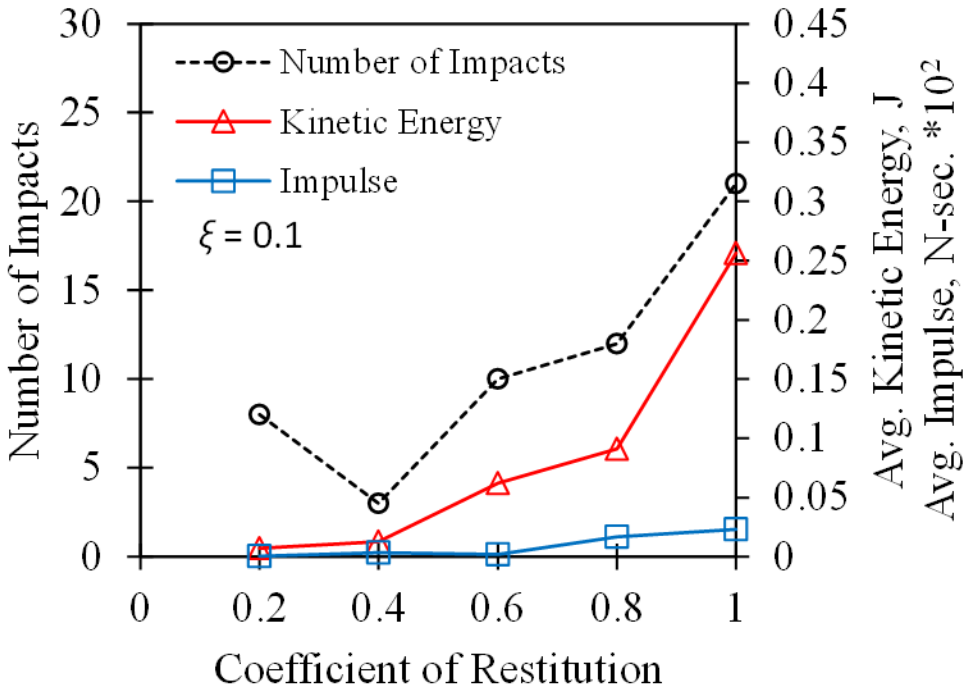

Fig. 2.16: Number of impacts, average kinetic energy transferred and average impulse obtained from the simulation (t = 11.1 msec.) for different coefficients of restitution. (damped)

2.3 Contact Force due to Impact: Wave Propagation Method

To determine the contact force and duration of contact, the impact between the free mass and the drill rod is analyzed using the wave propagation method developed by St. Venant (1889). It is assumed that the free mass is rigid (undeformable) and that both surfaces (free mass and drill bit) are flat. The equation governing the axial vibration of the rod is given by:

$$\frac{\partial^2 u_r}{\partial x^2} - \frac{1}{c^2}\frac{\partial^2 u_r}{\partial t^2} = 0 \tag{2.14}$$

The wave propagation solution of Eqn. (2.14) is given by (Goldsmith 1960):

$$u_r = f(ct - x) + g(ct + x) = f(\xi) + g(\xi) \tag{2.15}$$

where, $f(\xi)=f(ct-x)$, $g(\xi)=g(ct+x)$, $\xi = ct \pm x$, and $f(\xi)$ and $g(\xi)$ are wave functions propagating in the positive and negative x-direction , respectively. Considering the rod fixed at $x = L$ and applying the boundary condition, $u = 0$ at $x = L$, in Eqn. (2.15) gives:

$$u_r = f(ct - L) + g(ct + L) = 0 \tag{2.16}$$

Or $f(ct-L) = -g(ct+L)$. This indicates that whenever the arguments differ by 2L, $f = -g$. Thus Eqn. (2.16) can be expressed as:

$$u_r = f(ct - x) - f(ct + x - 2L) = f(\xi) - f(\xi - 2L) \tag{2.17}$$

Applying the principle of impulse-momentum to the free mass, and assuming that the velocity of the free mass during contact is the same as that of the drill bit rod, we obtain:

$$-\int_0^{\Delta\tau} EA\frac{\partial u_r}{\partial x}\,dt = m_{fm}\left[v_{fm} - \frac{\partial u_r}{\partial t}\right] \tag{2.18}$$

where m_{fm} and v_{fm} are the mass and velocity of the free mass, respectively. By substituting Eqn. (2.17) in Eqn. (2.18), and integrating the left side with respect to $d\xi$, where $d\xi = cdt$ (at $x = 0$), the following differential equation is obtained:

$$f'(\xi) + \frac{M}{L} f(\xi) = \frac{v_{fm}}{c} + f'(\xi - 2L) - \frac{M}{L} f(\xi - 2L) \tag{2.19}$$

where M is the mass ratio m_r/m_{fm}, v_{fm} is the approaching velocity (before impact) of the free mass, and c is the velocity of wave propagation. The solution to Eqn. (2.19) is given by (Greenberg 1978):

$$f(\xi) = e^{-M\left(\frac{\xi}{L}\right)} \int_0^{\xi} e^{M\frac{\xi}{L}} \left[\frac{v_{fm}}{c} + f'(\xi - 2L) - \frac{M}{L} f(\xi - 2L)\right] d\xi \tag{2.20}$$

or

$$f(\xi) = \frac{L}{M}\frac{v_{fm}}{c}\left[1 - e^{-M\frac{\xi}{L}}\right] + e^{-M\frac{\xi}{L}} \int_0^{\xi} e^{M\frac{\xi}{L}} \left[f'(\xi - 2L) - \frac{M}{L} f(\xi - 2L)\right] d\xi \tag{2.21}$$

The wave function $f(\xi)$ can be determined by Eqn. (2.21) for intervals of $2iL$ to $2(i+1)L$ once the wave function for the previous interval has been determined, where $i = 0,1,2,\ldots$ To evaluate the wave function $f(\xi)$, it is necessary to substitute the wave function of the previous interval evaluated in $(\xi\text{-}2L)$ inside the integral of Eqn. (2.21) and change the lower limit of the integral to the lower limit of the interval under consideration (or $2iL$). $f'(\xi)$ can be calculated by differentiation of the wave function $f(\xi)$. The wave functions for the intervals $0 \le \xi \le 2L$ and $2L \le \xi \le 4L$ are shown in Eqns. (2.22).

<u>Interval $0 \le \xi \le 2L$</u>

$$f_1(\xi) = \frac{L}{M}\frac{v_{fm}}{c}\left[1 - e^{-M\frac{\xi}{L}}\right] \tag{2.22a}$$

$$f'_1(\xi) = \frac{v_{fm}}{c} e^{-M\frac{\xi}{L}} \tag{2.22b}$$

<u>Interval $2L \le \xi \le 4L$</u>

$$f_2(\xi) = f_1(\xi) + \frac{L}{M}\frac{v_{fm}}{c}\left[-1 + \left\{1 + 2M\left(\frac{\xi}{L} - 2\right)\right\} e^{-M\left(\frac{\xi}{L} - 2\right)}\right] \tag{2.22c}$$

$$f'_2(\xi) = f'_1(\xi) + \frac{v_{fm}}{c}\left[1 - 2M\left\{\frac{\xi}{L} - 2\right\}\right] e^{-M\left(\frac{\xi}{L}-2\right)} \quad (2.22d)$$

The displacement of the rod during contact is determined by Eqn. (2.17), where *f(ξ)* is determined from Eqn. (2.21) and *f(ξ-2L)* is the wave function of the previous interval evaluated in *(ξ-2L).* After the contact ceases, the rod undergoes free vibration. The velocity and acceleration of the rod during contact is obtained by differentiation of the displacement function.

$$v_r = \frac{\partial u_r}{\partial t} = c[f'(\xi) - f'(\xi - 2L)] \quad (2.23)$$

$$a = \frac{\partial^2 u_r}{\partial t^2} = c^2[f"(\xi) - f"(\xi - 2L)] \quad (2.24)$$

Once the wave functions have been determined, the stress in the rod can be calculated by substituting the corresponding wave equations in Eqn. (2.25).

$$\sigma = E\frac{\partial u_r}{\partial x} = -E[f'(\xi) + f'(\xi - 2L)] \quad (2.25)$$

The condition that controls the end of contact is zero stress at the point of contact ($x = 0$).

From Eqn. (2.25), $\sigma = E\frac{\partial u_r}{\partial x} = 0$ or $\partial u_r / \partial x = 0$ or

$$[f'(\xi) + f'(\xi - 2L)] = 0 \quad (2.26)$$

The duration, τ, of contact is obtained by substituting Eqn. (2.22b) evaluated in $\xi - 2L$, and Eqn. (2.22d) into Eqn. (2.26). That is:

$$\frac{v_{fm}}{c} e^{-\frac{M}{L}(\xi - 2L)} + \frac{v_{fm}}{c} e^{-M\frac{\xi}{L}} + \frac{v_{fm}}{c}\left[1 - 2M\left\{\frac{\xi}{L} - 2\right\}\right] e^{-M\left(\frac{\xi}{L}-2\right)} = 0 \quad (2.27)$$

Considering the motion at the striking end (x = 0), $\xi = ct$, and letting $t = \tau$, the duration, τ, of contact is given by:

$$\tau = \frac{L(e^{-2M} + 4M + 2)}{2Mc} \quad (2.28)$$

It can be seen that the duration, τ, of impact depends upon mass ratio M, length, L, of the rod, and velocity, c, of wave propagation. The displacement and velocity of the rod at the end of contact given by Eqns. (2.17) and (2.23) serve as the initial conditions for its free vibration after the impact.

2.3.1 Determination of Contact Stress/Force

The contact force between the free mass and the drill bit is determined by stress wave propagation analysis on the rod. Once the wave functions (Eqn. 2.22) have been determined, the stress on the rod can be calculated using Eqn. (2.25). Figure 2.17 shows the contact force at the free end (x = 0) of the drill bit for the material properties shown in Table 2.1 (M = 13.24).

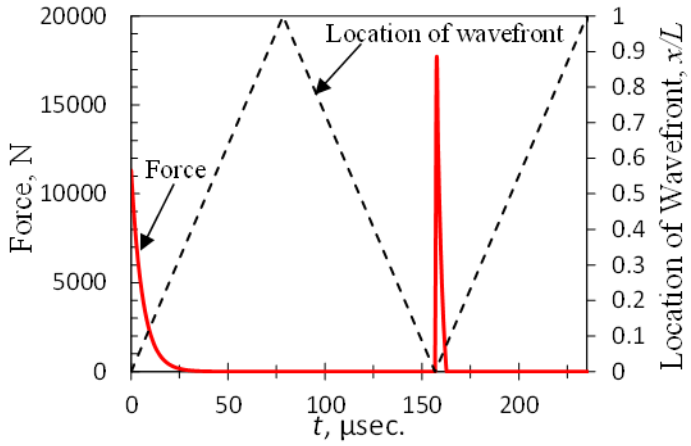

Figure 2.17: Impact force time history obtained from wave propagation method.

The diagonal lines show the location of wave front in the rod. The contact stress is observed to increase impulsively at the moment of contact, and then it starts decreasing while the wave is propagating through the rod. When the reflected wave reaches the point of contact

(x = 0), the stress is again increased impulsively. Finally, it starts decreasing until it becomes equal to zero (end of contact).

2.4 Contact Force due to Impact: Energy Balance Method (Cox Equation)

Other important parameters in the analysis of percussive drilling systems are the contact force developed between the hammer and the drill rod during impact and the duration of such impact. The contact force for a mass, m_{fm}, with a velocity $v_{fm,0}$ striking an elastic rod of mass m_r will be determined by performing an energy balance in the system (see Fig. 2.18), also known as Cox (1849) method. The rod is regarded as a spring with stiffness $k = EA/L$ (see Fig. 2.18b).

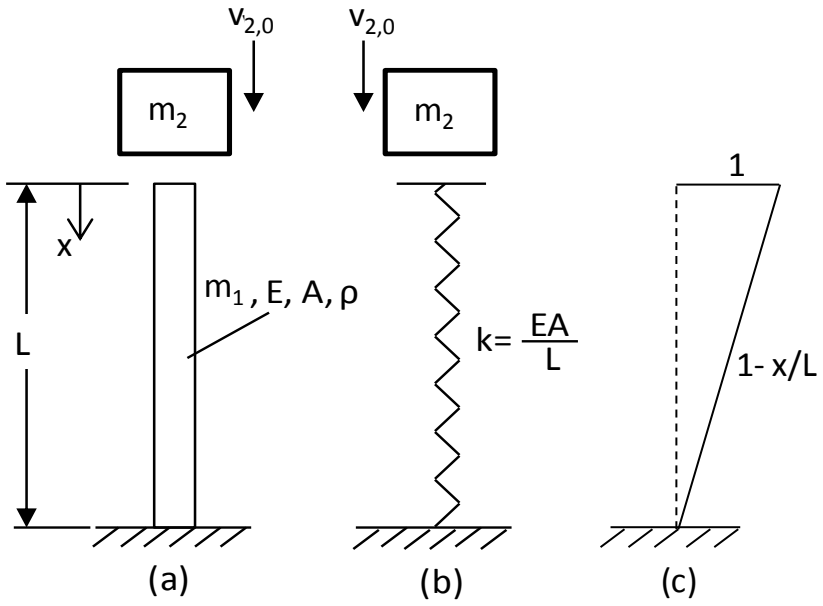

Fig. 2.18: (a) Mass striking an elastic rod, (b) Equivalent spring system, and (c) Assumed mode shape

It is assumed that the mass and the rod will move together during impact, thus both acquire the same velocity, *v,* immediately after impact. The mass of the rod is considered as an effective mass (χm_r) which is a fraction of the total mass of the rod. Thus applying the law of conservation of momentum for the system gives (Goldsmith 1960):

$$m_{fm}v_{fm,0} = (m_{fm} + \chi m_r)v \quad or \qquad v = \frac{m_{fm}v_{fm,0}}{(m_{fm} + \chi m_r)} \tag{2.29}$$

The axial deformation, u_r, of the rod is assumed to be of the form:

$$u_r(x,t) = \eta(t)f(x) \tag{2.30}$$

where $\eta(t)$the generalized dynamic axial deformation and *f (x)* is the axial mode shape. The deformation of the rod is assumed to be linear (see Fig. 2.18c), therefore, the axial mode shape, *f(x)*, is given by:

$$f(x) = 1 - \frac{x}{L} \tag{2.31}$$

The total kinetic energy, *T*, of the rod is given by:

$$T = \frac{1}{2}\rho A \int_0^L \left(\frac{\partial u_r}{\partial t}\right)^2 dx \tag{2.32}$$

where ρ is the mass density of the drill rod material and *A* is the cross sectional area. Substituting Eqn. (2.30) into Eqn. (2.32) and carrying out the integration yields a total kinetic energy, *T*, of:

$$T = \frac{1}{2}\rho A \int_0^L [\dot{\eta}^2(1 - {}^{x}/_{L})^2]dx = \frac{m_1\dot{\eta}^2}{6} \tag{2.33}$$

where $m_r = \rho AL$. From Eqn. (2.33), it can be seen that the effective mass, χm_r, of the rod is ${}^{1}/_{3}\, m_r$. Considering a differential element of the rod (see Fig. 2.19), $\varepsilon = \frac{\partial u}{\partial x}$, thus the strain energy is given by:

$$V = \int_0^L \frac{AE}{2}\varepsilon^2 dx = \frac{AE}{2}\int_0^L \left(\frac{\partial u_r}{\partial x}\right)^2 dx \tag{2.34}$$

Thus, substituting $\partial u/\partial x$ in Eqn. (2.34) and carrying out the integration, the total strain energy in the rod is obtained as:

$$V = \frac{EA\eta^2}{2L} \tag{2.35}$$

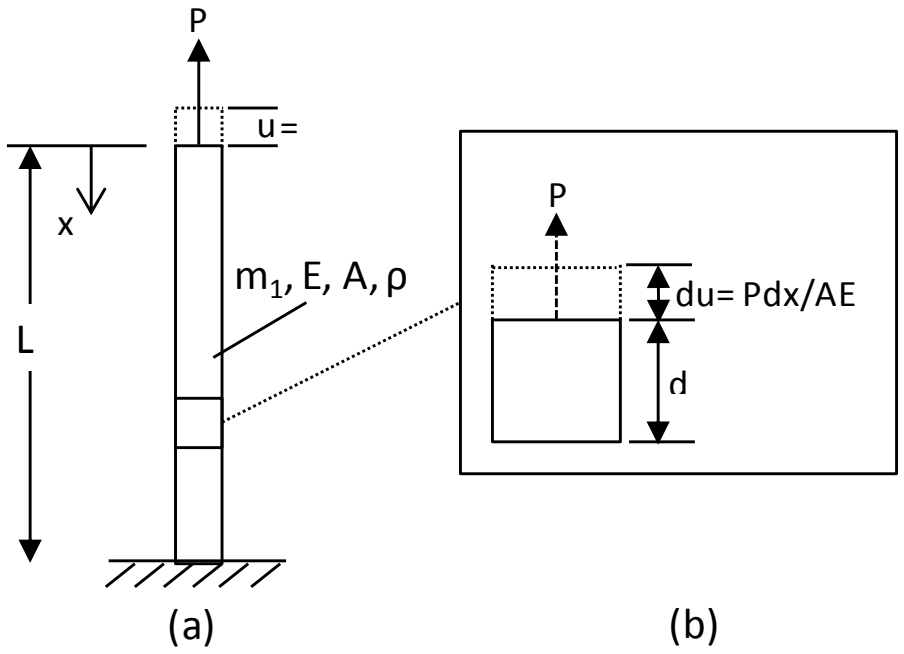

Fig. 2.19: (a) Elastic rod subjected to axial load P, and (b) Differential element subjected to axial load *P*.

Introducing the Lagrange equation for impulsive motion (Goldsmith 1960):

$$\frac{d}{dt}\left(\frac{\partial T}{\partial \dot{q}_\iota}\right) - \frac{\partial T}{\partial q_i} + \frac{\partial V}{\partial q_i} = Q_i \qquad i = 1,2,3,\ldots.n \tag{2.36}$$

where Q_i is the generalized external force corresponding to the generalized coordinate q_i. Substituting Eqns. (2.33) and (2.35) into the Lagrangian equation of motion (Eqn. (2.36)), with $q_i = \eta$ and $\dot{q}_i = \dot{\eta}$, gives the equation of motion of the rod as:

$$Q = \frac{1}{3} m_r \ddot{\eta} + \frac{EA}{L} \eta \tag{2.37}$$

Then the equation of motion for the striking mass, m_2, is obtained as:

$$m_{fm} g - Q = m_{fm} \ddot{\eta} \tag{2.38}$$

Finally, combining the equations of motion for the rod and the mass gives the equation of motion for the system as:

$$\left[m_{fm} + \frac{1}{3} m_r \right] \ddot{\eta} + k\eta = m_{fm} g \tag{2.39}$$

where $k = EA/L$, or

$$\ddot{\eta} + \omega^2 \eta = \frac{m_{fm} g}{m_{eff}} \tag{2.40}$$

where $m_{eff} = m_{fm} + \frac{1}{3} m_r$ and ω_{eff} is the effective frequency given by:

$$\omega_{eff} = \sqrt{\frac{k}{m_{eff}}} \tag{2.41}$$

2.4.1 Contact Force

The solution of Eqn. (2.40) is of the form:

$$\eta = A sin(\omega_{eff} t) + B cos(\omega_{eff} t) + \frac{m_{fm} g}{m_{eff} \omega_{eff}^2} \tag{2.42}$$

The constants A and B are determined from the following initial conditions:

$$u_r(x, 0) = 0 \qquad and \qquad \dot{u}_r(x, 0) = v = \frac{m_{fm} v_{fm,0}}{m_{fm} + \frac{1}{3} m_r} \tag{2.43}$$

Substituting the first initial condition of Eqn. (2.43) into Eqn. (2.30), we obtain:

$$\eta(0) = 0 \tag{2.44}$$

The remaining initial condition $\dot{\eta}(0)$ is given by:

$$\dot{\eta}(0) = v = \frac{m_{fm} v_{fm,0}}{m_{fm} + \frac{1}{3} m_r} \tag{2.45}$$

After applying the initial conditions (Eqn. (2.44) and Eqn. (2.45)), η and $\ddot{\eta}$ are obtained as:

$$\eta = \frac{m_{fm} g}{m_{eff} \omega_{eff}^2} \left[1 - \cos\left(\omega_{eff} t\right)\right] + \frac{m_{fm} v_{fm,0}}{m_{eff} \omega_{eff}} \sin\left(\omega_{eff} t\right) \tag{2.46}$$

$$\ddot{\eta} = \frac{m_{fm} g}{m_{eff}} \cos\left(\omega_{eff} t\right) - \frac{m_{fm} v_{fm,0} \omega_{eff}}{m_{eff}} \sin\left(\omega_{eff} t\right) \tag{2.47}$$

Finally, the impact force, *Q*, can be calculated by substituting Eqn. (2.46) and Eqn. (2.47) into Eqn. (2.37). Thus the contact force is given by:

$$Q = \frac{1}{3} m_r \ddot{\eta} + \frac{EA}{L} \eta \tag{2.48}$$

The geometric and material properties shown in Table 2.1 are used to analyze the impact of the free mass on the drill rod. The cross sectional area of the rod is taken as equal to 2.85 cm^2 and the free mass is taken with an initial velocity equal to 1 m/s. The initial displacement of the drill rod is taken as equal to zero and the initial velocity equal to 0.185 m/s (as obtained from Eqn. (2.43)). The Young's modulus is taken as equal to 203 GPa. The effective frequency, ω_{eff}, obtained from Eq. (2.41) is equal to 19,961 rad/s. The contact force and displacement of the drill rod and the free mass are shown in Fig. 2.20. It is observed that a maximum contact force of 248 N was obtained. The force obtained from the energy method is observed to be smaller (and with a different shape) than that of obtained from the wave propagation method (see Fig. 2.17). The high force obtained from the wave propagation method compared to other methods is consistent with the material presented by Hu and Eberhard (2003).

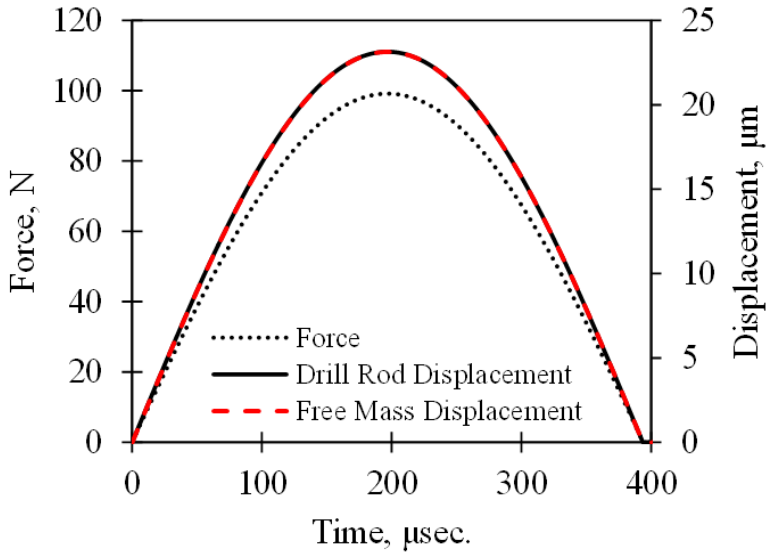

Fig. 2.20: Impact force time history for longitudinal impact between a free mass and a uniform cantilever rod.

In addition, in the wave propagation method the wave equations need to be determined every time the wave reach the impacted end of the rod. This makes it difficult, and inconvenient, for applications in which the simulations needs to be done for a long time period.

2.4.2 Duration of Contact

The time, t_{max}, where the maximum force occurs is obtained by differentiating Eqns. (2.46) and (2.47) and equating to zero. Thus we obtain,

$$\dot{\eta} = \frac{g}{\sqrt{k(m_{fm} + \frac{1}{3}m_r)}}\sin(\omega_{eff}t_{max}) + \frac{v_{fm,0}}{m_{fm} + \frac{1}{3}m_r}\cos(\omega_{eff}t_{max}) = 0 \qquad (2.49)$$

$$\ddot{\eta} = \frac{-k^{1/2}m_{fm}g}{\left(m_{fm} + \frac{1}{3}m_r\right)^{3/2}}\sin(\omega_{eff}t_{max}) - \frac{km_{fm}v_{fm,0}}{\left(m_{fm} + \frac{1}{3}m_r\right)^{2}}\cos(\omega_{eff}t_{max}) = 0 \qquad (2.50)$$

Solving Eqns. (2.49) and (2.50) for t_{max}, it is seen that the maximum compression, η_{max}, and the maximum acceleration, $\ddot{\eta}_{max}$, occur at the same time:

$$t_{max} = \frac{1}{\omega_{eff}} tan^{-1}\left(\frac{-v_{fm,0}\omega_{eff}}{g}\right) \tag{2.51}$$

Since for the particular case of a perfectly elastic impact, the maximum force occurs at one-half of the duration of contact (Goldsmith 1960), then the duration, τ, of contact can be obtained by:

$$\tau = 2t_{max} = \frac{2}{\omega_{eff}} tan^{-1}\left(\frac{-v_{fm,0}\omega_{eff}}{g}\right) \tag{2.52}$$

Substituting the properties of the rod into Eqn. (2.52), the duration of contact for these properties is equal to 157 μsec. The duration of contact for this system using wave propagation theory can be obtained from Eqn. (2.28). Subtituting the mass ratio (M = 13.24) and the velocity of wave propagation (c = 5105 m/s) into Eqn. (2.28) the duration of contact is obtained as equal to 159 μsec. For a general case, the duration of contact may be determined by letting the force (Eqn. (2.37)) equal to zero. Thus, for a general impact case, Eqn. (2.53) can be solved iteratively to obtain the duration of contact.

$$m_2 g + \left[\left(\frac{1}{3}m_1\right)\left(\frac{m_2 g}{m_{eff}}\right) - m_2 g\right]\cos(\omega t)$$

$$+\left[\frac{1}{\sqrt{m_{eff}}} - \left(\frac{1}{3}m_1\right)\frac{1}{\left(m_{eff}\right)^{3/2}}\right]\left(m_2 v_{2,0} k^{1/2}\right)\sin(\omega t) = 0 \tag{2.53}$$

2.5 Conclusions

In this chapter, the hammering mechanism of an ultrasonic percussive system was analyzed. The study focused on analyzing the interaction between the ultrasonic horn, free

mass and drill rod for both, undamped and underdamped cases. The impulse and energy transferred to the drill rod during the impact from the free mass, the contact force and duration of contact between the free mass and the drill rod were determined. Based on the results obtained from the present study, the following conclusions can be made:

- The free mass converts the high frequency oscillations of the ultrasonic horn into lower frequency impacts on the drill rod.
- Including the energy losses through the coefficient of restitution affects significantly the operation of the ultrasonic percussive drill. The number of impacts, average kinetic energy and average impulse transferred to the drill rod by the free mass increase as the energy loss decreases.
- Applying an energy balance to the (free mass/rod) system, the equivalent dynamic contact force and duration of contact can be determined by a relatively simple procedure.
- The duration of contact obtained from Cox method is similar to that obtained from wave propagation theory of previous studies, considering the difference in the assumptions of each method.

It should be noted that in this chapter the free mass was taken as rigid and the surfaces in contact were considered to be flat. However, in practical applications this is not always true and a detailed analysis of the impact phenomena including the local deformation at the point of contact should be considered. Such detailed impact analysis is presented in Chapter 3.

Chapter 3

Longitudinal Impact of a Spherical Striker on a Rod

This chapter presents a general methodology to perform the dynamic contact analysis of the longitudinal impact of the free mass on the drill rod considering the structural vibration and damping of the rod. The contact force due to impact is obtained using Hertz force-indentation relation coupled with the structural vibration obtained using mode superposition method and finite element technique. Numerical solution, with equilibrium iterations, of the equations of motion is implemented.

3.1 Analytical Formulation

Consider a uniform cantilever rod of length, *L*, struck by a spherical mass with an initial velocity, $v_{2,0}$. as shown in Fig. 3.1. In this study this situation is analyzed as the structural vibration of an axial member under an end force, *P(0,t)*, caused by the impact; where *P(0,t)* is the contact force that is to be determined.

The equation of motion of axial vibration of a rod subjected to a distributed to a load *P(x,t)* along its length (Fig. 3.2a), obtained from a differential element (Fig. 3.2b), of the rod is given by:

$$\bar{m}\frac{\partial^2 u_1(x,t)}{\partial t^2} + C\frac{\partial u_1(x,t)}{\partial t} - EA\ \frac{\partial^2 u_1(x,t)}{\partial x^2} = P(x,t) \tag{3.1}$$

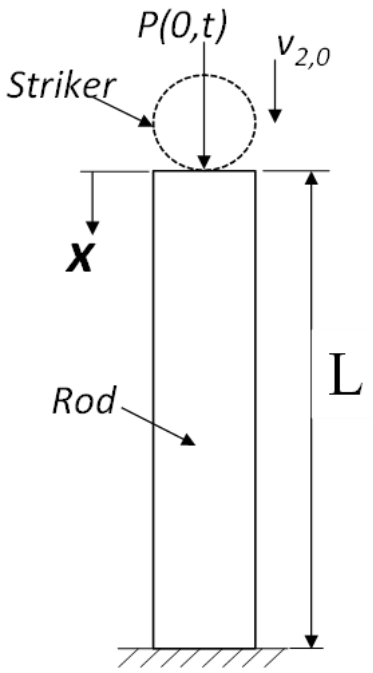

Fig. 3.1: Impact of a spherical striker on a rod.

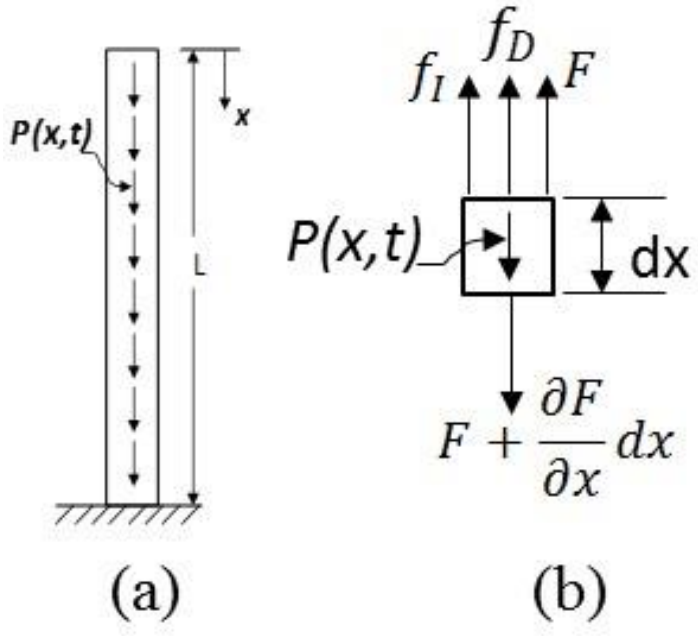

Fig. 3.2: (a) Rod with fixed support subjected to distributed time varying load $P(x,t)$ and **(b)** Free body diagram of an element of a uniform rod subjected to a distributed axial force.

where $f_I = \bar{m} \cdot \partial^2 u_1(x,t)/\partial t^2$ is the inertial force, $f_D = C \cdot \partial u_1(x,t)/\partial t$ is the damping force, $F = EA \cdot \partial u_1(x,t)/\partial x$ is the internal axial force, E is the Young's modulus, and A is the cross sectional area of the rod. Introducing the velocity of wave propagation $c = \sqrt{E/\rho}$, letting the mass per unit length of the rod $\bar{m} = \rho A$, where ρ is the density of the rod, and defining the distributed load as $\underline{P}(x,t) = P(x,t)/\bar{m}$, Eqn. (3.1) can be expressed as:

$$\frac{\partial^2 u_1(x,t)}{\partial t^2} + \frac{C}{\bar{m}}\frac{\partial u_1(x,t)}{\partial t} - c^2 \frac{\partial^2 u_1(x,t)}{\partial x^2} = \underline{P}(x,t) \tag{3.2}$$

3.1.1 Free Vibration: Frequencies and Mode Shapes

By separation of variables, the displacement, $u_1(x,t)$, of the rod is defined as:

$$u_1(x,t) = \varphi(x)q(t) \tag{3.3}$$

where $\varphi(x)$ is the mode shape and $q(t)$ is the generalized coordinate. The general solution of Eqn. (3.2) for undamped free vibration ($C = 0, \underline{P}(x,t) = 0$) is obtained by substituting Eqn. (3.3) into Eqn. (3.2) and is given by (Clough and Penzien 1975; Tedesco et al. 1999):

$$\varphi(x) = C_1 cos\left(\frac{\omega x}{c}\right) + C_2 sin\left(\frac{\omega x}{c}\right) \tag{3.4a}$$

$$q(t) = C_3 cos(\omega t) + C_4 sin(\omega t) \tag{3.4b}$$

where ω is the undamped natural frequency, and C_1, C_2, C_3, and C_4 are constants. Therefore, the total solution of Eqn. (3.2) is given by Eqn. (3.3) where $\varphi(x)$ and $q(t)$ are given by Eqns. (3.4a, 3.4b). The frequency (ω) and one of the constants C_1 and C_2 can be obtained by applying the boundary conditions. The coefficients C_3 and C_4 are obtained by applying the initial conditions.

Considering the uniform cantilever rod shown in Fig. 3.2a without force *P(x,t)*, the boundary conditions are given by (i) the axial stress equal to zero at $x = 0$ (free end), and (ii) the displacement equal to zero at $x = L$ (fixed end), for all time, *t*. Applying the first boundary condition we obtain $C_2 = 0$. Thus the mode shape for this case is given by:

$$\varphi(x) = C_1 cos\left(\frac{\omega x}{c}\right) \tag{3.5}$$

Applying the second boundary condition we obtain the characteristic equation, $\cos(\omega L/c) = 0$, from which $\omega L/c = (2i + 1)\pi/2$ and the natural frequencies are obtained as:

$$\omega_i = \frac{(2i + 1)\pi c}{2L} \quad i = 0,1,2 \ldots \tag{3.6}$$

3.1.2 Dynamic Response under applied load by Mode Superposition

Applying mode superposition, the longitudinal motion of the rod can be expressed in terms of the sum of the normal mode shapes, $\varphi_i(x)$, times the generalized coordinates, $q_i(t)$. Thus the response of the rod is expressed as:

$$u_1(x,t) = \sum_{i=1}^{\infty} \varphi_i(x) q_i(t) \tag{3.7}$$

Substituting Eqn. (3.7) into Eqn. (3.2), assuming a damping proportional to mass and stiffness, and after applying the boundary conditions and orthogonality relations (Clough and Penzien 1975; Timoshenko et al. 1974; Rao 2007), the equation of motion of the rod under the action of a distributed applied force along the length is obtained as:

$$\ddot{q}_i + 2\zeta_i\omega_i\dot{q}_i + \omega_i^2 q_i = \int_0^L \varphi_i(x)\underline{P}(x,t)\,dx \tag{3.8}$$

where ω_i are the natural frequencies of the system and $\zeta_i = (a_0/2\omega_i) + (a_1\omega_i/2)$ is the damping ratio. The proportionality factors a_0 and a_1 can be found once two modal damping ratios are known (see Clough and Penzien 1975). In this study the same modal damping ratio is used for all modes. The solution to Eqn. (3.8) can be obtained from Duhamel's integral (Clough and Penzien 1975; Rao 2007) and for the case of an underdamped system and a concentrated load applied at $x = 0$ is given by:

$$q_i(t) = \frac{1}{\omega_{D,i}}\int_0^L \varphi_i(x)\int_0^t \underline{P}(0,t)e^{-\zeta_i\omega_i(t-\tau)}\sin\left[\omega_{D,i}(t-\tau)\right]d\tau\cdot dx \tag{3.9}$$

where $\omega_{D,i} = \omega_i\sqrt{1-\zeta_i^2}$ is the damped natural frequency for the underdamped case. Substituting Eqn. (3.9) into Eqn. (3.7), the response $u(x,t)$ of the rod is given by:

$$u_1(x,t) = \sum_{i=1}^{\infty}\frac{\varphi_i(x)}{\omega_{D,i}}\int_0^L \varphi_i(x)\int_0^t \frac{P(0,t)}{\rho A}e^{-\zeta_i\omega_i(t-\tau)}\sin\left[\omega_{D,i}(t-\tau)\right]d\tau\cdot dx \tag{3.10}$$

For the case of a concentrated load, $P(x_m,t)$, applied at x = x_m, the Dirac delta function (Kreyszig 2011)

$$\int \varphi(x)\delta(x-x_m)\,dx = \varphi(x_m) \tag{3.11}$$

can be applied to the first integral, and the response of the rod is then given by:

$$u_1(x,t) = \sum_{i=1}^{\infty}\frac{\varphi_i(x)\varphi_i(x=0)}{\omega_{D,i}}\int_0^t \frac{P(0,t)}{\rho A}e^{-\zeta_i\omega_i(t-\tau)}\sin\left[\omega_{D,i}(t-\tau)\right]d\tau \tag{3.12}$$

For a critically damped system the generalized coordinate and the total solution, respectively, are given by:

$$q_i(t) = \varphi_i(x=0)\cdot t\int_0^t \frac{P(0,t)}{\rho A}e^{-\omega_i(t-\tau)}\cdot d\tau \tag{3.13}$$

$$u_1(x,t) = \sum_{i=1}^{\infty} \varphi_i(x)\varphi_i(x=0) \cdot t \int_0^t \frac{P(0,t)}{\rho A} e^{-\omega_i(t-\tau)} \cdot d\tau \tag{3.14}$$

Similarly the solution for an overdamped system is given by:

$$q_i(t) = \frac{\varphi_i(x=0)}{\widehat{\omega}_{D,i}} \int_0^t \underline{P}(0,t) e^{-\zeta_i \omega_i (t-\tau)} \sinh[\widehat{\omega}_{Di}(t-\tau)]\, d\tau \cdot dx \tag{3.15}$$

$$u_1(x,t) = \sum_{i=1}^{\infty} \frac{\varphi_i(x)\varphi_i(x=0)}{\widehat{\omega}_{D,i}} \int_0^t \frac{P(0,t)}{\rho A} e^{-\zeta_i \omega_i (t-\tau)} \sinh\left[\widehat{\omega}_{D,i}(t-\tau)\right] d\tau \tag{3.16}$$

where $\widehat{\omega}_{D,i} = \omega_i \sqrt{\zeta_i^2 - 1}$ is the damped natural frequency for the overdamped case.

3.2 Longitudinal Impact of a Spherical Mass on a Rod

The longitudinal impact of a striker on a rod is analyzed using Hertz theory of elastic contact. This theory considers the contact between two elastic bodies. The contact force is computed based on the contact area (or contact ellipse) that forms when the two bodies are compressed to each other. Consider, two bodies 1 and 2 that become in contact at time t = 0 (see Fig. 3.3). As the bodies become in contact, due to the contact force it will experience a deformation δ_1 and δ_2 for body 1 and body 2, respectively.

Hertz (1881) found that the contact force P between two elastic bodies is proportional to the local indentation, α, to the 1.5th power. Hence, the Hertz force-indentation relation is given by (Hertz 1881):

$$P = k_2 \alpha^{3/2} \tag{3.17}$$

where $k_2 = \left({}^{4}/_{3}\right) E^* R^{*1/2}$ is the contact stiffness. The effective Young's modulus (E^*) and the effective radius (R^*) are given by (Goldsmith 1960; Vu-Quoc and Zhang 1999):

$$E^* = \left[\frac{1-\nu_1^2}{E_1} + \frac{1-\nu_2^2}{E_2}\right]^{-1} \tag{3.18}$$

$$R^* = \left[\frac{1}{R_1} + \frac{1}{R_2}\right]^{-1} \tag{3.19}$$

For a sphere of radius R_2 striking a flat ended rod ($R_1 = \infty$), the effective radius R^* is equal to R_2.

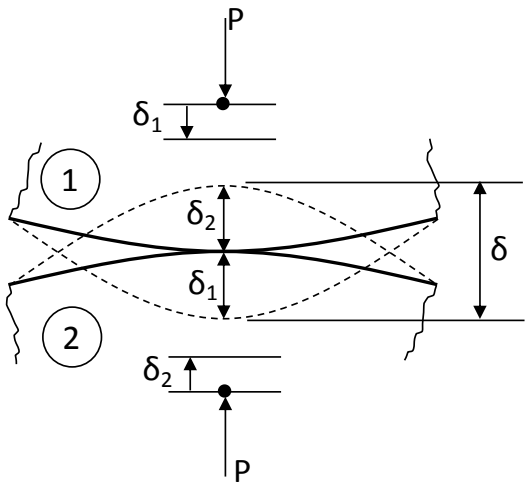

Fig. 3.3: Two spherical elastic bodies in contact.

To determine the contact force it is necessary to find the indentation, α, resulting from the impact of the two bodies. Timoshenko's (1913) approach is used to determine the indentation due to impact of the striker and the drill rod. In this approach, the motion/response of each body to the contact force is obtained independently. Fig. 3.4 shows a spherical mass, with an initial velocity $v_{2,0}$, striking a cantilever rod on the free end. At $t = 0$ the rod is at rest and the striker becomes in contact with the top surface of the rod. At a time $t > 0$ the two bodies are compressed together and a contact force $P(0,t)$ is developed between them. The equation of motion of the striker (neglecting the gravitational acceleration) subjected to this force is given by:

$$m_2 \frac{d^2 u_2}{dt^2} + P(0,t) = 0 \tag{3.20}$$

From which by integration, the position of the striker is given by (see Figure 3.4):

$$u_2(t) = v_0 t - \frac{1}{m_2} \int_0^t dt \int_0^t P(0,t)\, dt = v_0 t - u_2^* \tag{3.21}$$

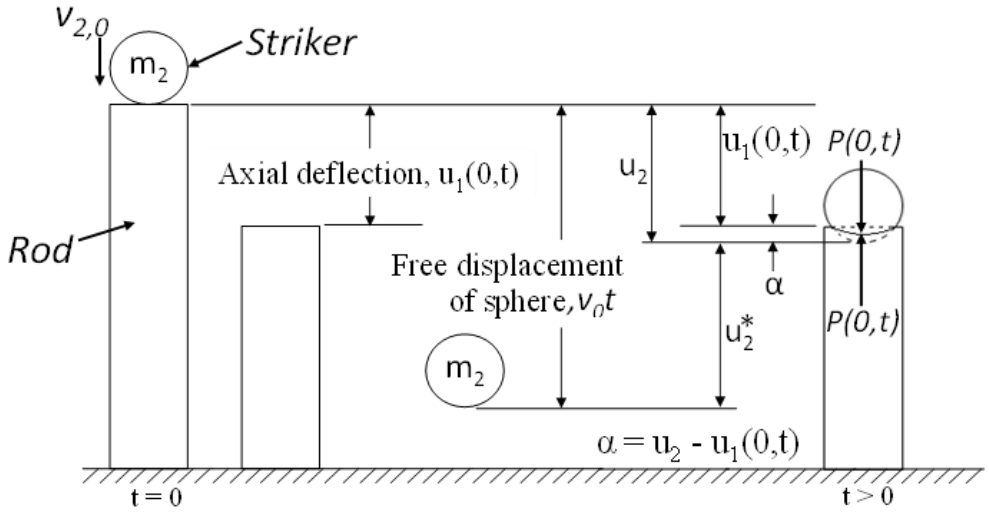

Fig. 3.4: Schematic of Timoshenko's approach to determine the indentation for two elastic bodies in contact.

The displacement of the rod due to the applied contact force *P(0,t)* for an underdamped, critically damped, and overdamped system is determined from Eqns. (3.12), (3.14), and (3.16), respectively. For the undamped case Eqn. (3.12) is utilized with ζ_i = 0. The displacement of the striker is determined from Eqn. (3.21). The indentation α is then obtained by the difference in the displacement, $u_2(t)$, of the striker and the displacement, $u_1(0,t)$, of the top end of the rod. Thus,

$$\alpha = u_2(t) - u_1(0,t) \tag{3.22}$$

Equations (3.12), (3.17) and (3.21) are coupled. That is, displacements $u_1(x,t)$ and $u_2(t)$ depend on the contact force *P(0,t)*, which in turn depends on the displacements $u_1(x,t)$ and

$u_2(t)$. Because of this coupling, it is not possible to solve these equations directly for the contact force or displacements. Therefore these equations need to be solved numerically (Fathi and Popplewell 1994).

A numerical solution with equilibrium iterations is performed. The flowchart for the numerical solution process is shown in Fig. 3.5. To begin the simulation, it is assumed that the contact force is constant during the small time increments, $\Delta t = 1*10^{-6}$ s. The first approximation of the displacement of the rod and the striker under the initial force ($P(0,0)=0$) is calculated at time $t_i = \Delta t$ using Eqns. (3.12) and (3.21), respectively. At $t_i = \Delta t$ the displacement, $u_{2,i}(t)$, of the striker is equal to the initial velocity times the time increment ($u_{2,i}(t_i) = v_0 * \Delta t$) and the displacement, $u_{1,i}(x,t_i)$, of the rod is equal to zero. The indentation, α, and the first approximation of the contact force, $P^1(0,t_i)$, are calculated for time $t_i = \Delta t$ using Eqns. (3.22) and (3.17), respectively. Then the second approximation of the displacement of the rod and the striker (at the same time step $t_i = \Delta t$) under the updated contact force, $P^1(0,t_i)$, is calculated. The updated values of $u_{1,i}(x,t_i)$ and $u_{2,i}(t_i)$ are used to calculate the second approximation, $P^2(0,t_i)$, of the contact force. The process is repeated within the same time step until the difference between the updated contact force and its previous approximation is less than the specified value of the tolerance ($\varepsilon = 1*10^{-5}$ N). When the tolerance value is met the time step is increased and the iterative process is repeated.

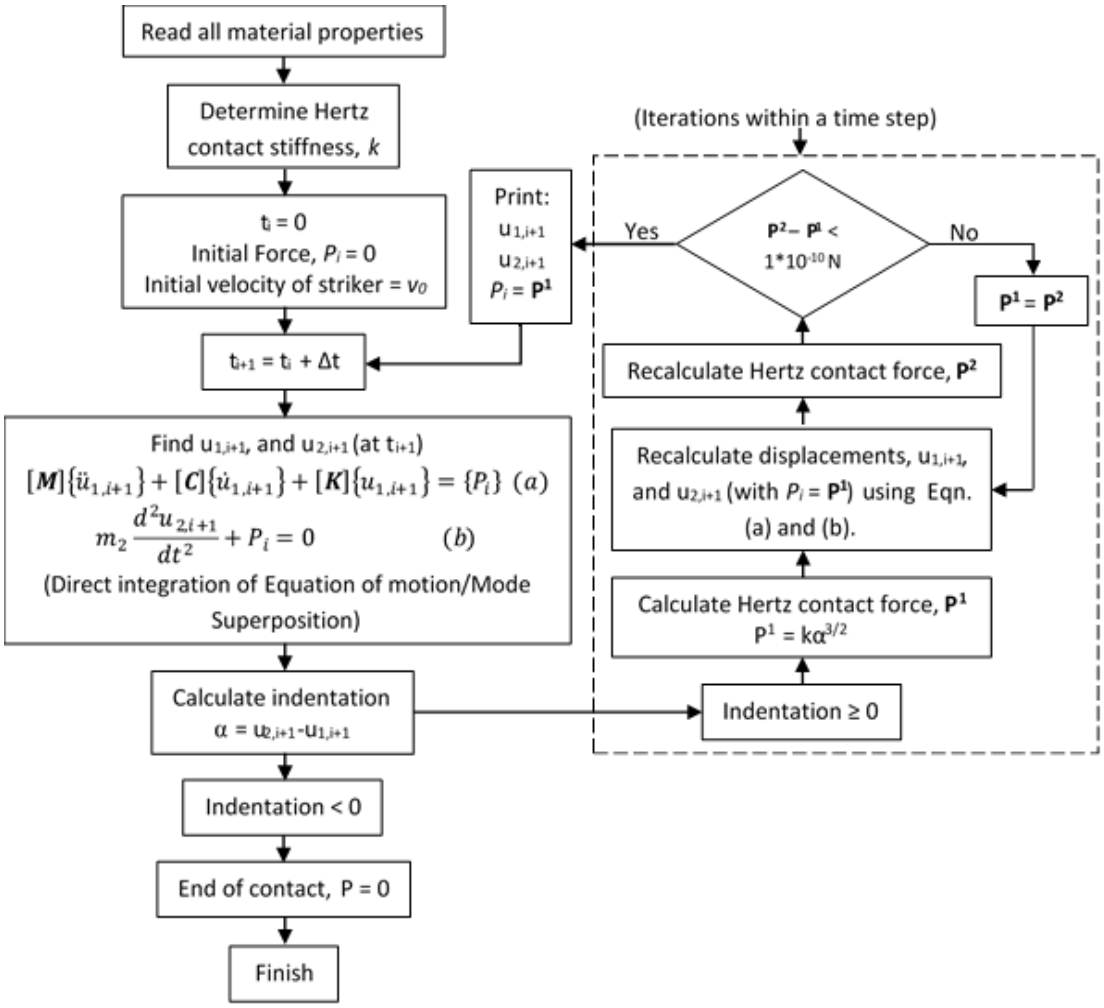

Fig. 3.5: Flowchart of the iterative procedure to obtain the contact force

3.3 In-House Finite Element Model

An in-house finite element model (FEM) was also developed in MATLAB (2010) to solve the non-linear problem of the longitudinal impact of a mass on a rod. The rod was modeled by bar elements (Cook et al. 2002). The equation of motion of the entire rod can be written in matrix form as (Clough and Penzien 1975; Tedesco et al. 1999):

$$[\boldsymbol{M}]\{\ddot{u}_1\} + [\boldsymbol{C}]\{\dot{u}_1\} + [\boldsymbol{K}]\{u_1\} = \{P\} \tag{3.23}$$

where **[*M*]** is the global mass matrix, **[*C*]** is the global damping matrix**,** **[*K*]** is the global stiffness matrix, $\{P\}$ is the externally applied dynamic load vector, and $\{\ddot{u}_1\}$, $\{\dot{u}_1\}$, and $\{u_1\}$ are the acceleration, velocity, and displacement vectors, respectively. The damping is taken as proportional to mass and stiffness, with the damping matrix **[*C*]** equal to η**[*M*]** + θ**[*K*]**, where η and θ are the proportional factors determined using the first two longitudinal frequencies of the rod (see Craig 1981). The dynamic load vector *{P}* (containing the contact force) is nonlinear and depends on the response of the rod and the striker, which in turn depend on the contact force. The response of the rod and the striker is obtained from step-by-step integration using the Newmark average acceleration method (γ = ½, β = ¼) (Clough and Penzien 1975; Craig 1981; Paz 1997; Tedesco et al. 1999). The Newmark average acceleration method assumes a constant (average) acceleration between time steps, with the relations for velocity and displacement given by:

$$\{\dot{u}\}_{i+1} = \{\dot{u}\}_i + [(1-\gamma)\{\ddot{u}\}_i + \gamma\{\ddot{u}\}_{i+1}]\Delta t \tag{3.24}$$

$$\{u\}_{i+1} = \{u\}_i + \{\dot{u}\}_i(\Delta t) + \left[\left(\frac{1}{2} - \beta\right)\{\ddot{u}\}_i + \beta\{\ddot{u}\}_{i+1}\right](\Delta t)^2 \tag{3.25}$$

where Δt is the time increment, $u_{i+1}$is the displacement at the next time step (i.e. $t = t + \Delta t$), and u_i is the displacement at the current time. The iterative relations used to obtain the displacements, velocities, and accelerations are given by (Tedesco et al. 1999):

$$\{\hat{P}\}_{i+1} = \{P\}_{i+1} + [M]\left[\left(\frac{1}{\beta(\Delta t)^2}\right)\{u\}_i + \left(\frac{1}{\beta(\Delta t)}\right)\{\dot{u}\}_i + \left(\frac{1}{2\beta} - 1\right)\{\ddot{u}\}_i\right] + C\left[\left(\frac{\gamma}{\beta(\Delta t)}\right)\{u\}_i + \left(\frac{\gamma}{\beta} - 1\right)\{\dot{u}\}_i + \frac{\Delta t}{2}\left(\frac{\gamma}{\beta} - 2\right)\{\ddot{u}\}_i\right] \quad (3.26)$$

$$\{u\}_{i+1} = [\hat{K}]^{-1} \cdot \{\hat{P}\}_{i+1} \quad (3.27)$$

$$\{\dot{u}\}_{i+1} = \{\dot{u}\}_i + \Delta t(1-\gamma)\{\ddot{u}\}_i + \gamma(\Delta t)\{\ddot{u}\}_{i+1} \quad (3.28)$$

$$\{\ddot{u}\}_{i+1} = \left(\frac{1}{\beta(\Delta t)^2}\right)[\{u\}_{i+1} - \{u\}_i] - \left(\frac{1}{\beta(\Delta t)}\right)\{\dot{u}\}_i - \left(\frac{1}{2\beta} - 1\right)\{\ddot{u}\}_i \quad (3.29)$$

where $[\hat{K}] = [K] + (1/\beta(\Delta t)^2)[M] + (\gamma/\beta\Delta t)[C]$. In Eqns. (3.24) to (3.29) $u = u_1$ for the rod and $u = u_2$ for the striker. Additionally, to obtain the response of the striker the stiffness **[*K*]** and the damping **[*C*]** are set as equal to zero. Equilibrium iterations (as described in Section 3.2, Fig. 3.5) are performed at each time step to account for the nonlinearity and coupling of the problem. At each iteration, Eqns. (3.26) to (3.29) are used to update the displacement of the striker and the rod; while Eqn. (3.17) is used to update the contact force.

3.4 Verification using Abaqus FEA

A model of the rod and the striker was created in Abaqus FEA (2012) to verify the in-house code. The cross- section of the rod is modeled with 144 elements (hexahedron and wedge elements) as shown in Fig. 3.6. This mesh is repeated 50 times along its length.

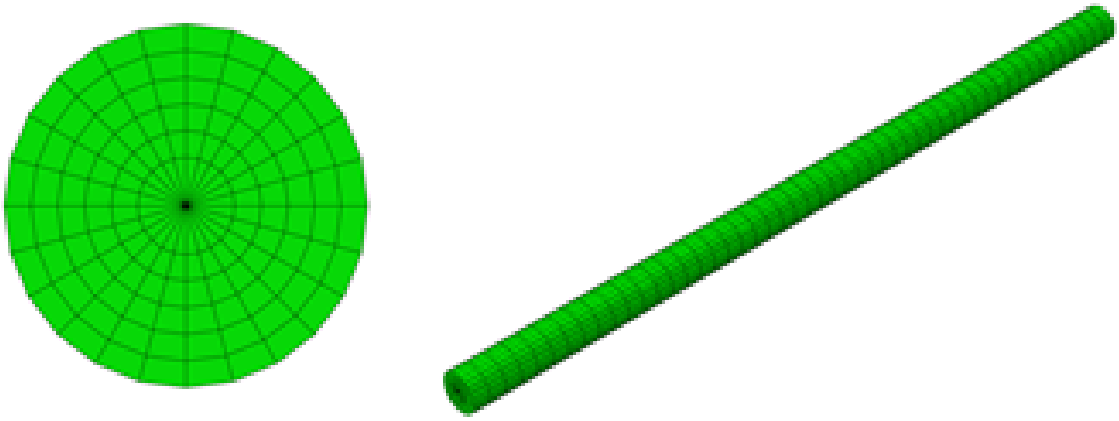

Fig. 3.6: Cross-section of the finite element mesh of the rod **(left)** and 3D view of the rod **(right)**.

The striker is modeled with 3709 tetrahedron elements. The geometric and material properties of the rod and the striker are used as given in Table 3.1. The contact between the striker and the rod is modeled using the general contact interaction with a hard contact pressure-overclosure relation in the normal direction. The results from Abaqus FEA are presented in Section 3.5 along with the results from the in-house codes.

3.5 Results and Discussion

The theory presented above is applicable to an elastic impact. It is common in the longitudinal impact of a drill/pile/rod to have an anvil of material with a higher yield strength on top of the rod where the impact takes place causing the impact to remain elastic (Tavares 1999). This is also verified by King and Bourgeois (1993). To verify the developed methodology a numerical example is presented. A 40 cm long steel rod with 1.91 cm diameter is considered. The impactor/striker is taken as a steel sphere with a diameter of 2.54 cm. The geometric and material properties of the rod and the striker are shown in Table 3.1 (Vila and Malla 2014b).

Table 3.1: Geometric and material Properties of the striker and the rod

Rod Properties		
Area	0.000285	m^2
E_1	209	GPa
ν_1	0.3	-
L	0.4	m
Density, ρ_1	7788.6	kg/m^3
c	5180	m/s
Striker Properties		
m_2	0.06705	kg
E_2	203	GPa
ν_2	0.3	-
Radius, R_2	12.7	mm
Density, ρ_2	7800	kg/m^3
$v_{2,0}$	0.77	m/s

3.5.1 Experimental Verification of Model

To verify the contact force obtained from the present model the results are compared to the experimental data obtained by King and Bourgeois (1993) for a similar problem. In their investigation, King and Bourgeois (1993) developed a theoretical contact force curve by considering the stress on the top of the rod. However, the actual structural vibration response of the continuous rod cannot be obtained from such method. Fig. 3.7 shows the experimental data obtained by King and Bourgeois (1993) for a drop height of 5 cm along with the results obtained from the FEM model presented in this study for an undamped system.

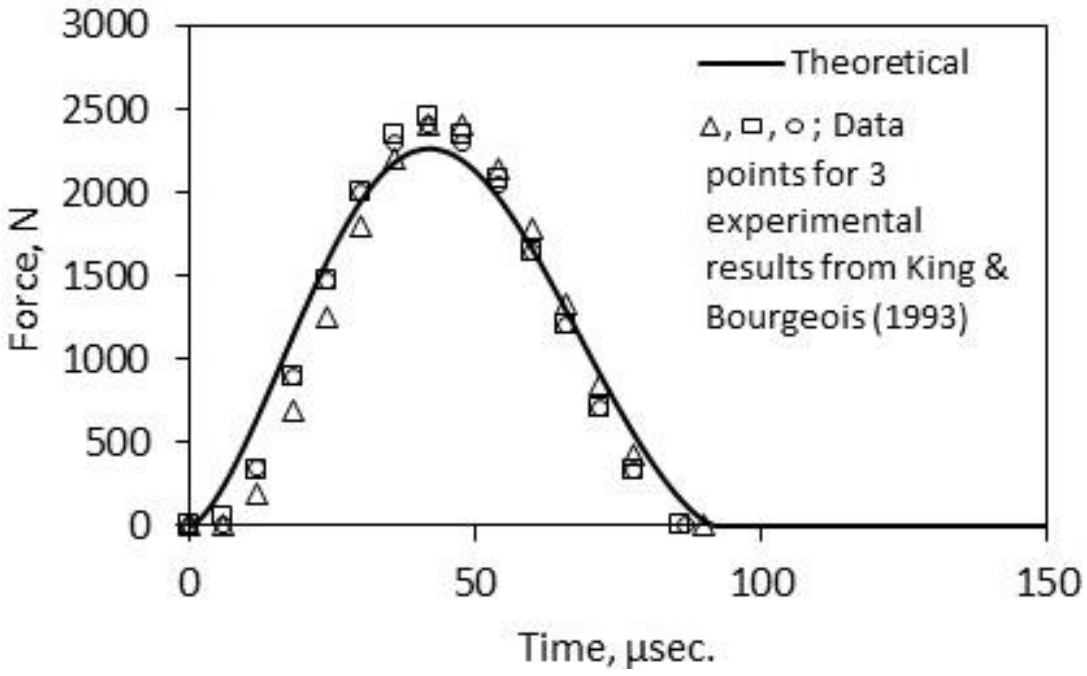

Fig. 3.7: Comparison of contact force obtained from FEM and experimental results from King and Bourgeois (1993) for a drop height of 5 cm.

The results confirm that the impact remains elastic as evidenced by the very good match between the experimental data and the results of the model developed in this study. A

similar match in the contact force was also found by King and Bourgeois (1993). However, in their theoretical formulation the structural vibration of the rod due to impact was not obtained. An in depth analysis including the structural vibration and damping of the rod is presented in the sections below.

3.5.2 Mode Shapes and Frequencies

The first ten natural frequencies of the rod obtained from Eqn. (3.6), the in-house finite element model, and Abaqus FEA are shown in Table 3.2. The first 5 mode shapes of the structural vibration of the rod computed using these three methods are shown in Fig. 3.8. They all match each other very well. Also these mode shapes and frequency values are observed to be consistent with those found in literature (e.g. see Craig 1981) for the support condition presented.

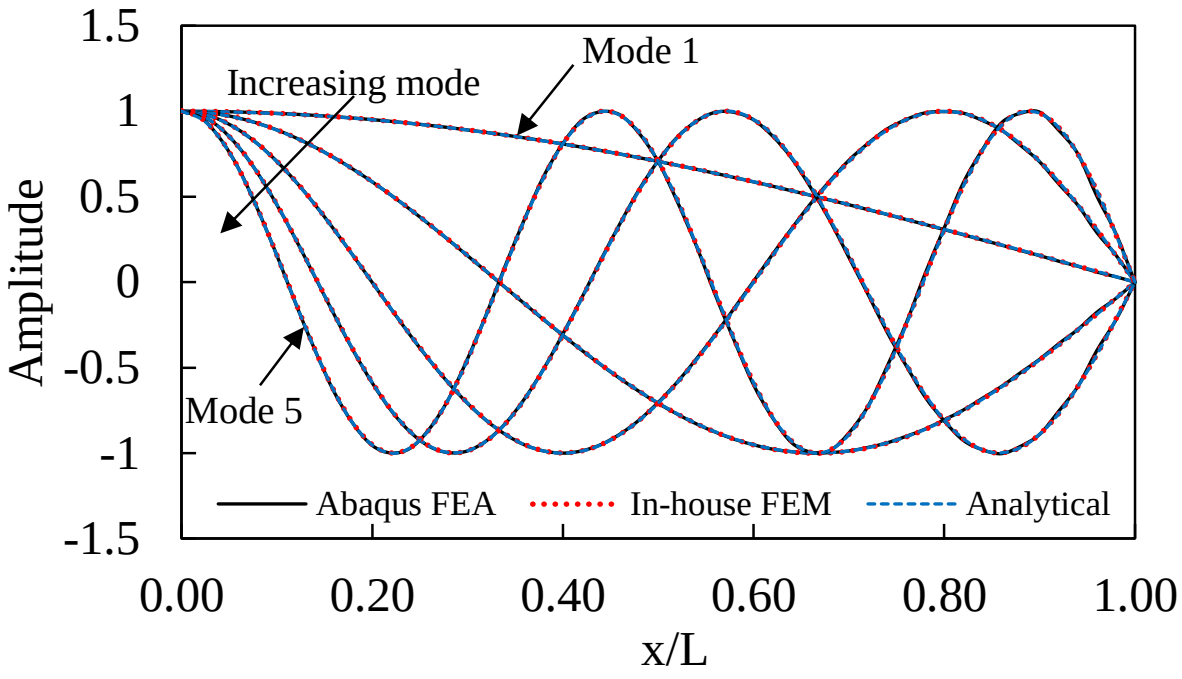

Fig. 3.8: First five axial vibration mode shapes of the rod.

Table 3.2: Natural frequencies of the rod for the first 10 modes of vibration.

Mode, *i*		**1**	**2**	**3**	**4**	**5**
ω_i (rad/sec)	Analytical (Eqn. 6)	20342	61025	101709	142393	183076
	In-house FEM	20343	61050	101817	142684	183693
	Abaqus FEA	20367	61065	101656	142069	182231
Mode, *i*		**6**	**7**	**8**	**9**	**10**
ω_i (rad/sec)	Analytical (Eqn. 6)	223760	264444	305127	345811	386494
	In-house FEM	224882	266293	307967	349945	392267
	Abaqus FEA	222067	261475	300418	338727	376388

3.5.3 Impact/Contact Force Simulation

Two simulations were performed separately using the mode superposition method, one considering 10 and another considering 20 vibration mode shapes. No difference was observed in the results of the contact force and response of the rod. Therefore, to reduce computational effort the final results presented here-in were obtained using a total of 10 modes (i = 10). For the in-house finite element model a total of 50 bar elements are used. The contact force and the response/displacement of the top end of the drill rod and the striker obtained from mode superposition method, the in-house finite element model and the Abaqus FEA model for an undamped (ξ = 0) system are shown in Fig. 3.9, where τ denotes the duration of contact. A very good agreement is observed between the three models in both, displacements and contact force results. It is observed that, consistent with the contact force for similar cases (see Goldsmith 1960), the contact force shows a smooth

curve similar to a half sine wave. The contact force is present while the displacement, $u_2(t)$, of the striker is greater than the displacement, $u_1(0,t)$, of the top end of the rod (i.e. $\alpha = u_2(t) - u_1(0,t) > 0$). When the displacement of the striker becomes equal to the displacement of the top end of the rod the indentation, α, becomes zero hence the contact force vanishes and the rod undergoes free vibration. This condition, indicated in Fig. 3.9 by a vertical dotted line, is observed to occur at $t = 97$ μsec. It is also observed that the displacement of the top end of the rod remains constant for a period of time after contact ends. This behavior is discussed in detail in Section 3.5.4.

The contact force and displacement time history for an underdamped ($\zeta = 0.5$), critically damped ($\zeta = 1$), and overdamped ($\zeta = 1.5$) system obtained from the mode superposition method and in-house finite element model are shown in Figs. 3.10, 3.11, and 3.12, respectively. Similarly, as in the undamped case, a very good agreement is observed in the displacements and the contact force results from these methods. For verification of these results with other independent approach, the impact/contact force obtained from the in-house finite element model was applied to the Abaqus FEA model and the displacement responses of the striker and the rod were obtained. These results are also shown in Figs. 3.10-3.12. They match very well with those obtained from the analytical and in-house finite element techniques.

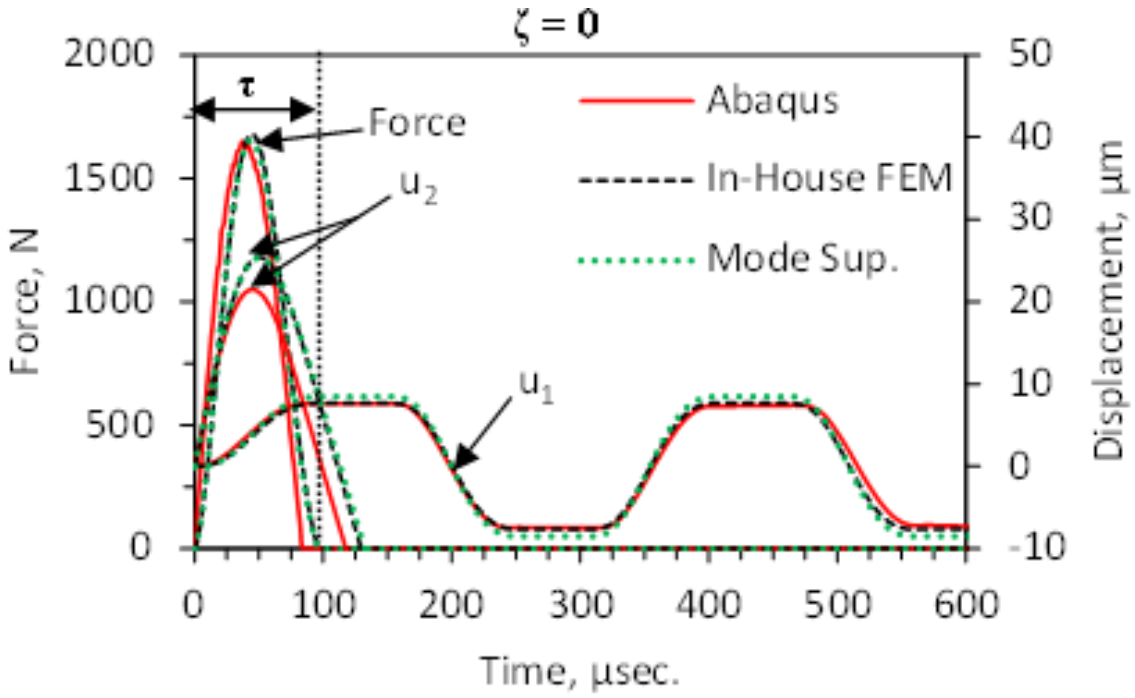

Fig. 3.9: Contact force and displacement time history ($\zeta = 0$).

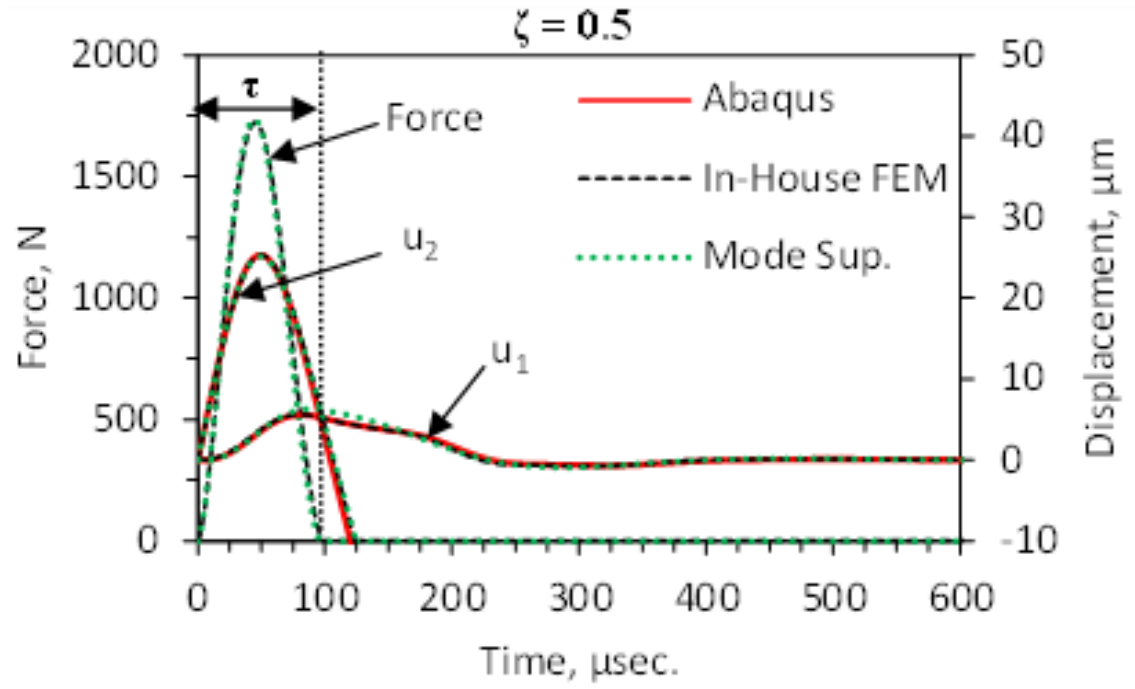

Fig. 3.10: Contact force and displacement time history ($\zeta = 0.5$).

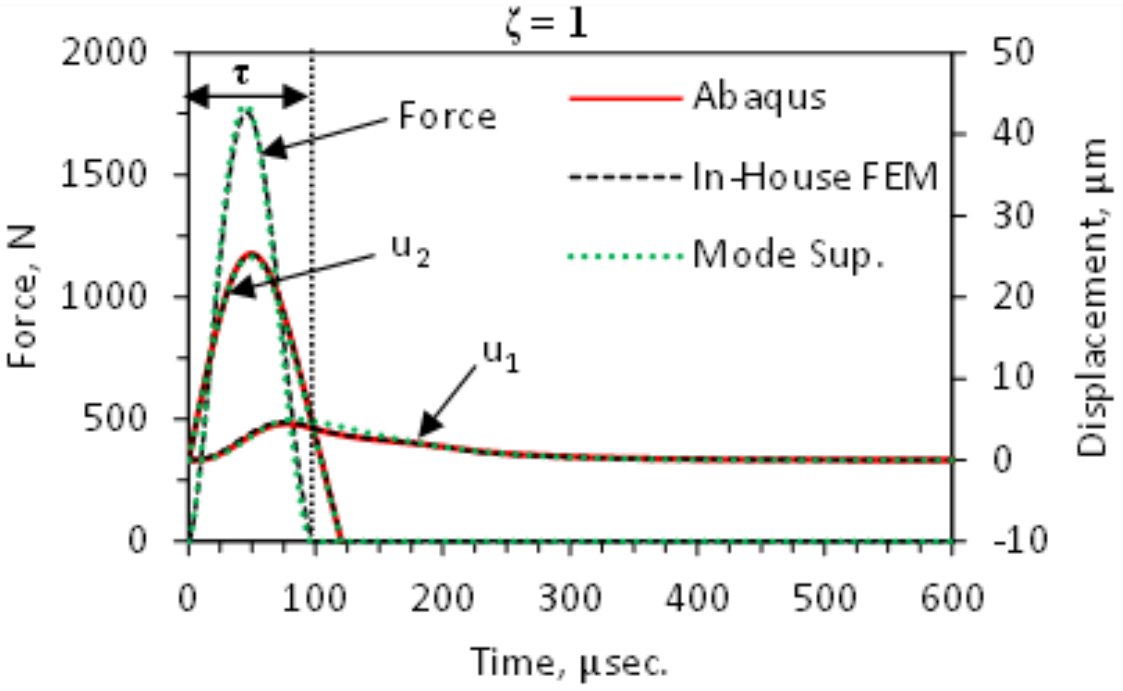

Fig. 3.11: Contact force and displacement time history ($\zeta = 1$).

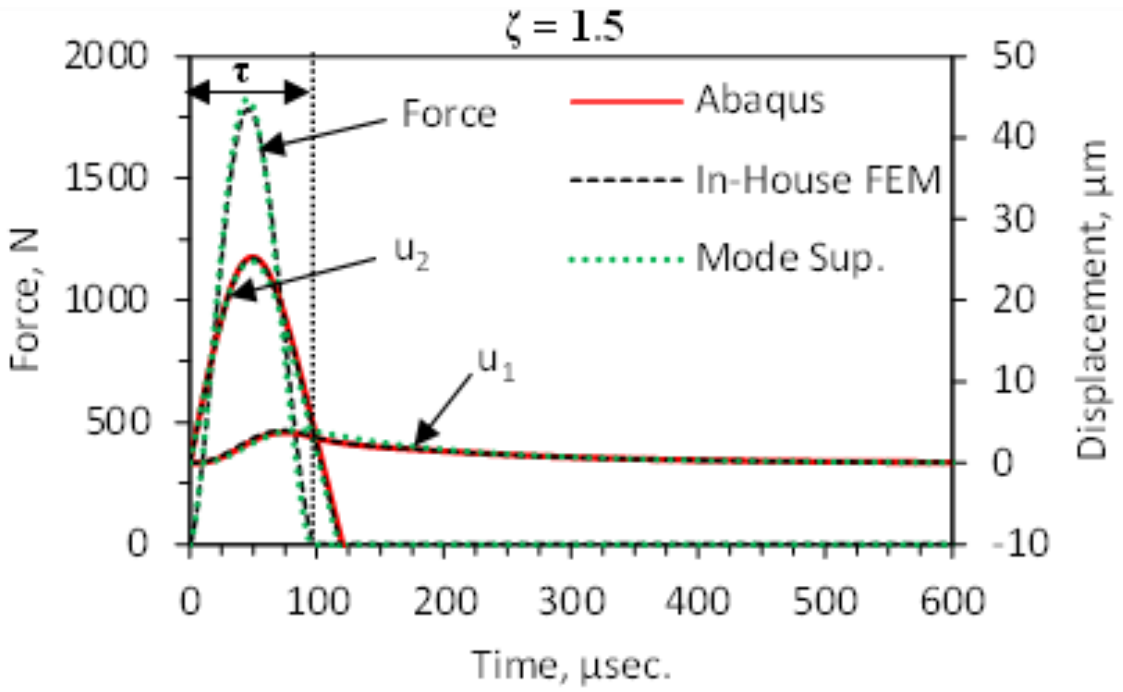

Fig. 3.12: Contact force and displacement time history ($\zeta = 1.5$).

The maximum contact force (P_{max}) and the duration of contact (τ) are shown in Fig. 3.13 as a function of the damping ratio along with the time history of the contact force for ζ = 0, 0.5, 1, and 1.5. It is observed that the maximum contact force increases with the damping ratio, while the duration of contact remains virtually unaffected. An increase of 13% is observed in the maximum contact force between the undamped case and the largest damping ratio considered (ζ = 2.5), while a decrease of 2% is observed on the duration of contact. This can be attributed to the fact that an increase in damping causes the rod to deform less during impact, causing the striker to exert a larger force on it compared to the undamped case.

3.5.4 Displacements and Stresses on the Rod

The variation of displacement along the length of the rod at different times for the undamped case obtained from the in-house finite element model is shown in Fig. 3.14. It is observed that the displacement of the top end of the rod remains constant from t = 97 μsec. to t = 154 μsec. This can be attributed to the fact that when the contact ends (t = 97 μsec) the reflected wave has not arrived to the top end of the rod, therefore at this point in time there is no force to affect the displacement of the top end of the rod. The displacement on the top end remains constant until it begins to be affected by the reflected wave. This can be seen in Fig. 3.14 when, after the contact ends (t = 97 μsec.), the displacement at x = 0 is observed to remain constant until the reflected wave arrives to the top end of the rod at t = 154 μsec. After this, the top end of the rod is now affected by the reflected wave and the displacement begins to decrease as seen by the curve at t = 165 μsec. The variation of displacement along the length of the rod for the underdamped case is shown in Fig. 3.15.

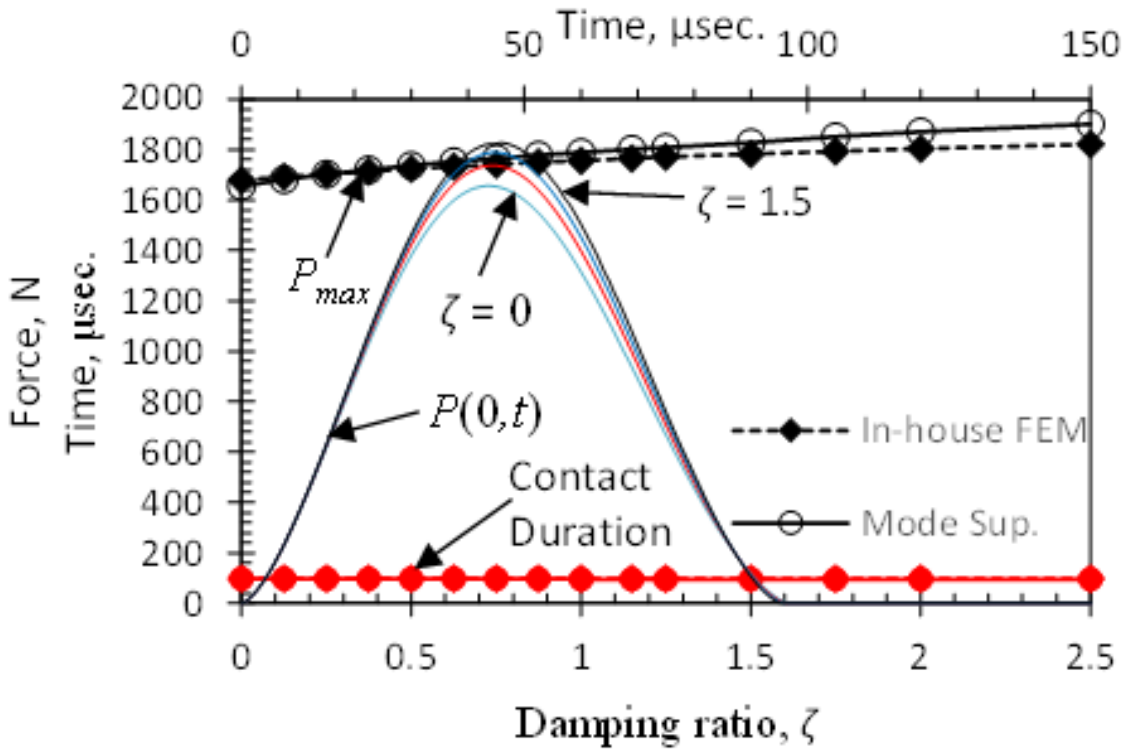

Fig. 3.13: Maximum contact force and duration of contact for different damping ratios.

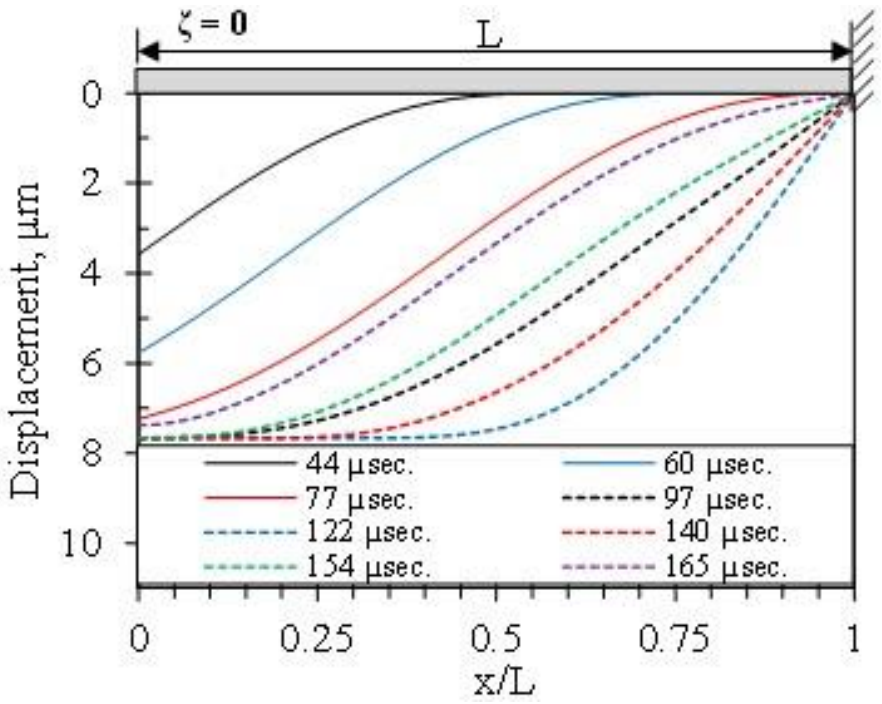

Fig. 3.14: Distribution of displacement along the rod at different times. ($\zeta = 0$)

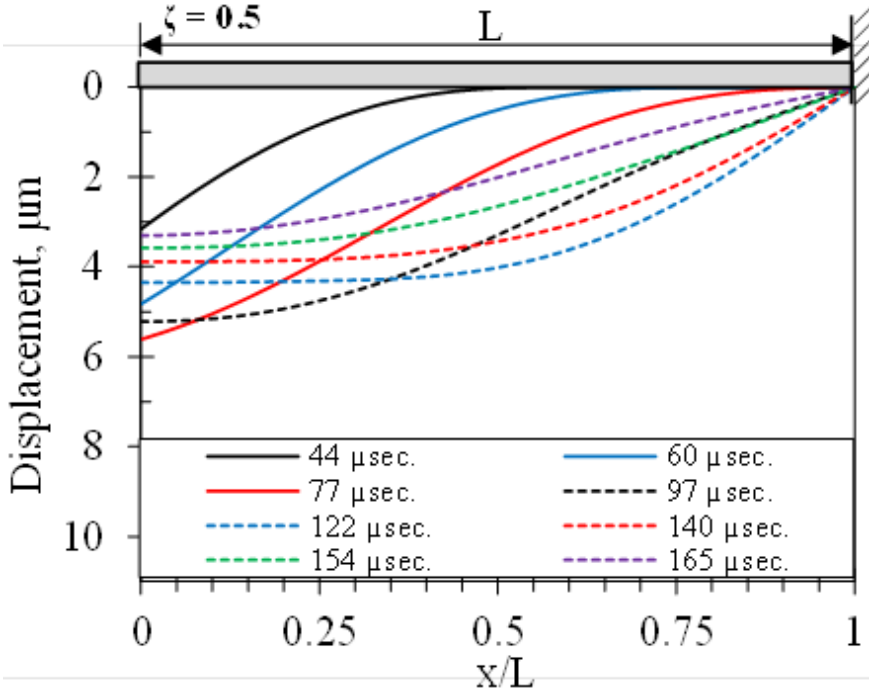

Fig. 3.15: Distribution of displacement along the rod at different times. ($\zeta = 0.5$)

Contrary to the undamped case, the top end of the rod does not remain constant after the contact ends. This can be attributed to the fact that, even though the reflected wave has not arrived to the contact end, now a damping force is present when the load is removed and the displacement is therefore affected.

The variation of stress along the length of the rod at different times obtained from the finite element model is shown in Fig. 3.16. The stress distribution along the rod at t = 44 μsec. corresponds to the time of maximum stress on the top end. It is observed that the stress wave propagates through the rod with a shape similar to that of the contact force (see Fig. 3.9). The stress on the free end becomes equal to zero when contact ends (t = 97 μsec.). The maximum stress, $\sigma_{I,max}$ of the incident wave is observed to be $\sigma_{I,max} = -5.89\ MPa$. At t = 77 μsec. the stress wave reaches the lower end of the rod and, consistent with the fixed boundary condition (see for example Clough and Penzien 1975; Malla et al. 2010; Malla and Shrestha 2010), the combination of the incident and reflected wave causes the stress on the lower end of the rod to double the value of the incident stress. This can be observed in Fig. 3.16 at t = 122 μsec., where the maximum stress of the reflected wave, $\sigma_{R,max}$, is observed to have a value of $\sigma_{R,max} = -11.78\ MPa$. Finally, at t = 154 μsec. it is observed that the reflected stress wave reaches the contact end (x = 0). The distribution of the stress for the underdamped case is shown in Fig. 3.17. The stress distribution is observed to be similar to the undamped case (i.e. stress equal to zero at the top end of the rod when contact ends) but, as expected, the magnitude of the stress waves decreases with time due to damping.

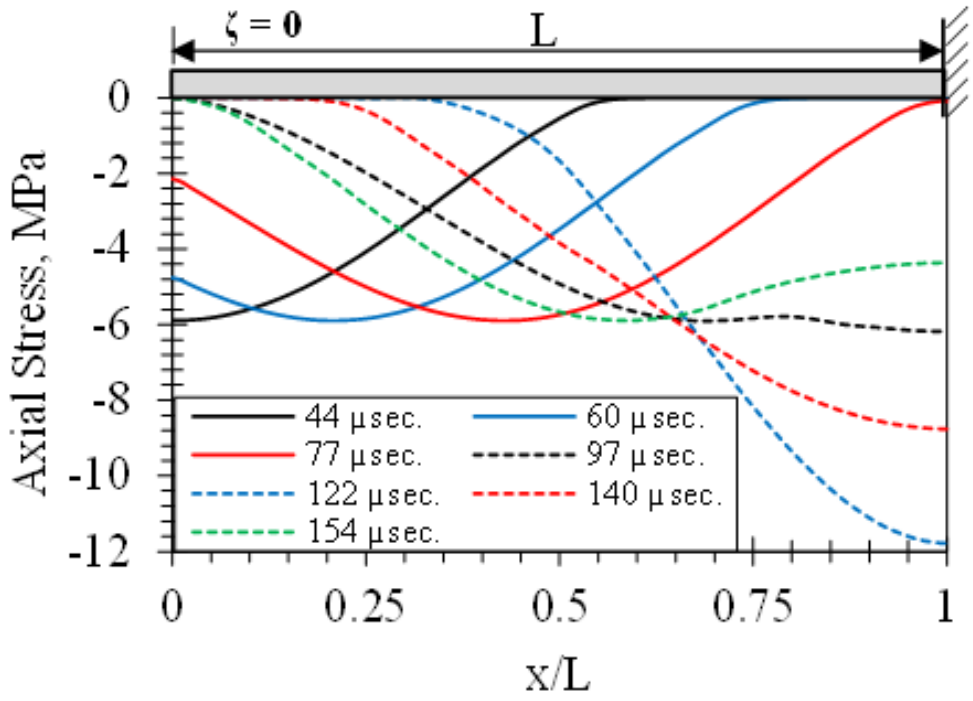

Fig. 3.16: Distribution of axial stress along the rod at different times. ($\zeta = 0$)

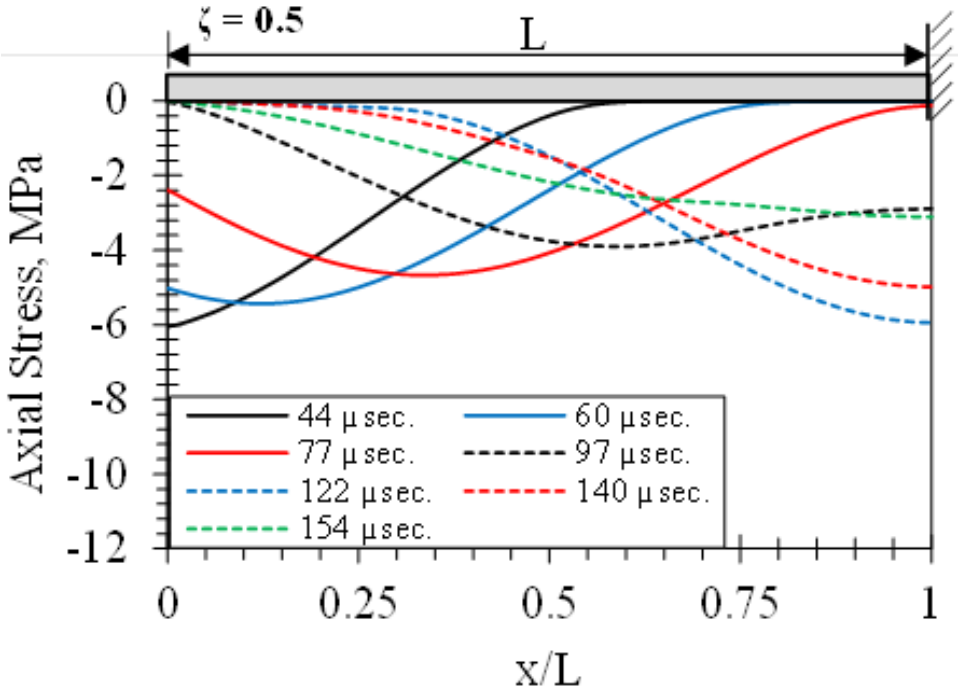

Fig. 3.17: Distribution of axial stress along the rod at different times. ($\zeta = 0.5$)

3.6 Conclusions

A methodology to analyze the longitudinal impact on a rod by a spherical striker considering structural vibration and damping of the rod was developed. The displacement response of the striker and the rod were obtained from the dynamic analysis of each body subjected to the contact force. The Hertz force-indentation relation was used to obtain the contact force from the local indentation obtained as the difference in the displacements of the rod and the striker. The closed form solution to obtain the response of the rod was obtained using mode superposition method while the motion of the striker was obtained using particle motion analysis. Due to coupling of the displacement of the rod and the striker with the contact force a numerical integration scheme with equilibrium iterations was performed to solve for these displacements and the contact force. The methodology developed was also implemented to analyze the impact problem using an in-house finite element code. Additionally, the presented model was verified with experimental data available in literature and Abaqus FEA. Based on the results obtained from the present study, the following conclusions can be made:

- The presented methodology can be applied for different methods (e.g. mode superposition, finite element) to accurately model the longitudinal impact of a striker on a rod as verified by the experimental data and the Abaqus FEA model.
- In the undamped case, the displacement of the top end of the rod remains constant for a period of time after end of contact. This is attributed to the fact that when contact ends, the reflected wave has not arrived to the top end of the rod. Therefore, after contact ends there is no force acting on the top end of the rod until the reflected wave arrives.

- The maximum contact force increases as the damping in the rod increases, while the duration of contact was observed to remain virtually unaffected. The increase in the magnitude of the force is attributed to the fact that the damping force causes the rod to deform less, hence a higher indentation and contact force is observed.
- The variation of displacement and axial stress along the rod at a given time was observed to be consistent with the boundary conditions considered. Consistent with the fixed support condition, the displacement of the rod was observed to decrease as it gets closer to the fixed end (bottom) of the rod, while the stress doubles when it reaches the bottom end of the rod. The contact force and the response of the striker and the rod were observed to be consistent with similar problems available in literature (see for example Goldsmith 1960).
- The methodology presented in this study should be readily applicable to the longitudinal impact between a spherical striker on a rod having other support conditions (e.g. free support, elastic support, etc.) to investigate the effect of the support condition of the rod on the contact force.

Chapter 4

Longitudinal Impact on a Rod with Rigid, Elastic and Free Support Conditions

This chapter presents the dynamic contact analysis of the longitudinal impact of a mass on a rod with rigid, free and deformable support conditions. Focus is given to capture how and under what conditions the impact force is affected by the support conditions. The contact force was obtained using Hertz force-indentation relation coupled with the structural vibration. Both the contact force and the rod structural response are determined using mode superposition method as well as an in-house finite element code.

4.1 Axial vibration of uniform rods with various end conditions

This section presents a summary of free and forced vibration response of uniform rods with different boundary conditions. Consider a uniform rod with fixed support subjected to a distributed load *P(x,t)* along its length as shown in Fig. 4.1. The equation of motion of axial vibration of the rod is given by:

$$\bar{m}\frac{\partial^2 u_1(x,t)}{\partial t^2} + C\frac{\partial u_1(x,t)}{\partial t} - EA\ \frac{\partial^2 u_1(x,t)}{\partial x^2} = P(x,t) \tag{4.1}$$

where *E* is the Young's modulus, *C* is the damping coefficient, and *A* is the cross sectional area of the rod. Introducing the velocity of wave propagation $c = \sqrt{E/\rho}$, letting the mass per unit length of the rod $\bar{m} = \rho A$, where ρ is the density of the rod, and defining the distributed load as $\underline{P}(x,t) = P(x,t)/\bar{m}$, Eqn. (4.1) can be expressed as:

$$\frac{\partial^2 u_1(x,t)}{\partial t^2} + \frac{C}{\bar{m}}\frac{\partial u_1(x,t)}{\partial t} - c^2\ \frac{\partial^2 u_1(x,t)}{\partial x^2} = \underline{P}(x,t) \tag{4.2}$$

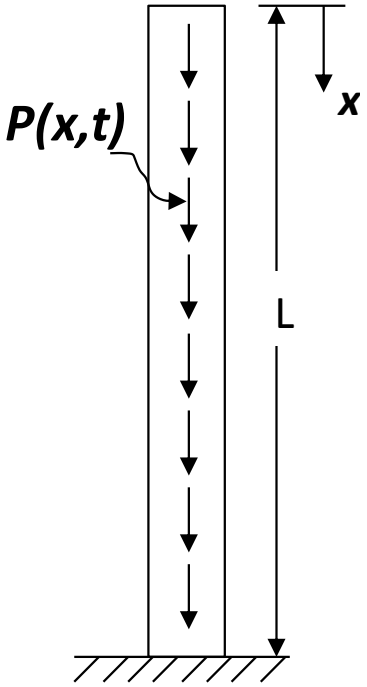

Fig. 4.1: Rod with fixed support subjected to distributed time varying load *P*(*x*,*t*).

4.1.1 Free Vibration, Mode Shapes and Frequencies

Consider the longitudinal free vibration of a uniform rod. By separation of variables, the displacement, *u(x,t)*, of the rod is defined as:

$$u_1(x,t) = \varphi(x)q(t) \tag{4.3}$$

where *φ(x)* is the mode shape and *q(t)* is the generalized coordinate. The general solution of Eqn. (4.2) for free vibration ($\underline{P}(x,t) = 0$) is obtained by substituting Eqn. (4.3) into Eqn. (4.2) and is given by (Clough and Penzien 1975; Tedesco et al. 1999):

$$q(t) = C_3 cos(\omega t) + C_4 sin(\omega t) \tag{4.4a}$$

$$\varphi(x) = C_1 cos\left(\frac{\omega x}{c}\right) + C_2 sin\left(\frac{\omega x}{c}\right) \tag{4.4b}$$

where ω is the undamped natural frequency, and C_1, C_2, C_3, and C_4 are constants. Therefore, the total solution of Eqn. (4.2) is given by:

$$u_1(x,t) = \left[C_1 cos\left(\frac{\omega x}{c}\right) + C_2 sin\left(\frac{\omega x}{c}\right)\right] \cdot [C_3 cos(\omega t) + C_4 sin(\omega t)] \quad (4.5)$$

The frequency (ω) and the constants C_1 and C_2 determine the vibration mode shape and can be obtained by applying the boundary conditions. The coefficients C_3 and C_4 are obtained by applying the initial conditions.

4.1.2 Rod with Fixed Support

Considering the rod with fixed support (shown in Fig. 4.1) with $P(x,t) = 0$, the boundary conditions are given by letting the force equal to zero at x = 0, and letting the displacement equal to zero at x = L. Applying these boundary conditions (see Chapter 3) the axial vibration mode shape and frequency of the rod are given by:

$$\varphi(x) = C_1 cos\left(\frac{\omega x}{c}\right) \quad (4.6)$$

$$\omega_i = \frac{(2i+1)\pi c}{2L} \quad i = 0,1,2 \ldots \quad (4.7)$$

4.1.3 Rod with Free Support

Considering a rod with free-free support condition, the boundary conditions are given by letting the force equal to zero at x = 0 and at x = L. These boundary conditions are shown in Eqns. (4.8a) and (4.8b) respectively.

$$EA\frac{\partial u(0,t)}{\partial x} = 0 \quad (4.8a)$$

$$EA\frac{\partial u(L,t)}{\partial x} = 0 \quad (4.8b)$$

Applying the first boundary condition (Eqn. (4.8a)) into Eqn. (4.5) we obtain $C_2 = 0$. Thus the mode shape for this case is the identical expression as given by Eqn. (4.7) for the fixed

support case. Applying the second boundary condition (Eqn. (4.8b)) we obtain the characteristic equation, $\sin(\omega L/c) = 0$, from which $\omega L/c = i\pi$ and the natural frequencies are obtained as (Rao 2007):

$$\omega_i = \frac{i\pi c}{L} \quad i = 0,1,2 \ldots \tag{4.9}$$

4.1.4 Rod with Elastic Support

Consider now the free vibration of the uniform rod with an elastic support represented by a spring as shown in Fig. 4.2(a) with *P(x,t)* = 0. The two boundary conditions are obtained by letting the stress at the free end equal to zero, and letting the internal force at *x* = *L* be equal to the spring force (Fig. 4.2(b)). These boundary conditions are shown in Eqn. (4.10a) and (4.10b) respectively (Rao 2007).

$$EA\frac{\partial u(0,t)}{\partial x} = 0 \tag{4.10a}$$

$$EA\frac{\partial u(L,t)}{\partial x} = -Ku(L,t) \tag{4.10b}$$

where *K* is the external spring stiffness. Applying the first boundary condition (i.e. Eqn. (4.10a)) into Eqn. (4.5) we obtain $C_2 = 0$.

Thus, the mode shape for this case is the identical expression as given by Eqn. (4.6) for the fixed end support case. However, the frequency equation for the present case is different and is obtained by applying the boundary condition (Eqn. (4.10b)) corresponding to the bottom end of the rod, from which we obtain (Rao 2007; Laura 1974):

$$\tan\left(\frac{\omega L}{c}\right) = \frac{Kc}{EA\omega} \tag{4.11}$$

Eqn. (4.11) can be expressed more conveniently as:

$$\lambda \tan(\lambda) = \mu \tag{4.12}$$

where $\lambda = \omega L/c$ is the non-dimensional natural frequency; and $\mu = K/k$ is the ratio of the stiffness (*K)* of the external spring to the axial stiffness (*k = EA/L)* of the rod. The transcendental equation (Eqn. (4.12)) can be solved for an infinite number of non-dimensional frequencies (λ_i) for a given value of μ, and the natural frequencies can be determined from:

$$\omega_i = \frac{\lambda_i c}{L} \tag{4.13}$$

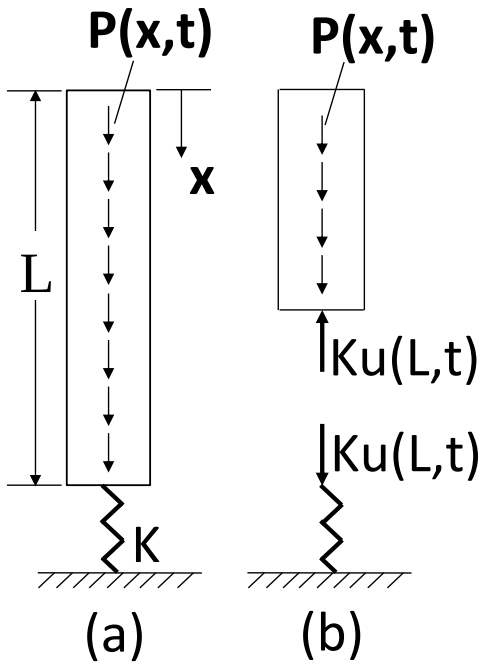

Fig. 4.2: (a) Uniform rod with spring attached at *x = L* and (b) Free body diagram of forces acting at the lower end of the rod.

The expression for the natural frequencies of a cantilever rod and a free-free rod can be obtained from Eqn. (4.12) as limiting cases (i.e. $\mu = \infty$ and $\mu = 0$) of the stiffness ratio. The stiffness ratio $\mu = \infty$ represents a rigid support (an infinitely stiff external spring). Substituting this condition ($\mu = \infty$) into Eqn. (4.12), the natural frequency is obtained as the expression (Eqn. (4.7)) presented in Section 4.1.2. for the rod with fixed support. The

stiffness ratio μ = 0 represents an infinitely flexible external spring (free support). Substituting μ = 0 into Eqn. (4.12) yields $\sin(\lambda) = 0$, from which the expression for the natural frequency (Eqn. (4.9)) is obtained identical to that of a free-free rod (Rao 2007). The variation of λ (or natural frequency ω) with the stiffness ratio μ is shown in Fig. 4.3 for the first 5 modes (i = 1,…, 5) of vibration. The dashed lines represent the value of the frequency corresponding to a rod with fixed support ($\mu = \infty$). It is observed that (for all modes) the natural frequencies begins with the value corresponding to a free-free rod (μ = 0) then it gradually increase with the stiffness ratio as it approach the value of the frequency corresponding to the fixed rod ($\mu = \infty$).

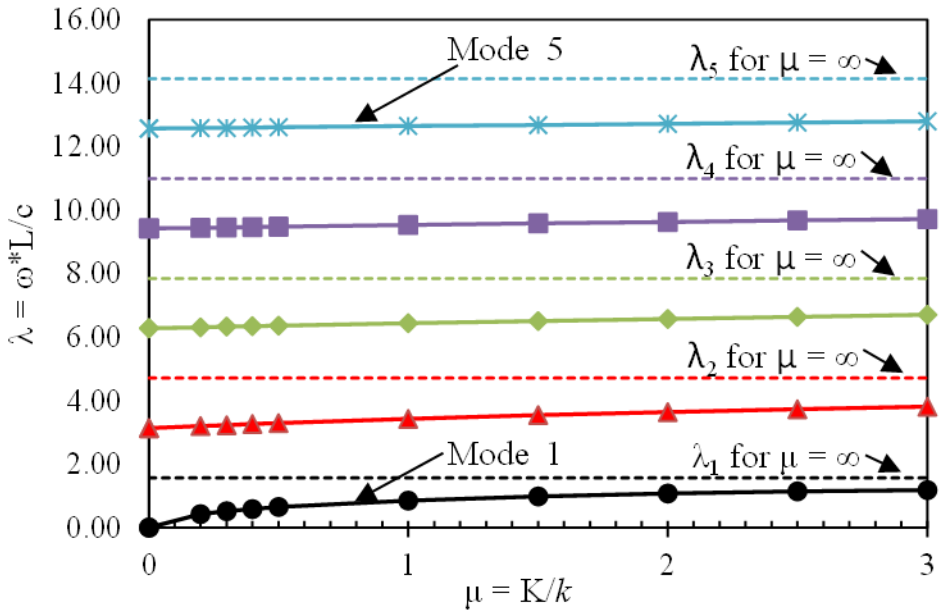

Fig. 4.3: Variation of the non-dimensional natural frequency ($\lambda_i = \omega_i L/c$) with the stiffness ratio (μ) for the first 5 modes of vibration.

4.2 Dynamic Response by Mode Superposition

Applying mode superposition, the longitudinal motion of the rod can be expressed in terms of the sum of the displacement functions, $\varphi_i(x)$, times the generalized coordinates, $q_i(t)$. Thus the response of the rod is expressed as:

$$u_1(x,t) = \sum_{i=1}^{\infty} \varphi_i(x) q_i(t) \tag{4.14}$$

Substituting Eqn. (4.14) into Eqn. (4.1), and after applying the corresponding boundary conditions and orthogonality relations (Rao 2007; Timoshenko et al. 1974), the equation of motion of the rod is obtained as:

$$\ddot{q}_i + \omega_i^2 q_i = \int_0^L \varphi_i(x) \underline{f}(x,t)\, dx \tag{4.15}$$

where ω_i are the natural frequencies of the system and $\underline{P}(x,t) = P(x,t)/m$. Eqn. (4.15) is equally valid for the rod with fixed support and the rod with elastic support when the corresponding mode shapes and frequencies (presented in Sections 4.1.2, 4.1.3, and 4.1.4) are used. The detailed derivation of the equation of motion for the rod with elastic support is presented in Appendix A. The equation of motion for free vibration is obtained by letting the force $\underline{P}(x,t) = 0$. For all cases (i.e. fixed rod, free rod and rod with elastic support) the mode shape, $\varphi_i(x)$, is given by Eqn. (4.6); while the frequencies (ω_i) are given by Eqn. (4.7), Eqn. (4.9) and Eqn. (4.13) for the fixed, free and elastic support, respectively. Solution to Eqn. (4.15) can be obtained from Duhamel's integral as (Clough and Penzien 1975; Rao 2007):

$$q_i(t) = \frac{1}{\omega_{D,i}} \int_0^L \varphi_i(x) \int_0^t \underline{P}(0,t) e^{-\zeta_i \omega_i (t-\tau)} \sin\left[\omega_{D,i}(t-\tau)\right] d\tau \cdot dx \tag{4.16}$$

where $\omega_{D,i} = \omega_i\sqrt{1-\zeta_i^2}$ is the damped natural frequency for the underdamped case. The response of the rod is given by (see Chapter 3):

$$u_1(x,t) = \sum_{i=1}^{\infty} \frac{\varphi_i(x)\varphi_i(x=0)}{\omega_{D,i}} \int_0^t \frac{P(x_m,t)}{\rho A} e^{-\zeta_i\omega_i(t-\tau)} \sin\left[\omega_{D,i}(t-\tau)\right] d\tau \tag{4.17}$$

The response of the rod for a critically damped and an overdamped system is given by Eqn. (4.18) and Eqn. (4.19), respectively,

$$u_1(x,t) = \sum_{i=1}^{\infty} \varphi_i(x)\varphi_i(x=0) \cdot t \int_0^t \frac{P(0,t)}{\rho A} e^{-\omega_i(t-\tau)} \cdot d\tau \tag{4.18}$$

$$u_1(x,t) = \sum_{i=1}^{\infty} \frac{\varphi_i(x)\varphi_i(x=0)}{\widehat{\omega}_{D,i}} \int_0^t \frac{P(0,t)}{\rho A} e^{-\zeta_i\omega_i(t-\tau)} \sinh\left[\widehat{\omega}_{D,i}(t-\tau)\right] d\tau \tag{4.19}$$

where $\widehat{\omega}_{D,i} = \omega_i\sqrt{\zeta_i^2-1}$ is the damped natural frequency for the overdamped case.

4.3 Longitudinal Impact of a Mass on a Rod

As discussed in Chapter 3, Hertz theory is used to analyze the contact interaction between the striker and the rod. Hertz (1881) found that the contact force between two elastic bodies is proportional to the local indentation, α, to the 1.5th power. Hence, the Hertz force-indentation relation is given by (Hertz 1881):

$$P = k_2\alpha^{3/2} \tag{4.20}$$

where k_2 is the contact stiffness that depends on the Young's modulus, Poisson's ratio and radius of curvature of each body as shown in Chapter 3.

Timoshenko's (1913) approach is used to determine the indentation due to impact of the striker and the drill rod. The displacement of each body (striker and rod) due to the

applied force *P(0,t)* is determined. The indentation α is given by the difference in the displacement, u_2, of the striker and the displacement, u_1, of the top end of the rod. Thus,

$$\alpha = u_2 - u_1 \tag{4.21}$$

Figure 4.5 shows a spherical mass, with an initial velocity v_0, striking a rod with on the free end. The position of the striker and the rod are obtained separately by dynamic analysis of each body subjected to force (contact force) *P(0,t).* The equation of motion of the striker (neglecting the gravitational acceleration) subjected to the contact force *P(0,t)* is given by:

$$m_2 \frac{d^2 u_2}{dt^2} + P(0,t) = 0 \tag{4.22a}$$

From which by integration, the position of the striker is given by (see Fig. 4.4):

$$u_2 = v_0 t - \frac{1}{m_2} \int_0^t dt \int_0^t P(0,t)\, dt = v_0 t - u_2^* \tag{4.22b}$$

where $u_2^* = \frac{1}{m_2} \int_0^t dt \int_0^t P(0,t)\, dt$.

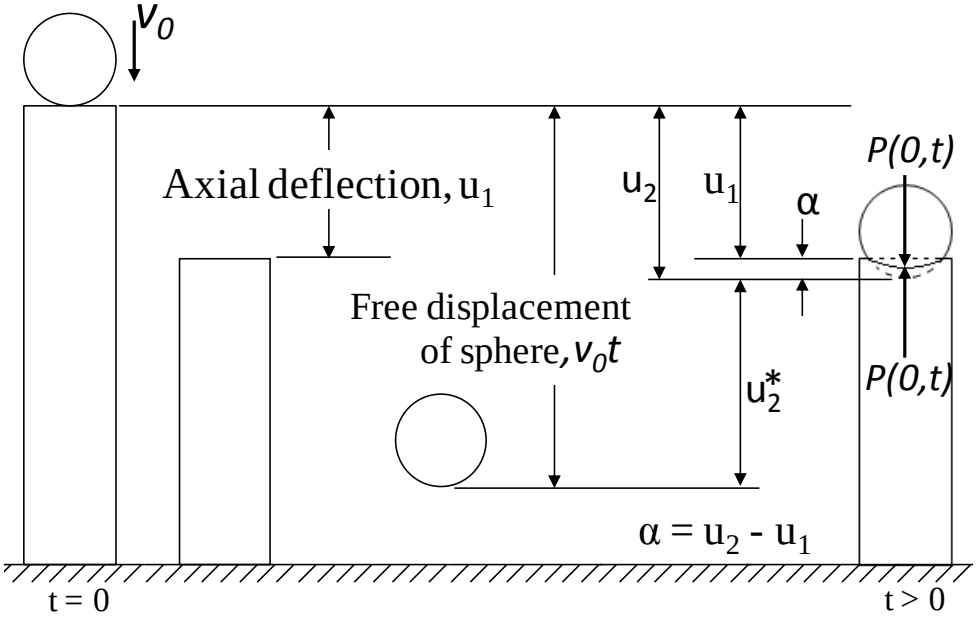

Fig. 4.4: Schematic of Timoshenko's approach to determine the indentation for two elastic bodies in contact.

The axial vibration displacement of the rod is given by Eqn. (4.17) and can be written for the contact force *P(0,t)* applied at $x = 0$ as:

$$u_a(x,t) = \sum_{i=1}^{\infty} C_{1,i}^2 \frac{\cos(\omega_i x/c)}{\omega_i} \int_0^t \frac{P(x_m,t)}{\rho A} e^{-\zeta_i \omega_i (t-\tau)} \sin\left[\omega_{D,i}(t-\tau)\right] d\tau \tag{4.23}$$

The modal amplitude, $C_{1,i}$, is obtained by normalizing such that the generalized mass, M^*, is unity, that is:

$$M^* = \int_0^L \rho C_{1,i} [\varphi_i(x)]^2 dx = 1 \tag{4.24}$$

Substituting the mode shape and carrying out the integration, $C_{1,i} = \sqrt{2/m_1}$ (Rao 2007). Eqn. (4.23) gives the axial vibration displacement, u_a, of the rod, but does not include additional displacement of the rod as a rigid body, u_{rigid}. Therefore, the rigid body motion of the rod must be added to the axial vibration displacement in order to determine the total displacement (Timoshenko et al. 1974), u_1, given by:

$$u_1(x,t) = u_a(x,t) + u_{rigid} \tag{4.25}$$

Finally, the contact force *P(0,t)* is obtained from Eqn. (4.20) as:

$$P(0,t) = k_2[u_2 - u_1(0,t)]^{3/2} \tag{4.26}$$

For the case of the rod with fixed support the rigid body motion of the rod is zero. Therefore in this case the total response of the rod is equal to the axial vibration response (i.e. $u_1(x,t) = u_a(x,t)$). In the case of the elastic support, in addition to the axial vibration response, the rod oscillates as a rigid body due to the external spring. Similarly, the rod with free ends experiences rigid body motion that in addition to the axial vibration response.

4.4 Methodology

The equation of motion of the rod is given by Eqn. (4.2), in which the applied force is $\underline{f}(x,t) = P(0,t)/\rho A$, where *P(0,t)* is the contact force. Equations (4.22), (4.23) and (4.26) are coupled. That is, displacements u_1 and u_2 depend on the contact force *P(0,t)*, which in turns depends on the displacements u_1 and u_2. Because of this nonlinearity, it is not possible to obtain a closed form solution for this problem and equations (4.22), (4.23) and (4.26) must be solved numerically (Lo 1980; Yongqiang and Lili 2011; Fathi and Popplewell 1994). The response, u_1, of the rod is obtained by numerical evaluation of Duhamel's integral for mode superposition approach (Clough and Penzien 1975) and by direct integration with Newmark average acceleration scheme for the finite element approach. The motion of the striker (for both mode superposition and finite element method) is obtained by direct integration of Eqn. (4.22b) applying the Newmark average acceleration method. A steel rod with 1.91 cm diameter and 40 cm length is considered. The impactor/striker is taken as a steel sphere with a diameter of 2.54 cm. The geometric and material properties of the rod and the striker shown in Table 4.1, where v is the Poisson's ratio and $v_{2,0}$ is the initial velocity of the striker, were used for all cases unless otherwise specified.

4.4.1 Determination of Contact Force

The computation of contact force is performed by numerical methods because of the non-linearity nature of the problem due to equations coupling. MATLAB (2010) codes are used to compute the contact force for mode superposition method and the finite element

analysis for all the cases studied. To begin the simulation, it is assumed that the contact force is constant during the small time increments, Δt. The response of the rod and the position of the striker under the initial force ($P(0,0)=0$) is calculated at time $t_i = \Delta t = 1*10^{-6}$ s. Therefore, at $t = \Delta t$ the position, $u_{2,i}$, of the striker is equal to the initial velocity times the time increment ($u_2 = v_0*\Delta t$) and the position, $u_{1,i}$, of the rod is equal to zero. The indentation, α, and the first approximation of the contact force, $P^1(0,t_i)$, are calculated for time $t = \Delta t$ using Hertz force-indentation relation (Eqn (4.20)).

Table 4.1: Geometric and material properties of the striker and the rod.

Rod Properties		*Striker Properties*	
Area (m^2)	0.00029	m_2 (kg)	0.06705
E_1 (GPa)	209	E_2 (GPa)	203
ν_1	0.3	ν_2	0.3
Radius, R_1 (mm)	∞	Radius, R_2 (mm)	12.7
L (m)	0.4	Density, ρ_2 (kg/m^3)	7833.5
Density, ρ_1 (kg/m^3)	7788.6	$v_{2,0}$ (m/s)	0.77

The response, $u_{1,i}$, of the rod and the position, $u_{2,i}$, of the striker, at the same time step ($t_i = \Delta t$), are recalculated based on the first approximation of the contact force, $P^{(1)}(0,t_i)$. Then the second approximation of the contact force $P^{(2)}(0,t_i)$ is calculated based on the updated values of $u_{1,i}$ and $u_{2,i}$. Finally, the difference, ε, between the first and second approximation of the contact force ($\varepsilon = P^{(2)}(0,t_i) - P^{(1)}(0,t_i)$) is calculated. If the difference, ε, is less than the specified value of the tolerance ($\varepsilon = 1*10^{-5}$ N), the first approximation of the contact force, $P^{(1)}(0,t_i)$, becomes the final contact force, $P(0,t_i)$for that specific time. On the contrary, if the difference, ε, is larger than the specified tolerance, the response, $u_{1,i}$, of the rod and the position, $u_{2,i}$, of the striker are updated based on the second

approximation of the contact force and a third approximation of the contact force, $P^{(3)}(0,t_i)$, is calculated. The difference, ε, between the third and second approximation of the contact force ($\varepsilon = P^{(3)}(0,t_i) - P^{(2)}(0,t_i)$) is calculated and compared to the tolerance. If the difference, ε, is less than the specified value of the tolerance, the second approximation of the contact force, $P^{2}(0,t_i)$, becomes the final contact force, $P(0,t)$ for that specific time. Otherwise, the procedure is repeated until the difference, ε_i, between the current (i) and the previous (i-1) approximation of the contact force ($\varepsilon_i = P^{(i)}(0,t_i) - P^{(i-1)}(0,t_i)$) is less than the tolerance. After the tolerance is met, the final contact force for that time step is used to find the response, $u_{1,i+1}$, of the rod and the position, $u_{2,i+1}$, of the striker at the next time step.

4.4.2 Mode Superposition

A MATLAB (2010) code has been developed to obtain the response of the rod by numerical evaluation of Eqn. (4.23) and of the striker by direct integration of Eqn. (4.22b) using the Newmark average acceleration method. Equilibrium iterations (as described in Chapter 3) are performed at each time step to account for the non-linearity of the problem. A total of 10 modes of vibration (i = 10) were considered. For the case of the rod with elastic support the oscillatory motion of the rod due to the external spring is obtained by modeling the rod as a single degree of freedom (SDOF) system subjected to force $P(0,t)$. At each time step, the contact force $P(0,t)$ is also applied to the SDOF system and the total response of the rod is used to calculate the contact force. For the case of the free-free rod, since Eqn. (4.23) does not include the rigid body motion of the rod, only the non-zero frequencies are used to determine the axial response of the rod (i.e. the rigid body mode is not considered). The rigid body motion of the rod is obtained by determining the rigid body

displacement of the rod subjected to force *P(0,t)* and, similar to the rod with elastic support, the contact force is calculated based on the total response of the rod.

4.4.3 Finite Element Model (FEM)

An in-house finite element model (FEM) was coded in MATLAB (2010) to solve the non-linear problem of the longitudinal impact of a mass on a rod. The rod was modeled by 50 bar elements (Cook et al. 2002). The undamped equation of motion of the entire rod can be written in matrix form as (Clough and Penzien 1975; Tedesco et al. 1999):

$$[\boldsymbol{M}]\{\ddot{u}_1\} + [\boldsymbol{K}]\{u_1\} = \{P\} \tag{4.27}$$

where **[*M*]** is the global mass matrix, **[*K*]** is the global stiffness matrix, $\{P\}$ is the externally applied dynamic load vector, and $\{\ddot{u}_1\}$ and $\{u_1\}$ are the acceleration and displacement vectors, respectively. The dynamic load vector, *{P}*, (containing the contact force) is nonlinear and depends on the response of the rod and the striker, which in turn depend on the contact force. The equation of motion of the striker is given by Eqn. (4.22a). The response of the rod and the striker are obtained from step-by-step integration using the Newmark average acceleration method as presented in Chapter 3.

4.4.4 Verification using Abaqus FEA

A model of the rod and the striker was created in Abaqus FEA (2012) to verify the in-house code. The rod was modeled using a wire-model with 50 bar elements. To verify the results, the contact force obtained from the in-house finite element model was applied to the Abaqus FEA model. The results are shown along with the results of the in-house codes in Section 4.5.

4.5 Results and Discussion

The theory presented above is applicable to an elastic impact. It is common in the longitudinal impact of a drill/pile/rod to have an anvil of material with a higher yield strength on top of the rod where the impact takes place causing the impact to remain elastic (Tavares 1999). This is also verified by King and Bourgeois (1993).

4.5.1 Verification of model

To verify the contact force obtained from the present model of the rod for the fixed, free, and elastic supports, the experimental data obtained by King and Bourgeois (1993) for a similar problem is compared with the results obtained in the present model. Fig. 4.5 shows the experimental data obtained by King and Bourgeois (1993) for a drop height of 5 cm along with the results obtained from the FEM model presented in this study for the fixed, free and elastic support. The results confirm that the impact remains elastic as evidenced by the very good match between the experimental data and the results of the model developed in this study for all support conditions. A similar match in the impact force was also found by King and Bourgeois (1993). However, since their theoretical formulation ignores the support condition of the rod the possible effect of the boundary condition on the contact force is not captured. An in depth analysis showing the different possible scenarios in which the contact force is affected by the support condition of the rod is presented in the sections below.

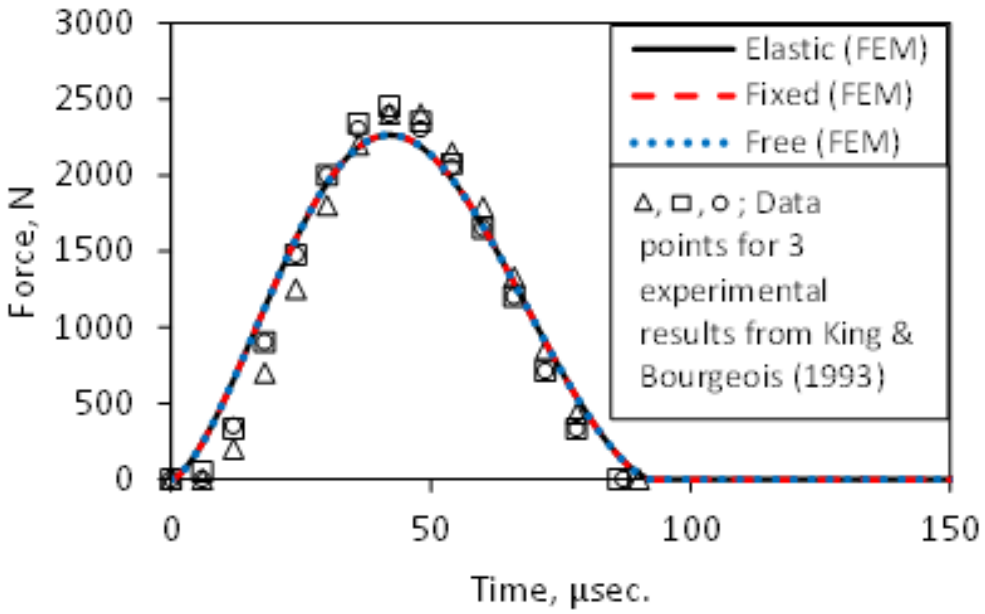

Fig. 4.5: Comparison of contact force obtained from FEM and experimental results from King and Bourgeois (1993) for a drop height of 5 cm.

4.5.2 Rod with Fixed Support

The contact force and the response of the drill rod and the striker for the case of the rod with fixed support determined by mode superposition and the in-house finite element model are shown in Fig. 4.6 for the material properties shown in Table 4.1. The contact force obtained from the in-house finite element model was applied to the Abaqus FEA model of the rod. The response for the Abaqus FEA model is also shown in Fig. 4.6. A very good agreement in the contact force and response of the rod and the striker is observed between the three methods. It is observed that the contact force shows a smooth curve similar to a half sine wave.

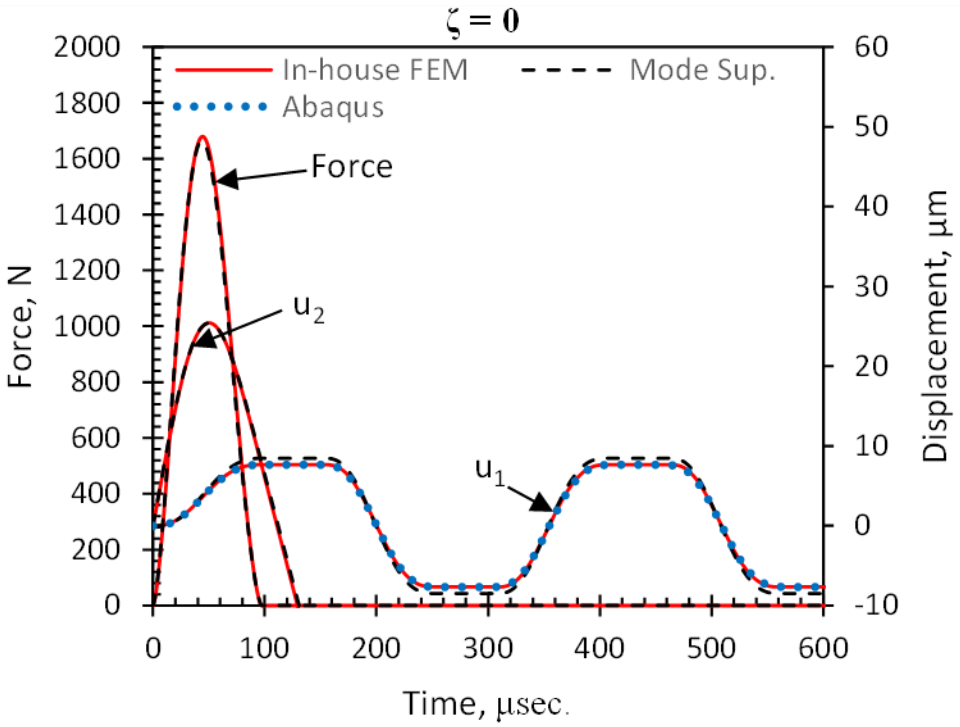

Fig. 4.6: Force and displacement time history for the longitudinal impact on a rod with fixed support. ($\zeta = 0$)

4.5.3 Rod with Free Support

The contact force and the response of the drill rod and the striker for the case of the rod with free support determined by mode superposition and the in-house finite element model are shown in Fig. 4.7. The contact force obtained from the in-house finite element model was applied to the Abaqus FEA model of the rod. The response for the Abaqus FEA model is also shown in Fig. 4.7. Similarly, a very good agreement in the contact force and response of the rod and the striker is observed between mode superposition, in-house finite element model, and Abaqus FEA. It is observed that the magnitude and duration of the contact force is similar to that of the fixed rod while in this case the rod experiences both axial vibration as well as rigid body motion.

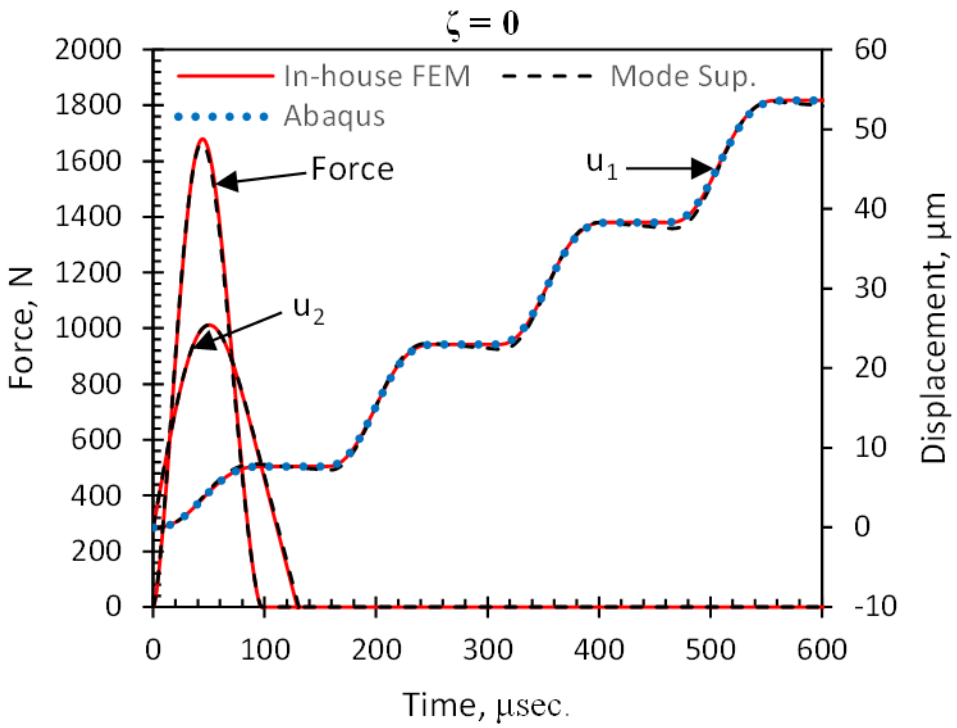

Fig. 4.7: Force and displacement time history for the longitudinal impact on a rod with free support. ($\zeta = 0$)

4.5.4 Rod with Elastic Support

The rod with elastic support is analogous to a drill rod supported by an elastic medium. Since the external spring represents the supporting medium, the stiffness of the spring is selected as $K = 5 * 10^6\, N/m$ based on the stiffness of sandstone, limestone, and granite (Batako et al. 2004).The contact force and the response of the drill rod and the striker for the case of the rod with the elastic support determined by mode superposition and the in-house FEM code is shown in Fig. 4.8 for the geometric and materials properties shown in Table 4.1. The contact force obtained from the in-house finite element model was applied to the Abaqus FEA model of the rod. The response for the Abaqus FEA model is also shown in Fig. 4.8.The shape of the force curve is similar to that of the rod with fixed

support. Similarly, a very good agreement is found between the mode superposition method and the FEM results. The response of the rod for all support conditions for a larger/extended time period is shown in Fig. 4.9. It is observed that the rod with the elastic support experiences two types of oscillations. The small oscillations are due to axial vibration of the rod, whereas the larger period oscillations are due to oscillatory motion due to the external spring at the support.

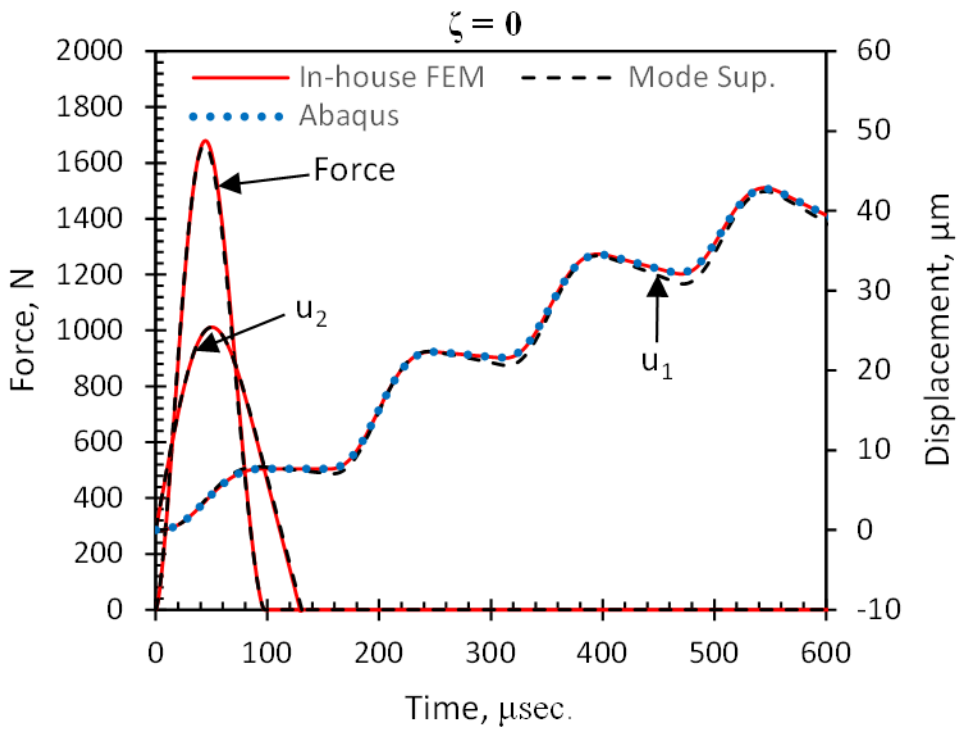

Fig. 4.8: Force and displacement time history for the longitudinal impact on a rod with elastic support. ($\zeta = 0$)

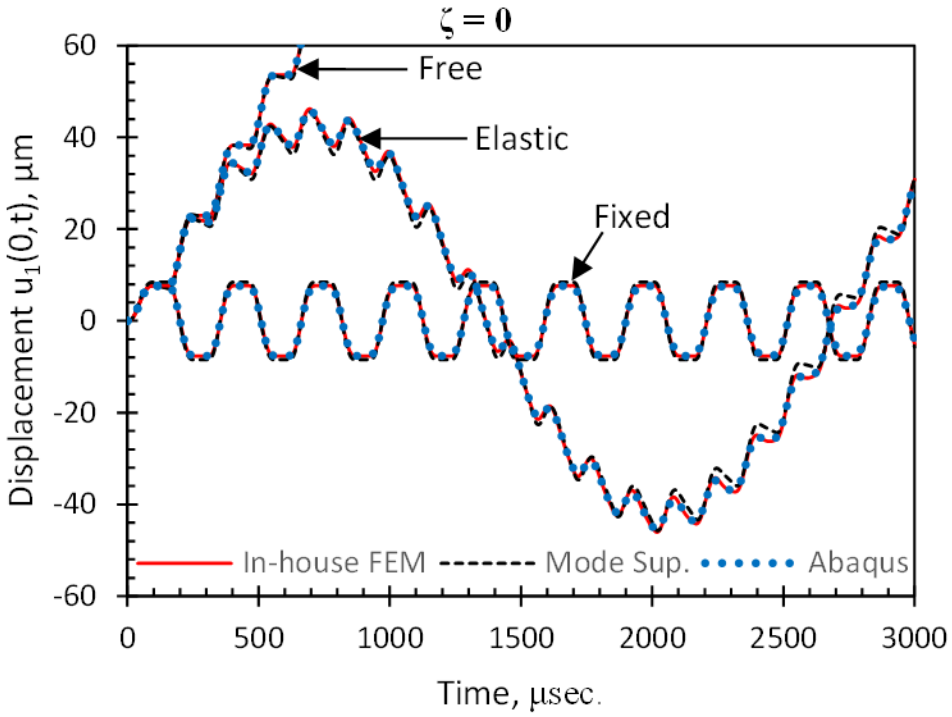

Fig. 4.9: Displacement time history of the top end of the rod, subjected to impact by a striker, for fixed, elastic and free support. ($\zeta = 0$)

The contact force time history for the three support conditions are shown in Fig. 4.10. The *x*-axis is normalized by the time of arrival, $t_a = 2L/c$, of the reflected wave to the contact end. It is observed that in this case the contact force is not affected by the support/boundary condition of the rod. Figure 4.11 shows the response of the rod and the striker for all cases (i.e. fixed, free, and elastic supports), where τ is the duration of contact and the subscripts *f, fr*, and *e* are for fixed, free, and elastic supports, respectively. The dashed diagonal lines represent the location of the waves traveling through the rod. It is observed that in this case the response of the rod remains the same during the short duration of the contact regardless of the boundary condition. This can be attributed to the fact that the duration, τ, of contact between the striker and the rod is less than the time, t_a, equal to $2L/c$, the displacement wave takes to travel through the rod to the other end and return back to the contact end. This is consistent with the material presented in (Goldsmith 1960; Johnson 1985).

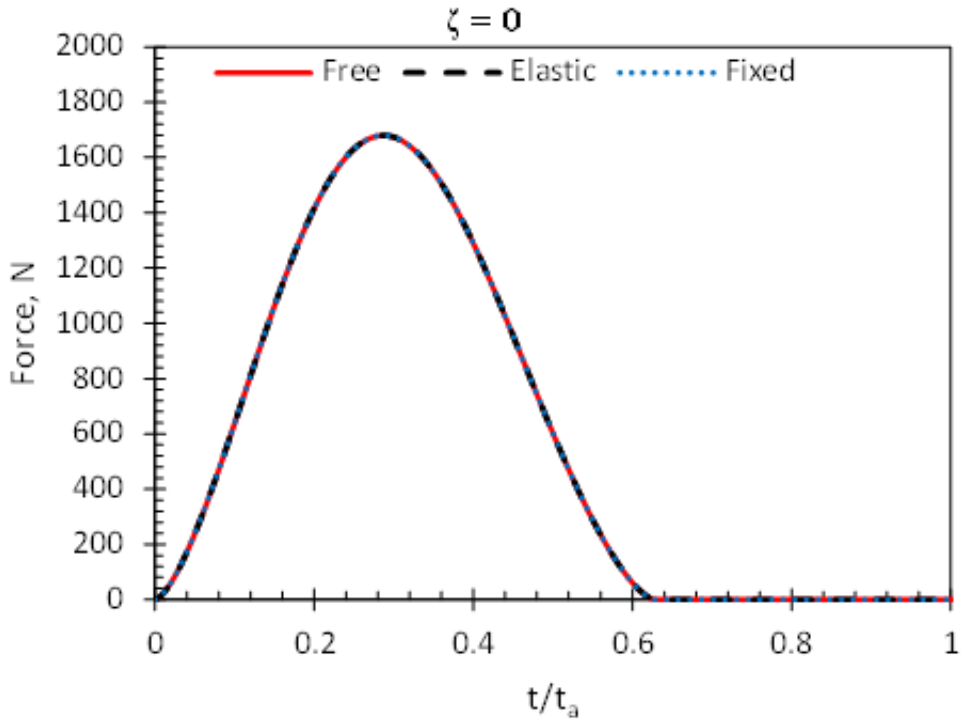

Fig. 4.10: Force time history for fixed, free, and elastic support. (L = 0.4 m, t_a = 154 μsec., ζ = 0)

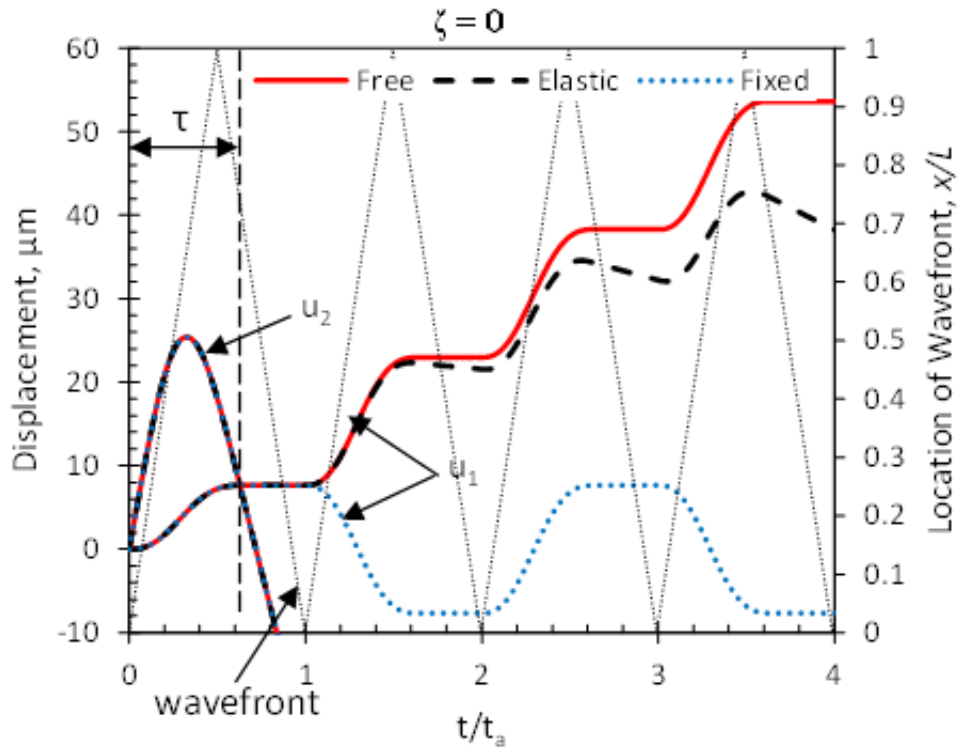

Fig. 4.11: Displacement time history for fixed, free, and elastic support. (L = 0.4 m, t_a = 154 μsec., ζ = 0)

In order to observe the effect of the boundary conditions of the rod on the contact force, it is necessary to analyze the case in which the time of arrival of the reflected wave is less than the duration of contact. Figure 4.12 and Fig. 4.13 show the contact force and rod response, respectively, for a shorter rod (L = 0.15 m). In this case, the duration of contact (τ_f = 111 μs, $\tau_{fr} = \tau_e$ = 90 μs) for both support cases is larger than the time of arrival of the wave (t_a = 58 μs); therefore the effect of the boundary condition on the structural response of the rod begins before the end of contact. In this case the contact force is seen to be affected by the boundary condition. The magnitude of the contact force is similar for all boundary conditions but the duration of contact is larger for the rod with the fixed support.

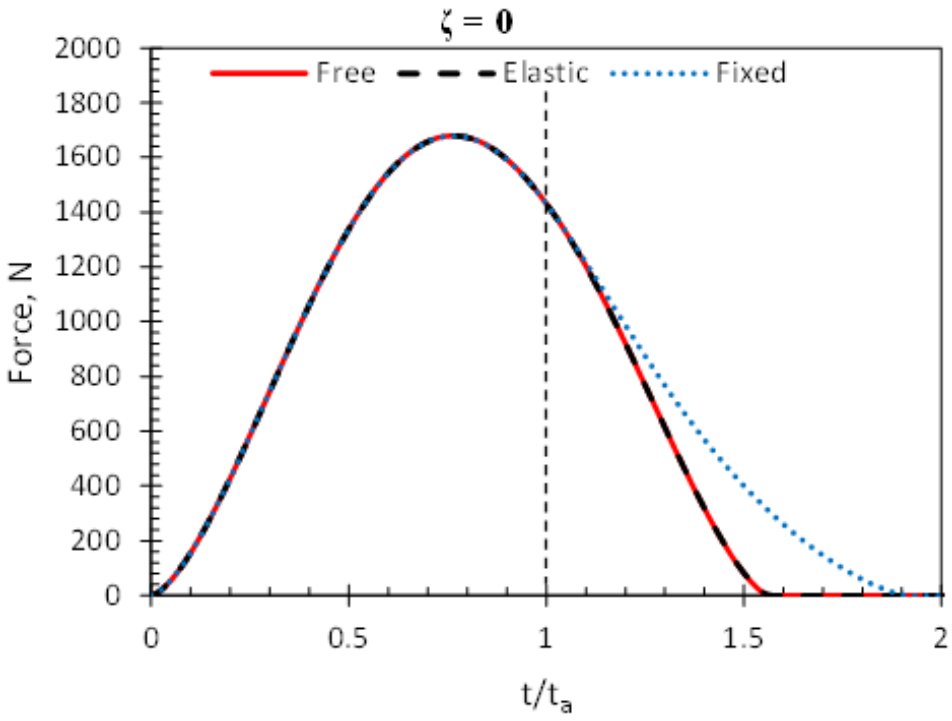

Fig. 4.12: Force time history for fixed, free, and elastic support. (L = 0.15 m, t_a = 58 μsec., ζ = 0)

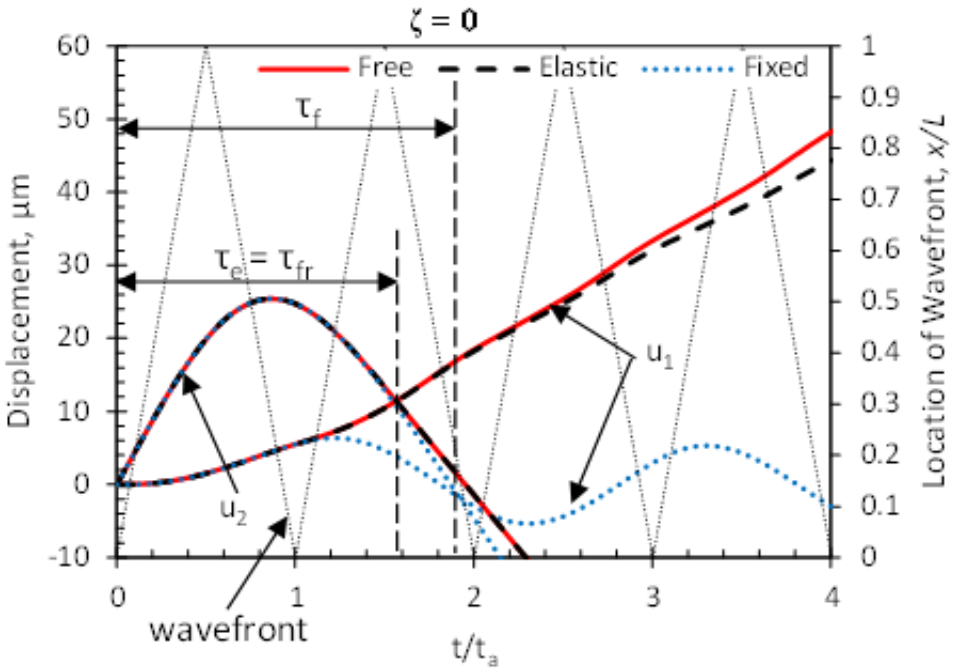

Fig. 4.13: Displacement time history for fixed, free, and elastic support. (L = 0.15 m, t_a = 58 μsec. $\zeta = 0$)

It is observed that the force curve for the free support is equal to that of the elastic support even though the duration of contact for both cases is larger than the time of arrival of the reflected wave. This can be attributed to the fact that for the geometric and material properties used the rod with elastic support has a stiffness ratio (μ = 0.03) close to the limiting case (μ = 0) of the free-free rod. Therefore the response of the rod for the elastic and the free support are seen to be similar for a time period longer than the time of arrival of the reflected wave. Figure 4.14 and Fig. 4.15 show the contact force and rod response, respectively, for a shorter rod (L = 0.05 m). Similarly to the previous case, the duration of contact (τ_f = 97 μs, $\tau_{fr} = \tau_e$ = 78 μs) is larger than the time of arrival of the wave (t_a = 19 μs). However, in this case $\tau \gg t_a$, therefore the difference in boundary condition has a larger effect in the contact force (magnitude and duration), with the rod with fixed support

showing the larger contact force. Similar to the previous case, the force for the free and the elastic support are observed to be the same.

Fig. 4.16 shows the peak (maximum) contact force plotted against the ratio of the duration of contact, τ, to the time of arrival, $t_a = 2L/c$; here in referred to as the time ratio. The vertical dashed line shows the time ratio $\tau/t_a = 1$. It is observed that if the time ratio (τ/t_a) is less than one (i.e. the duration of contact is less than the time of arrival of the wave), the force remains the same regardless of the boundary condition. In such cases, a simpler approach, such as presented by King and Bourgeois (1993), may suffice. However, if this time ratio is larger than one, the magnitude and/or the duration of the force is affected by the boundary condition and a more detailed analysis, such as presented in this study, is required to incorporate the effects of the support on the contact force.

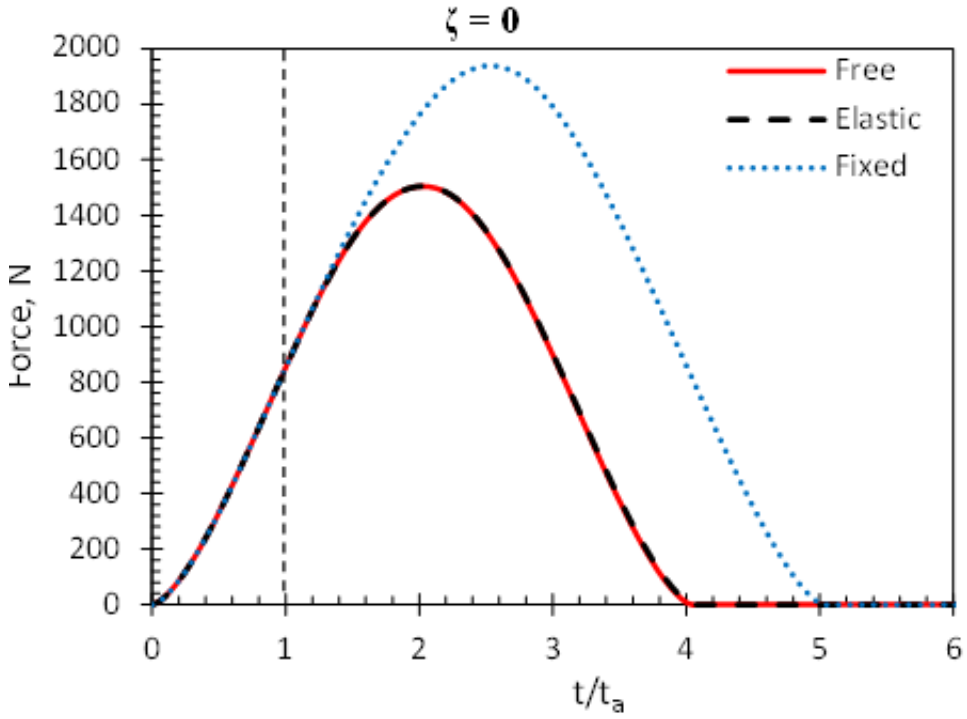

Fig. 4.14 Force time history for fixed, free, and elastic support. (L = 0.05 m, t_a = 19 μsec., $\zeta = 0$)

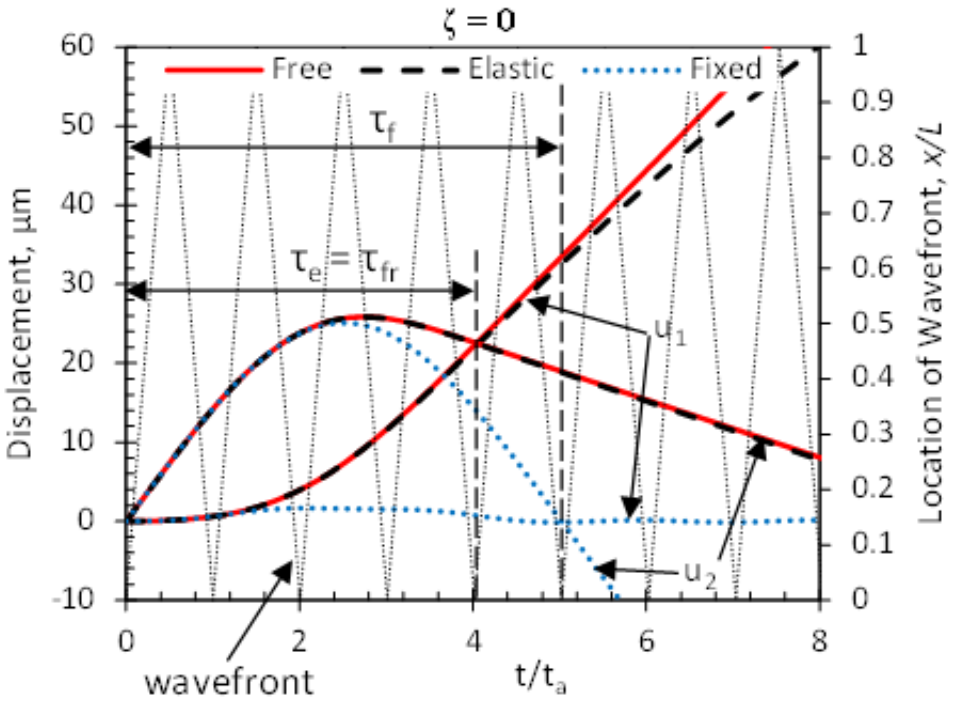

Fig. 4.15: Displacement time history for fixed, free, and elastic support. (L = 0.05 m, t_a = 19 μsec., ζ = 0)

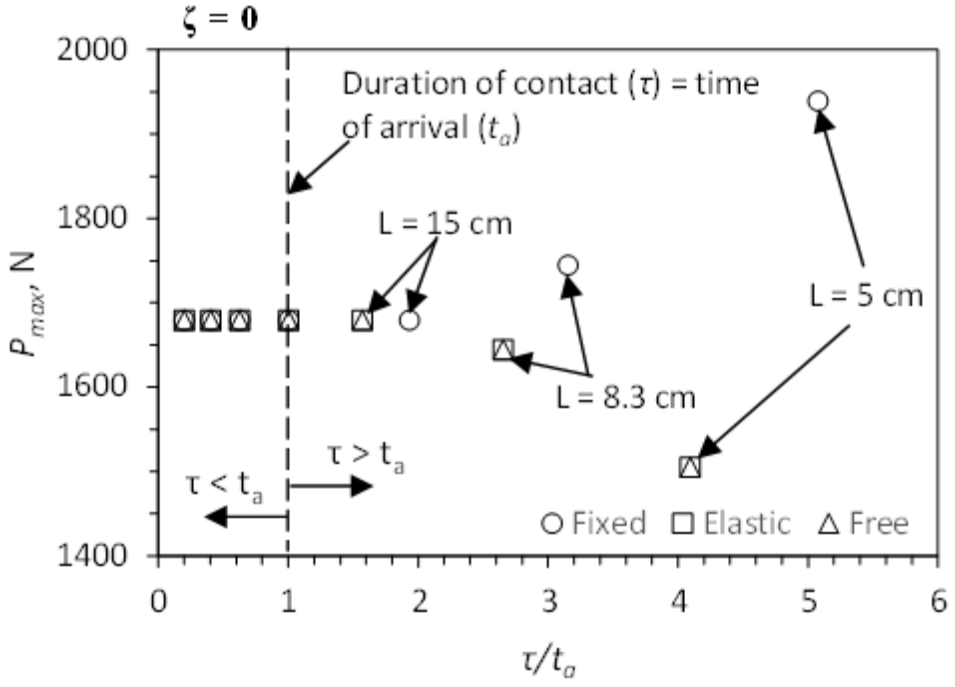

Fig. 4.16: Force amplitude vs time ratio for fixed, free, and elastic support. (ζ = 0)

4.5.5 Impact simulations including damping in the rod

The contact force and the response of the drill rod and the striker for an underdamped ($\zeta = 0.5$) rod for fixed, free, and elastic support determined by mode superposition and the in-house finite element model are shown in Fig. 4.17 for the material properties shown in Table 4.1. The contact force obtained from the in-house finite element model was applied to the Abaqus FEA model of the rod. The response for the Abaqus FEA model is also shown in Fig. 4.6. Similarly to the undamped case, a very good agreement in the contact force and response of the rod and the striker is observed between the three methods. The response of the rod for all support conditions for a larger/extended time period is shown in Fig. 4.18. It is observed that the larger oscillation due to the external spring (elastic support) are damped out as well. However, this larger oscillation takes much longer to be reduced to zero because there is now damping element in the support condition.

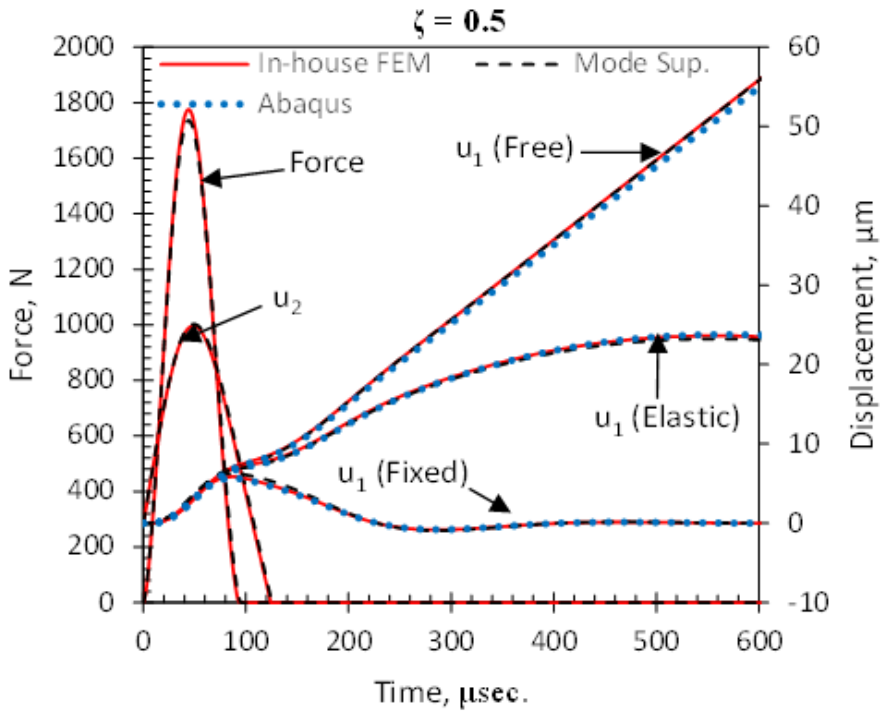

Fig. 4.17: Force and displacement time history for the rod with fixed, elastic and free support. ($\zeta = 0.5$)

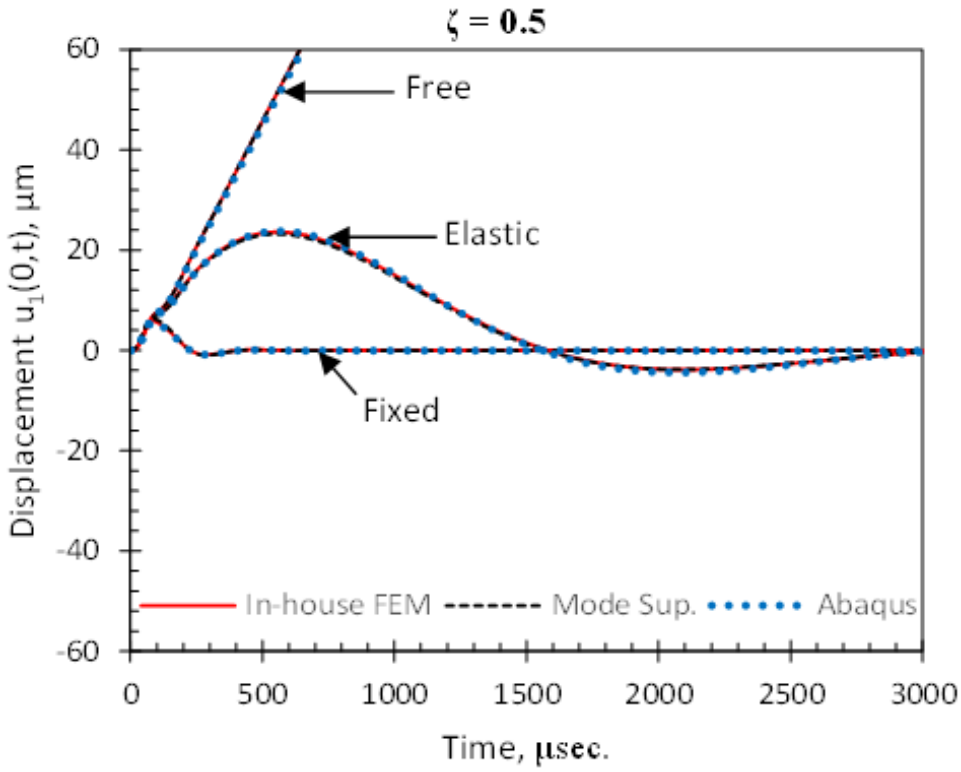

Fig. 4.18: Displacement time history of the top end of the rod for fixed, free and elastic support. ($\zeta = 0.5$)

The contact force time history for all three support conditions, for an underdamped rod, is shown in Fig. 4.19. Even though the contact ends before the reflected wave arrives to the contact end (i.e. $\tau < t_a$), a slight difference in the contact force for the fixed support is observed. The response of the striker and the rod for all three support conditions is shown in Fig. 4.20. It is observed that, contrary to the undamped case, the response of the rod for each support condition begins to differ before the reflected wave arrives to the contact end. This suggests that when damping of the rod is considered, the time of arrival of the reflected wave is no longer the only governing parameter. This is attributed to the fact that the damping force becomes effective starting at the very beginning of the response of the rod. The effect of damping on the contact force is different for each support condition. This is

due to the fact that the damping ratio is a function of the damping coefficient, mass and frequency of the rod. Since the frequency of the rod is different for each of the support conditions, the response of the rod for the same damping ratio differs before the arrival of the reflected wave. Hence, contrary to the undamped case, the contact force is affected by the support condition even when the contact ends before the arrival of the reflected wave.

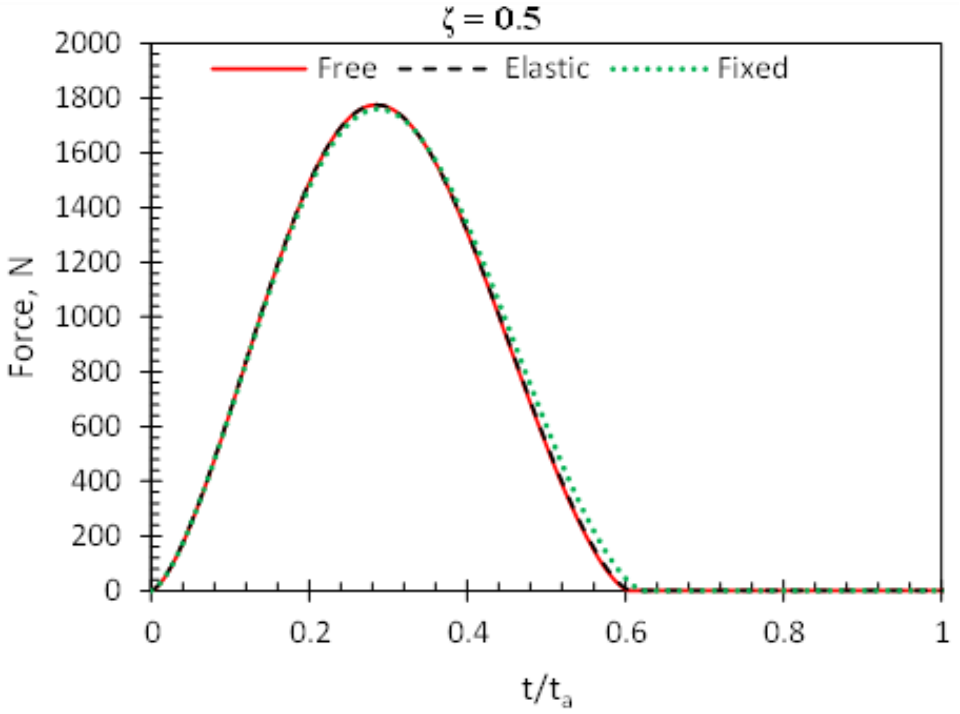

Fig. 4.19: Force time history for and underdamped rod with fixed, free, and elastic support. (L = 0.4 m, t_a = 154 μsec., ζ = 0.5)

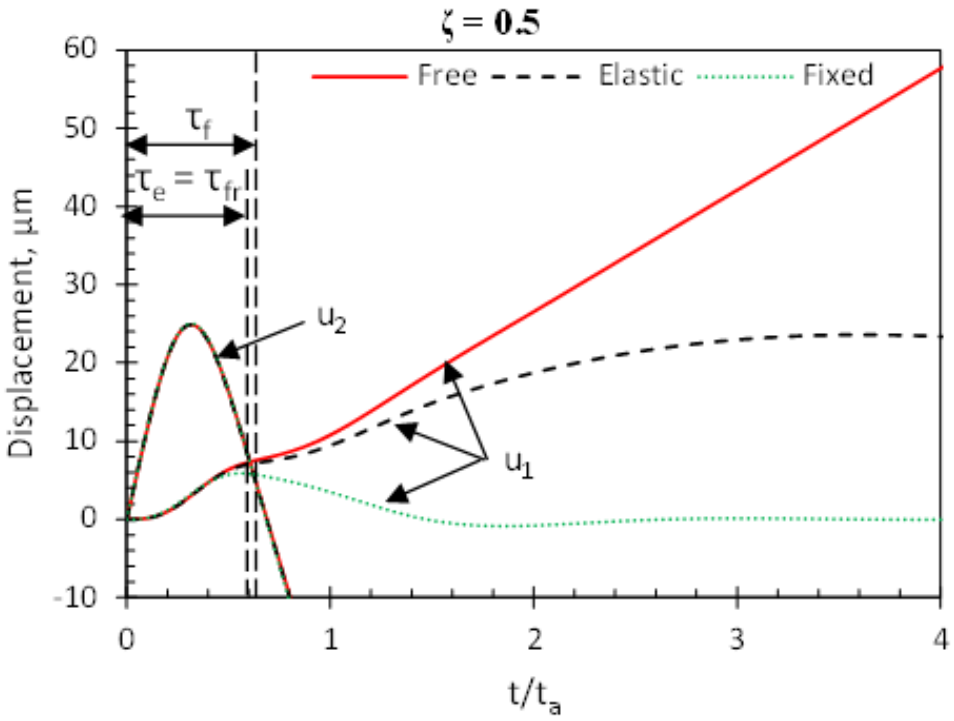

Fig. 4.20: Displacement time history for an underdamped rod with fixed, free, and elastic support. (L = 0.4 m, t_a = 154 μsec., ζ = 0.5)

The contact force and displacement time history for a shorter rod (L = 0.15 m) are shown in Figs. 4.21 and 4.22, respectively. In this case, the contact ends after the reflected wave arrival to the contact end. It is observed that the contact force for the fixed support varies significantly from that of the free and elastic support, whereas a slight difference is observed between the free and the elastic support. As can be observed in Fig. 4.22, the response of the rod for the fixed support during the contact period varies significantly from that of the free and the elastic support. The response of the rod for the elastic support is observed to deviate slightly from that of the free support towards the end of the contact duration.

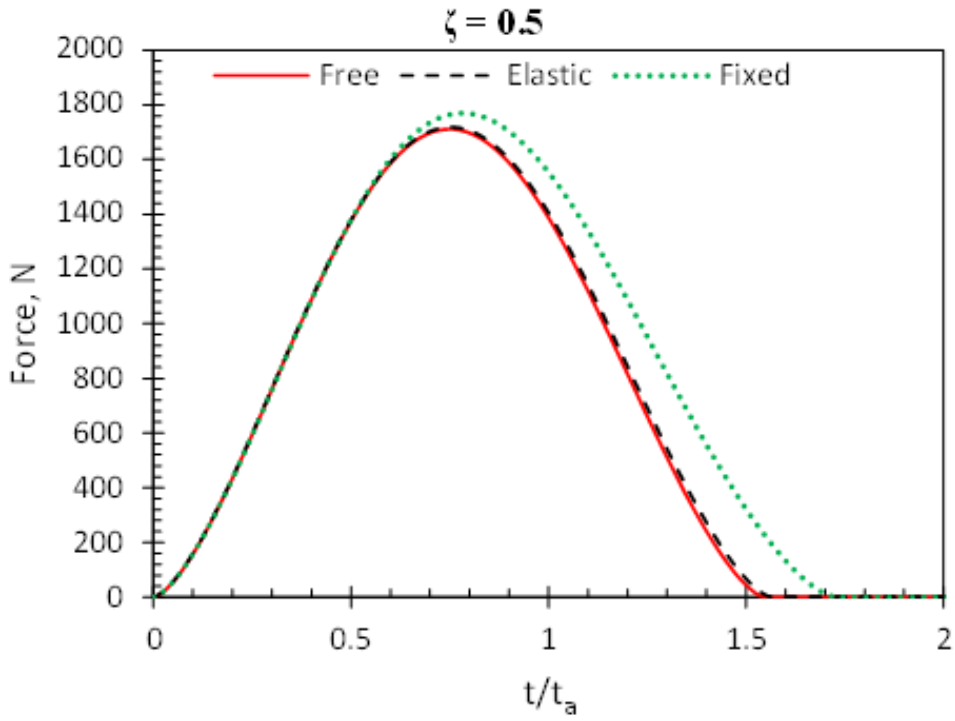

Fig. 4.21: Force time history for and underdamped rod with fixed, free, and elastic support. (L = 0.15 m, t_a = 58 μsec., ζ = 0.5)

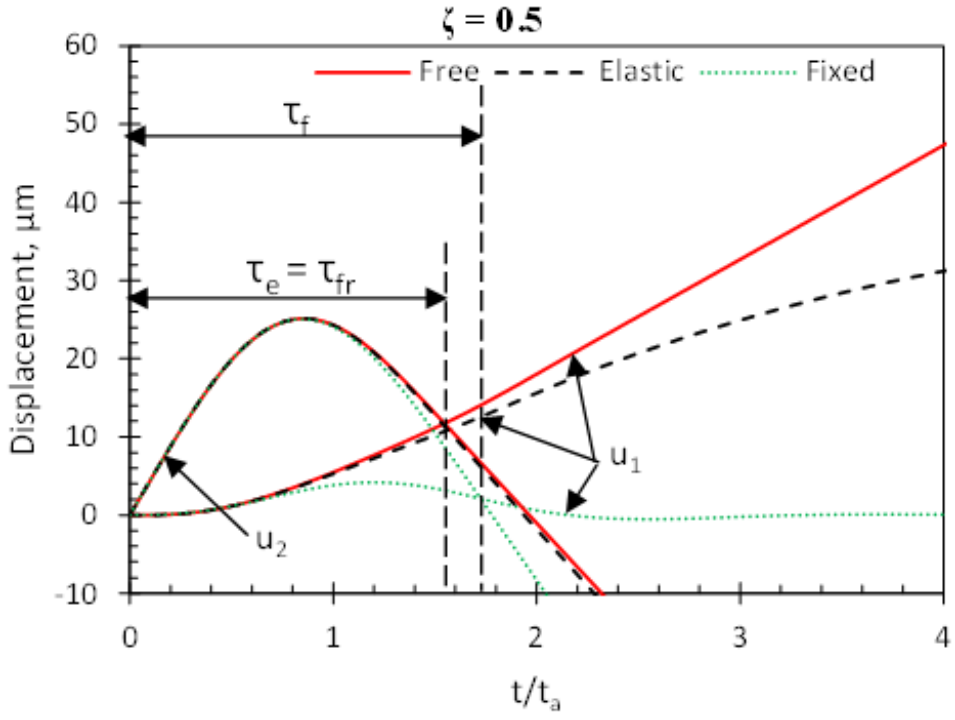

Fig. 4.22: Displacement time history for an underdamped rod with fixed, free, and elastic support. (L = 0.15 m, t_a = 58 μsec., ζ = 0.5)

The peak (maximum) contact force plotted against the ratio of the duration of contact, τ, to the time of arrival, $t_a = 2L/c$, is shown in Fig. 4.23. Contrary to the undamped case it is observed that even for cases when the contact ends before the arrival of the reflected wave to the contact end (i.e. $\tau < t_a$) the contact force is affected by the support condition. However, it is important to point that the effect of the support condition on the contact force is observed to be much higher when the contact ends after the time of arrival of the reflected wave to the contact end. Figs. 4.24 and 4.25 show the peak force versus time ratio for a critically damped and over damped system, respectively. The observations made for the underdamped case are seen to remain true for the critically damped and overdamped cases.

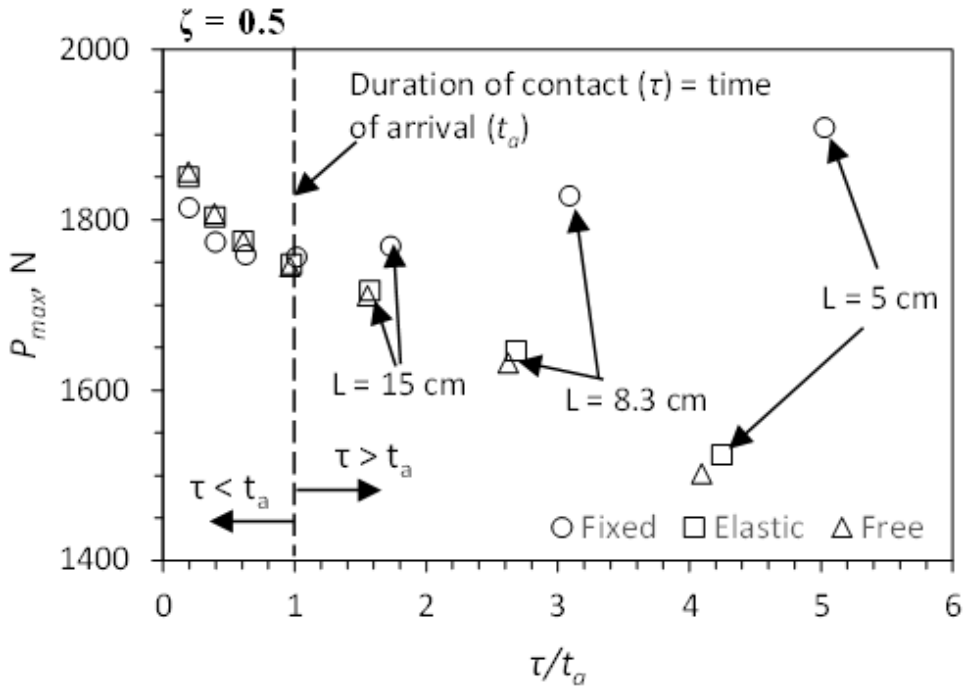

Fig. 4.23: Force amplitude vs time ratio for fixed, free, and elastic support. (ζ = 0.5)

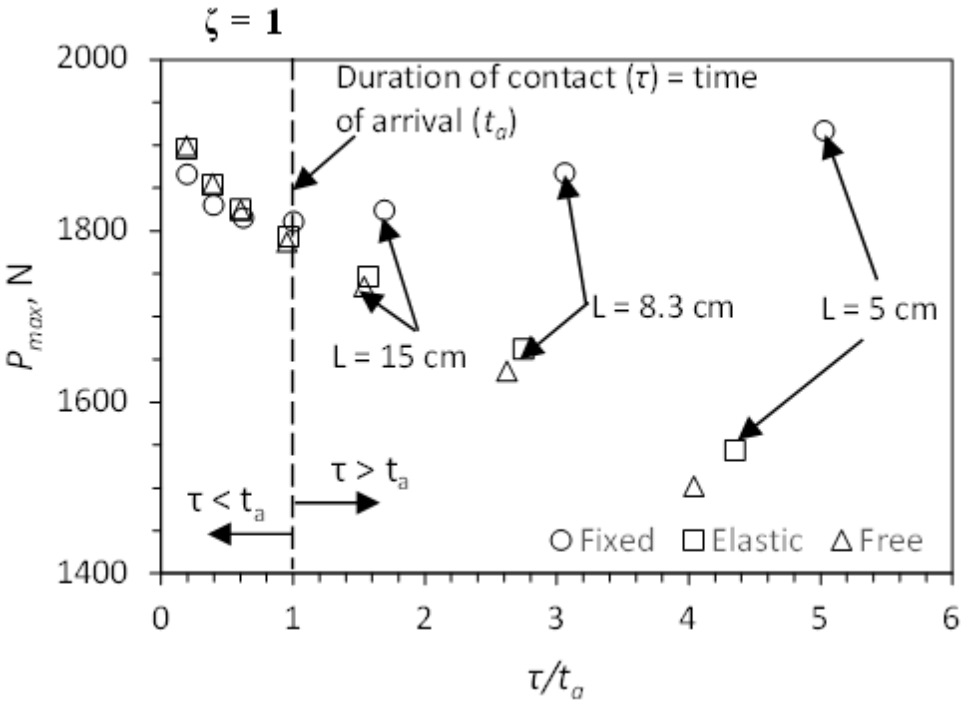

Fig. 4.24: Force amplitude vs time ratio for fixed, free, and elastic support. (ζ = 1)

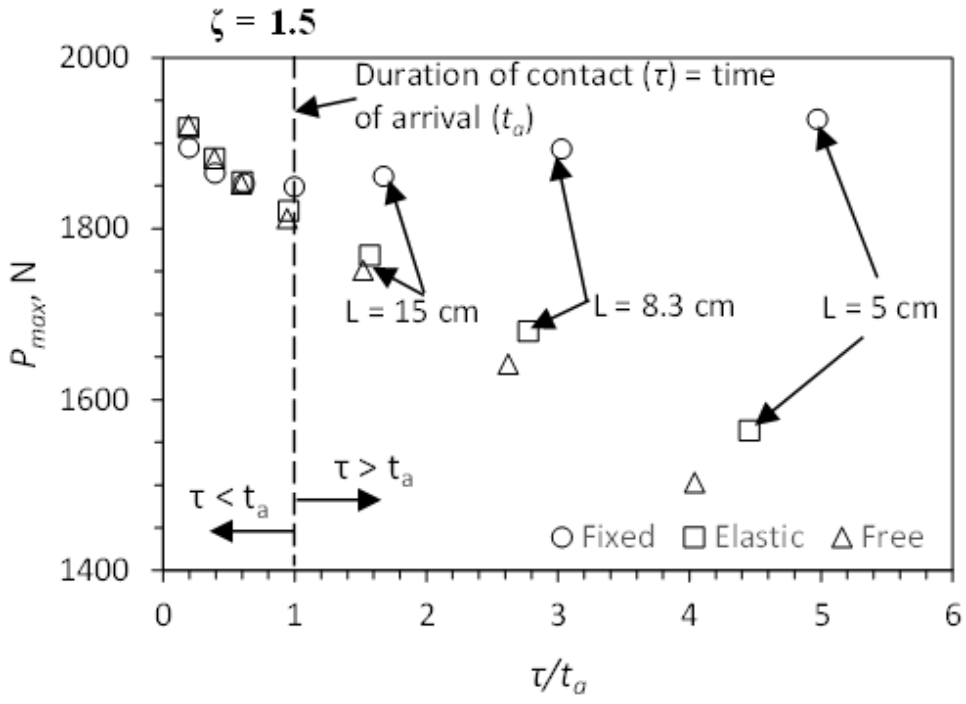

Fig. 4.25: Force amplitude vs time ratio for fixed, free, and elastic support. (ζ = 1.5)

4.6 Conclusions

The dynamic response of longitudinal impact of a mass on one end of a uniform rod with different support conditions, e. g. fixed, free, and elastic (spring attached) supports was analyzed using Hertz theory of contact. The contact force and the rod response were obtained using mode superposition technique and an in-house finite element code. The response of the rod and the contact force for each support condition were compared and the conditions under which the support condition of the rod affects the contact force were discussed. Based on the results obtained from the present study, the following conclusions can be made:

- For an undamped rod the contact force is not affected by the boundary condition of the supporting end of the rod (i.e. fixed, free or elastic support) if the duration of contact is less than the time it takes to the displacement wave to return to the contact end (time of arrival, t_a). This is because the effect of the boundary conditions is carried by the reflected wave. Therefore, if the contact between the striker and the rod ceases before the reflected wave reaches the contact end of the rod, the response of the rod during the contact period is the same regardless of the boundary condition.
- On the other hand, if the duration of contact is larger than the time of arrival of the reflected wave ($\tau > t_a$), the contact force is affected by the support condition of the rod. The larger the duration of contact is with respect to the time of arrival, (i.e. the larger the ratio τ / t_a), the larger the effect of the boundary condition on the contact force.
- If the duration, τ, of contact is less than the time of arrival, t_a, the contact force is not affected by the boundary condition on the bottom of the rod and a more simple analysis

such as the one presented by King and Bourgeois (1993) may be performed with reasonably accurate results.

- When damping of the rod is considered, the time of arrival of the reflected wave is no longer the only governing parameter. The support conditions are observed to affect the contact force even for the case of a contact ending before the time of arrival. However, the effect of the support condition on the contact force is higher when the contact ends after the time of arrival of the reflected wave.

Chapter 5

Impact on a Rod with Viscous and Viscoelastic Support Conditions

This chapter presents the dynamic and contact analysis of the longitudinal impact of a mass on a rod with viscous and visco-elastic support conditions. The support condition of the rod represents the medium (soil or rock) on which the rod is resting. Additionally, the case of a rod supported by a visco-elasto-plastic support is presented to model drill rod penetration into the supporting medium. Focus is given to find the dynamic response of the rod for the different support conditions and how the impact force is affected by the dissipative support conditions. The contact force was obtained using Hertz force-indentation relation coupled with the structural vibration. Both the contact force and the rod structural response are determined using an in-house finite element code.

5.1 Longitudinal vibration of uniform rods with viscous and viscoelastic end conditions

In the context of percussive drilling it is important to understand the soil-tool interaction. In the case of percussive drilling of rocks, the interaction between the drill rod and the rock, before rock breakage, can be considered as linear elastic (Lundberg (1993)). However, for a supporting medium other than rock (e.g. soil) energy dissipation must be taken into account. This energy dissipation is mainly due to energy radiation to the soil (Bachman et al. 1995). This section presents a summary of the free vibration response of uniform rods with dissipative boundary conditions. Consider a uniform rod with viscous

support subjected to a distributed load *P(x,t)* along its length as shown in Fig. 5.1(a). The equation of motion of undamped vibration, obtained from a differential element (Fig. 5.1(b)), of the rod is given by (Clough and Penzien 1975; Tedesco et al. 1999):

$$\bar{m}\frac{\partial^2 u(x,t)}{\partial t^2} - EA\,\frac{\partial^2 u(x,t)}{\partial x^2} = P(x,t) \tag{5.1}$$

where $f_I = \bar{m}\cdot\partial^2 u/\partial t^2$ is the inertial force,$F = EA\cdot\partial u/\partial x$ is the internal axial force, E is the Young's modulus, and A is the cross sectional area of the rod. Introducing the velocity of wave propagation ($c = \sqrt{E/\rho}$), letting the mass per unit length of the rod $\bar{m} = \rho A$, where ρ is the density of the rod, and defining the distributed load as $\underline{f}(x,t) = P(x,t)/\bar{m}$, Eqn. (5.1) can be expressed as:

$$\frac{\partial^2 u(x,t)}{\partial t^2} - c^2\,\frac{\partial^2 u(x,t)}{\partial x^2} = \underline{f}(x,t) \tag{5.2}$$

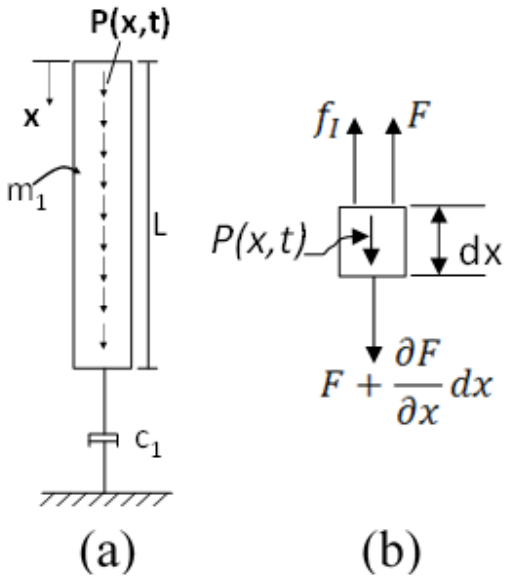

Fig. 5.1: (a) Rod with viscous support subjected to distributed time varying load *P(x,t)* and (b) Free body diagram of an element of a uniform rod subjected to a distributed axial force.

5.1.1 Free Vibration: Mode Shapes and Frequencies

Consider the longitudinal free vibration ($\underline{P}(x,t) = 0$) of a uniform rod. The solution to Eqn. (5.2) is assumed of the form (Udwadia 2012):

$$u(x,t) = \varphi(x)e^{\lambda t} \tag{5.3}$$

where $\varphi(x)$ is the mode shape and $e^{\lambda t}$ is the solution to the time component. Substituting Eqn. (5.3) into Eqn. (5.2) yields:

$$\varphi''(x) - \frac{\lambda^2}{c^2}\varphi(x) = 0 \tag{5.4}$$

The general solution to Eqn. (5.4) is given by:

$$\varphi(x) = D_1 sinh\left(\frac{\lambda x}{c}\right) + D_2 cosh\left(\frac{\lambda x}{c}\right) \tag{5.5}$$

where D_1 and D_2 are constants. The natural frequencies are obtained by applying the boundary conditions into Eqn. (5.5).

5.1.2 Rod with Viscous Support

Considering the rod with viscous support (shown in Fig. 5.1(a)) with $P(x,t) = 0$, the boundary conditions are given by letting the force equal to zero at $x = 0$, and the force on the bottom ($x = L$) equal to the force exerted by the viscous damper. These boundary conditions are given by Eqns. (5.6) and (5.7), respectively.

$$EA\frac{\partial u(0,t)}{\partial x} = 0 \tag{5.6}$$

$$EA\frac{\partial u(L,t)}{\partial x} = -c_1\frac{\partial u(L,t)}{\partial t} \tag{5.7}$$

where c_1 is the external damper coefficient. Applying the boundary condition at $x = 0$ (i.e. Eqn. (5.6)) into Eqn. (5.5) gives $D_1 = 0$. Thus the mode shape for this case is given by:

$$\varphi(x) = D_2 cosh\left(\frac{\lambda x}{c}\right) \tag{5.8}$$

Introducing the boundary condition at $x = L$ yields:

$$\frac{1}{c}\sinh\left(\frac{\lambda L}{c}\right) = -\frac{c_1}{AE}\cosh\left(\frac{\lambda L}{c}\right) \tag{5.9}$$

Or

$$\tanh\left(\frac{\lambda L}{c}\right) = -\frac{c_1 c}{AE} \tag{5.10}$$

Recalling the exponential form of the hyperbolic tangent function given by:

$$\tanh\left(\frac{\lambda L}{c}\right) = \frac{e^{\frac{\lambda L}{c}} - e^{-\frac{\lambda L}{c}}}{e^{\frac{\lambda L}{c}} + e^{-\frac{\lambda L}{c}}} \tag{5.11}$$

and multiplying by $e^{\frac{\lambda L}{c}}/e^{\frac{\lambda L}{c}}$ Eqn. (5.10) can be expressed as:

$$\frac{e^{\frac{2\lambda L}{c}} - 1}{e^{\frac{2\lambda L}{c}} + 1} = -\frac{c_1 c}{AE} \tag{5.12}$$

Letting $h = -c_1 c/AE$ Eqn. (5.12) can then be expressed as:

$$e^{\frac{2\lambda L}{c}} = \frac{(1-h)}{(1+h)} = \tilde{\alpha} \tag{5.13}$$

where $\tilde{\alpha}$ is a real number. Letting $\frac{\lambda L}{c} = q + ip$, Eqn. (5.13) gives:

$$e^{2q}[\cos(2p) + isin(2p)] = \tilde{\alpha} \tag{5.14}$$

Since $\tilde{\alpha}$ is real, then from Eqn. (5.13) we obtain $sin(2p) = 0$, or $2p = n\pi$. Therefore, Eqn. (5.13) reduces to:

$$e^{2q} = \pm\tilde{\alpha} \tag{5.15}$$

Using the property $\mathrm{Ln}(e^x) = 2x \pm n\pi i$ (Kreyszig 2011) we obtain (from Eqn. (5.15)):

$$q = \frac{1}{2}Ln(\tilde{\alpha}) + i\frac{n\pi}{2} \tag{5.16}$$

Now, recalling that $\frac{\lambda L}{c} = q + ip$, and using Eqn. (5.16) we obtain:

$$\lambda_n = \frac{c}{L}(q + ip_n) = \frac{c}{L}\left(\frac{1}{2}Ln(\tilde{\alpha}) + i\frac{n\pi}{2} + i\frac{n\pi}{2}\right) \tag{5.17}$$

Or

$$\lambda_n = \frac{c}{2L}Ln(\tilde{\alpha}) + i\frac{n\pi c}{L} \tag{5.18}$$

Noting that $Ln(x) = \ln(x) + iArg(x)$ (Kreyszig 2011), Eqn. (5.18) can be expressed as:

$$\lambda_n = \frac{c}{2L}[\ln(\tilde{\alpha}) + iArg(\tilde{\alpha})] + i\frac{n\pi c}{L} \tag{5.19}$$

Where

$$Arg(\tilde{\alpha}) = \begin{bmatrix} 0 & if\ \tilde{\alpha} > 0 \\ \pi & if\ \tilde{\alpha} < 0 \end{bmatrix} \tag{5.20}$$

Therefore, the eigenvalues of the system shown in Fig. 5.1(a) are given by (Udwadia 2012):

$$\lambda_n = \frac{c}{2L}ln(\tilde{\alpha}) + i\frac{n\pi c}{L} \qquad for\ \tilde{\alpha} > 0 \tag{5.21a}$$

$$\lambda_n = \frac{c}{2L}ln(\tilde{\alpha}) + i\frac{(2n+1)\pi c}{2L} \qquad for\ \tilde{\alpha} < 0 \tag{5.22b}$$

5.1.3 Rod with Visco-elastic Support

Considering the rod with visco-elastic support shown in Fig. 5.2, with *P(x,t)* = 0, the boundary conditions are given by letting the force equal to zero at *x* = 0, and the force on the bottom (*x* = *L*) equal to the force exerted by the viscous damper and the linear spring. These boundary conditions are given by Eqns. (5.22) and (5.23), respectively.

$$EA\frac{\partial u(0,t)}{\partial x} = 0 \tag{5.22}$$

$$EA\frac{\partial u(L,t)}{\partial x} = -K_1 u(L,t) - c_1\frac{\partial u(L,t)}{\partial t} \tag{5.23}$$

Applying the boundary condition at $x = 0$ (i.e. Eqn. (5.22)) into Eqn. (5.5) gives $D_1 = 0$. Thus, the mode shape for this case is the identical expression as given by Eqn. (5.8) for the viscous end support case.

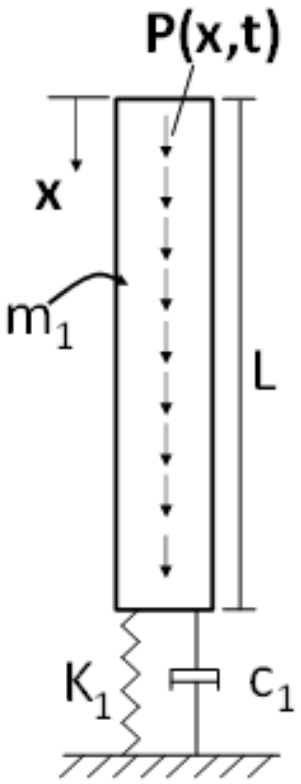

Fig. 5.2: Uniform rod with viscoelastic support subjected to a time varying load along its length.

However, the frequency equation for the present case is different and is obtained by applying the boundary condition (Eqn. (5.23)) corresponding to the bottom end of the rod, from which we obtain:

$$\tanh\left(\frac{\lambda L}{c}\right) = \frac{1}{EA}\left[-\frac{K_1 c}{\lambda} - c_1 c\right] \tag{5.24}$$

Rearranging terms, the characteristic equation is obtained as:

$$\frac{\lambda L}{c}\left[\tanh\left(\frac{\lambda L}{c}\right) + \frac{c_1 c}{EA}\right] = -\frac{K_1}{k} \tag{5.25}$$

Or

$$\frac{\lambda L}{c}\left[\tanh\left(\frac{\lambda L}{c}\right)+\frac{c_1 c}{EA}\right]=-\mu \tag{5.26}$$

where $\mu = K_1/k$ is the ratio of the stiffness (K_1) of the external spring to the axial stiffness ($k = EA/L$) of the rod. Equation (5.26) can be solved numerically to obtain the natural frequencies (λ) of the system.

5.1.4 Rod with Visco-elasto-plastic Support

A model considered here to estimate the penetration of the drill rod into the supporting medium due to the impact force generated by the striking mass is shown in Fig. 5.3.

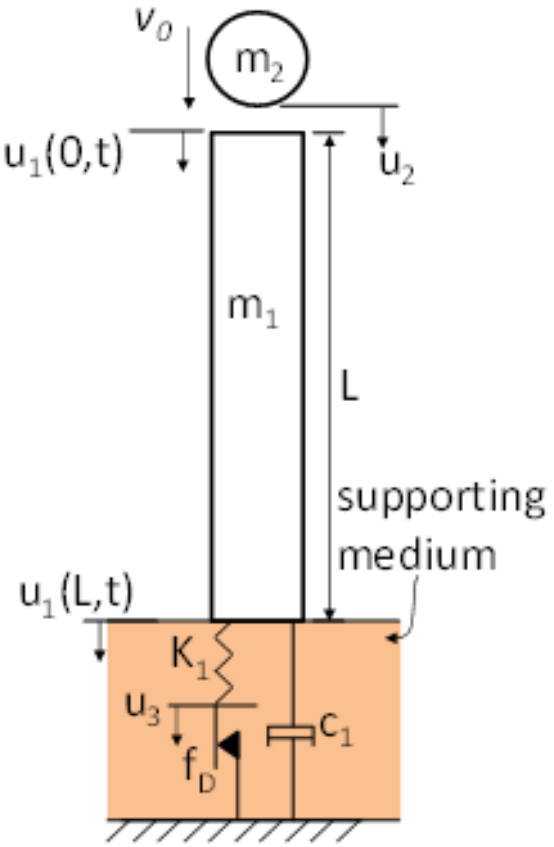

Fig. 5.3: Continuous model of the drill rod with visco-elasto-plastic support.

The supporting medium is modeled by a visco-elasto-plastic element (Batako et al., 2004). Batako et al. (2004) modeled the drill rod as a single degree of freedom (SDOF) system, thus axial vibration of the rod is not considered. Here, a continuous model that considers longitudinal vibration of the rod as well as oscillation and penetration due to the visco-elasto-plastic support is presented. The model considers a spherical mass, m_2, striking the rod with initial velocity, v_0 (Fig. 5.3). The visco-elasto-plastic penetration model is applied as a boundary condition. The model consists of a linear elastic spring, a viscous damping element, and a dry friction element. The linear spring represents the bearing resistance of the supporting medium and the viscous damper represents the energy radiated to the soil. The friction element force, f_D, represents the bearing capacity of the supporting medium. When the spring force reaches the supporting medium's bearing capacity, the supporting medium yields and penetration begins. This is a special case of the viscoelastic support, in which the support is viscoelastic while the rod is not penetrating. When the penetration begins then the support becomes equal to the viscous support case. Therefore the natural frequencies for this case are equal to that of the rod with viscous support (see Section 5.1.2) while the rod is penetrating and equal to the frequencies of the rod with viscoelastic support (see Section 5.1.3) when the rod is not penetrating.

Consider a spherical striker of mass m_2 hitting a drill rod of mass m_1 as shown in Fig. 5.3. A force, $P(0,t)$, will be generated on the top end of the drill due to impact of the striker. The visco-elastic motion, $u_1(x,t)$, is governed by the following equation of motion:

$$m_1\ddot{u}_1(x,t) + c\dot{u}_1(L,t) + K\big(u_3 - u_1(L,t)\big) = P(0,t) \tag{5.27}$$

If the spring force (i.e. $K(u_3 - u_1(L,t))$) is less than the dry friction element force, f_D, the drill rod will only experience visco-elastic motion, thus the permanent penetration, u_3, is

equal to zero. Once the internal spring force reaches the threshold force, f_D, permanent penetration, u_3, occurs and the bottom end of the drill rod moves with the same velocity as the friction element (i.e. $\dot{u}_1(L,t) = \dot{u}_3$). The equation of motion of the drill rod during this stage is given by:

$$m_1\ddot{u}_1(x,t) + c\dot{u}_1(L,t) = P(0,t) - f_D \tag{5.28}$$

The permanent penetration, u_3, will continue until the forces opposing the motion (i.e. f_D, damping force, and inertial force) cause a change in the direction of motion. The permanent penetration, u_3, is only allowed to move downward; therefore a change in the direction of motion means a stop in the penetration. After penetration stops, Eqn. (5.27) applies and the drill rod will oscillate with respect to the penetrated position.

5.2 Longitudinal Impact of a Mass on a Rod

The longitudinal impact of a spherical striker on a rod is analyzed using Hertz theory of contact as described in Chapter 3. Therefore the force-indentation relation is given by (Hertz 1881):

$$P = k_2\alpha^{3/2} \tag{5.29}$$

where k_2 is the contact stiffness given by (Goldsmith 2001):

$$k_2 = \frac{4}{3}E^*R^{*1/2} \tag{5.30}$$

The effective Young's modulus (E^*) and the effective radius (R^*) are given by (Goldsmith 2001; Vu-Quoc and Zhang 1999):

$$E^* = \left[\frac{1-\nu_1^2}{E_1} + \frac{1-\nu_2^2}{E_2}\right]^{-1} \tag{5.31}$$

$$R^* = \left[\frac{1}{R_1} + \frac{1}{R_2}\right]^{-1} \tag{5.32}$$

where E is the Young's modulus, v is the Poisson's ratio, R is the radius of the contact surface, and the subscripts 1 and 2 correspond to body 1 (rod) and body 2 (striker), respectively. For a sphere of radius R_2 striking a flat ended rod ($R_1 = \infty$), the effective radius is $R^* = R_2$. Timoshenko's (1913) approach is used to determine the indentation due to impact of the striker and the drill rod. The displacement of each body (striker and rod) due to the applied force $P(0,t)$ is determined. The indentation α is given by the difference in the displacement, u_2, of the striker and the displacement, $u_1(0,t)$, of the top end of the rod. Thus,

$$\alpha = u_2 - u_1(0,t) \tag{5.33}$$

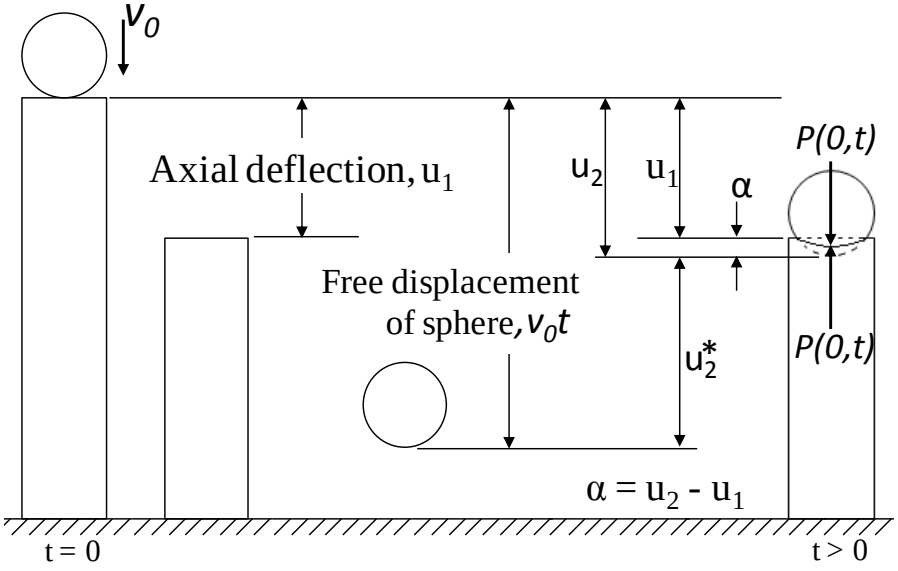

Fig. 5.4: Schematic of Timoshenko's approach to determine the indentation for two elastic bodies in contact.

Fig. 5.4 shows a spherical mass, with an initial velocity v_0, striking a rod with on the free end. The position of the striker and the rod are obtained separately by dynamic analysis of each body subjected to force (contact force) $P(0,t)$. The equation of motion of the striker (neglecting the gravitational acceleration) subjected to the contact force $P(0,t)$ is given by:

$$m_2 \frac{d^2 u_2}{dt^2} + P(0,t) = 0 \tag{5.34a}$$

From which by integration, the position of the striker is given by (see Fig. 5.4):

$$u_2 = v_0 t - \frac{1}{m_2} \int_0^t dt \int_0^t P(0,t)\, dt = v_0 t - u_2^* \tag{5.34b}$$

where $u_2^* = \frac{1}{m_2} \int_0^t dt \int_0^t P(0,t)\, dt$. The axial vibration displacement of the rod is obtained by applying the finite element method. Finally, the contact force *P(0,t)* is obtained from Eqn. (5.29) as:

$$P(0,t) = k_2 [u_2 - u_1(0,t)]^{3/2} \tag{5.35}$$

The procedure to obtain the contact force and the response of the rod and the striker is presented in Chapter 3.

5.3 Methodology

A steel rod with 1.91 cm diameter and 40 cm length is considered. The impactor/striker is taken as a steel sphere with a diameter of 2.54 cm. The geometric and material properties of the rod and the striker shown in Table 5.1 (Vila and Malla 2014), where *v* is the Poisson's ratio and $v_{2,0}$ is the initial velocity of the striker, were used for all cases unless otherwise specified.

5.3.1 Dynamic Response by Finite Element Method (FEM)

An in-house finite element model (FEM) was coded in MATLAB (2010) to solve the non-linear problem of the longitudinal impact of a mass on a rod. The rod was modeled by

50 bar elements (Cook et al. 2002). The undamped equation of motion of the entire rod can be written in matrix form as (Clough and Penzien 1975; Tedesco et al. 1999):

$$[\boldsymbol{M}]\{\ddot{u}_1\} + [\boldsymbol{K}]\{u_1\} = \{P\} \tag{5.36}$$

where **[*M*]** is the global mass matrix, **[*K*]** is the global stiffness matrix, $\{P\}$ is the externally applied dynamic load vector, and $\{\ddot{u}_1\}$ and $\{u_1\}$ are the acceleration and displacement vectors, respectively. The equation of motion of the striker (neglecting the gravitational acceleration) subjected to the contact force *P(0,t)* is given by is given by:

$$m_2\ddot{u}_2 + P = 0 \tag{5.37}$$

The dynamic load vector, *{P}*, (containing the contact force) is nonlinear and depends on the response of the rod and the striker, which in turn depend on the contact force. The response of the rod and the striker are obtained from step-by-step integration using the Newmark average acceleration method. The detailed process of the numerical simulation and the equilibrium iterations to find the contact force is discussed in Chapter 3.

5.4 Results and Discussion

The theory presented above is applicable to an elastic impact. It is common in the longitudinal impact of a drill/pile/rod to have an anvil of material with a higher yield strength on top of the rod where the impact takes place causing the impact to remain elastic (Tavares 1999). This is also verified by King and Bourgeois (1993).

5.4.1 Verification of Natural Frequencies

To verify that the finite element model correctly represents the system studied, the natural frequencies obtained from the analytical formulation presented in previous sections

are compared to that obtained from the finite element model using a numerical eigenvalue solver.

Table 5.1: Geometric and material Properties of the striker and the rod

Rod Properties		
Area	0.000285	m^2
E_1	209	GPa
ν_1	0.3	-
L	0.4	m
Density, ρ_1	7788.6	kg/m^3
c	5180	m/s
Striker Properties		
m_2	0.06705	kg
E_2	203	GPa
ν_2	0.3	-
Radius, R_2	12.7	mm
Density, ρ_2	7800	kg/m^3
$v_{2,0}$	0.77	m/s

5.4.2 Rod with Viscous Support

The imaginary and the real component of the natural frequencies for the rod with viscous support are shown in Fig. 5.5 for the first 10 modes. It is observed that the numerical imaginary component agrees very well with the exact value for all modes shown. The numerical real component matches very well with the exact value for the first mode, then it deviates from the exact solution as the mode number increases. The largest difference (for mode 10) is about 0.8 % (≈ 20 rad/sec). The percent error of the real and imaginary components are shown in Fig. 5.6. It is observed that even though a difference of up to 20 rad/sec. is seen in the real component, the percent error for both, the real and the imaginary components, is still below 1 percent. Therefore, we conclude that the finite element model represents correctly the rod with viscous support.

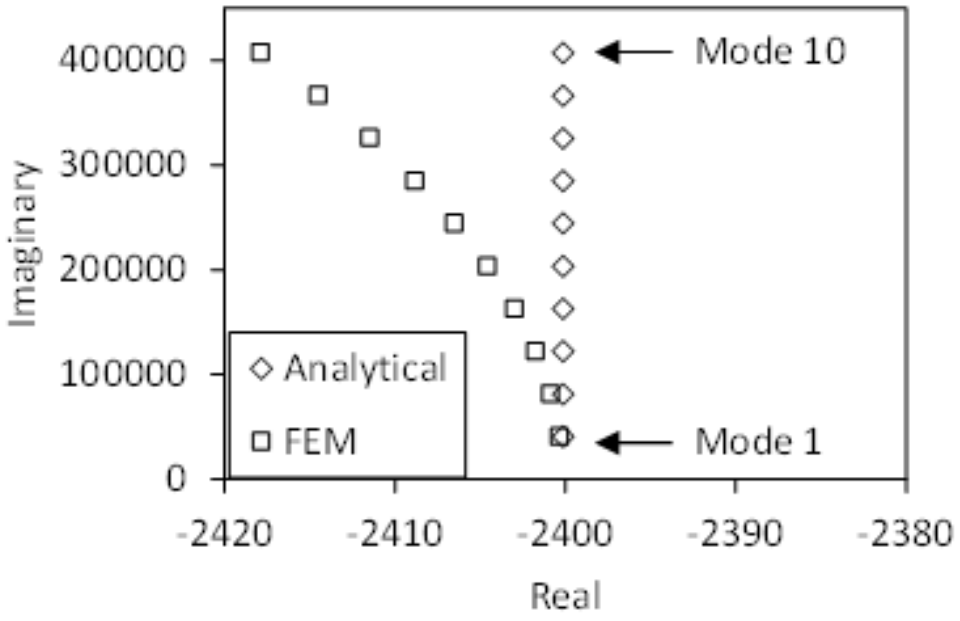

Fig. 5.5: Analytical and numerical imaginary and real component of the natural frequencies for the rod with viscous support.

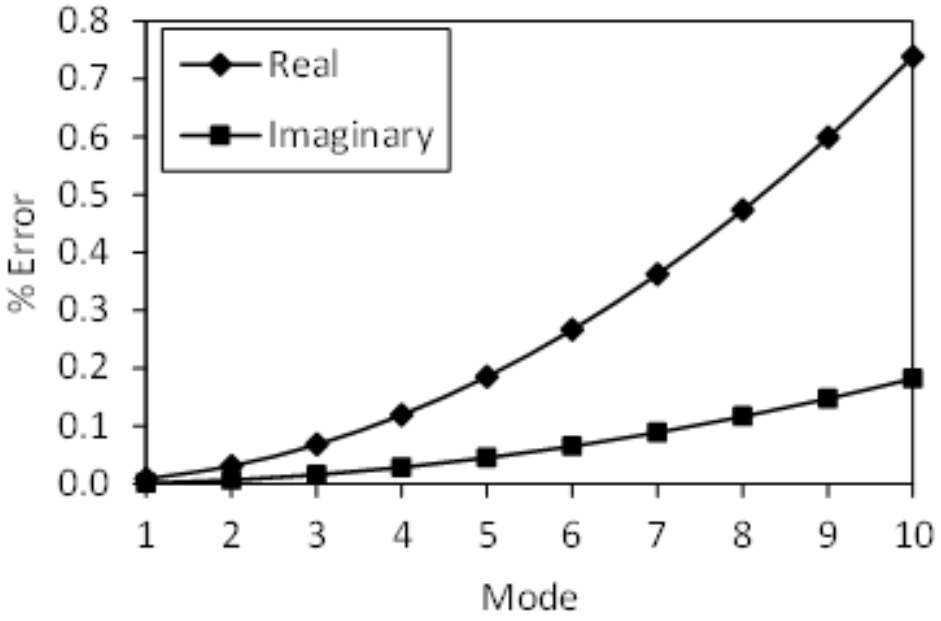

Fig. 5.6: Percentage error of the natural frequencies for a rod with viscous support.

5.4.3 Impact Simulation of Rod with Viscous Support

The contact force and the response of the drill rod and the striker for the case of the rod with viscous support is shown in Fig. 5.7 for a damping ratio (for the external damper) equal to 0.5. It is observed that the contact force curve shows the typical smooth sinusoidal like shape. The contact force is present while the displacement, u_2, of the striker is greater than the displacement, $u_1(0,t)$, of the top end of the rod (i.e. $\alpha = u_2 - u_1(0,t) > 0$). The contact force vanishes when the displacement of the striker becomes less than the displacement of the rod, which happens at $t = 97$ μsec.

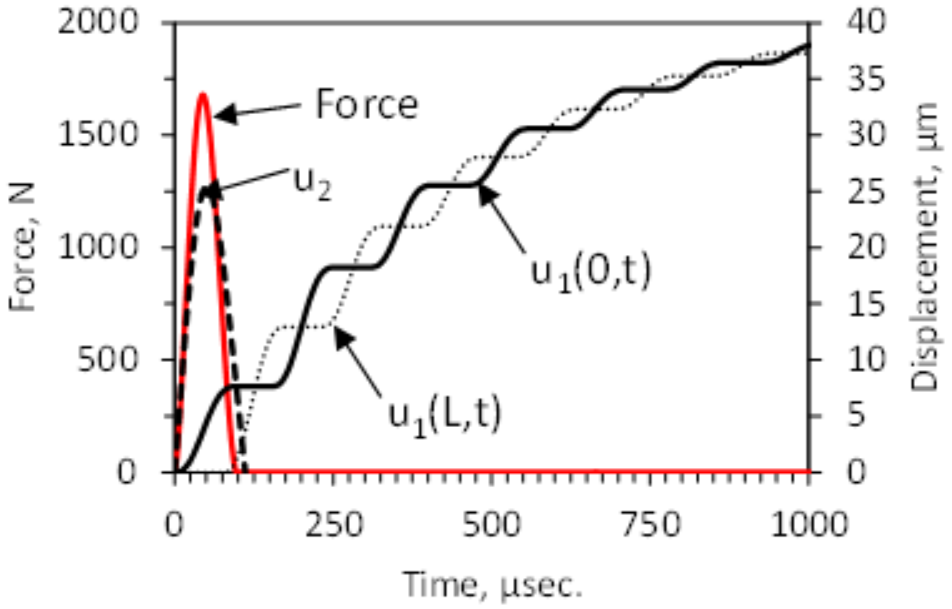

Fig. 5.7: Force and displacement time history for the rod with viscous support. ($\zeta = 0.5$)

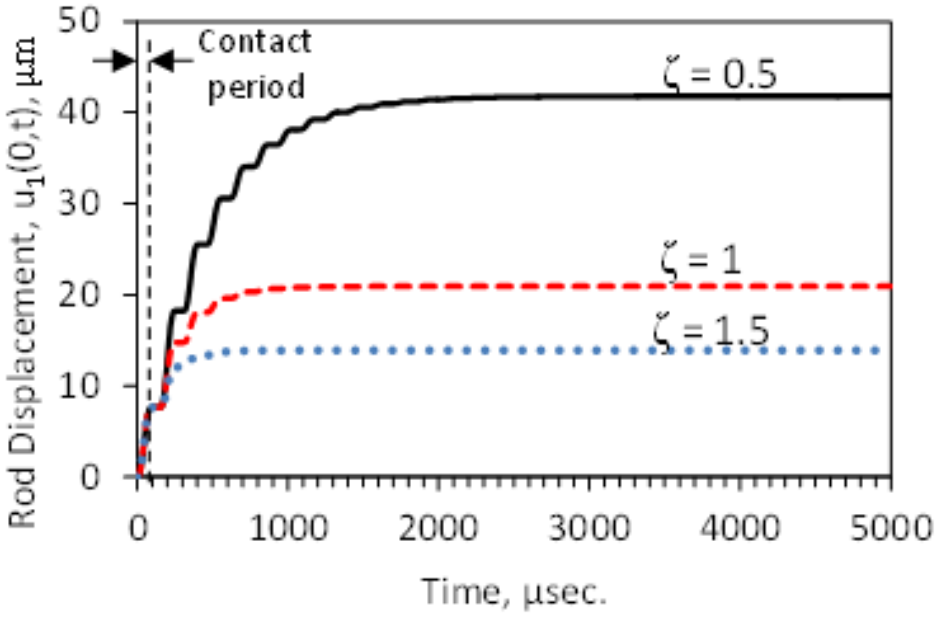

Fig. 5.8: Response of the rod with viscous support for different damping ratios.

The impact simulation was run for damping ratios of $\zeta = 1$ and $\zeta = 1.5$. It was observed that the contact force was the same for all damping ratios. Fig. 5.8 shows the response of the rod for all damping ratios considered (i.e. $\zeta = 0.5$, 1, and 1.5). It is observed that the response of the rod during the short duration of impact is the same for all damping ratio.

Therefore, since the contact force depends on the response of the rod (and the striker), the force is the same for all damping ratios. This is consistent with the results shown in previous chapters in which it was found that the contact force is not affected by the support condition of the rod if the duration, τ, of contact is less than the time, $t_a = 2L/c$, it takes the reflected wave to travel through the rod and return to the contact end. For the present case, the duration of contact $\tau = 97$ μsec. while the time of arrival of the reflected wave $t_a = 154.4$ μsec.

To verify the effect of the support condition the impact of the striker on a shorter rod (L = 0.05 m) is analyzed. The contact force obtained for all three damping ratios is shown in Fig. 5.9. In this case the duration of contact is larger than the time of arrival (t_a = 19.3 μsec.). It is observed that even though the reflected wave arrives early in the contact period, and the force is affected by the damping ratio, the difference in the contact force for each damping ratio is very small.

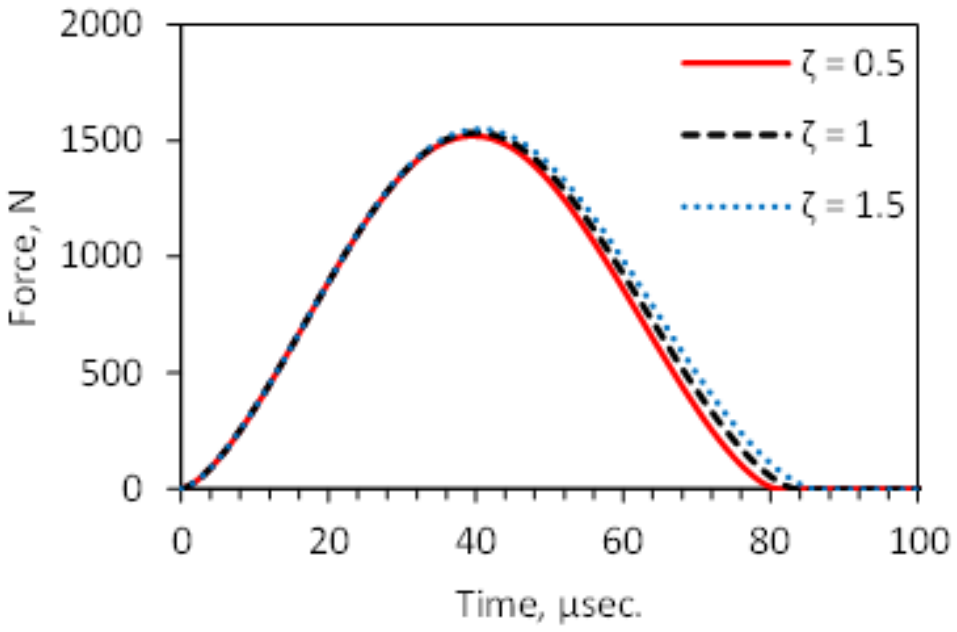

Fig. 5.9: Contact force for a shorter rod (L = 0.05 m) with viscous support for different damping ratios.

5.4.4 Impact Simulation of Rod with Visco-elastic Support

The rod with visco-elastic support is analogous to a drill rod supported by a visco-elastic medium where the elastic resistance of the supporting medium is represented by the external spring. Similar to previous chapters, the stiffness of the spring is selected as $K_1 = 5 * 10^6\ N/m$. The damping ratios (ζ = 0.5, 1, 1.5) are selected to cover underdamped, critically damped, and overdamped cases. The contact force and the response of the drill rod and the striker for the case of the rod with viscoelastic support is shown in Fig. 5.10 for a damping ratio $\zeta = 0.5$.

It is observed that the contact force curve is similar to that of the rod with viscous support. Similar to the rod with viscous support it is observed that the contact force is the same for all damping ratios since the duration of contact is less than the time of arrival of the reflected wave. Fig. 5..11 shows the response of the rod with viscoelastic support for different damping ratios. Similarly, it is observed that although the response of the rod is different for each damping ratio, this difference occurs after the contact has ended. Therefore the contact force remains same for all damping ratios. To see the effect of the damping ratio on the contact force for the viscoelastic support the analysis was performed with the shorter rod (L = 0.05 m). It was observed that the results followed those obtained for the viscous support, i.e. the difference in the contact force with the damping ratio is very small.

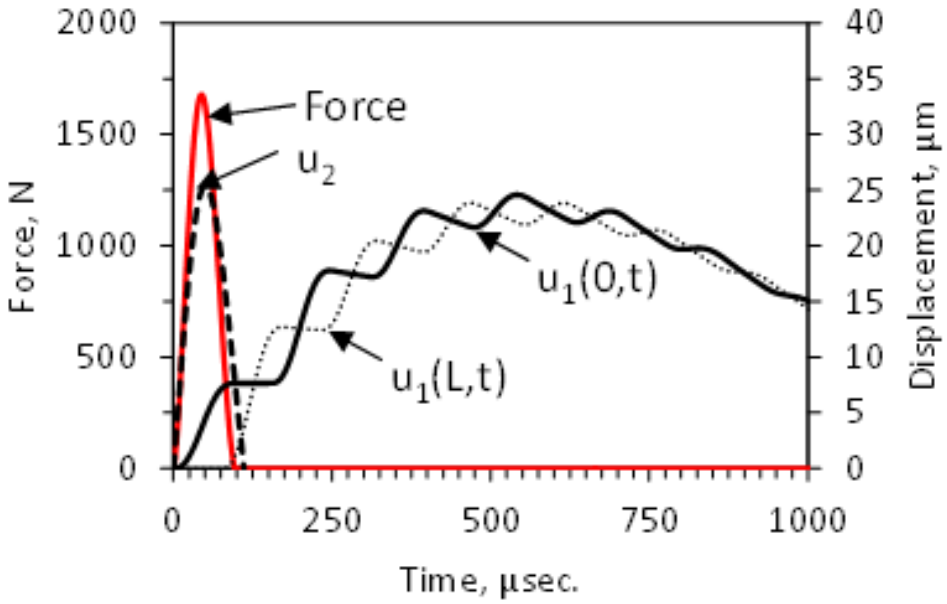

Fig. 5.10: Force and displacement time history for the rod with viscoelastic support. ($\zeta = 0.5$)

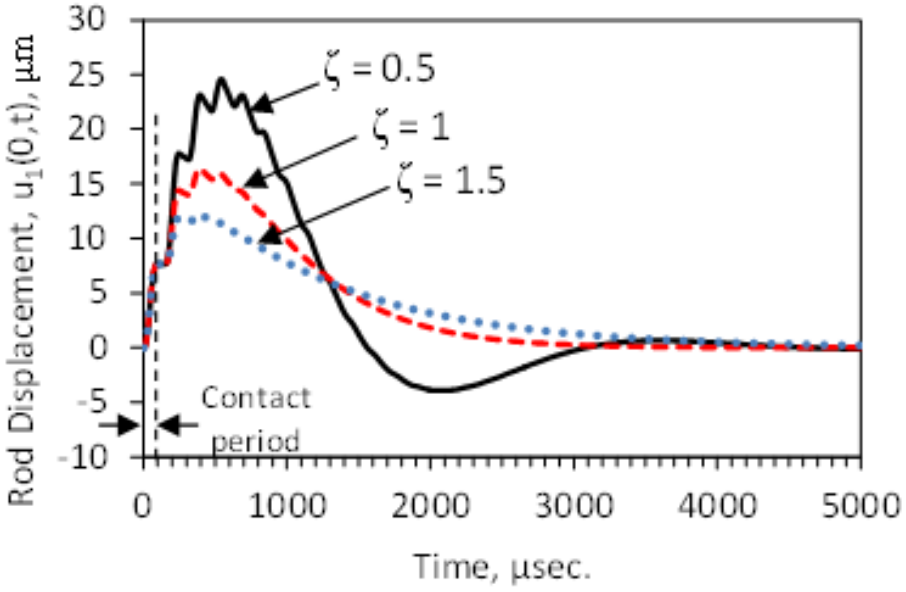

Fig. 5.11: Response of the rod with viscoelastic support for different damping ratios.

5.4.5 Impact Simulation of Rod with Visco-elasto-plastic Support

The contact force and the response of the drill rod and the striker for the case of the rod with visco-elasto-plastic support is shown in Fig. 5.12 for a damping ratio $\zeta = 0.5$ and a friction threshold value of $f_D = 100$ N. The contact force is observed to be similar to the previous cases presented. Fig. 5.13 shows the response of the rod with visco-elasto-plastic support for different damping ratios.

The observations made for the rod with viscous support and the rod with viscoelastic support remain true (i.e. response of the rod is the same for all damping ratios during the short duration of contact). However, in this case it is important to note that the penetration of the rod is affected by the damping ratio. For the damping ratio $\zeta = 0.5$ it is observed that a total penetration of 3.25 μm is achieved, whereas no penetration is observed to a damping ratio of 1 and 1.5.

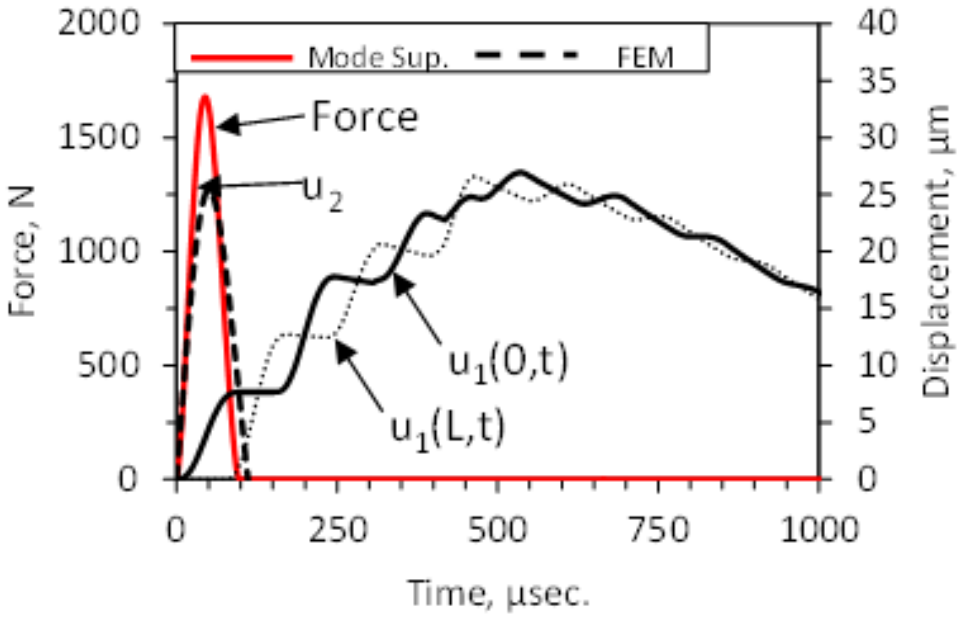

Fig. 5.12: Force and displacement time history for the rod with visco-elasto-plastic support. ($\zeta = 0.5$)

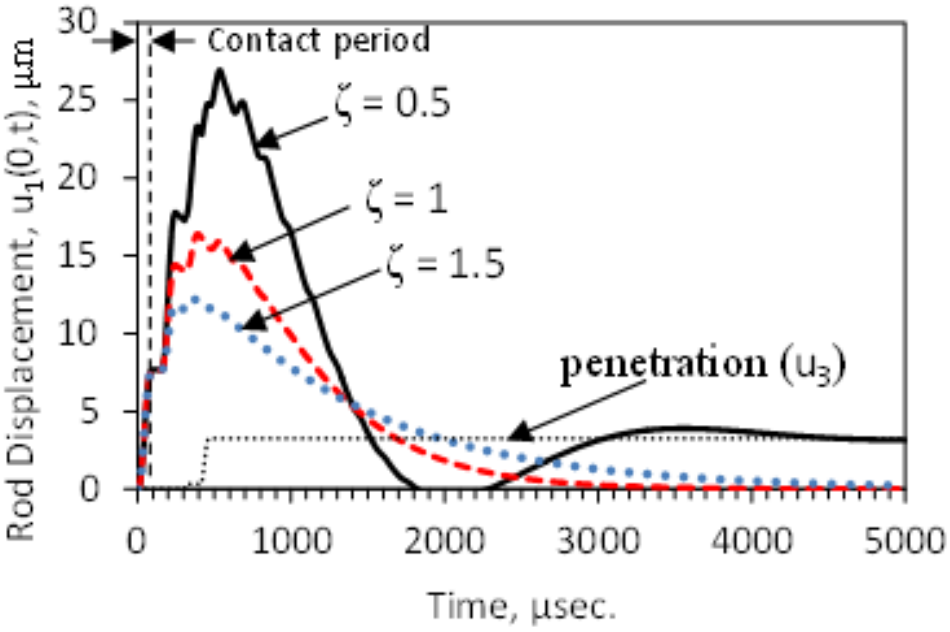

Fig. 5.13: Response of the rod with visco-elasto-plastic support for different damping ratios.

Fig. 5.14 shows the external spring force for all damping ratios. The friction threshold (f_D = 100 N) force is represented by the horizontal dotted line. It is observed that for ζ = 0.5 penetration occurs while the spring force equals the friction threshold force. For the damping ratios of ζ = 1 and ζ = 1.5 the friction threshold is not reached and no penetration is observed. The impact of the striker was analyzed on a shorter rod (L = 0.05 m) and the contact force was observed to differ slightly with the damping ratio. In the case of the shorter rod it was also observed that the friction threshold force was reached for ζ = 0.5 and ζ = 1.

The visco-elasto-plastic support has another scenario in which the contact force could be affected by the support condition. That is, if penetration begins before the end of contact, the contact force is affected. Consider the case of a rod supported by a material with a lower bearing capacity (represented by a lower friction threshold force). The response of the rod of length L = 0.05 m to the impact of the striker is shown in Fig. 5.15 for two friction

threshold values (i.e. f_D = 100 N, and f_D = 25 N). It is observed that the model with the lower friction threshold (f_D = 25 N) experiences a larger penetration. A higher penetration compared to the model with the friction threshold of f_D = 100 N is expected, since the bearing capacity of the supporting medium has been reduced. More important, it is observed that for the model with the lower friction threshold, penetration begins before the end of contact, therefore the contact force is affected by penetration.

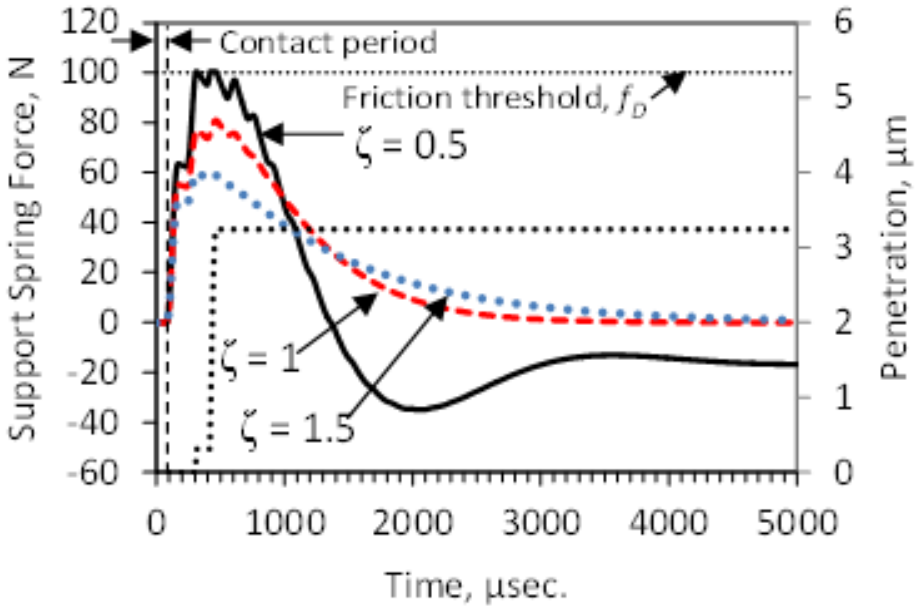

Fig. 5.14: External spring force and penetration for the rod with visco-elasto-plastic support for different damping ratios.

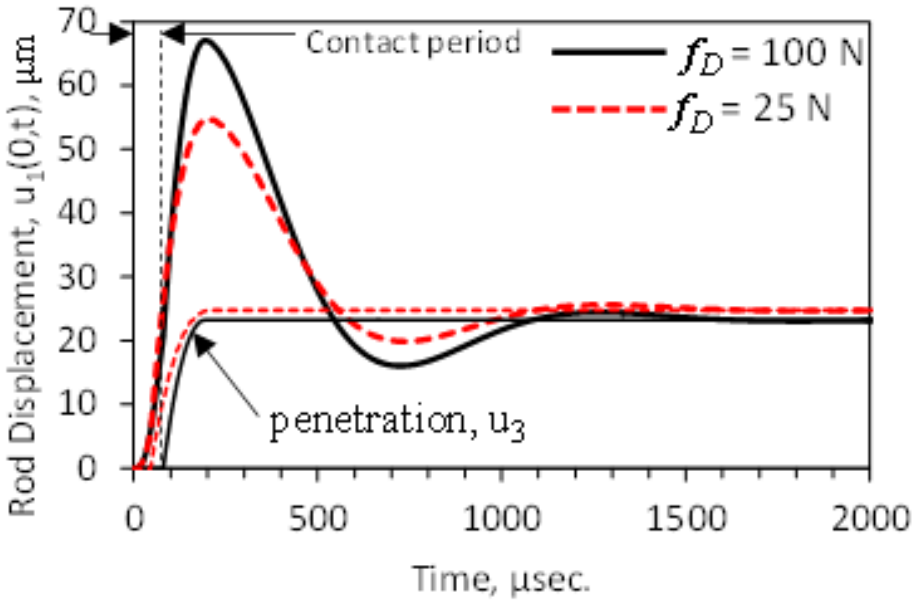

Fig. 5.15: Response and penetration of the rod (L = 0.05 m) with visco-elasto-plastic support for two friction threshold force values.

The contact force time history for both cases (f_D = 100 N and f_D = 25 N) is shown in Fig. 5.16. It is observed that the contact force is the same for both cases until t = 47 µsec. At that point, the rod on the supporting medium with lower bearing capacity starts penetrating and a difference in the contact force is observed. Specifically, it is observed that the force (shown with a dashed curve) decreases at a higher rate for the model with penetration during contact, compared to the force (shown with a solid line) where penetration is not present during contact. This is because the force depends on the indentation ($\propto = u_2 - u_1(0,t)$), or relative position of the sphere and the top of the rod. When penetration of occurs, the displacement of the top of the rod (during contact) is larger than when there is no penetration, which results in a lower indentation (α) , hence a lower force is observed.

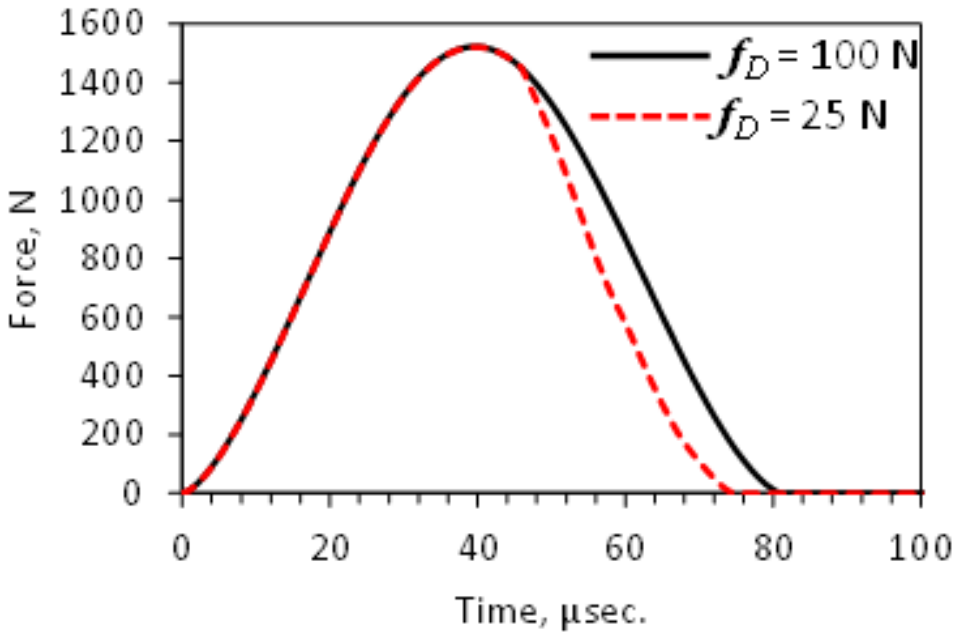

Fig. 5.16: Contact force for the rod (L = 0.05 m) with visco-elasto-plastic support for two friction threshold force values.

5.5.5 Comparison between support conditions

The results presented above analyze the effect of the damping ratio and friction threshold force on the contact force. Here the contact force and response of the rod for all the support conditions studied are compared. As it has been discussed, for the rod of length L = 0.4 m the duration of contact is less than the time of arrival of the reflected wave. Therefore the contact force for all the support conditions analyzed is the identical force curve shown in Fig. 5.7. The response of the rod for all support conditions is shown in Fig. 5.17. The response of the rod with viscous, viscoelastic and visco-elasto-plastic supports shown correspond to a damping ratio of ζ = 1.5. It is observed that regardless of the boundary condition the response of the rod is the same during the short duration of the contact period.

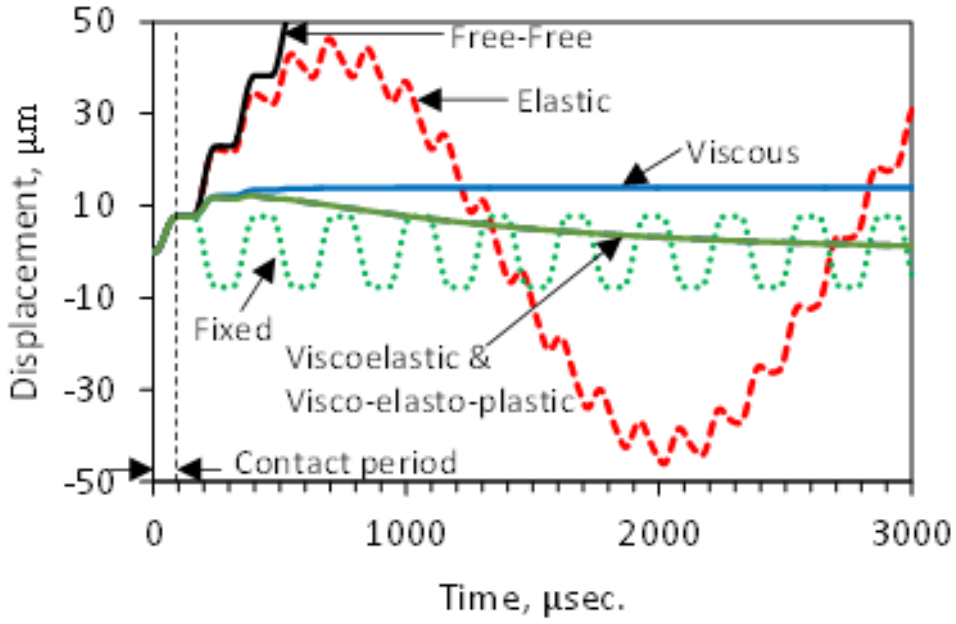

Fig. 5.17: Response of the rod (L = 0.4 m) for all support conditions considered (ζ = 1.5).

The contact force for all support conditions for a shorter rod (L = 0.05 m) in which the duration of contact is larger than the time of arrival of the reflected wave is shown in Fig. 5.18. Similarly a damping ratio of ζ = 1.5 was used. It is observed that the contact force is affected by the support conditions. Specifically, a 25 percent difference in the magnitude is observed between the force on the rod with fixed support and the rod with elastic and free supports; the rod with fixed support showing the largest force. The magnitude of the contact force obtained for the rod with viscous, viscoelastic, and visco-elasto-plastic is observed to be the same, with a magnitude and a duration slightly larger than the rod with elastic and free supports.

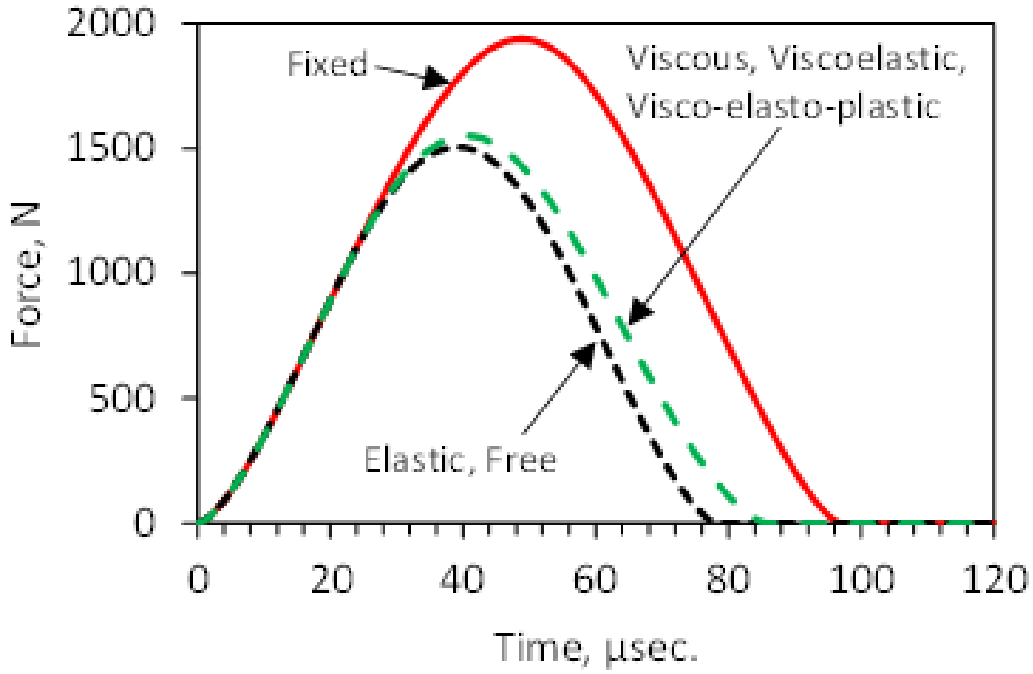

Fig. 5.18: Contact force time history for different support conditions. ($\zeta = 1.5$)

Fig. 5.19 shows the response of the rod for all support conditions studied. It is observed that the response of the rod is different during the contact period. An inset of Fig. 5.19 is shown in Fig 5.20. It is observed that the response of the rod with viscous, viscoelastic, and visco-elasto-plastic supports is the same during the duration of impact even though the duration of contact is larger than the time of arrival of the reflected wave. Similar observation was found for the rod with elastic and free supports. Finally, the response of the rod with fixed support during the contact period is observed significantly different than for the other support conditions, resulting in the different contact force shown in Fig. 5.18.

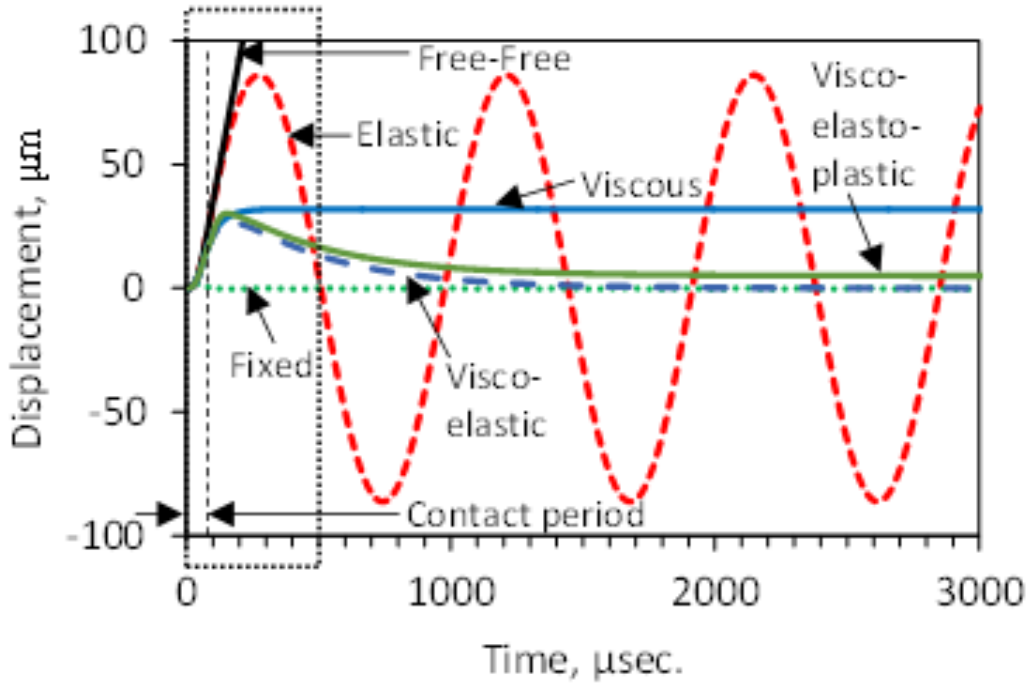

Fig. 5.19: Response of the rod (L = 0.5 m) for all support conditions considered. (ζ = 1.5)

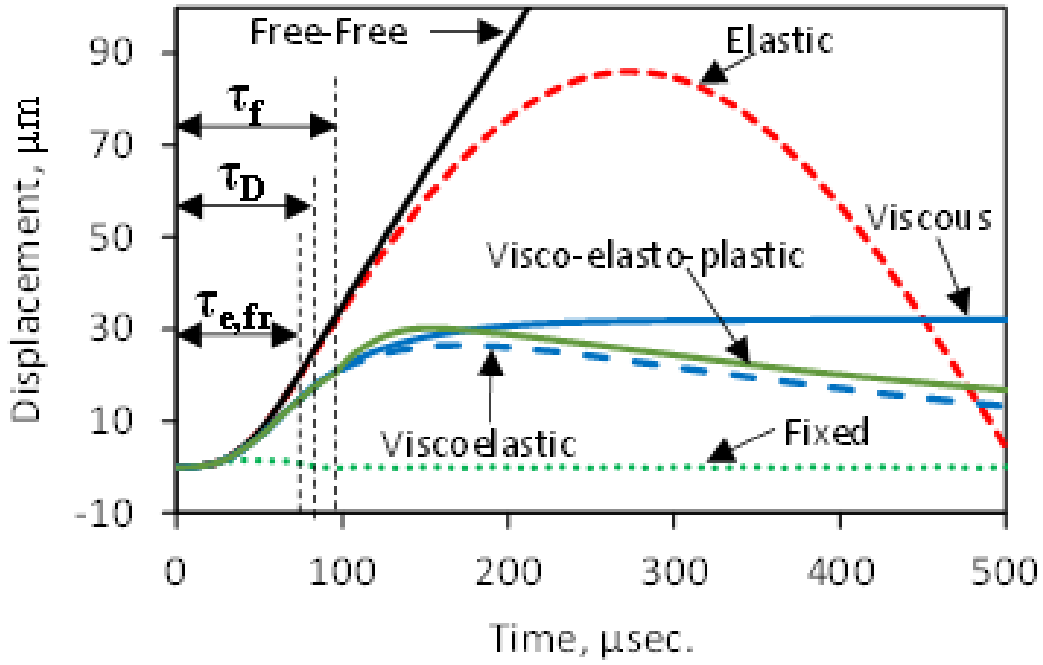

Fig. 5.20: Inset of the response of the rod for all support conditions. (L = 0.05 m) (ζ = 1.5).

5.5 Conclusions

The dynamic response of longitudinal impact of a mass on one end of a uniform rod with different support conditions, e. g. viscous, viscoelastic, and visco-elasto-plastic was analyzed using Hertz theory of contact. The contact force and the rod response were obtained using an in-house finite element code. The response of the rod and the contact force for each support condition, including rigid, free, and elastic supports analyzed in previous chapters were compared and the conditions under which the support condition of the rod affects the contact force were discussed. Based on the results obtained from the present study, the following conclusions can be made:

- Similarly to the results found in previous chapters the effect of the boundary condition of the supporting end of the rod (i.e. viscous, viscoelastic or visco-elasto-plastic support) on the contact force between the striker and the top of the rod is not present if the duration of contact is less than the time it takes the displacement wave to travel through the rod and return to the contact end (time of arrival, t_a).
- When the duration of contact is larger than the time of arrival of the reflected wave the contact force is only slightly affected by the damping ratio of the support viscous damper.
- If the duration of contact is larger than the time of arrival of the reflected wave the contact force is significantly different between rigid and deformable (i.e. elastic, free, viscous, viscoelastic, and visco-elasto-plastic) supports. The contact force does not seem to be significantly affected by different types of deformable supports.
- If the duration, τ, of contact is less than the time of arrival, t_a, the contact force is not affected by the boundary condition on the bottom of the rod and a more simple analysis

such as the one presented by Volterra and Zachmanoglou (1965) may be performed with reasonably accurate results.

- When drill rod penetration is considered (i.e. visco-elasto-plastic support), there are two possible cases in regard to the contact force. First, the contact may cease before penetration begins. In this case the force would not be affected by penetration. Second, drill bit penetration may begin while the contact is still present. In such case the contact force will decrease at a higher rate compared to the case where penetration is not present during contact.
- If a supporting medium with lower bearing capacity is considered, the overall response of the rod is different and as expected, a larger penetration is reached (compared to the same system on a supporting with a higher bearing capacity).

Chapter 6

Impact Force Including Plastic Deformation

In previous chapters the presence of an anvil of a material with a higher yield strength on the top end of the rod was assumed. This caused the impact to remain elastic. In this chapter this assumption is no longer used. The impact of a spherical striker on a rod is analyzed and the contact force, including plastic deformation of the rod, is obtained using a modified Hertz theory. Furthermore, repetitive identical impacts are considered to study the effect of the history of the plastic deformation of the rod on the contact force.

6.1 Elastic Contact

Consider a spherical mass striking a uniform cantilever rod as shown in Fig. 6.1. The force generated between the striker and the top of the rod acts in a very small area where the two bodies (i.e. the striker and the rod) are in contact. This leads to high stresses that may exceed the material yield strength. Therefore, when modeling the impact of the sphere on the rod, the plastic deformation of the rod due to impact of the striker should be taken into account. For this purpose, the rod is considered as an elastic-perfectly plastic material. During the elastic loading phase the total (elastic) contact force, P_e, acting over the circular contact area of radius a is obtained from the well-known Hertz force-indentation relation given by (Goldsmith 2001; Hertz 1881):

$$P_e = k_H \alpha^{3/2} \tag{6.1}$$

where α is the local indentation and k_H is the Hertz contact stiffness given by (Goldsmith 2001):

$$k_H = \frac{4}{3} E^* R^{*1/2} \tag{6.2}$$

The effective Young's modulus (E^*) and the effective radius (R^*) are given by (Goldsmith 2001; Thornton and Ning 1998; Vu-Quoc and Zhang 1999; Wojtkowski et al. 2010):

$$E^* = \left[\frac{1 - \nu_1^2}{E_1} + \frac{1 - \nu_2^2}{E_2} \right]^{-1} \tag{6.3}$$

$$R^* = \left[\frac{1}{R_1} + \frac{1}{R_2} \right]^{-1} \tag{6.4}$$

where E is the Young's modulus, ν is the Poisson's ratio, R is the radius of the contact surface, and the subscripts 1 and 2 correspond to body 1 (rod) and body 2 (striker), respectively.

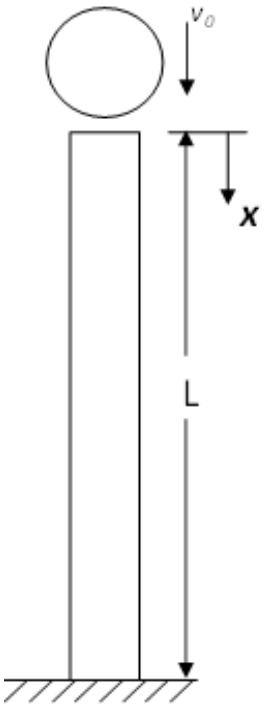

Fig. 6.1: Uniform cantilever rod struck by a spherical mass with initial velocity v_0.

For a sphere of radius R_2 striking a flat ended rod ($R_1 = \infty$), the effective radius is $R^* = R_2$. When the two bodies are compressed onto each other a circular contact area of radius a

and a compressive pressure *p* develops. The radius of the contact area and the compressive pressure acting on it are given by (Goldsmith 2001; Thornton and Ning 1998; Wojtkowski et al. 2010):

$$a^2 = R^* \alpha \tag{6.5}$$

$$a = \left(\frac{3PR^*}{4E^*}\right)^{1/3} \tag{6.6}$$

$$p(r) = \frac{3P}{2\pi a^2}\left[1 - \left(\frac{r}{a}\right)^2\right]^{1/2} \tag{6.7}$$

where *F* is the total force acting over the contact area. The distribution of the stress over the contact area is shown in Fig. 6.2. The maximum pressure, p_0, occurs in the center of the contact area (i.e. $r = 0$) and the pressure vanishes when $r = a$.

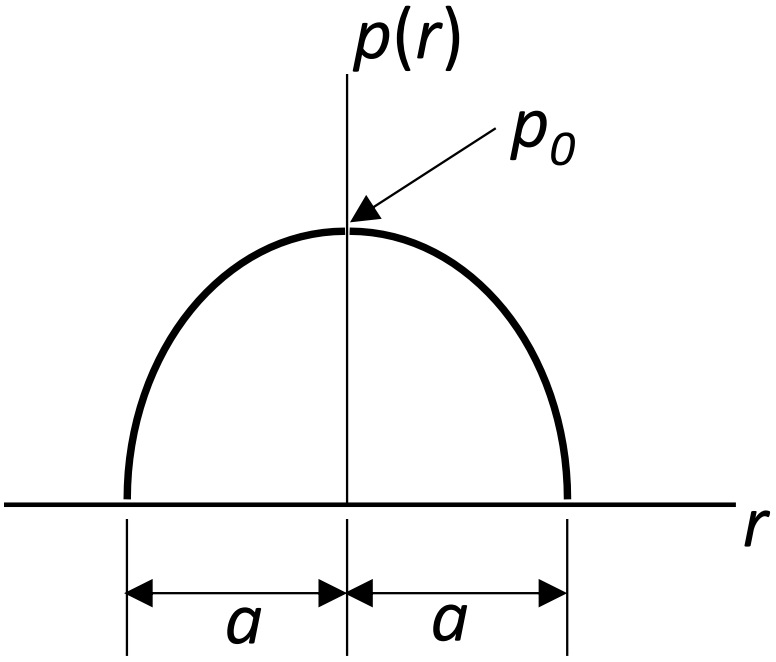

Fig. 6.2: Stress distribution over the elastic contact area of radius *a*.

6.2 Plastic Yielding

When the maximum stress exceeds the yielding strength of the material, plastic deformation initiates. Letting $r = 0$ and $P = P_Y$ in Eqn. (6.7), the yielding pressure can be expressed as (Wojtkowski et al. 2010):

$$p_Y = \frac{3P_Y}{2\pi a_Y^2} \tag{6.8}$$

The radius corresponding to yield initiation can be obtained from Eqns. (6.1), (6.2), (6.5) and (6.8). Substituting Eqns. (6.2) and (6.5) (with $a = a_Y$ and $\alpha = \alpha_Y$) into Eqn. (6.1) we obtain:

$$P_Y = \frac{4a_Y^3 E^*}{3R^*} \tag{6.9}$$

Finally, substituting Eqn. (6.9) into Eqn. (6.8) and solving for a_Y we obtain:

$$a_Y = \frac{R^* \pi p_Y}{2E^*} \tag{6.10}$$

The radius, a_Y, of the contact area corresponding to yield initiation can be related to the local indentation, α_Y, indicating initiation of yielding by using Eqn. (6.5). Thus we obtain (Wojtkowski et al. 2010):

$$\alpha_Y = R^* \left(\frac{\pi p_Y}{2E^*}\right)^2 \tag{6.11}$$

When yielding occurs the contact force is the sum of the elastic force (corresponding to the elastic contact area, A_e) and the plastic force (corresponding to the plastic contact area, A_p) (Wojtkowski et al. 2010). Therefore, the total force, P, can be expressed by:

$$P = P_e + P_p \tag{6.12}$$

During plastic deformation the elastic force, P_e, is given by Eqn. (6.1) with $\alpha = \alpha_Y$. The plastic force is obtained multiplying the plastic contact area ($A_p = \pi a_p^2$)) by the yield pressure p_Y. Thus the total force during plastic deformation is given by:

$$P = k_H \alpha_Y^{3/2} + p_Y \pi a_p^2 \tag{6.13}$$

From Eqn. (6.8) and Eqn. (6.7), noting from Fig. 6.3 (Thornton and Ning 1998) that the maximum elastic stress is equal to the yield pressure (i.e. $p(a_p) = p_Y$), we obtain:

$$p_Y = \frac{3P_Y}{2\pi a_Y^2} = \frac{3P_e}{2\pi a^2}\left[1 - \left(\frac{a_p}{a}\right)^2\right]^{1/2} \tag{6.14}$$

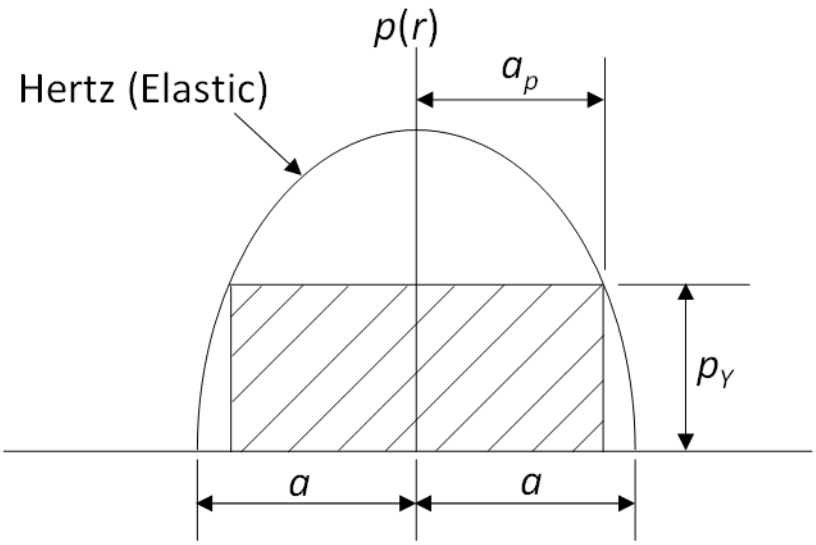

Fig. 6.3: Pressure distribution over the elastic-perfectly plastic circular contact area of radius a (Thornton and Ning 1998).

Noting that Eqn. (6.6) can be solved for P_e and P_Y (with $a = a$ and $a = a_Y$, respectively) and substituting into Eqn. (6.14) we obtain:

$$a_p^2 = a^2 - a_Y^2 \tag{6.15}$$

Therefore, Eqn. (6.13) can be expressed as (Wojtkowski et al. 2010):

$$P = k_H \alpha_Y^{3/2} + \sigma_Y \pi (a^2 - a_Y^2) \tag{6.16}$$

or (substituting Eqn. (6.5) into Eqn. (6.16))

$$P = k_H \alpha_Y^{3/2} + \sigma_Y \pi R^* (\alpha - \alpha_Y) \tag{6.17}$$

During unloading the force-indentation relation is elastic (Cristescu 1967), therefore is in the same form as Eqn. (6.1). However due to plastic deformation a residual indentation (α_{res}) will remain in the rod when the contact force becomes equal to zero. The residual indentation can be obtained by subtracting the elastic indentation, $\alpha_e = (3/4) * P_{max}/(E^* R^{*1/2})$ (obtained from Eqn. (6.1)) corresponding to the actual maximum force, from the actual maximum indentation α_{max}. Therefore, the residual indentation, α_{res}, can be expressed as:

$$\alpha_{res} = \alpha_{max} - \left(\frac{3}{4}\frac{P_{max}}{E^* R^{*1/2}}\right)^{2/3} \tag{6.18}$$

The final expression for the elastic unloading, after plastic deformation occurs, is then given by:

$$P = k_H (\alpha - \alpha_{res})^{3/2} \tag{6.19}$$

The contact force will be present until the indentation α is equal to the residual indentation, α_{res}. The contact force for the impact of a spherical striker on a rod with elasto-plastic material properties can be summarized as shown in Eqn. (6.20). A graphical explanation of the impact process is shown in the Appendix B.

$$P = P_e + P_p = \begin{bmatrix} k_H \alpha^{3/2} & \alpha < \alpha_y \quad and\ \dot{\alpha} > 0 \\ k_H \alpha_y^{3/2} + p_y \pi R^* (\alpha - \alpha_y) & \alpha \geq \alpha_y \quad and\ \dot{\alpha} > 0 \\ k_H (\alpha - \alpha_{res})^{3/2} & \alpha \geq \alpha_{res}\ and\ \dot{\alpha} < 0 \\ 0 & \alpha < \alpha_{res}\ \ and\ \dot{\alpha} < 0 \end{bmatrix} \tag{6.20}$$

6.3 Repeated Impacts

In mechanical tools, such as percussive drills, the different components are subjected to multiple impacts. Therefore, it is of interest to understand how the parameters governing the contact phenomena (e.g. contact force, duration of contact) behave under repeated impacts. The formulation presented in Section 6.2 applies for the first impact as well as for subsequent impacts. As presented in Section 6.2, a residual indentation (α_{res}) will remain in the rod after the first impact. For the analysis of repeated impacts, the deformation history (i.e. residual indentation, α_{res}) of the rod due to previous impacts is used to analyze the subsequent impacts. Fig. 6.4 shows the local deformation and stress history of the rod for repeated impacts, where a_Y and a_p is the yielding radius and plastic radius, and the subscripts indicate the number of impact.

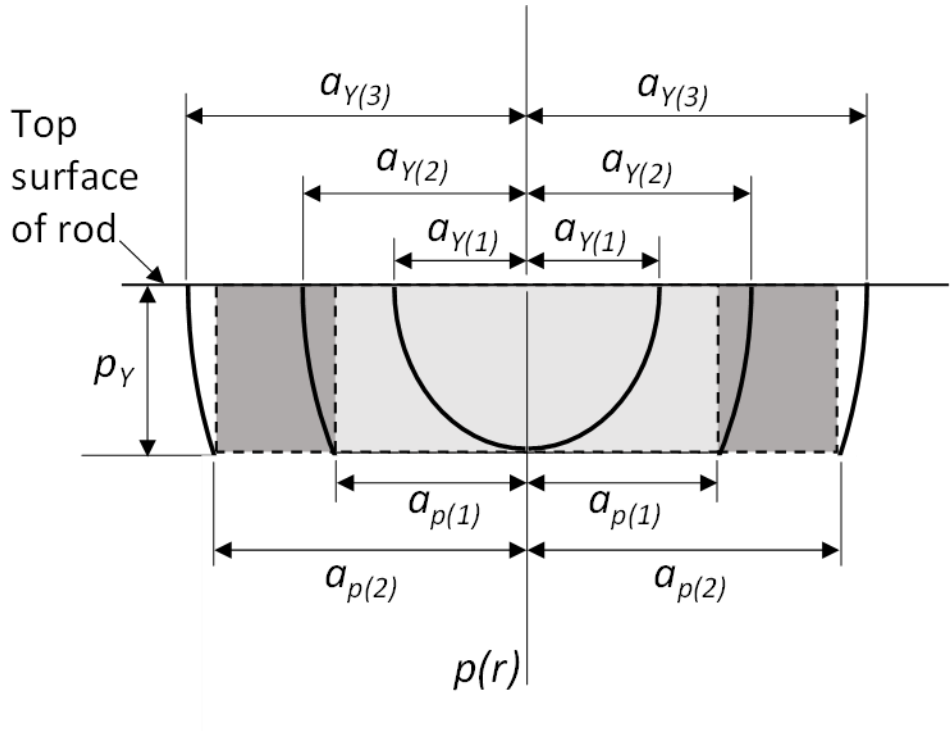

Fig. 6.4: Local contact area and pressure history of the rod during repeated impacts.

For the first impact, the initiation of yielding is governed by the yield radius, $a_{Y(1)}$, (Eqn. (6.10)). At the maximum indentation of the first impact (i.e. indentation when unloading begins) the contact area consists of a plastic area with radius $a_{p(1)}$ and an elastic area with radius $a_{Y(2)} - a_{p(1)}$ (see Fig. 6.4). For the second impact (on the fully unloaded rod) the loading will be elastic up to the previously strained point (Pytel and Kiusalaas 2011) (i.e. until the contact area is equal to the maximum contact area of the previous impact). Therefore, the yield radius ($a_{Y(2)}$) of the second impact is equal to the total radius corresponding to the maximum force of the previous impact. For example, for impact *i* ($i > 1$) the condition for yield initiation is governed by:

$$a_{(i)}^2 = a_{\max(i-1)}^2 \tag{6.21}$$

or (using the relation on Eqn. (6.15))

$$a_{(i)}^2 = a_{p(i-1)}^2 + a_{Y(i-1)}^2 \tag{6.22}$$

From Eqns. (6.5) and (6.15) we obtain the plastic radius as:

$$a_p^2 = R^*(\alpha_{max} - \alpha_Y) \tag{6.23}$$

Substituting Eqns. (6.5) and (6.23) into Eqn. (6.22) the yield initiation for repeated impacts (after the first impact) is governed by:

$$R^*\alpha_{(i)} = R^*\left[\alpha_{\max(i-1)} - \alpha_{Y(i-1)}\right] + R^*\alpha_{Y(i-1)} \tag{6.24}$$

or

$$\alpha_{(i)} = \alpha_{\max(i-1)} \tag{6.25}$$

Therefore, after the first impact, additional plastic deformation will occur when the indentation is equal to the maximum indentation of the previous impact (i.e. $\alpha_{Y(i)} = \alpha_{\max(i-1)}$). The force relations for subsequent impacts are the same as given in Eqn. (6.20). However, the corresponding $\alpha_{Y(i)}$ must be used. A qualitative force-indentation diagram

for the first two impacts is shown in Fig. 6.5. The loading and unloading curve of each impact is shown by an arrow next to the number of the impact. During the first impact a maximum indentation is reached at point A, where unloading then takes place. The loading curve for the second impact will follow the unloading curve of the first impact until the maximum indentation (point A in Fig. 6.5) of the first impact is reached (Schiehlen et al. 2006; Weir and Tallon 2005). After reaching point A, plastic deformation begins until elastic unloading begins (at point B). Similarly, the loading curve for the third impact follows the unloading curve of the second impact until the maximum indentation (point B in Fig. 6.5) of the second impact is reached.

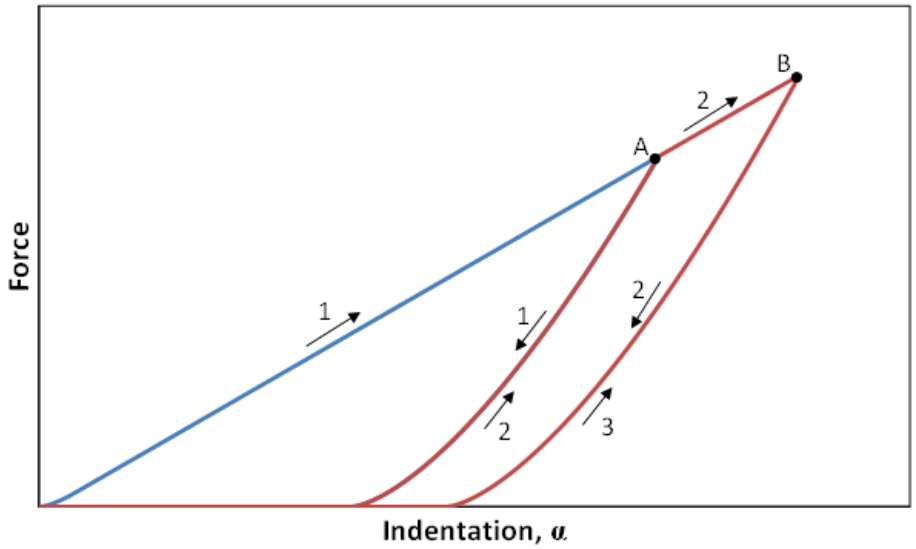

Fig. 6.5: Loading and unloading curves for repeated impacts of a mass on a rod with elasto-plastic material properties.

6.4 Results and Discussion

6.4.1 Single Impact

The formulation presented was used to analyze the longitudinal impact of a spherical striker on an elastic-perfectly plastic rod. The local indentation, α, is obtained using Timoshenko's (1913) approach as discussed in Chapter 3. The displacement of each body (striker and rod) due to the applied contact force *P(t)* is determined. The indentation α is given by the difference in the displacement of the striker and the displacement of the top end of the rod. The results shown in this section were obtained by an in-house finite element code written in MATLAB. Figure 6.6 shows the time history of the contact force for different yield strengths of the rod. It is observed that the amplitude of the force curve where plastic deformation occurs is less than that of the purely elastic case. On the contrary, the duration of contact is seen to increase with decreasing yield strength of the rod.

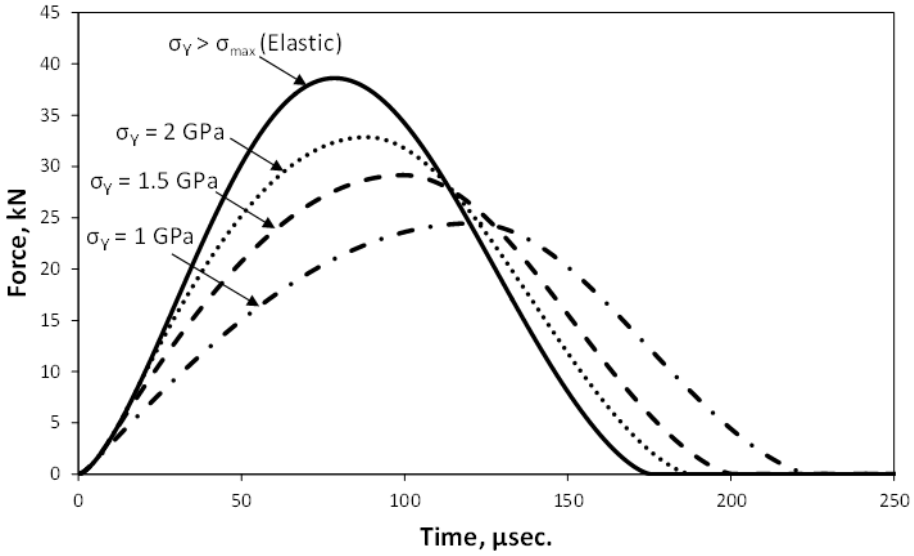

Fig. 6.6: Force time history for different yield strengths of the rod obtained from the in-house FE code.

The force-indentation curve is shown in Fig. 6.7 for the different yield strengths of the rod. It is observed that the maximum indentation, as expected, is larger for the lowest yield strength of the rod. The maximum indentation decreases as the yield strength of the material is increased. The lowest maximum indentation is seen when the yield strength of the material is larger than the maximum stress experienced by the rod during impact (i.e. purely elastic impact). Additionally, it is observed that the curve for the elasto-plastic model follows the purely elastic curve until yield initiation.

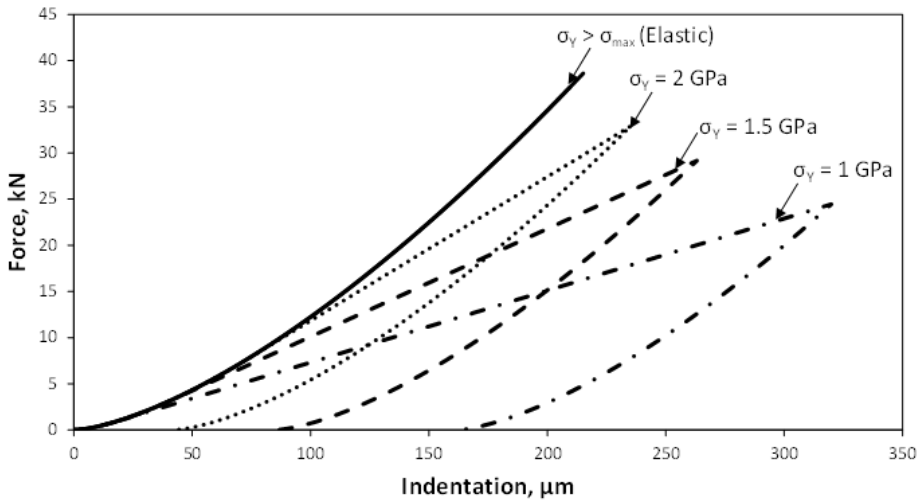

Fig. 6.7: Force-indentation curve for elastic and elasto-plastic rod with different yield strength.

6.4.2 Repeated Impacts

An in-house finite element model written in MATLAB was used to simulate repeated impacts as formulated in Section 6.3. For all impacts the same value for the initial velocity of the striker was used. The rod was considered as made of aluminum, with a yield pressure, p_Y , equal to the yield strength, σ_Y, of aluminum equal to 200 MPa. The geometric and material properties of the rod and the striker are shown in Table 6.1. Two support

conditions (as shown in Fig. 6.8) of the rod are considered for this study: (i) fixed and (ii) elastic.

Table 6.1: Geometric and material properties of the striker and the rod.

Rod Properties		
Area	0.0028274	m^2
E_1	70	GPa
ν_1	0.33	-
L	0.4	m
Density, ρ_1	2700	kg/m^3
c	5091.75	m/s

Striker Properties		
m_2	0.6	kg
E_2	197	GPa
ν_2	0.3	-
Radius, R_2	24.8	mm
Density, ρ_2	7800	kg/m^3
$v_{2,0}$	4.4294	m/s

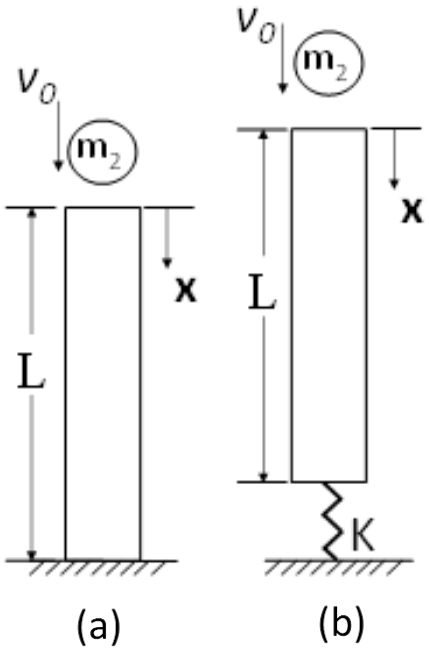

Fig. 6.8: Supporting conditions of the rod considered in the present study (a) Uniform cantilever rod, (b) Uniform rod with elastic support.

6.4.2.1 Fixed Support

The force indentation curve for the rod with fixed support for 15 impacts is shown in Fig. 6.9. The force indentation curve for the purely elastic impact is also shown for reference. It is observed that the plastic deformation is largest for the first impact. As the number of impact progresses, the plastic deformation decreases.

The force time history for the 15 impacts is shown in Fig. 6.10 along with the force for the purely elastic case. The amplitude of the contact force is observed to increase with the number of impacts while the duration of contact decreases; both approaching, but never reaching, the values for the elastic case. The results shown in Fig. 6.10 are qualitatively similar to those shown in Fig. 6. The repeated impacts have the same effect (i.e. increases the amplitude of the force and decreases the duration of contact) as increasing the yield strength of the material after each impact.

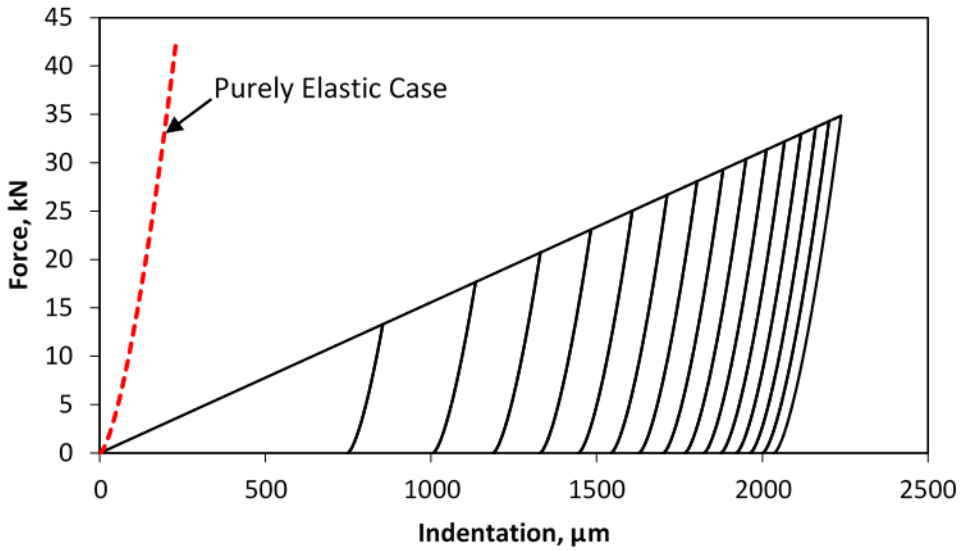

Fig. 6.9: Force-indentation curve for repetitive impacts with elasto-plastic model and perfectly elastic impact case. (Rod with fixed support)

The time history of the velocity of the striker is shown in Fig. 6.11 for the first 15 impacts. It is observed that the final velocity of the striker for the first impact is significantly different from that of the elastic case. As the number of impact increases, the velocity of the striker is observed to approach that of the elastic case.

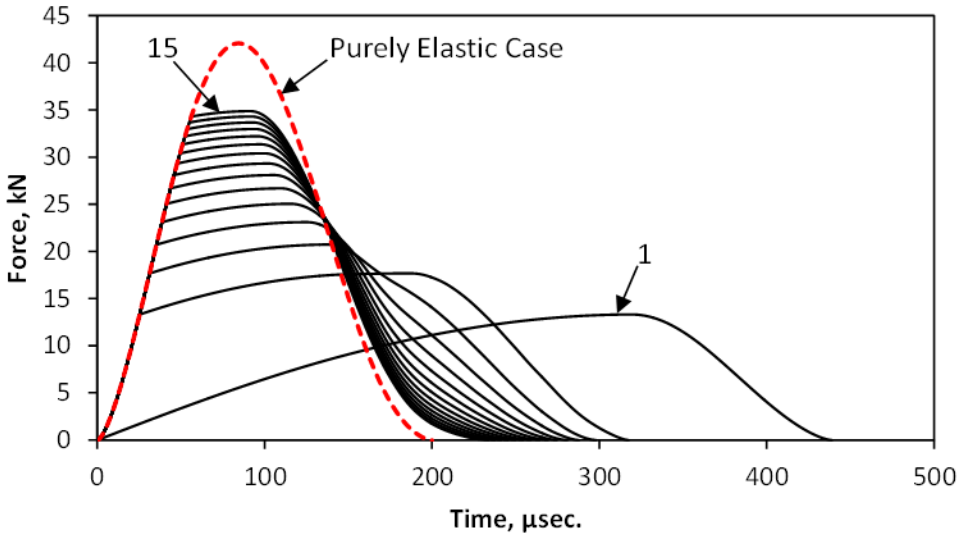

Fig. 6.10: Force time history curves for repetitive impacts with elasto-plastic model and perfectly elastic impact case. (Rod with fixed support)

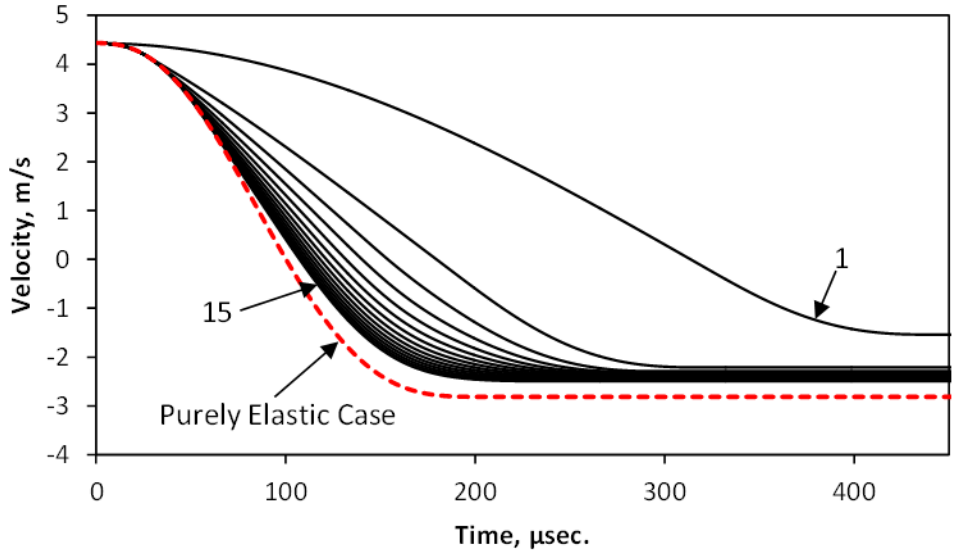

Fig. 6.11: Velocity of the striker time history curves for repetitive impacts with elasto-plastic model and perfectly elastic impact case.(Rod with fixed support)

6.4.2.2 Elastic Support

The force indentation curve for the rod with elastic support for 15 impacts is shown in Fig. 6.12. The force indentation curve for the purely elastic impact is also shown for reference. Similar to the case of the rod with the fixed support, it is observed that the plastic deformation is largest for the first impact, with the plastic deformation decreasing as the number of impacts increase. The force time history for the 15 impacts is shown in Fig. 6.13 along with the force for the purely elastic case. The results are consistent with those obtained for the rod with the fixed support. The amplitude of the contact force increases with the number of impacts while the duration of contact decreases. The time history of the velocity of the striker is shown in Fig. 6.14 for the 15 impacts. The results match qualitatively with those obtained for the rod with fixed support.

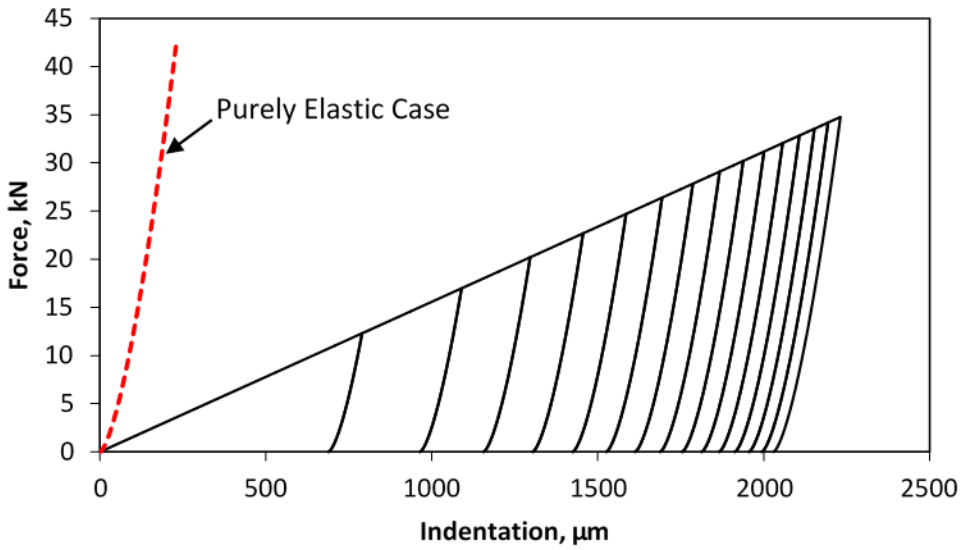

Fig. 6.12: Force-indentation curve for repetitive impacts with elasto-plastic model and perfectly elastic impact case. (Rod with elastic support)

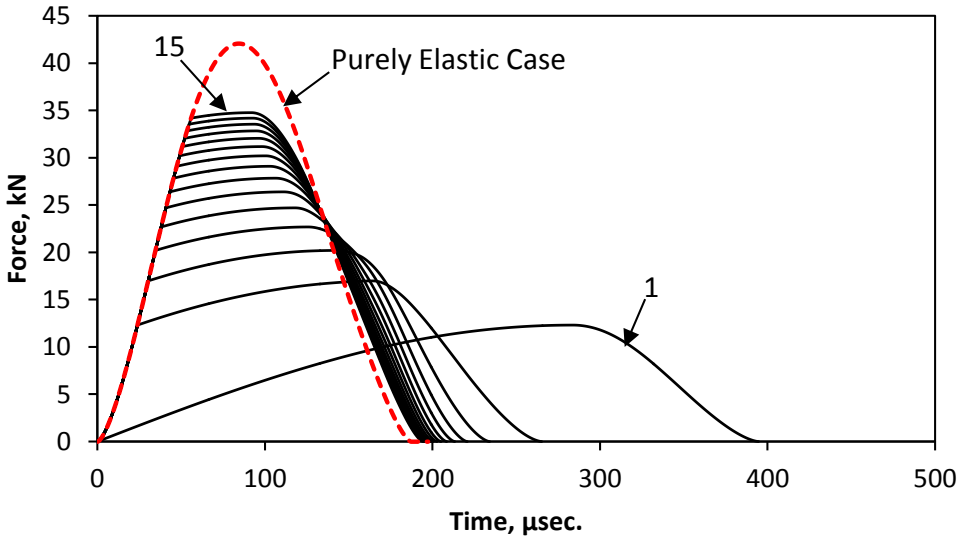

Fig. 6.13: Force time history curves for repetitive impacts with elasto-plastic model and perfectly elastic impact case. (Rod with elastic support)

The coefficient of restitution is obtained from (Minamoto et al. 2011):

$$e = \frac{(m_2 - m_1)}{m_1}\frac{(v_{2,0} - v_2')}{v_{2,0}} - 1 \qquad (6.26)$$

where $v_{2,0}$ is the velocity of the striker before impact, v_2' is the velocity of the striker after impact, and m_1 and m_2 are the mass of the rod and the striker, respectively. The coefficient of restitution for both support conditions as a function of the number of impacts is shown in Fig. 6.15. It is observed that the coefficient of restitution for the elastic impact case is not equal to one for neither of the support conditions. This is attributed to the fact that, even though it is a perfectly elastic collision, energy is lost into wave propagation (Schiehlen et al. 2006). In the case of the rod with elastic support, it is observed that the coefficient of restitution for the first impact is approximately 0.34. The coefficient of restitution is observed to increase with the number of impacts, eventually reaching a constant value close to that of the elastic collision/impact case. The coefficient of restitution for the rod with

fixed support is about 0.6 for the first impact and is also observed to increase with the number of impacts.

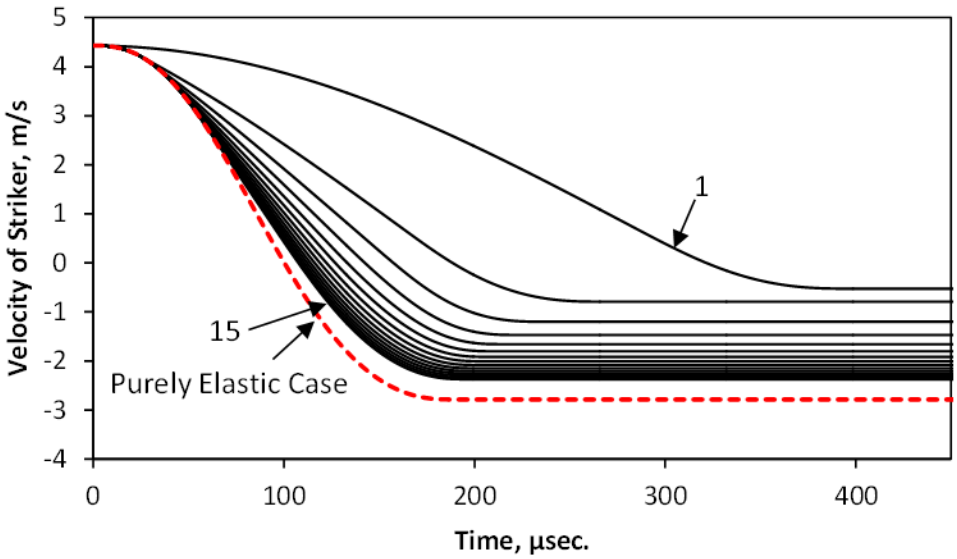

Fig. 6.14: Velocity of the striker time history curves for repetitive impacts with elasto-plastic model and perfectly elastic impact case. (Rod with elastic support)

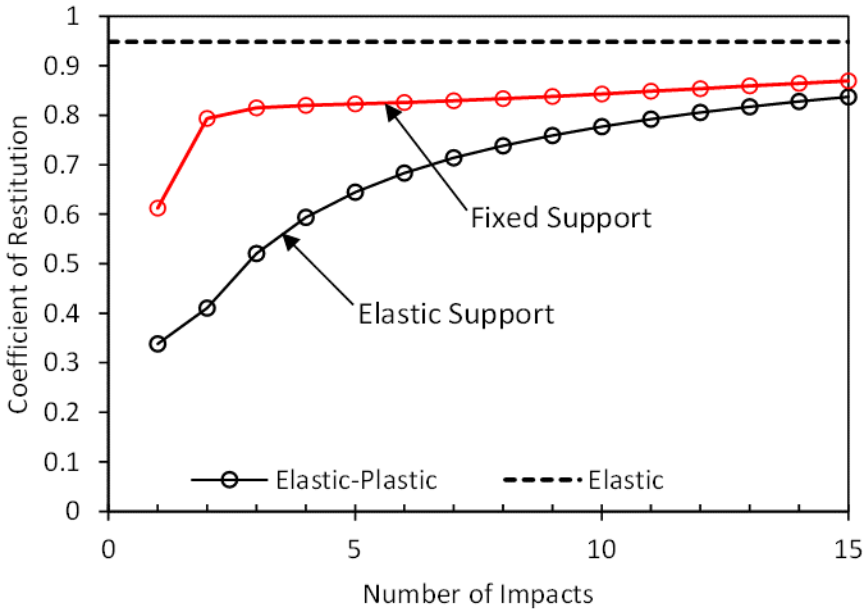

Fig. 6.15: Coefficient of restitution for the rod with fixed and elastic support. The horizontal dashed line represents the coefficient of restitution for the case of a perfectly elastic impact.

Finally, the contact force time history for the rod with fixed and elastic support is shown in Figs. 6.16-6.19 for the 1st, 5th, 10th, and 15th impact respectively. For the first impact a significant difference is observed in the force results, with the amplitude of the contact force and the duration of contact for the rod with fixed support being larger than that of the rod with elastic support. From Figs. 6.17-6.19 it is observed that the effect of the support condition of the rod on the contact force is reduced as the number of impacts increase. This is attributed to the fact that the duration of contact decreases as the number of impacts increase. This causes the ratio of the duration of contact to the time of arrival of the reflected wave to decrease. Therefore, as shown in Chapter 4, the effect of the support condition of the rod on the contact force is less than that of the first impacts. Moreover, for all the impacts presented in this chapter the duration of contact is larger than the time of arrival of the reflected wave. If the duration of contact is less than that of the reflected wave, as shown in Chapter 4, that the contact force is not affected by the support condition of the rod.

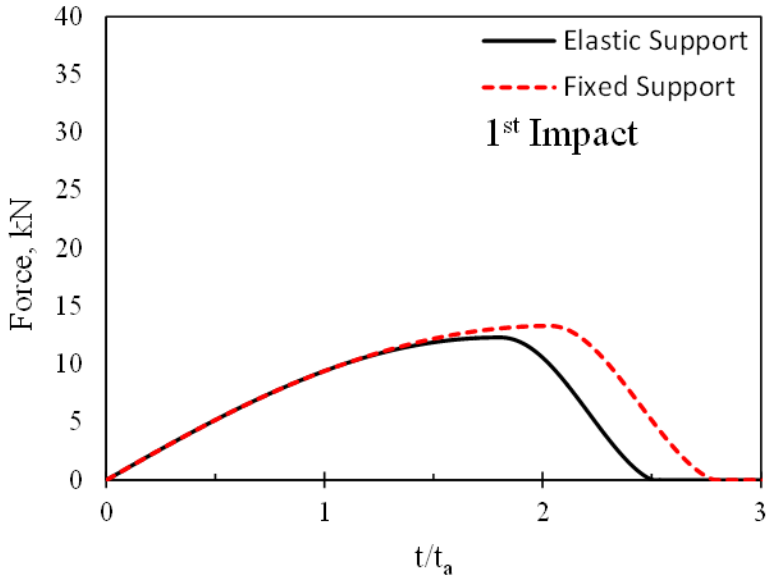

Fig. 6.16: Force time history for the rod with fixed and elastic support. (1st impact)

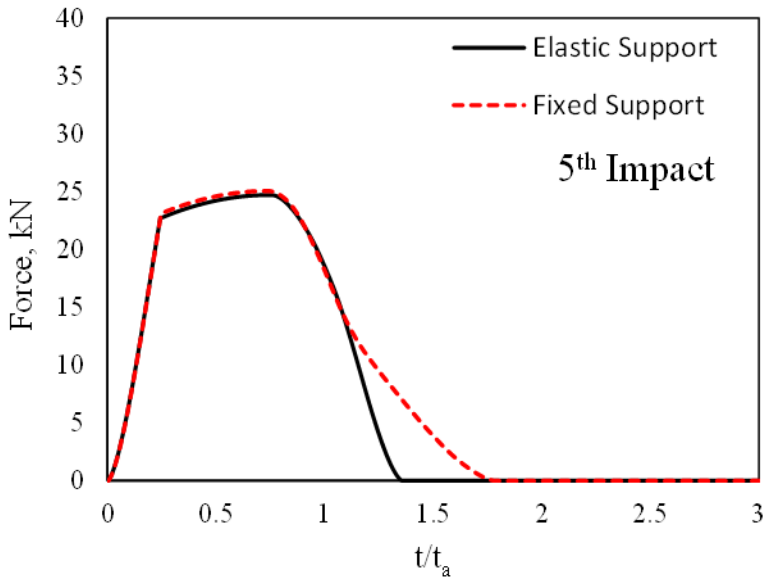

Fig. 6.17: Force time history for the rod with fixed and elastic support. (5^{th} impact)

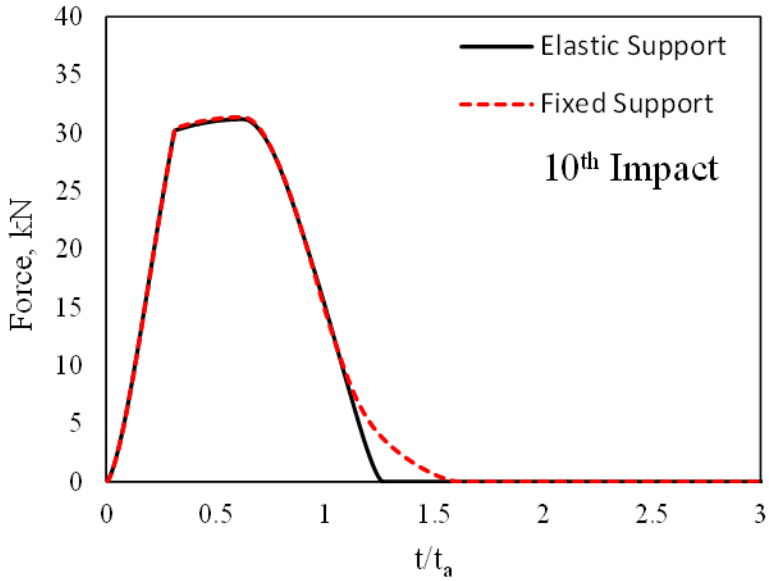

Fig. 6.18: Force time history for the rod with fixed and elastic support. (10^{th} impact)

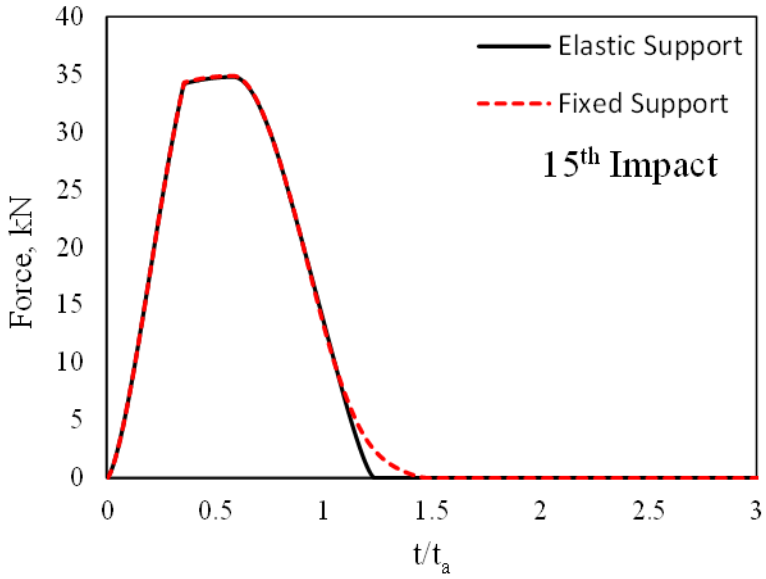

Fig. 6.19: Force time history for the rod with fixed and elastic support. (15^{th} impact)

6.5 Conclusions

The dynamic contact force due to impact of a striker on an elasto-plastic rod with fixed and elastic support conditions was analyzed using a modified Hertz theory of contact. The contact force and the rod response were obtained using an in-house finite element code. Based on the results obtained from the present study, the following conclusions can be made:

- When plastic deformation of the rod is considered, the contact force is smaller, with a larger duration, than that of the case of an elastic rod. As the yield strength of the rod is increased, the contact force increases and the duration of contact decreases, approaching the results of the case of an elastic rod.
- In the case of repetitive impacts, the first impact shows the largest plastic deformation on the rod. As the number of impacts increases the plastic deformation on the rod

decreases, the magnitude of the contact force increases and the duration of contact decreases.

- The velocity of the striker at the end of contact for the first impact is significantly lower than that of the elastic case. As the number of impacts increase the velocity of the striker at the end of contact increases, approaching that of the elastic case.
- The coefficient of restitution for both support conditions was observed to increase with the number of impacts.
- The effects of the support conditions of the rod on the contact force is more significant in the first impacts, while it decreases as the number of impacts increase.

Chapter 7

Finite Element Simulation of Ultrasonic Percussive Mechanism

In this chapter the interaction of the components of the percussive mechanism of the ultrasonic percussive drill is studied. The impact of the free mass on the drill rod and the ultrasonic horn is analyzed using Hertz theory of contact. The response of the drill rod is obtained using the in-house finite element model presented in previous chapters. Since the response of the ultrasonic horn is controlled by the piezoelectric stack, it is assumed that the ultrasonic horn remains unaffected by the impact of the free mass. The effect of the support condition (e.g. fixed, elastic, visco-elasto-plastic) of the rod on important contact parameters of the percussive mechanism such as duration of contact, maximum contact force, and free mass oscillation frequency is studied.

7.1 Free Mass and Ultrasonic Horn Impact

Consider the percussive mechanism of the ultrasonic percussive drill, shown in Fig. 7.1, consisting of an ultrasonic horn, a free mass, and a drill rod. The operation of the ultrasonic percussive system begins with the excitation of the ultrasonic horn by imparting high frequency voltage to the piezoelectric stack. The ultrasonic horn vibrates harmonically with a frequency of about 22.5 kHz and amplitude, B_0, of around 10 μm (Bao et al. 2003). For convenience, the horn position function is selected so that the horn tip is able to move up and down from its initial position (t = 0). The position and the velocity of the horn tip are given by:

$$u_h = B_0 \sin(\varpi t + \beta) \tag{7.1}$$

$$v_h = B_0\omega \cdot \cos(\varpi t + \beta) \tag{7.2}$$

where B_0 is the amplitude of vibration, ϖ is the vibration frequency, and β is the phase angle.

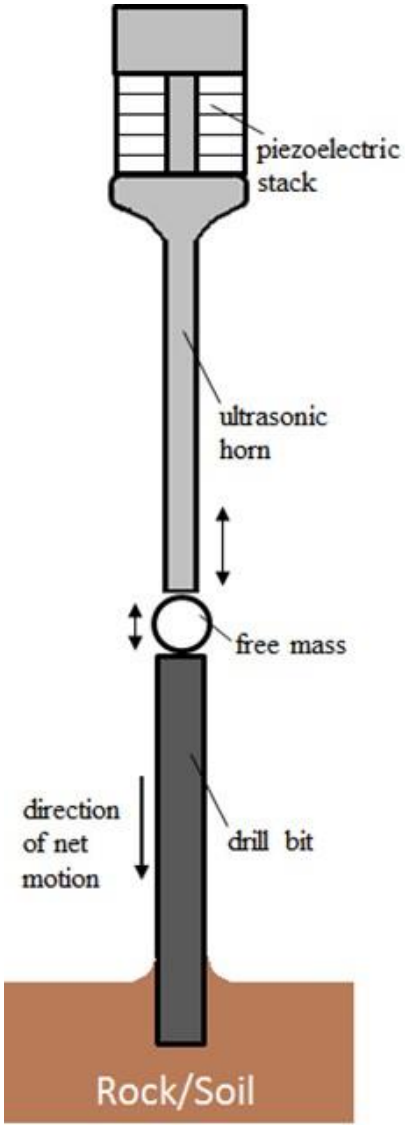

Fig. 7.1: Interaction between vibrating ultrasonic horn, free mass, and drill bit.

The excitation imparted to the horn causes it to impact the free mass. The impact of the free mass and the ultrasonic horn is analyzed using Hertz (1881) theory of contact. Therefore, the contact force, P_H, developed between the free mass and the ultrasonic horn is given by:

$$P_H = k_{2,H}\alpha_H^{3/2} \tag{7.3}$$

where α_H is the local indentation between the ultrasonic horn and the free mass, and $k_{2,H}$ is the contact stiffness given by (Goldsmith 1960):

$$k_{2,H} = \frac{4}{3}E^* R^{*1/2} \tag{7.4}$$

The effective Young's modulus (E^*) and the effective radius (R^*) are given by (Goldsmith 1960; Vu-Quoc and Zhang 1999):

$$E^* = \left[\frac{1-\nu_1^2}{E_1} + \frac{1-\nu_2^2}{E_2}\right]^{-1} \tag{7.5}$$

$$R^* = \left[\frac{1}{R_1} + \frac{1}{R_2}\right]^{-1} \tag{7.6}$$

where E is the Young's modulus, ν is the Poisson's ratio, R is the radius of the contact surface, and the subscripts 1 and 2 correspond to body 1 (drill rod) body 2 (free mass). As in previous chapters, Timoshenko's approach is used to find the local indentation. In this case, the motion of the ultrasonic horn (given by Eqn. (7.1)) is governed by the piezoelectric actuator and is therefore assumed to remain unaffected by the impact of the free mass. The equation of motion of the free mass (neglecting the gravitational acceleration) subjected to the contact force, P_H, is given by:

$$m_2\frac{d^2u_2}{dt^2} + P_H(t) = 0 \tag{7.7}$$

The response of the free mass is obtained by direct integration of Eqn. (7.7). The local indentation is then obtained by:

$$\alpha = u_h(t) - u_2(t) \tag{7.8}$$

The procedure to obtain the contact force and the response of the rod and the free mass is presented in Chapter 3, but in this case the displacement of one of the bodies (i.e. the ultrasonic horn) is known. Therefore, the equilibrium iterations are only used to update the contact force and the displacement response of the free mass.

7.2 Free Mass and Drill Rod

The contact between the free mass and the drill rod is analogous to the case of the impact between the striker and the rod discussed in previous chapters. In this case the contact force, P_D, between the free mass and the drill rod is given by:

$$P_D = k_{2,D}\alpha_D^{3/2} \tag{7.9}$$

where the contact stiffness, $k_{2,D}$, can be obtained by substituting the corresponding geometric and material properties into Eqns. (7.4), (7.5), and (7.6). The displacement response of the rod and the free mass and the local indentation, α_D, are obtained using the same methods presented in Chapter 3.

7.3 Results and Discussion

A 15 cm long steel rod with 1.91 cm diameter is considered. The impactor/striker is taken as a steel sphere with a diameter of 1.5 cm. The geometric and material properties of the rod and the striker are shown in Table 7.1.

Table 7.1: Geometric and material properties of the free mass and the drill rod.

Drill Rod Properties		
Area	0.00285	m^2
E_1	197	GPa
ν_1	0.3	-
L	0.15	m
Density, ρ_1	7800	kg/m^3
c	5025	m/s

Free Mass Properties		
m_2	0.0137	kg
E_2	197	GPa
ν_2	0.3	-
Radius, R_2	7.5	mm
Density, ρ_2	7800	kg/m^3
$v_{2,0}$	1.72	m/s

7.3.1 Percussive Mechanism Simulation: Fixed Support

The displacement/position time history of the ultrasonic horn, the free mass and the drill rod is shown in Fig. 7.2 for the drill rod with fixed support along with the contact force due to impact of the free mass. To initiate the simulation it is considered that the free mass strikes the drill rod with an initial velocity, $v_{2,0}$, of the free mass of 1.72 m/s. After this the velocity of the free mass is used as obtained from the impact simulation.

It is observed that for one cycle of oscillation of the free mass, several cycles of the ultrasonic horn occur. This is consistent with the purpose of the free mass of producing impact of a frequency lower than that of the ultrasonic horn (Sherrit 1999). The displacement results shown in Fig. 7.2 are shown in Fig. 7.3 for a longer/extended time period (t = 10000 μsec.). It is observed that 31 impacts occur within the duration of the simulation.

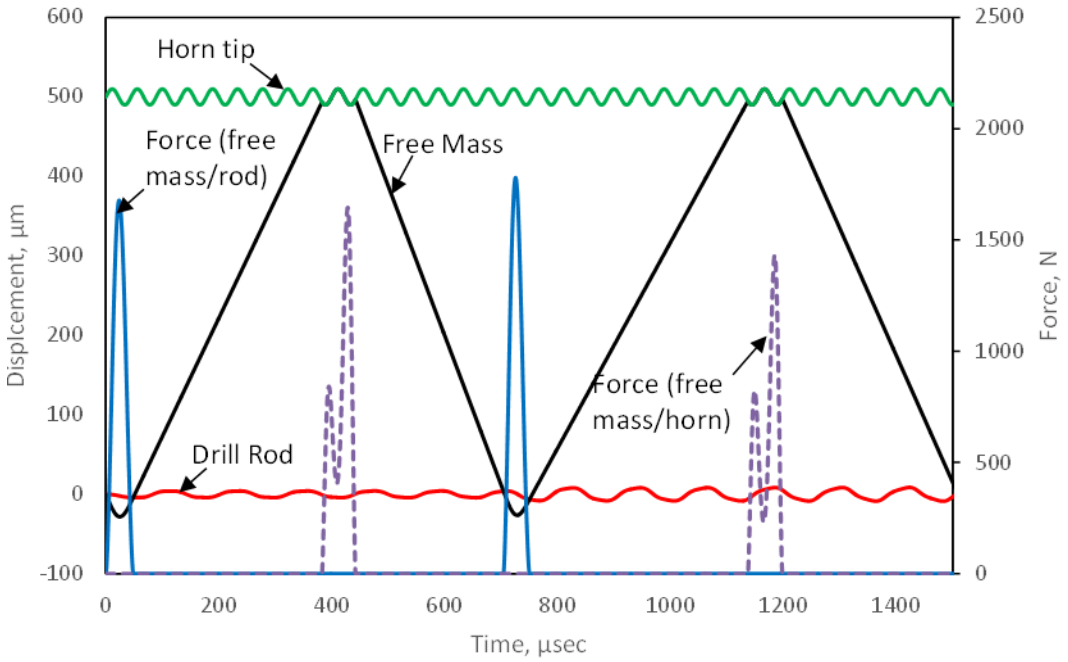

Fig. 7.2: Displacement and contact force time history for the percussive mechanism simulation. (Fixed support)

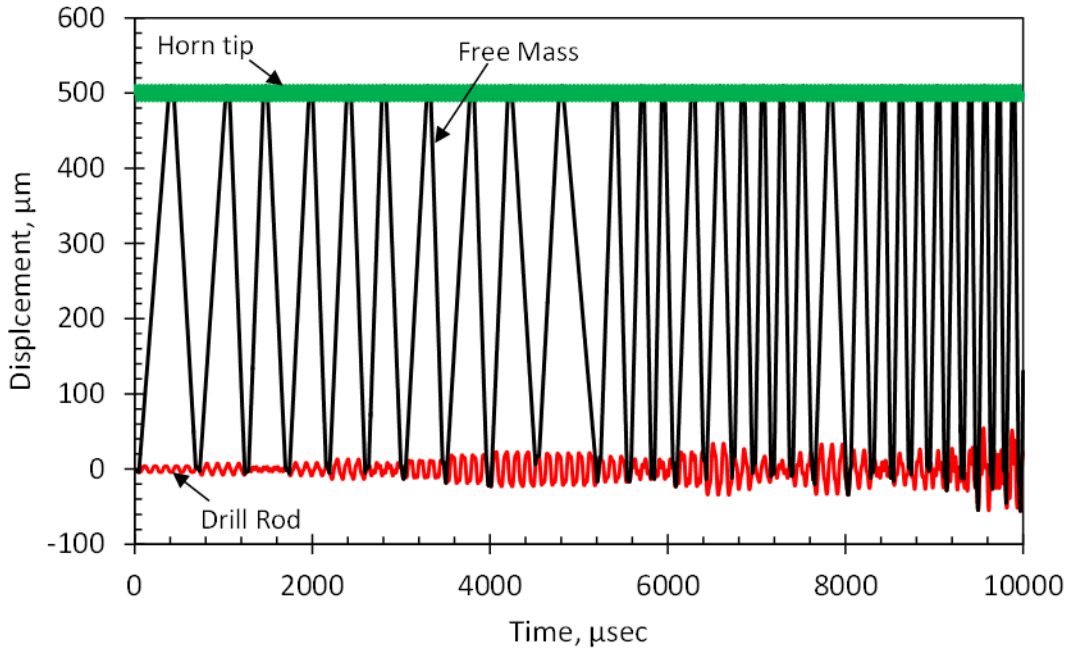

Fig. 7.3: Displacement and contact force time history for the percussive mechanism simulation. (Fixed support. Extended time period)

7.3.2 Percussive Mechanism Simulation: Elastic Support

The displacement/position time history of the ultrasonic horn, the free mass and the drill rod is shown in Fig. 7.4 for the drill rod with elastic support along with the contact force due to impact of the free mass. Since the external spring represents the supporting medium, the stiffness of the spring is selected as $K = 5 * 10^6\, N/m$ based on the stiffness of sandstone, limestone, and granite (Batako et al. 2004). The geometric and material properties are taken as shown in Table 7.1.

Similar to the case of the drill rod with fixed support, it is observed that several cycles of the ultrasonic horn occurs for one cycle of oscillation of the free mass. Additionally, the drill rod is observed to experience small oscillations due to axial vibration of the rod and larger oscillations due to the elastic support. The results shown in Fig. 7.4 are shown in Fig. 7.5 for a longer/extended time period (t = 10000 μsec.). It is observed that 8 impacts occur within the duration of the simulation. As discussed in previous chapters, if the duration of contact is less than the time of arrival of the reflected wave the contact force is not affected by the support condition. This is the case for the first impact in this simulation, with a duration of contact, τ, equal to 48 μsec. and a time of arrival, t_a, of 59 μsec. However, the response of the drill rod after the first impact is significantly different for each support condition.

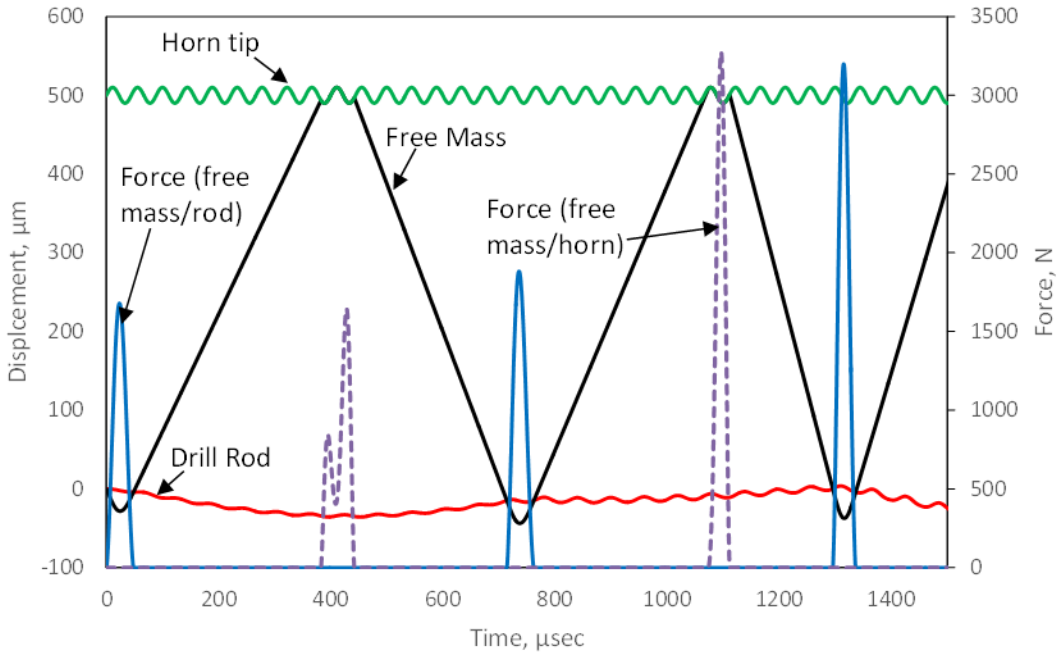

Fig. 7.4: Displacement and contact force time history for the percussive mechanism simulation. (Elastic support)

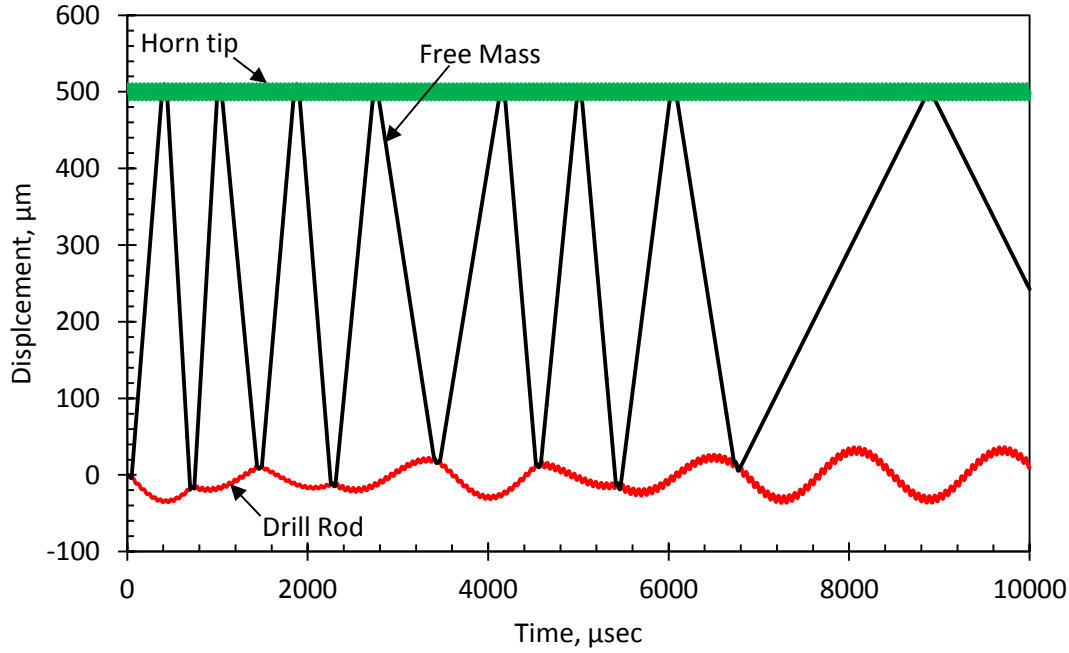

Fig. 7.5: Displacement and contact force time history for the percussive mechanism simulation. (Elastic support. Extended time period)

7.3.3 Percussive Mechanism Simulation: Visco-elasto-plastic Support

The displacement/position time history of the ultrasonic horn, the free mass and the drill rod is shown in Fig. 7.6 for the drill rod with the visco-elasto-plastic support along with the contact force due to impact of the free mass. The threshold force for penetration initiation is taken as equal to 100 N, while the stiffness of the spring is taken as equal to $5*10^6$ N/m. The drill rod is observed to experience small oscillations due to axial vibration of the rod, larger oscillations due to the external spring and permanent penetration into the supporting medium. The results shown in Fig. 7.6 are shown in Fig. 7.7 for a longer/extended time period (t = 10000 μsec.). It is observed that 15 impacts occur within the duration of the simulation. Additionally, a total penetration of 48 μm is observed.

Table 7.2 shows the number of impacts, average duration of contact, average maximum force, and average oscillation frequency of the free mass for the duration of the simulation. It is observed that the number of impacts, the average maximum force and the oscillation frequency of the free mass is higher for the drill rod with fixed support. This is consistent with the common knowledge of percussive drilling that it is more effective for brittle/harder materials.

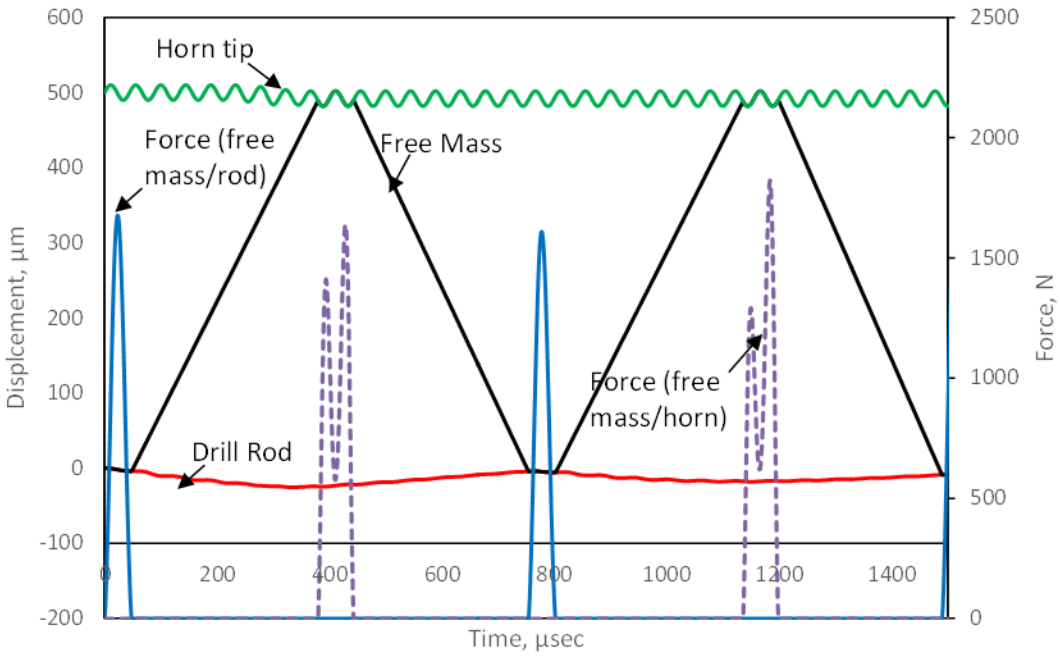

Fig. 7.6: Displacement and contact force time history for the percussive mechanism simulation. (Visco-elasto-plastic support)

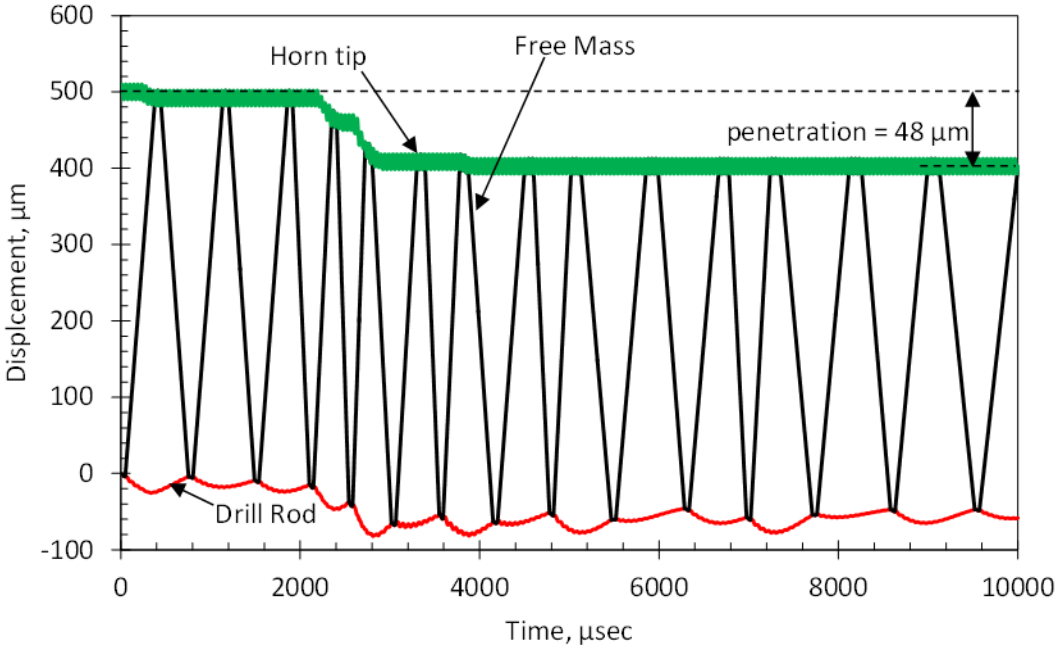

Fig. 7.7: Displacement and contact force time history for the percussive mechanism simulation. (Visco-elasto-plastic support. Extended time period)

Table 7.2: Contact results for the ultrasonic percussive mechanism simulation.

Rod Support	No. of Impacts with Drill Rod	Avg. Duration, μsec. (τ_{AVG})	Avg. Max Force, N ($P_{max,\,AVG}$)	Avg. Frequency, Hz. (f_{AVG})
Fixed	31	39	7919	3674
Elastic	8	55	1270	1093
Visco-elasto-plastic (Penetration model)	15	47	2058	1538

7.4 Conclusions

The dynamic and contact simulation of the full ultrasonic mechanism was performed using an in-house finite element code. The contact between the different components was analyzed using Hertz theory of contact. The dynamic response of the system and the contact parameters were obtained for a drill rod with fixed and elastic support condition. Based on the results obtained from the present study, the following conclusions can be made:

- The frequency of oscillation of the free mass is smaller than that of the ultrasonic horn. This is consistent with the purpose of including the free mass to convert the high frequency oscillation of the ultrasonic horn into lower frequency impacts on the drill rod.
- The support condition affects the overall dynamic response of the ultrasonic percussive mechanism.
- The drill rod with fixed support resulted in a percussive system with higher oscillation frequency of the free mass and higher contact force compared to that of the drill rod with elastic support and the rod with visco-elasto-plastic support. This is consistent with the common knowledge of percussive drilling that it is more effective for brittle/harder materials.

Chapter 8

Conclusions and Recommendations

As presented in the first chapter, the objectives of this work are to develop a model to determine the position of each component of the ultrasonic percussive mechanism, deeply analyze the contact between the free mass and the drill rod considering various support conditions of the drill rod, and analyze the repetitive impacts of the percussive mechanism including the effect of the loading history of the drill rod.

8.1 Summary of the Study

The methods and techniques used in this study are briefly summarized in the following:

- An initial simplified model of the interaction between the ultrasonic horn, the free mass and the drill rod was presented. Methods such as conservation of momentum, impulse momentum principle, and particle motion analysis were employed to find the position of each component during operation and the energy and impulse transferred to the drill rod by the free mass.
- A methodology to analyze the longitudinal impact of a striker (free mass) on a rod was developed based on Hertz theory of contact. The structural vibration of the rod was used to find the local indentation on the top end of the rod and subsequently the contact force. The methodology developed was implemented using mode superposition method and finite element technique.
- The methodology developed to analyze the impact between the free mass and the rod was implemented to investigate the effect of the support conditions of the drill rod on the contact force.

- A modified Hertz model was used to include the effect of plastic deformation of the rod on the contact force. This model was implemented to investigate the impact phenomena for identical repetitive impacts.
- A finite element model of the percussive mechanism was used to investigate the effect of the support conditions of the drill rod on the overall dynamic response of the ultrasonic drill.

8.2 Conclusions of the Research

This study presented (i) a model to determine the position of each component of the ultrasonic percussive mechanism,(ii) a methodology to analyze the contact between the free mass and the drill rod considering various support conditions of the drill rod, structural damping and plastic deformation of the drill rod, and (iii) a finite element model to investigate the overall dynamic response of the ultrasonic drill on different supporting media. Based on the results obtained from this study, the following conclusions can be made:

- The free mass converts the high frequency oscillations of the ultrasonic horn into lower frequency impacts on the drill rod.
- Including the energy losses through the coefficient of restitution affects significantly the operation of the ultrasonic percussive drill. The number of impacts, average kinetic energy and average impulse transferred to the drill rod by the free mass increase as the energy loss decreases.

- Applying an energy balance to the (free mass/rod) system, the equivalent dynamic contact force and duration of contact can be determined by a relatively simple procedure.
- The duration of contact obtained from Cox method is similar to that obtained from wave propagation theory of previous studies, considering the difference in the assumptions of each method.
- The methodology developed to analyze the contact between the free mass and the drill rod can be applied for different methods (e.g. mode superposition, finite element) to accurately model the longitudinal impact of a striker on a rod as verified by the experimental data and the Abaqus FEA model.
- For an undamped rod, the displacement of the top end of the rod remains constant for a period of time after end of contact. This is attributed to the fact that when contact ends, the reflected wave has not arrived to the top end of the rod. Therefore, after contact ends there is no force acting on the top end of the rod until the reflected wave arrives.
- The maximum contact force increases as the damping in the rod increases, while the duration of contact was observed to remain virtually unaffected. The increase in the magnitude of the force is attributed to the fact that the damping force causes the rod to deform less, hence a higher indentation and contact force is observed.
- The methodology developed to analyze the impact between the free mass and the drill rod is applicable to the longitudinal impact between a spherical striker on a rod having other support conditions (e.g. free support, elastic support, etc.) to investigate the effect of the support condition of the rod on the contact force.

- For an undamped rod the contact force is not affected by the boundary condition of the supporting end of the rod (i.e. fixed, free or elastic support) if the duration of contact is less than the time it takes to the displacement wave to return to the contact end (time of arrival, t_a). This is because the effect of the boundary conditions is carried by the reflected wave. Therefore, if the contact between the striker and the rod ceases before the reflected wave reaches the contact end of the rod, the response of the rod during the contact period is the same regardless of the boundary condition.
- On the other hand, if the duration of contact is larger than the time of arrival of the reflected wave ($\tau > t_a$), the contact force is affected by the support condition of the rod. The larger the duration of contact is with respect to the time of arrival, (i.e. the larger the ratio τ / t_a), the larger the effect of the boundary condition on the contact force.
- If the duration, τ, of contact is less than the time of arrival, t_a, the contact force is not affected by the boundary condition on the bottom of the rod and a more simple analysis such as the one presented by Volterra and Zachmanoglou (1965) may be performed with reasonably accurate results.
- When damping of the rod is considered, the time of arrival of the reflected wave is no longer the only governing parameter. The support condition are observed to affect the contact force even for the case of a contact ending before the time of arrival. However, the effect of the support condition on the contact force is higher when the contact ends after the time of arrival of the reflected wave.
- When drill rod penetration is considered (i.e. visco-elasto-plastic support), there are two possible cases in regard to the contact force. First, the contact may cease before penetration begins. In this case the force would not be affected by penetration. Second,

drill bit penetration may begin while the contact is still present. In such case the contact force will decrease at a higher rate compared to the case where penetration is not present during contact.

- When plastic deformation of the rod is considered, the contact force is smaller, with a larger duration, than that of the case of an elastic rod. As the yield strength of the rod is increased, the contact force increases and the duration of contact decreases, approaching the results of the case of an elastic rod.
- In the case of repetitive impacts, the first impact shows the largest plastic deformation on the rod. As the number of impacts increases the plastic deformation on the rod decreases, the magnitude of the contact force increases and the duration of contact decreases.
- The coefficient of restitution was observed to be less than one even for the case of an elastic impact. This is attributed to the fact that, even though the impact is elastic, energy is lost in wave propagation. The coefficient of restitution for both support conditions was observed to increase with the number of impacts.
- The support condition affects the overall response and performance of the percussive mechanism.
- The drill rod with fixed support resulted in a percussive system with higher oscillation frequency of the free mass and higher contact force compared to that of the drill rod with elastic and visco-elasto-plastic support.

8.3 Recommendations for Future Work

Whereas the interaction between the different components (i.e. ultrasonic horn, free mass, and drill rod), including the supporting medium, and the overall dynamic response of

the percussive system has been thoroughly examined in the scope of this work, there are several aspects of the system that needs to be investigated further to better understand the overall performance of this special ultrasonic percussive drill. The following future work are recommended to be undertaken:

- Although the model developed in this study was verified with experimental data available in literature, this data was obtained for a system in which the contact ends before the reflected wave arrives to the contact end. This causes the force not to be affected by the support condition. Experimental data on the longitudinal impact of a spherical striker on a rod with various support conditions, in which the contact force is affected by the support condition of the rod, could be gathered to verify the effect of the support conditions on the contact force.
- This study focused on ultrasonic percussive mechanisms. However, in some drills, such as the Auto-Gopher, rotary drilling is combined with the percussive mechanism to increase the penetration rate. A model including both rotary and percussive motion will give a much better understanding performance of the system under both, percussive and rotary motion.
- Finally, manufacturing an ultrasonic percussive drill with a similar mechanism and carry out experiments to monitor the interaction between each component and track its position during operation will be important to calibrate the developed model.

Appendix A:

Orthogonality Relations for the Rod with Elastic Support

Consider the case of a rod with elastic support (represented by a spring) subjected to a distributed load *P(x,t)* along the length as shown in Fig. 4.2(a). The two boundary conditions are obtained by letting the stress at the free end equal to zero (Eqn. (4.10a)), and letting the internal force at $x = L$ be equal to the spring force as given by Eqn. (4.10b) (Fig. 4.2(b)).

In this case the external spring must be included in the orthogonality relations. The orthogonality relations are given by the following expressions (Timoshenko et al. 1974):

$$\bar{m}\int_0^L \varphi_i(x)\varphi_j(x)\,dx = \begin{Bmatrix} 0 & for\ i \neq j \\ \bar{m} & for\ i = j \end{Bmatrix} \qquad (A-1a)$$

$$-EA\int_0^L \varphi_i'(x)\varphi_j'(x)\,dx - K\varphi_i(L)\varphi_j(L) = \begin{Bmatrix} 0 & for\ i \neq j \\ -\bar{m}\omega_i^2 & for\ i = j \end{Bmatrix} \qquad (A-1b)$$

$$EA\int_0^L \varphi_i''(x)\varphi_j(x)\,dx - EA\varphi_i'(L)\varphi_j(L) - K\varphi_i(L)\varphi_j(L)$$

$$= \begin{Bmatrix} 0 & for\ i \neq j \\ -\bar{m}\omega_i^2 & for\ i = j \end{Bmatrix} \qquad (A-1c)$$

Substituting Eqn. (4.16) into Eqn. (4.1) (without damping), multiplying by $\varphi_j(x)$ and integrating from 0 to L, we obtain the equation of motion of the rod as:

$$\sum_{i=1}^{\infty}\left[\ddot{q}_i \cdot m\int_0^L \varphi_i(x)\varphi_j(x)\,dx - EAq_i\int_0^L \varphi_i''(x)\varphi_j(x)\,dx\right]$$

$$= \int_0^L \varphi_j(x)P(x,t)\,dx \qquad (A-2)$$

Substituting Eqn. (4.14) into the relation of the boundary condition of the bottom end of the rod (Fig. 4.2(b)), given by Eqn. (4.10b), and multiplying by $\varphi_j(L)$ we obtain:

$$\sum_{i=1}^{\infty}\left[EAq_i\varphi_i'(L)\varphi_j(L) + Kq_i\varphi_i(L)\varphi_j(L)\right] = 0 \qquad (A-3)$$

Adding Eqns. (A-2) and (A-3) we obtain the equation of motion of the rod as:

$$\sum_{i=1}^{\infty}\left[\ddot{q}_i \cdot \overline{m}\int_0^L \varphi_i(x)\varphi_j(x)\,dx - q_i\left[EA\int_0^L \varphi_i''(x)\varphi_j(x)\,dx - EA\varphi_i'(L)\varphi_j(L) - K\varphi_i(L)\varphi_j(L)\right]\right]$$

$$= \int_0^L \varphi_j(x)P(x,t)\,dx \qquad (A-4)$$

After applying the orthogonality relations (i.e. Eqns. (A-1)) and dividing by $\overline{m} = \rho A$, the equation of motion of the rod is obtained as shown in Eqn. (4.15).

Appendix B:

Graphical explanation of the plastic impact process

Elastic Loading: $\boldsymbol{\alpha < \alpha_Y}$ & $\boldsymbol{\dot{\alpha} > 0}$

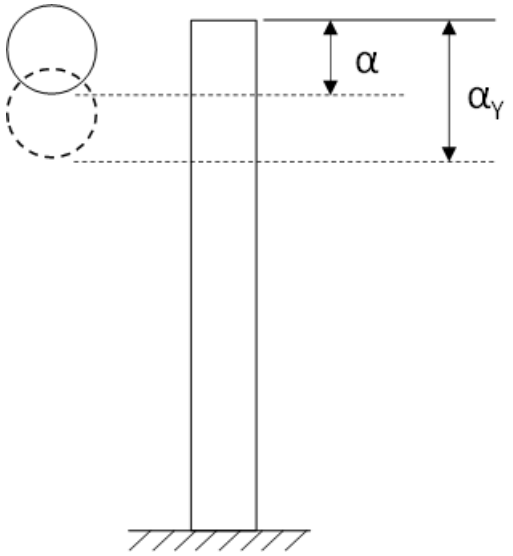

$$\boldsymbol{P = k_H \alpha^{3/2}}$$

Elasto-Plastic Loading: $\boldsymbol{\alpha \geq \alpha_Y}$ & $\boldsymbol{\dot{\alpha} > 0}$

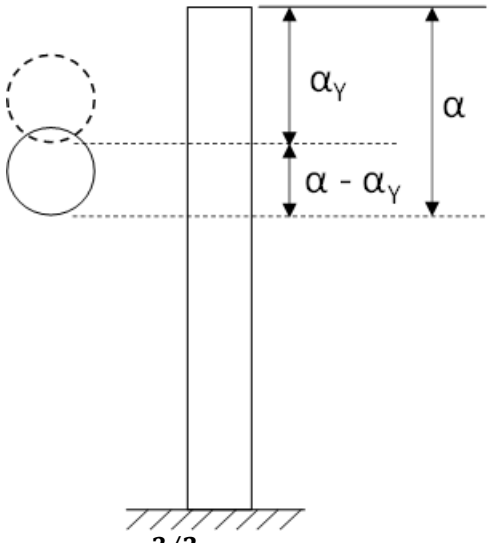

$$\boldsymbol{P = k_H \alpha_Y^{3/2} + \pi p_Y R^* (\alpha - \alpha_Y)}$$

Elastic Unloading (after plastic deformation): $\boldsymbol{\alpha > \alpha_{res}}$ & $\boldsymbol{\dot{\alpha} < 0}$

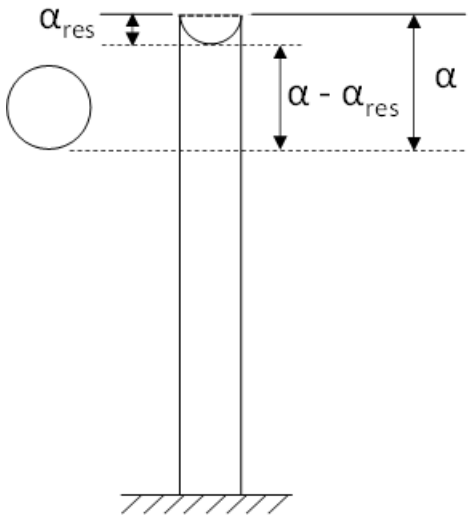

$$\boldsymbol{P = k_H(\alpha - \alpha_{res})^{3/2}}$$

End of contact: $\boldsymbol{\alpha \leq \alpha_{res}}$ & $\boldsymbol{\dot{\alpha} < 0}$

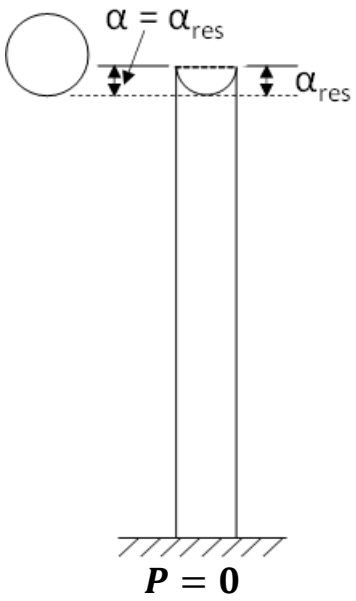

$$\boldsymbol{P = 0}$$

Appendix C:

MATLAB code for mode superposition method

```
%%%% LONGITUDINAL IMPACT OF A SPHERICAL STRIKER AND A UNIFORM ROD %%%%%%%
%%%% MODELED AS A SDOF SYSTEM, SOLVED BY NEWMARK METHOD %%%%%%%%%%%%%%%%%
%%%% (AVERAGE ACCELERATION METHOD) %%%%%%%%%%%%%%%%%%%%%%%%%%%%%%%%%%%%%

clear all

dt=0.000001;%0.00002;
duration=0.003;%0.003;%0.002;%
t=[0:dt:duration];
TOL=0.5;%1e-10;
prog=dt/duration;

%%%%%%PROPERTIES OF THE STRIKER%%%%%%%%%%%%%%%%%%%%%%%%
m2=0.067053;%0.06721;%
Emass=203*10^9; %Pa 203*10^9;
vmass=0.3;
Rmass=0.0254/2;%0.014986/2;%0.0127;%  %RADIUS OF THE STRIKER
rhomass=7833.5; %kg/m3 (STRIKER)7833.5;
h=0.03;%0.15;%Drop Altittude, m
v0=sqrt(2*9.81*h);%0.5; %m/s INITIAL VELOCITY OF THE STRIKER


%%%%%%PROPERTIES OF THE ROD%%%%%%%%%%%%%%%%%%%%%%%%%%%%
L=0.4; %m (ROD) 1;%
D=0.06;
area=0.000285;%pi*(D/2)^2;%0.000285;%0.00114;%0.00028502;
rho=7788.6; %kg/m3 (ROD)7788.6;%
Erod=209*10^9; %Pa 209*10^9;%
vrod=0.3;%0.33;
m1=rho*area*L;
c=sqrt(Erod/rho);
k1=Erod*area/L;
ksoil=5*10^6;
Rrod=0;
psi=1.5;
w_SDOF=sqrt(ksoil/m1); %SDOF Frequency of the rod
```

```
damp=2*psi*m1*w_SDOF; %Damping coefficient "c" bottom end of rod


for i=1:length(t);
   iteration(i)=0;
end

%%%%%DEFINE PROPERTIES OF PLASTIC MODEL%%%%%%%%%%%%%%%%%%%%%%%%%%%%%%%%%%%%
sigma_y=250*10^60000000000000000000000;%1.5*10^9;%2.1435*10^9; %Yield strength of the rod(Pa)
E_star=((1-vrod^2)/Erod+(1-vmass^2)/Emass)^(-1);
if Rrod==0;
   R_star=Rmass;
else
   R_star=(1/Rmass+1/Rrod)^(-1);
end
ind_res1=0;
ind_y=(pi*sigma_y/(2*E_star))^2*R_star;%0.000025; 2.352521382479062e-04-ind_res1;%
Fy=sigma_y*ind_y*2*pi*R_star/3;
plastic=0;
check=0;
ind_max=0;
ind_res=0;
Fmax=0;

%%%%%DEFINE HERTZ CONTACT PARAMETERS%%%%%%%%%%%%%%%%%%%%%%%%%%%%%%%%%%%%%%
deltarod=(1-vrod^2)/(Erod*pi);
deltamass=(1-vmass^2)/(Emass*pi);
kh=(4/3)*E_star*sqrt(R_star);
%kh=(4/(3*pi))*sqrt(Rmass)*(1/(deltarod+deltamass));

%%%%%CALCULATE CONSTANTS FOR NEWMARK BETA METHOD%%%%%%%%%%%%%%%%%%%%%%%%%%
alpha=0.25;
delta=0.5;

a0=1/(alpha*dt^2);
a1=a0*dt;
a2=1.d0/(2*alpha)-1.d0;
a3=dt*(1.d0-delta);
a4=delta*dt;
a5=1/(2*alpha);
```

```
a6=delta/alpha-1;
a7=dt/2*(delta/alpha-2);

%%%%%INITIAL
CONDITIONS%%%%%%%%%%%%%%%%%%%%%%%%%%%%%%%%%%%%
%%%%%%%%%%%%%%%%%

%%%STRIKER%%%%%
u2(1)=0;
u2d(1)=v0;
u2dd(1)=0;

%%%%%ROD%%%%%%
u1(1)=0;
u1d(1)=0;
u1dd(1)=0;

us(1)=0;
usd(1)=0;
usdd(1)=0;
ud_bot(1)=0;

uf(1)=0;
ufd(1)=0;
ufdd(1)=0;
%%%%DETERMINE EFFECTIVE
STIFFNESSES%%%%%%%%%%%%%%%%%%%%%%%%%%%%%%%%%%%
%%%%

%%%%%%ROD%%%%%%
KSeff=ksoil+a0*m1+(delta/(alpha*dt))*damp;
%%%ROG RIGID MOTION%%%%
KFeff=a0*m1;
%%%%STRIKER%%%%
K2eff=a0*m2;

%%INITIAL FORCE (t=0)%%
Ft(1)=0;
R(1)=0;
A1(1)=0;
A_bar1(1)=0;
B1(1)=0;
B_bar1(1)=0;

BC=input('Enter the boundary condition for the rod at x = L? (Elastic = 1, Fixed= 2, Free
= 3)');
```

```
n=10;%50; %%% NUMBER OF MODES TO CONSIDER
h = waitbar(0,'Initializing waitbar...');

if BC==1;
    for j=1:n;
     alphan(j)=j*3.26;
     w(j)=j*pi*c/L;%alphan(j)*c/L;
     C(j)=sqrt(2/m1);%% Normalized so that generalized mass = 1
     if psi==1;
        wD(j)=w(j);
     end
     if psi<1;
        wD(j)=w(j)*sqrt(1-psi^2);
     end
     if psi>1;
        wD(j)=w(j)*sqrt(psi^2-1);
     end
    end
else if BC==2
    for j=1:n;
     w(j)=(2*j-1)*pi*c/(2*L);
     C(j)=sqrt(2/m1);%% Normalized so that generalized mass = 1
     if psi==1;
        wD(j)=w(j);
     end
     if psi<1;
        wD(j)=w(j)*sqrt(1-psi^2);
     end
     if psi>1;
        wD(j)=w(j)*sqrt(psi^2-1);
     end
    end
    else if BC==3;
        for j=1:n;
        w(j)=j*pi*c/L;
         C(j)=sqrt(2/m1);%% Normalized so that generalized mass = 1
        if psi==1;
         wD(j)=w(j);
        end
        if psi<1;
         wD(j)=w(j)*sqrt(1-psi^2);
        end
        if psi>1;
         wD(j)=w(j)*sqrt(psi^2-1);
        end
    end
```

```
      else
     h=msgbox('Enter a valid value for the boundary condition at x = L ...( 1= Elastic , 2=
Fixed)','Boundary Condition Error','error');
     return
      end
   end
end
mult=2;
sum1=0;
sumUQUART1=0;
sumUBOT1=0;
sumUHALF1=0;
sumUTHREEQUARTERS1=0;

sumstressUQUART1=0;
sumstressUBOT1=0;
sumstressUHALF1=0;
sumstressUTHREEQUARTERS1=0;
A_bar1=zeros(n,n);
B_bar1=zeros(n,n);

for i=2:length(t);
   %%%%%%ROD%%%%%%%
   for j=1:n;
      if psi<1;
      %%DUE TO FORCE ON TOP (X = 0)%%
      A_bar1(i,j)=(A_bar1(i-1,j)+Ft(i-1)*cos(wD(j)*(t(i)-dt)))*exp(-psi*w(j)*dt)+...
         Ft(i-1)*cos(wD(j)*t(i));

      B_bar1(i,j)=(B_bar1(i-1,j)+Ft(i-1)*sin(wD(j)*(t(i)-dt)))*exp(-psi*w(j)*dt)+...
         Ft(i-1)*sin(wD(j)*t(i));

      G=dt/((m1)*wD(j)*mult);
      u1(i)=C(j)^2*(G*(A_bar1(i,j)*sin(wD(j)*t(i))-B_bar1(i,j)*cos(wD(j)*t(i))))+sum1;
      u1quarter(i)=C(j)^2*cos(w(j)*(L/4)/c)*(G*(A_bar1(i,j)*sin(w(j)*t(i))-
B_bar1(i,j)*cos(w(j)*t(i))))+sumUQUART1;
      u1half(i)=C(j)^2*cos(w(j)*(L/2)/c)*(G*(A_bar1(i,j)*sin(w(j)*t(i))-
B_bar1(i,j)*cos(w(j)*t(i))))+sumUHALF1;
      u1threequarters(i)=C(j)^2*cos(w(j)*(30*L/32)/c)*(G*(A_bar1(i,j)*sin(w(j)*t(i))-
B_bar1(i,j)*cos(w(j)*t(i))))+sumUTHREEQUARTERS1;
      u_bot1(i)=C(j)^2*cos(w(j)*L/c)*(G*(A_bar1(i,j)*sin(w(j)*t(i))-
B_bar1(i,j)*cos(w(j)*t(i))))+sumUBOT1;

      u1stressquarter(i)=Erod*(C(j)^2*(-
w(j)/c)*sin(w(j)*(L/4)/c)*(G*(A_bar1(i,j)*sin(w(j)*t(i))-
B_bar1(i,j)*cos(w(j)*t(i)))))+sumstressUQUART1;
```

```
    u1stresshalf(i)=Erod*(C(j)^2*(-
w(j)/c)*sin(w(j)*(L/2)/c)*(G*(A_bar1(i,j)*sin(w(j)*t(i))-
B_bar1(i,j)*cos(w(j)*t(i)))))+sumstressUHALF1;
    u1stressthreequarters(i)=Erod*(C(j)^2*(-
w(j)/c)*sin(w(j)*(3*L/4)/c)*(G*(A_bar1(i,j)*sin(w(j)*t(i))-
B_bar1(i,j)*cos(w(j)*t(i)))))+sumstressUTHREEQUARTERS1;
    u_stressbot1(i)=Erod*(C(j)^2*(-
w(j)/c)*sin(w(j)*L/c)*(G*(A_bar1(i,j)*sin(w(j)*t(i))-
B_bar1(i,j)*cos(w(j)*t(i)))))+sumstressUBOT1;

    sum1=u1(i);
    sumUQUART1=u1quarter(i);
    sumUHALF1=u1half(i);
    sumUTHREEQUARTERS1=u1threequarters(i);
    sumUBOT1=u_bot1(i);

    sumstressUQUART1=u1stressquarter(i);
    sumstressUHALF1=u1stresshalf(i);
    sumstressUTHREEQUARTERS1=u1stressthreequarters(i);
    sumstressUBOT1=u_stressbot1(i);

    end

    if psi==1;
    A_bar1(i,j)=A_bar1(i-1,j)+Ft(i-1)*exp(w(j)*(t(i)-dt))+Ft(i-1)*exp(w(j)*t(i));
    B_bar1(i,j)=B_bar1(i-1,j)+Ft(i-1)*(t(i)-dt)*exp(w(j)*(t(i)-dt))+Ft(i-
1)*t(i)*exp(w(j)*t(i));

    u1(i)=C(j)^2*(dt/(mult*m1)*(A_bar1(i,j)*t(i)*exp(-w(j)*t(i))-B_bar1(i,j)*exp(-
w(j)*t(i))))+sum1;

    sum1=u1(i);

    end

    if psi>1;
    A_bar1(i,j)=(A_bar1(i-1,j)+Ft(i-1)*cosh(wD(j)*(t(i)-dt)))*exp(-psi*w(j)*dt)+...
       Ft(i-1)*cosh(wD(j)*t(i));
    B_bar1(i,j)=(B_bar1(i-1,j)+Ft(i-1)*sinh(wD(j)*(t(i)-dt)))*exp(-psi*w(j)*dt)+...
       Ft(i-1)*sinh(wD(j)*t(i));

        G=dt/(m1*wD(j)*mult);

    u1(i)=C(j)^2*(G*(A_bar1(i,j)*sinh(wD(j)*t(i))-
B_bar1(i,j)*cosh(wD(j)*t(i))))+sum1;
```

```
    sum1=u1(i);

    end
  end
  sum1=0;
  sumUQUART1=0;
  sumUBOT1=0;
  sumUHALF1=0;
  sumUTHREEQUARTERS1=0;

  sumstressUQUART1=0;
  sumstressUHALF1=0;
  sumstressUTHREEQUARTERS1=0;
  sumstressUBOT1=0;
  %%%%STRIKER%%%%
  R2(i-1)=-Ft(i-1);
  R2eff(i)=R2(i-1)+m2*(a0*u2(i-1)+a1*u2d(i-1)+a2*u2dd(i-1));
  u2(i)=R2eff(i)*inv(K2eff);
  u2dd(i)=a0*(u2(i)-u2(i-1))-a1*u2d(i-1)-a2*u2dd(i-1);
  u2d(i)=u2d(i-1)+a3*u2dd(i-1)+a4*u2dd(i);

  %%SPRING DISPLACEMENT %%%
  if BC==1;
  RS(i-1)=Ft(i-1);%+damp*ud_bot(i-1);
  RSeff(i)=RS(i-1)+m1*(a0*us(i-1)+a1*usd(i-1)+a2*usdd(i-
1))+damp*((delta/(alpha*dt))*us(i-1)+(delta/alpha-1)*usd(i-1)+(dt/2)*(delta/alpha-
2)*usdd(i-1));
  us(i)=RSeff(i)*inv(KSeff);
  usdd(i)=a0*(us(i)-us(i-1))-a1*usd(i-1)-a2*usdd(i-1);
  usd(i)=usd(i-1)+a3*usdd(i-1)+a4*usdd(i);
   end

  %%RIGID BODY ROD DISPLACEMENT%%(FOR FREE-FREE BC)
  RF(i-1)=Ft(i-1);
  RFeff(i)=RF(i-1)+m1*(a0*uf(i-1)+a1*ufd(i-1)+a2*ufdd(i-1));
  uf(i)=RFeff(i)*inv(KFeff);
  ufdd(i)=a0*(uf(i)-uf(i-1))-a1*ufd(i-1)-a2*ufdd(i-1);
  ufd(i)=ufd(i-1)+a3*ufdd(i-1)+a4*ufdd(i);

  if BC==1;
    u1(i)=u1(i)+us(i);
    %u_bot1(i)=u_bot1(i)+us(i);
    %u1threequarters(i)=u1threequarters(i)+us(i);
    %ud_bot(i)=(u_bot1(i)-u1threequarters(i))/dt;
  else
    %ud_bot(i)=0;
```

```
end

if BC==3;
   u1(i)=u1(i)+uf(i);
   %u_bot1(i)=u_bot1(i)+uf(i);
end

%%%%INDENTATION FOR HERTZ FORCE%%%%%
ind(i)=u2(i)-u1(i);

%%% ELASTIC RANGE %%%%%%%%%%%%%%%%%%
if (ind(i)-ind_res1)<ind_y;
   if (ind(i)-ind_res1)<0;
      ind(i)=0;
      Ft(i)=0;
   else
      Probando=1;
      Ft(i)=kh*(ind(i)-ind_res1)^(1.5);
   end
end

%%% PLASTIC RANGE %%%%%%%%%%%%%%%%%%
if (ind(i)-ind_res1)>=ind_y;
   plastic=1;
end

if check==0;
   if ind(i)<ind(i-1);
      check=1;
      Fmax=Ft(i-1);
      ind_max=ind(i-1)-ind_res1;
      ind_res=ind_max-(3*Fmax/(4*E_star*R_star^(0.5)))^(2/3);
   end
end

if plastic==1;
   if check==0; %%% PLASTIC LOADING %%%%
      Ft(i)=kh*ind_y^(1.5)+pi*sigma_y*R_star*((ind(i)-ind_res1)-ind_y);
   else             %%%%%%% UNLOADING %%%%%%%%%
      if (ind(i)-ind_res1)>ind_res;
         Ft(i)=kh*((ind(i)-ind_res1)-ind_res)^(1.5);
      else
         Ft(i)=0;
      end
   end
end
```

```
%%%%%%%%%%%%%%%%%%%%%%%%%%%%%%%%%%%%%%%%%%%%%%%%%%%%%%%%%%%%%%%%%%%%%%%%%%%%%%%%%%%%%%
   %%%%%%   UPDATE THE DISPLACEMENTS BASED ON FORCE AT TIME t TO %%%%%%%
   %%%%%%                         SATISFY        EQUILIBRIUM %%%%%%%%%%%%%%%%%%%%%%%%%%%%%%%%%%%%%%%%%%%%%

%%%%%%%%%%%%%%%%%%%%%%%%%%%%%%%%%%%%%%%%%%%%%%%%%%%%%%%%%%%%%%%%%%%%%%%%%%%%%%%%%%%%%%
   diff=10;
   j=0;
   x=0;
   while diff>TOL;
   F_ref=Ft(i);
   iteration(i)=iteration(i)+1;
   Force_approx(iteration(i),i)=Ft(i);
   u1_approx(iteration(i),i)=u1(i);
   %%%%%%ROD%%%%%%%
   for j=1:n;
      if psi<1;

      A_bar1(i,j)=(A_bar1(i-1,j)+Ft(i-1)*cos(wD(j)*(t(i)-dt)))*exp(-psi*w(j)*dt)+...
         Ft(i)*cos(wD(j)*t(i));

      B_bar1(i,j)=(B_bar1(i-1,j)+Ft(i-1)*sin(wD(j)*(t(i)-dt)))*exp(-psi*w(j)*dt)+...
         Ft(i)*sin(wD(j)*t(i));

      G=dt/((m1)*wD(j)*mult);
      u1(i)=C(j)^2*(G*(A_bar1(i,j)*sin(wD(j)*t(i))-B_bar1(i,j)*cos(wD(j)*t(i))))+sum1;
      u1quarter(i)=C(j)^2*cos(w(j)*(L/4)/c)*(G*(A_bar1(i,j)*sin(w(j)*t(i))-B_bar1(i,j)*cos(w(j)*t(i))))+sumUQUART1;
      u1half(i)=C(j)^2*cos(w(j)*(L/2)/c)*(G*(A_bar1(i,j)*sin(w(j)*t(i))-B_bar1(i,j)*cos(w(j)*t(i))))+sumUHALF1;
      u1threequarters(i)=C(j)^2*cos(w(j)*(30*L/32)/c)*(G*(A_bar1(i,j)*sin(w(j)*t(i))-B_bar1(i,j)*cos(w(j)*t(i))))+sumUTHREEQUARTERS1;
      u_bot1(i)=C(j)^2*cos(w(j)*L/c)*(G*(A_bar1(i,j)*sin(w(j)*t(i))-B_bar1(i,j)*cos(w(j)*t(i))))+sumUBOT1;

      u1stresstop(i)=-1*Ft(i)/area;
      u1stressquarter(i)=Erod*(C(j)^2*(-w(j)/c)*sin(w(j)*(L/4)/c)*(G*(A_bar1(i,j)*sin(w(j)*t(i))-B_bar1(i,j)*cos(w(j)*t(i)))))+sumstressUQUART1;
```

```
    u1stresshalf(i)=Erod*(C(j)^2*(-
w(j)/c)*sin(w(j)*(L/2)/c)*(G*(A_bar1(i,j)*sin(w(j)*t(i))-
B_bar1(i,j)*cos(w(j)*t(i)))))+sumstressUHALF1;
    u1stressthreequarters(i)=Erod*(C(j)^2*(-
w(j)/c)*sin(w(j)*(3*L/4)/c)*(G*(A_bar1(i,j)*sin(w(j)*t(i))-
B_bar1(i,j)*cos(w(j)*t(i)))))+sumstressUTHREEQUARTERS1;
    u_stressbot1(i)=Erod*(C(j)^2*(-
w(j)/c)*sin(w(j)*L/c)*(G*(A_bar1(i,j)*sin(w(j)*t(i))-
B_bar1(i,j)*cos(w(j)*t(i)))))+sumstressUBOT1;

    sum1=u1(i);
    sumUQUART1=u1quarter(i);
    sumUHALF1=u1half(i);
    sumUTHREEQUARTERS1=u1threequarters(i);
    sumUBOT1=u_bot1(i);

    sumstressUQUART1=u1stressquarter(i);
    sumstressUHALF1=u1stresshalf(i);
    sumstressUTHREEQUARTERS1=u1stressthreequarters(i);
    sumstressUBOT1=u_stressbot1(i);

    end

    if psi==1;
    A_bar1(i,j)=A_bar1(i-1,j)+Ft(i-1)*exp(w(j)*(t(i)-dt))+Ft(i)*exp(w(j)*t(i));
    B_bar1(i,j)=B_bar1(i-1,j)+Ft(i-1)*(t(i)-dt)*exp(w(j)*(t(i)-
dt))+Ft(i)*t(i)*exp(w(j)*t(i));

    u1(i)=C(j)^2*(dt/(mult*m1)*(A_bar1(i,j)*t(i)*exp(-w(j)*t(i))-B_bar1(i,j)*exp(-
w(j)*t(i))))+sum1;

    sum1=u1(i);
    end

    if psi>1;
    A_bar1(i,j)=(A_bar1(i-1,j)+Ft(i-1)*cosh(wD(j)*(t(i)-dt)))*exp(-psi*w(j)*dt)+...
       Ft(i)*cosh(wD(j)*t(i));
    B_bar1(i,j)=(B_bar1(i-1,j)+Ft(i-1)*sinh(wD(j)*(t(i)-dt)))*exp(-psi*w(j)*dt)+...
       Ft(i)*sinh(wD(j)*t(i));

    G=dt/(m1*wD(j)*mult);
    u1(i)=C(j)^2*(G*(A_bar1(i,j)*sinh(wD(j)*t(i))-
B_bar1(i,j)*cosh(wD(j)*t(i))))+sum1;

    sum1=u1(i);
    end
```

```
end

 sum1=0;
 sumUQUART1=0;
 sumUBOT1=0;
 sumUHALF1=0;
 sumUTHREEQUARTERS1=0;

 sumstressUQUART1=0;
 sumstressUHALF1=0;
 sumstressUTHREEQUARTERS1=0;
 sumstressUBOT1=0;

 %%%% STRIKER
 R2(i)=-Ft(i);
 R2eff(i)=R2(i)+m2*(a0*u2(i-1)+a1*u2d(i-1)+a2*u2dd(i-1));
 u2(i)=R2eff(i)*inv(K2eff);
 u2dd(i)=a0*(u2(i)-u2(i-1))-a1*u2d(i-1)-a2*u2dd(i-1);
 u2d(i)=u2d(i-1)+a3*u2dd(i-1)+a4*u2dd(i);

 %%SPRING DISPLACEMENT %%%
 if BC==1;
 RS(i)=Ft(i);%+damp*ud_bot(i);
 RSeff(i)=RS(i)+m1*(a0*us(i-1)+a1*usd(i-1)+a2*usdd(i-
1))+damp*((delta/(alpha*dt))*us(i-1)+(delta/alpha-1)*usd(i-1)+(dt/2)*(delta/alpha-
2)*usdd(i-1));
 us(i)=RSeff(i)*inv(KSeff);
 usdd(i)=a0*(us(i)-us(i-1))-a1*usd(i-1)-a2*usdd(i-1);
 usd(i)=usd(i-1)+a3*usdd(i-1)+a4*usdd(i);
 end

 %%RIGID BODY ROD DISPLACEMENT%%(FOR FREE-FREE BC)
 RF(i-1)=Ft(i);
 RFeff(i)=RF(i-1)+m1*(a0*uf(i-1)+a1*ufd(i-1)+a2*ufdd(i-1));
 uf(i)=RFeff(i)*inv(KFeff);
 ufdd(i)=a0*(uf(i)-uf(i-1))-a1*ufd(i-1)-a2*ufdd(i-1);
 ufd(i)=ufd(i-1)+a3*ufdd(i-1)+a4*ufdd(i);

 if BC==1;
    u1(i)=u1(i)+us(i);
    %u_bot1(i)=u_bot1(i)+us(i);
    %u1threequarters(i)=u1threequarters(i)+us(i);
    %ud_bot(i)=(u_bot1(i)-u1threequarters(i))/dt;
 else
    %ud_bot(i)=0;
 end
```

```
if BC==3;
   u1(i)=u1(i)+uf(i);
   %u_bot1(i)=u_bot1(i)+uf(i);
end

%%CONTACT FORCE%%%%
ind(i)=u2(i)-u1(i);

%%%%% ELASTIC RANGE %%%%%%%%%%%%%%%%%%
if (ind(i)-ind_res1)<ind_y;
   if (ind(i)-ind_res1)<0;
      ind(i)=0;
      Ft(i)=0;
   else
      Ft(i)=kh*(ind(i)-ind_res1)^(1.5);
   end
end

%%% PLASTIC RANGE %%%%%%%%%%%%%%%%%%
if (ind(i)-ind_res1)>=ind_y;
   plastic=1;
end

if check==0;
   if ind(i)<ind(i-1);
      check=1;
      Fmax=Ft(i-1);
      ind_max=ind(i-1)-ind_res1;
      ind_res=ind_max-(3*Fmax/(4*E_star*R_star^(0.5)))^(2/3);
   end
end

if plastic==1;
   if check==0; %%% PLASTIC LOADING %%%%
      Ft(i)=kh*ind_y^(1.5)+pi*sigma_y*R_star*((ind(i)-ind_res1)-ind_y);
   else             %%%%%%% UNLOADING %%%%%%%%%
      if (ind(i)-ind_res1)>ind_res;
         Ft(i)=kh*((ind(i)-ind_res1)-ind_res)^(1.5);
      else
         Ft(i)=0;
      end
   end
end

j=j+1;
```

```
    diff=abs(F_ref-Ft(i));
    end

    perc(i)=i*prog;
    if perc(i)>0.10 && perc(i)<0.30;
        perc = 20;
        waitbar(perc/100,h,sprintf('%d%% along...',perc))
    else if perc(i)>0.31 && perc(i)<0.5;
        perc = 40;
        waitbar(perc/100,h,sprintf('%d%% along...',perc))
        else if perc(i)>0.51 && perc(i)<0.69;
        perc = 60;
        waitbar(perc/100,h,sprintf('%d%% along...',perc))
            else if perc(i)>0.7 && perc(i)<0.95;
            perc = 80;
            waitbar(perc/100,h,sprintf('%d%% along...',perc))
                else if perc(i)>0.96;
                perc = 100;
                waitbar(perc/100,h,sprintf('Analysis Completed'))
                    end
                end
            end
        end
    end

%%%%%%%%%%%%%%%%%%%%%%%%%%%%%%%%%%%%%%%%%%%%%%%%%%%%%%%%%%%%%%%%%%%%%%%%%%%%%
    %%%%%%     END OF UPDATING DISPLACEMENTS TO SATISFY EQUILIBRIUM   %%%%%%

%%%%%%%%%%%%%%%%%%%%%%%%%%%%%%%%%%%%%%%%%%%%%%%%%%%%%%%%%%%%%%%%%%%%%%%%%%%%%
end

%%%
ind=ind'*10^6;
Ft=Ft';%/1000;
t=t'*10^6;
u1=u1'*10^6;
u2=u2'*10^6;
u_bot1=u_bot1*10^6;
u1threequarters=u1threequarters*10^6;

forExcel(:,1)=Ft;
forExcel(:,2)=u1;
forExcel(:,3)=u2;
```

```
plot(t,u1)
% u1quarter=u1quarter'*10^6;
% u1half=u1half'*10^6;
% u1threequarters=u1threequarters'*10^6;
% u_bot1=u_bot1'*10^6;
% u1stresstop=u1stresstop'*10^-6;
% u1stressquarter=u1stressquarter'*10^-6;
% u1stresshalf=u1stresshalf';
% u1stressthreequarters=u1stressthreequarters'*10^-6;
% u_stressbot1=u_stressbot1'*10^-6;
%
% %%%%%%%%%%%%%%%%%%%%%%%%%%%%%%%%%%%%%%%%%%%%%%%%%%%%%%%%
% [AX,H1,H2] = plotyy(t,u1,t,Ft);
% %xlim(AX(2),[0 duration]);
% %xlim(AX(1),[0 duration]);
% hold on
% plot(t,u2,':','Color','k','LineWidth',2);ylim([0 3e-5])
% %set(AX(1),'ytick',[0:0.5e-5:3e-5]);
% set(AX,{'ycolor'},{'k';'r'},'fontsize',14)
% set(H1,'Color','k');
% set(H2,'Color','r','LineStyle','--','LineWidth',2);
% ylabel(AX(2),'Force (N)');
% ylabel('Displacement (m)');
% xlabel('Time(sec)');
% title('Displacement and Force History (Newmark)');
% legend('u1 (Rod)','u2 (Striker)','Force');
%
```

Appendix D:

MATLAB code for in-house finite element model

```
%%%% LONGITUDINAL IMPACT OF A SPHERICAL STRIKER AND A UNIFORM ROD %%%%%%%
%%%% FEM ANALYSIS, DIRECT INTEGRATION SOLVER: NEWMARK METHOD %%%%%%%%%%%
%%%% (AVERAGE ACCELERATION METHOD)%%%%%%%%%%%%%%%%%%%%%%%%%%%%%%%%%%%%%%%

clear all

dt=0.000001;%0.0000001;%0.00002;
duration=0.003;%0.002;%
t=[0:dt:duration];
TOL=1e-10;
prog=dt/duration;

%fd=30;%20*10^3;

%%%%%%PROPERTIES OF THE STRIKER%%%%%%%%%%%%%%%%%%%%%%%%%%%%
m2=0.067053;%0.4984;%0.013745;%0.06721;
Emass=203*10^9;%203*10^9;% %Pa
vmass=0.3;
Rmass=0.0254/2;%0.0248;%0.014986/2;%0.0127;%0.0254/2;  ;%%RADIUS OF THE STRIKER
rhomass=7833.5;% %kg/m3 (STRIKER)
h=0.03;%0.15;%Drop Altittude, m
v0=sqrt(2*9.81*h);%0.5; %m/s INITIAL VELOCITY OF THE STRIKER


%%%%%%PROPERTIES OF THE ROD%%%%%%%%%%%%%%%%%%%%%%%%%%%%%%%%
L=0.62;%0.15;%0.075; %m (ROD)
D=0.1; %m
area=0.000285;%pi*(D/2)^2;%%0.0028;%0.00114;%0.00028502;%%
rho=7788.6;%%kg/m3 (ROD)
Erod=209*10^9;%209*10^9;% %Pa
vrod=0.3;
m1=rho*area*L;
cwave=sqrt(Erod/rho);
k1=Erod*area/L;
```

```
ksoil=5*10^6; %N/m
psi=0.5;
psi_soil=0;
cwave=sqrt(Erod/rho);
Rrod=0; %RADIUS OF CURVATURE OF TOP SURFACE OF THE ROD


%%%%%DEFINE PROPERTIES OF PLASTIC MODEL%%%%%%%%%%%%%%%%%%%%%%%%%%%%%%%%%%%%
sigma_y=200*10^60000000000;%1.5*10^9;%2.1435*10^9; %Yield strength of the rod(Pa)
E_star=((1-vrod^2)/Erod+(1-vmass^2)/Emass)^(-1);
if Rrod==0;
   R_star=Rmass;
else
   R_star=(1/Rmass+1/Rrod)^(-1);
end
ind_res1=0;
ind_y=(pi*sigma_y/(2*E_star))^2*R_star;%0.000025;  2.352521382479062e-04-ind_res1;%
Fy=sigma_y*ind_y*2*pi*R_star/3;
plastic=0;
check=0;
ind_max=0;
ind_res=0;
Fmax=0;

%%%%%DEFINE HERTZ CONTACT PARAMETERS%%%%%%%%%%%%%%%%%%%%%%%%%%%%%%%%%%%%%%%%
deltarod=(1-vrod^2)/(Erod*pi);
deltamass=(1-vmass^2)/(Emass*pi);
kh=(4/3)*E_star*sqrt(R_star);
%kh=(4/(3*pi))*sqrt(Rmass)*(1/(deltarod+deltamass));

%%%%%CALCULATE CONSTANTS FOR NEWMARK BETA METHOD%%%%%%%%%%%%%%%%%%%%%%%%%%
alpha=0.25;
delta=0.5;

a0=1/(alpha*dt^2);
a1=delta/(alpha*dt);
a2=1/(alpha*dt);
a3=1.d0/(2*alpha)-1.d0;
a4=delta/alpha-1;
a5=dt/2*(delta/alpha-2);
```

```
a6=dt*(1.d0-delta);
a7=delta*dt;

Nels=input('Number of Elements');
BC=input('Enter the boundary condition for the rod at x = L? (Fixed= 1, Free= 2, Elastic
= 3)');
h = waitbar(0,'Initializing waitbar...');

if BC==1;  %CHECK FOR FIXED BOUNDARY CONDITION

%%%%%INITIAL
CONDITIONS%%%%%%%%%%%%%%%%%%%%%%%%%%%%%%%%%%
%%%%%%%%%%%%%%%%%%

%%%STRIKER%%%%%
u2(1)=0;
u2d(1)=v0;
u2dd(1)=0;

%%%%%ROD%%%%%%
u1(1,1)=0;
u1d(1,1)=0;
u1dd(1,1)=0;

R1=zeros(Nels,1);

K=zeros(Nels,Nels);
M=zeros(Nels,Nels);
u1=zeros(Nels,1);
u1d=zeros(Nels,1);
u1dd=zeros(Nels,1);

%%%%%%%%%%%%%%%%%%%%%%%%%%%%%%%%%%%%%%%%%
%%%%%%%%%%%%%%%%%%%%%%%%%%%%%%%%%%
%%%%%%%%%%%%%%%%%%%%%%%%%%%%%%%%%%%%%%%%%
%%%%%%%%%%%%%%%%%%%%%%%%%%%%%%%%%%

%%%%%%%%%%%%%%%%%%%%%%%%%%%%%%%%%%%%%%%%%
%%%%%%%%%%%%%%%%%%%%%%%%%%%%%%%%%%
%%%%%%%%%%%%% SYSTEM MATRICES ASSEMBLY (STIFFNESS AND
MASS)%%%%%%%%%%%%%%%%
%%%%%%%%%%%%% FOR FIXED BOUNDARY CONDITION AT X = L
%%%%%%%%%%%%%%%%%%%%%%%
for i=2:Nels;
   K(1,1)=1;
   K(1,2)=-1;
```

```
   K(Nels+1,Nels)=-1;
   K(Nels+1,Nels+1)=1;
   K(i,i)=2;
   K(i,i+1)=-1;
   K(i,i-1)=-1;

   M(1,1)=2;
   M(1,2)=1;
   M(Nels+1,Nels)=1;
   M(Nels+1,Nels+1)=2;
   M(i,i)=4;
   M(i,i+1)=1;
   M(i,i-1)=1;
end

K_initial=Erod*area/(L/Nels)*K;  %STIFFNESS MATRIX WITHOUT B.C.s
M_initial=rho*area*(L/Nels)/6*M; %MASS MATRIX WITHOUT B.C.s

K=K_initial(1:Nels,1:Nels);
M=M_initial(1:Nels,1:Nels);
%%%%%MODE SHAPE AND NATURAL FREQUENCIES %%%%%%
[mode_shape wsq]=eig(K,M);
wn=sqrt(diag(wsq));
wn=sort(wn);
 for i=1:Nels;                    %%%%%%%%%%%%%%%%
   c(i)=2*M(i,i)*wn(i)*psi;      %%%%%%%%%%%%%%%%
 end
 C=zeros(Nels,Nels);               %%%%%%%%%%%%%%%%
                          %%%%%%%%%%%%%%%%
 for i=1:Nels;                    %%%%%%%%%%%%%%%%
%     Eq1=[1,wn(1)^2;1,wn(Nels)^2];
%     Eq2=[2*wn(1)*psi;2*wn(Nels)*psi];
%     Eq3=inv(Eq1)*Eq2;
   Eq1=[1,wn(1)^2;1,wn(2)^2];
   Eq2=[2*wn(1)*psi;2*wn(2)*psi];
   Eq3=inv(Eq1)*Eq2;
 end
  alpha1=Eq3(1);
  beta1=Eq3(2);
  C=alpha1*M+beta1*K;

else if BC==2; %CHECK FOR FREE BOUNDARY CONDITION
       %%%INITIAL CONDITIONS %%%
       %%%STRIKER%%%%%
       u2(1)=0;
       u2d(1)=v0;
```

```
u2dd(1)=0;

%%%%%ROD%%%%%%
u1(1,1)=0;
u1d(1,1)=0;
u1dd(1,1)=0;

R1=zeros(Nels+1,1);
K=zeros(Nels+1,Nels+1);
M=zeros(Nels+1,Nels+1);
u1=zeros(Nels+1,1);
u1d=zeros(Nels+1,1);
u1dd=zeros(Nels+1,1);


%%%%%%%%%%%%%%%%%%%%%%%%%%%%%%%%%%%%%%%%%
%%%%%%%%%%%%%%%%%%%%%%%%%%
%%%%%%%%%%%%% SYSTEM MATRICES ASSEMBLY (STIFFNESS
AND MASS)%%%%%%%%
%%%%%%%%%%%%% FOR FREE BOUNDARY CONDITION AT X =L
%%%%%%%%%%%%%%%%%

for i=2:Nels;
   K(1,1)=1;
   K(1,2)=-1;
   K(Nels+1,Nels)=-1;
   K(Nels+1,Nels+1)=1;
   K(i,i)=2;
   K(i,i+1)=-1;
   K(i,i-1)=-1;

   M(1,1)=2;
   M(1,2)=1;
   M(Nels+1,Nels)=1;
   M(Nels+1,Nels+1)=2;
   M(i,i)=4;
   M(i,i+1)=1;
   M(i,i-1)=1;
end

K_initial=Erod*area/(L/Nels)*K;  %STIFFNESS MATRIX WITHOUT B.C.s
M_initial=rho*area*(L/Nels)/6*M; %MASS MATRIX WITHOUT B.C.s

%%%APPLY B.C.: FIXED AT X = L
K=K_initial;
M=M_initial;
```

```
    %%%%%MODE SHAPE AND NATURAL FREQUENCIES %%%%%%
    [mode_shape wsq]=eig(K,M);
    wn=sqrt(diag(wsq));
    wn=sort(wn);
    % %%%% MODAL DAMPING MATRIX %%%%
    for i=1:Nels+1;                  %%%%%%%%%%%%%%%%%
       c(i)=2*M(i,i)*wn(i)*psi;      %%%%%%%%%%%%%%%%%
    end
    C=zeros(Nels+1,Nels+1);              %%%%%%%%%%%%%%%%
                          %%%%%%%%%%%%%%%%%
    for i=1:Nels+1;                  %%%%%%%%%%%%%%%%%
%         Eq1=[1,wn(1)^2;1,wn(Nels+1)^2];
%         Eq2=[2*wn(1)*psi;2*wn(Nels+1)*psi];
%         Eq3=inv(Eq1)*Eq2;
       Eq1=[1,wn(1)^2;1,wn(2)^2];
       Eq2=[2*wn(1)*psi;2*wn(2)*psi];
       Eq3=inv(Eq1)*Eq2;
    end
      alpha1=Eq3(1);
      beta1=Eq3(2);
      C=alpha1*M+beta1*K;
      C=real(C);
  else if BC==3;
       %%%INITIAL CONDITIONS %%%
    %%%STRIKER%%%%%
    u2(1)=0;
    u2d(1)=v0;
    u2dd(1)=0;

    %%%%%ROD%%%%%%
    u1(1,1)=0;
    u1d(1,1)=0;
    u1dd(1,1)=0;

    R1=zeros(Nels+1,1);
    K=zeros(Nels+1,Nels+1);
    M=zeros(Nels+1,Nels+1);
    u1=zeros(Nels+1,1);
    u1d=zeros(Nels+1,1);
    u1dd=zeros(Nels+1,1);

     for i=2:Nels;
       K(1,1)=Erod*area/(L/Nels);
       K(1,2)=-Erod*area/(L/Nels);
       K(Nels+1,Nels)=-Erod*area/(L/Nels);
       K(Nels+1,Nels+1)=Erod*area/(L/Nels);
```

```
  K(i,i)=2*Erod*area/(L/Nels);
  K(i,i+1)=-Erod*area/(L/Nels);
  K(i,i-1)=-Erod*area/(L/Nels);
  K(Nels+1,Nels+2)=-ksoil;
  K(Nels+2,Nels+1)=-ksoil;
  K(Nels+2,Nels+2)=ksoil;

  M(1,1)=2;
  M(1,2)=1;
  M(Nels+1,Nels)=1;
  M(Nels+1,Nels+1)=2;
  M(i,i)=4;
  M(i,i+1)=1;
  M(i,i-1)=1;
  M(Nels+2,Nels+2)=0;
end

K_initial=K;  %STIFFNESS MATRIX WITHOUT B.C.s
M_initial=rho*area*(L/Nels)/6*M; %MASS MATRIX WITHOUT B.C.s

%%%APPLY B.C.: FIXED AT X = L
K=K_initial(1:Nels+1,1:Nels+1);
M=M_initial(1:Nels+1,1:Nels+1);
K_slide=K;
M_slide=M;
K(Nels+1,Nels+1)=K(Nels+1,Nels+1)+ksoil;

%%%%%MODE SHAPE AND NATURAL FREQUENCIES %%%%%%
[mode_shape wsq]=eig(K,M);
wn=sqrt(diag(wsq));
wn=sort(wn);

[ms_slide wsq_slide]=eig(K_slide,M_slide);
wn_slide=sqrt(diag(wsq_slide));
wn_slide=sort(wn_slide);
                    %%%%%%%%%%%%%%%%
for i=1:Nels+1;                 %%%%%%%%%%%%%%%%
%       Eq1=[1,wn(1)^2;1,wn(Nels+1)^2];
%       Eq2=[2*wn(1)*psi;2*wn(Nels+1)*psi];
%       Eq3=inv(Eq1)*Eq2;
  Eq1=[1,wn(1)^2;1,wn(2)^2];
  Eq2=[2*wn(1)*psi;2*wn(2)*psi];
  Eq3=inv(Eq1)*Eq2;
  Eq1_slide=[1,wn_slide(1)^2;1,wn_slide(Nels+1)^2];
  Eq2_slide=[2*wn_slide(1)*psi;2*wn_slide(Nels+1)*psi];
  Eq3_slide=inv(Eq1_slide)*Eq2_slide;
```

```
        end
         alpha1=Eq3(1);
         beta1=Eq3(2);
         C=alpha1*M+beta1*K;
         C=real(C);

         %C=zeros(Nels+1,Nels+1);              %%%%%%%%%%%%%%%%
         %C(Nels+1,Nels+1)=C(Nels+1,Nels+1)+2*m1*sqrt(5*10^6/m1)*psi_soil;
         C(Nels+1,Nels+1)=C(1,1);

      else
          h=msgbox('Enter a valid value for the boundary condition at x = L ...( 1= Fixed
, 2= free)','Boundary Condition Error','error');
          return
   end
end
end
%%%%              DETERMINE              EFFECTIVE              STIFFNESSES
%%%%%%%%%%%%%%%%%%%%%%%%%%%%%%%%%%%%%%%%%%%%%%%%%%%%%%%%%%%%%%%%%%%%%%%%
K1eff=K+a0*M+a1*C;
K2eff=a0*m2;

%%INITIAL FORCE (t=0)%%
Ft(1)=0;
for i=2:length(t);
   %%%%%%ROD%%%%%%%
   R1(1,i-1)=Ft(i-1);
   R1eff(:,i)=R1(:,i-1)+M*(a0*u1(:,i-1)+a2*u1d(:,i-1)+a3*u1dd(:,i-1))+...
      C*(a1*u1(:,i-1)+a4*u1d(:,i-1)+a5*u1dd(:,i-1));
   u1(:,i)=inv(K1eff)*R1eff(:,i);
   u1dd(:,i)=a0*(u1(:,i)-u1(:,i-1))-a2*u1d(:,i-1)-a3*u1dd(:,i-1);
   u1d(:,i)=u1d(:,i-1)+a6*u1dd(:,i-1)+a7*u1dd(:,i);


   %%%%STRIKER%%%%
   R2(i-1)=-Ft(i-1);
   R2eff(i)=R2(i-1)+m2*(a0*u2(i-1)+a2*u2d(i-1)+a3*u2dd(i-1));
   u2(i)=R2eff(i)*inv(K2eff);
   u2dd(i)=a0*(u2(i)-u2(i-1))-a2*u2d(i-1)-a3*u2dd(i-1);
   u2d(i)=u2d(i-1)+a6*u2dd(i-1)+a7*u2dd(i);

   %%%%INDENTATION FOR HERTZ FORCE%%%%%
   ind(i)=u2(i)-u1(1,i);

   %%% ELASTIC RANGE %%%%%%%%%%%%%%%%%%
   if (ind(i)-ind_res1)<ind_y;
```

```
      if (ind(i)-ind_res1)<0;
         ind(i)=0;
         Ft(i)=0;
      else
         Ft(i)=kh*(ind(i)-ind_res1)^(1.5);
      end
  end

   %%% PLASTIC RANGE %%%%%%%%%%%%%%%%%%
   if (ind(i)-ind_res1)>=ind_y;
      plastic=1;
   end

   if check==0;
      if ind(i)<ind(i-1);
         check=1;
         Fmax=Ft(i-1);
         ind_max=ind(i-1)-ind_res1;
         ind_res=ind_max-(3*Fmax/(4*E_star*R_star^(0.5)))^(2/3);
      end
   end

   if plastic==1;
      if check==0; %%% PLASTIC LOADING %%%%
         Ft(i)=kh*ind_y^(1.5)+pi*sigma_y*R_star*((ind(i)-ind_res1)-ind_y);
      else             %%%%%% UNLOADING %%%%%%%%
         if (ind(i)-ind_res1)>ind_res;
            Ft(i)=kh*((ind(i)-ind_res1)-ind_res)^(1.5);
         else
            Ft(i)=0;
         end
      end
   end



%%%%%%%%%%%%%%%%%%%%%%%%%%%%%%%%%%%%%%%%%%%%%%%%
%%%%%%%%%%%%%%%%%%%%%%%%%%%%%%%%%%%
   %%%%%%   UPDATE THE DISPLACEMENTS BASED ON FORCE AT TIME t
TO %%%%%%%
   %%%%%%                   SATISFY     EQUILIBRIUM          (EQUILIBRIUM
ITERATIONS)%%%%%%%%%%%%%%%

%%%%%%%%%%%%%%%%%%%%%%%%%%%%%%%%%%%%%%%%%%%%%%%%
%%%%%%%%%%%%%%%%%%%%%%%%%%%%%%%%%%%
```

```
diff=10;
j=0;
while diff>TOL;
F_ref=Ft(i);
R1(1,i)=Ft(i);
R1eff(:,i)=R1(:,i)+M*(a0*u1(:,i-1)+a2*u1d(:,i-1)+a3*u1dd(:,i-1))+...
   C*(a1*u1(:,i-1)+a4*u1d(:,i-1)+a5*u1dd(:,i-1));
u1(:,i)=inv(K1eff)*R1eff(:,i);
u1dd(:,i)=a0*(u1(:,i)-u1(:,i-1))-a2*u1d(:,i-1)-a3*u1dd(:,i-1);
u1d(:,i)=u1d(:,i-1)+a6*u1dd(:,i-1)+a7*u1dd(:,i);

R2(i)=-Ft(i);
R2eff(i)=R2(i)+m2*(a0*u2(i-1)+a2*u2d(i-1)+a3*u2dd(i-1));
u2(i)=R2eff(i)*inv(K2eff);
u2dd(i)=a0*(u2(i)-u2(i-1))-a2*u2d(i-1)-a3*u2dd(i-1);
u2d(i)=u2d(i-1)+a6*u2dd(i-1)+a7*u2dd(i);

ind(i)=u2(i)-u1(1,i);

%%%%% ELASTIC RANGE %%%%%%%%%%%%%%%%%%
if (ind(i)-ind_res1)<ind_y;
   if (ind(i)-ind_res1)<0;
      ind(i)=0;
      Ft(i)=0;
   else
      Ft(i)=kh*(ind(i)-ind_res1)^(1.5);
   end
end

%%% PLASTIC RANGE %%%%%%%%%%%%%%%%%%
if (ind(i)-ind_res1)>=ind_y;
   plastic=1;
end

if check==0;
   if ind(i)<ind(i-1);
      check=1;
      Fmax=Ft(i-1);
      ind_max=ind(i-1)-ind_res1;
      ind_res=ind_max-(3*Fmax/(4*E_star*R_star^(0.5)))^(2/3);
   end
end

if plastic==1;
   if check==0; %%% PLASTIC LOADING %%%%
      Ft(i)=kh*ind_y^(1.5)+pi*sigma_y*R_star*((ind(i)-ind_res1)-ind_y);
```

```
    else            %%%%%% UNLOADING %%%%%%%%
      if (ind(i)-ind_res1)>ind_res;
        Ft(i)=kh*((ind(i)-ind_res1)-ind_res)^(1.5);
      else
        Ft(i)=0;
      end
    end
  end

  j=j+1;
  diff=abs(F_ref-Ft(i));
  end

  perc(i)=i*prog;
  if perc(i)>0.10 && perc(i)<0.30;
    perc = 20;
    waitbar(perc/100,h,sprintf('%d%% along...',perc))
  else if perc(i)>0.31 && perc(i)<0.5;
    perc = 40;
    waitbar(perc/100,h,sprintf('%d%% along...',perc))
    else if perc(i)>0.51 && perc(i)<0.69;
    perc = 60;
    waitbar(perc/100,h,sprintf('%d%% along...',perc))
      else if perc(i)>0.7 && perc(i)<0.95;
      perc = 80;
      waitbar(perc/100,h,sprintf('%d%% along...',perc))
        else if perc(i)>0.96;
        perc = 100;
        waitbar(perc/100,h,sprintf('Analysis Completed'))
          end
        end
      end
    end
  end

%%%%%%%%%%%%%%%%%%%%%%%%%%%%%%%%%%%%%%
%%%%%%%%%%%%%%%%%%%%%%%%%%%
  %%%%%%%%%%%%%%%     END OF EQUILIBRIUM ITERATIONS
%%%%%%%%%%%%%%%%%%

%%%%%%%%%%%%%%%%%%%%%%%%%%%%%%%%%%%%%%
%%%%%%%%%%%%%%%%%%%%%%%%%%%
end

%%%%%%%%%%%%%%%%%%%%%%%%%%%%%%%%%%%%%%
%%%%%%%%%%%%%%%%%%%%%%%%%%%%%%
```

```
%%%%%%%%%%%%%%%%%%%%%%%%%%%%%%%%%%%%%%%%%%%%%%%
%%%%%%%%%%%%%%%%%%%%%%%%%%%%%%%%%%%%%%
u1=real(u1);
Ft=real(Ft);
u2=real(u2);
ind=real(ind);
a_res=sqrt(R_star*(ind_max-ind_y));
R_res=(ind_res^2+a_res^2)/(2*ind_res);
NextImpact_indres1=ind_res1+ind_res;
NextImpact_ind_y=ind_max+ind_res1;
NextImpact_R_star=(4*E_star/(3*Fmax))*((2*Fmax+Fy)/(2*pi*sigma_y))^(3/2);

%%%CALCULATE FORCE CONSIDERING ELASTIC DEFORMATION
ONLY%%%%%%%%%%%%%%%%%%
for i=1:length(t);
   Ft_elastic(i)=kh*(ind(i)-ind_res1)^(1.5);
   yield_ind(i)=(ind_res1+ind_y)*10^6;
end

for i=1:length(t);
   u1(Nels+1,i)=0;
end

for i=1:length(t);
   u1_stress(1,i)=-1*Ft(i)/area;
   for j=2:Nels+1;
      u1_stress(j,i)=Erod*((u1(j,i)-u1(j-1,i))/(L/Nels));
   end
end


%%%
ind=ind'*10^6;
Ft=Ft';
t=t'*10^6;
u1=u1'*10^6;
u2=u2'*10^6;
Ft_elastic=Ft_elastic'/1000;
u1_stress=u1_stress'*10^-6;

%
%%%%%%%%%%%%%%%%%%%%%%%%%%%%%%%%%%%%%%%%%%%%%%%
%%%%%%%%%%%%%%%%%%%%%%%%%%%%%%%%%%%%%%
% %%%%%%%%%%%%%%%%%%%%%% PLOT FORCE AND DISPLACEMENTS
%%%%%%%%%%%%%%%%%%%%%%%%%%%
```

```
%
%%%%%%%%%%%%%%%%%%%%%%%%%%%%%%%%%%%%%%%%%%%%%%%%%%%%%%%%%%%%%%%%%%%%%%%%%%%%%%%%%%%%
%
[AX,H1,H2] = plotyy(t,u1(:,1),t,Ft);
xlim(AX(2),[0 duration*10^6]);
xlim(AX(1),[0 duration*10^6]);
hold on
plot(t,u2,':','Color','k','LineWidth',2);ylim([min(u1(:,1)) 300])
set(AX(1),'ytick',[0:50:300]);
set(AX,{'ycolor'},{'k';'r'},'fontsize',12)
set(H1,'Color','k');
set(H2,'Color','r','LineStyle','--','LineWidth',2);
ylabel(AX(2),'Force (N)');
ylabel('Displacement (m)');
xlabel('Time(sec)');
title('Displacement and Force History (Newmark)');
legend('u1 (Rod)','u2 (Striker)','Force');
%
%
% %%% PLOT THE FORCE VS INDENTATION FOR PLASTIC AND ELASTIC IMPACT%%%%%%%%%%
% figure; plot(ind,Ft,'r',ind,Ft_elastic,'k',yield_ind,Ft_elastic,':b')
% ylabel('Force (N)');
% xlabel('Indentation(m*10^-6)');
% title('Force-Indentation Curve');
% legend('Elasto-Plastic','Elastic');
%
% %%% Surface Plot %%
%
for  i=1:Nels;
Length(1)=0;
Length(i+1)=i*(L/Nels);
end
Length=Length/L;
%
% figure;surf(Length,t,u1_stress);

%%%%% Stres Distribution Plot %%%
% figure; plot(Length,u1_stress(31,:),'k',Length,u1_stress(61,:),'b',...
%     Length,u1_stress(78,:),'r',Length,u1_stress(91,:),':k',Length,u1_stress(131,:),':b',...
%     Length,u1_stress(141,:),':r',Length,u1_stress(161,:),':g')

forexcel(:,1)=Ft;
forexcel(:,2)=u1(:,1);
forexcel(:,3)=u2;
```

References and Bibliography:

1. Abaqus FEA version 6.12. Providence, RI: Dassault Systemes Simulia Corp. 2012.

2. ASCE Task Committee. (1992). "Overview of Existing Lunar Base Structural Concepts." *ASCE – J. of Aerospace Engineering*, 5(2), 159-174.

3. Bachman, H., Ammann, W., Deischl, F., Eisenmann, J., Floegl, I., Hirsch, G., Klein, G., Lande, G., Mahrenholtz, O., Natke, H., Nussbaumer, H., Pretlove, A., Rainer, J., Saemann, E., Steinbeisser, L. (1995). *Vibration Problems in Structures: Practical Guidelines*. Birkhauser Verlag Basel, Germany.

4. Bao, X., Bar-Cohen, Y., Chang, Z., Dolgin, B., Sherrit, S., Pal, D., Du, S., and Peterson, T. (2003). "Modeling and Computer Simulation of Ultrasonic/Sonic/Driller/Corer (USDC)." *IEEE Transactions on Ultrasonics, Ferroelectrics, and Frequency Control*, 50(9), 1147-1160.

5. Badescu, M., Bar-Cohen, Y., Sherrit, S., Bao, X., Chang, Z., Donnelly, C., and Aldrich, J. (2012). "Percussive Augmenter of Rotary Drills (PARoD)." *Proc., SPIE: Sensors and Smart Structures for Civil, Mechanical, and Aerospace systems*, San Diego, CA.

6. Badescu, M., Sherrit, S., Bao, X., Bar-Cohen, Y., and Chen, B. (2011). "Auto-Gopher – a wire-line rotary-hammer ultrasonic drill." *Proc., SPIE: Sensors and Smart Structures for Civil, Mechanical, and Aerospace systems*, San Diego, CA.

7. Bar-Cohen, Y., Badescu, M., Sherrit, S., Zacny, K., Paulsen, G., Beegle, L., and Bao, X. (2012). "Deep Drilling and Sampling via the Wireline Auto-Gopher Driven by Piezoelectric Percussive Actuator and EM Rotary Motor." *Proc., SPIE: Sensors and Smart Structures for Civil, Mechanical, and Aerospace systems*, San Diego, CA.

8. Bar-Cohen, Y., and Sherrit, S. (2007). *Self Mountable Ultrasonic/Sonic Anchor and Extractable*. US Patent No. 7,156,189, Jan. 2, 2007.
9. Bar-Cohen, Y., Sherrit, S., Dolgin, B.P., Bao, X., Chang, Z., Pal, D.S., Krahe, R., Kroh, J., Du., S., and Peterson, T. (2001). "Ultrasonic/sonic drilling/coring (USDC) for planetary applications." *Proc. SPIE 8th Annual International Symposium on Smart Structures and Materials*, San Diego, CA.
10. Batako, A.D., Babitsky, V.I., and Halliwell, N.A. (2004). "Modelling of vibro-impact penetration of self-exciting percussive-rotary drill bit." *J. of Sound and Vibration*, 271(1-2), 209-225.
11. Clough, R.W., and Penzien, J. (1975). *Dynamics of Structures*. McGraw-Hill, Inc., New York City, NY.
12. Cook, R.D., Malkus, D.S., Plesha, M.E., Witt, R.J. (2002). *Concepts and Applications of Finite Element Analysis*. 4th Ed., John Wiley & Sons Inc., Hoboken, NJ.
13. Cox, H. (1849) "On Impact of Elastic Beams", *Transactions of the Cambridge Philosophical Society*, **9**, p. 73.
14. Craig, R. (1981). *Structural Dynamics: An Introduction to Computer Methods.* John Wiley & Sons, Inc., Hoboken, NJ.
15. Cristescu, N. (1967). *Dynamic Plasticity*. John Wiley & Sons, Inc, New York.
16. Das, B.M. (2006). *Principles of Geotechnical Engineering*. Cengage Learning, Stamford, CT.
17. Fathi, A., and Popplewell, N. (1994) "Improved Approximations for a Beam Impacting a Stop", *Journal of Sound and Vibration*, 170(3), 365-375.

18. Goldsmith, W. (1960). *Impact: The Theory and Physical Behaviour of Colliding Solids*, Edward Arnold Publishers LTD, London.
19. Greenberg, M. D. (1978). *Foundations of Applied Mathematics*, Prentice-Hall, Englewood Cliffs, NJ.
20. Heiken, G. H., Vaniman, D. T., and French, B. M. (1991). *Lunar Sourcebook : A User's Guide To The Moon,* Cambridge University Press., Cambridge, England.
21. Hertz, H. (1881). "On the Contact of Elastic Bodies." *J. für die reine und angewandte Mathematik*, 92**,** 56-171.
22. Hu, B., and Eberhard, P. (2003). "Comparison of Analytical and Experimental Results for Longitudinal Impacts on Elastic Rods." *J. of Vibration and Control*, 9(1-2), 157-174.
23. Johnson, K.L. (1985). *Contact Mechanics*. Cambridge University Press, Cambridge, UK.
24. Kaliski, M. (1989). "Rotary percussive drilling of mine holes with the aid of manual drills. Part I." *Archives of Mining Sciences*, 34(2), 273-297.
25. King, R.P., and Bourgeois, F. (1993). "Measurement of fracture energy during single-particle fracture." *Minerals Engineering*, 6(4), pp. 353-367.
26. Kreyszig, E. (2011). *Advanced Engineering Mathematics*, John Wiley & Sons Inc., Hoboken, NJ.
27. Laura, P.A.A. (1974). "Analysis of a cable-like system suddenly stopped at one end." *J. of Sound and Vibration*, 37(2), 195-204.
28. Lo, C.C. (1980). "A Cantilever Beam Chattering Against a Stop." *J. of Sound and Vibration*, 69(2), 245-255.

29. Lundberg, B. (1993). "Computer Modeling and Simulation of Percussive Drilling of Rock." *Comprehensive Rock Engineering: Principle, Practice & Projects*, Volume 4: Excavation, Support and Monitoring.
30. Malla, R., Adib-Jahromi, H. R., and Accorsi, M. L. (1995) "Simplified Design Method for Braced Double-Skinned Structure in Lunar Application." *J. of Aerospace Engineering,* 8(4), 189-195.
31. Malla, R. and Chaudhuri, D. (2008). "Dynamic Analysis of a 3-D Frame-Membrane Lunar Structure Subjected to Impact." *Proc., Earth and Space*, ASCE, Reston, VA.
32. Malla, R. B. and Gionet, T. (2013). "Dynamic Response of a Pressurized Frame-Membrane Lunar Structure with Regolith Cover Subjected to Impact Load." *J. of Aerospace Engineering,* 26(4), 855-873.
33. Malla, R.B., Shrestha, B.R., and Zacny, K. (2010a). "Stress and Displacement Wave Propagation in Percussive Tubular Mechanism for Space Applications." *Proc., 51st AIAA/ASME/ASCE/AHS/ASC Structures, Structural Dynamics, and Materials (SDM) Conference,* AIAA, Reston, VA; 18 pages.
34. Malla, R.B., Shrestha, B.R., Paulsen, G., and Craft, J. (2010b). "Variation in Wave Propagation in Lunar Percussive Drilling Instrument due to Presence of a Joint." *Proc., ASCE Earth and Space 2010: Engineering, Science, Construction, and Operations in Challenging Environments,* ASCE ASCE, Reston, VA, March 2010, pp 1513-1524.
35. Malla, R.B., Shrestha, B.R., and Zacny, K. (2012). "Stress and Displacement Propagation in a Drilling Tube due to Rebounding and Non-rebounding Impact Mechanisms." *Proc., ASCE Earth and Space 2012,* ASCE, Reston, VA: 11 pages.
36. MATLAB version 7.10. Natick, MA: The Mathworks Inc., 2010.

37. Minamoto, H., Seifried, R., Eberhard, P., Kawamura, S. (2011). "Analysis of repeated impacts on a steel rod with visco-plastic material behavior." *European Journal of Mechanics A/Solids*, 30, p. 336-344.

38. Mitchell, J. K. and Houston, W. N. (1974). "Static Penetration Testing on the Moon." *European Symposium in Penetration Testing: 1st Intl. Soc. for Soil Mech. and Found. Eng.*, Stockholm, Sweden, 277-284.

39. Paz, M. (1997). *Structural Dynamics: Theory and Computation*. Chapman & Hall, London.

40. Pytel, A. and Kiusalaas, J. (2011). *Mechanics of Materials*. *2nd Ed.* Cengage Learning, Stamford, CT.

41. Raj, P. (2008). *Soil Mechanics and Foundation Engineering*. Dorling Kindersley Pvt. Ltd., New Delhi, India.

42. Rao, S.S. (2007). *Vibration of Continuous Systems*. John Wiley & Sons, Inc., Hoboken, NJ.

43. Schiehlen, W., Seifried, R., and Eberhard, P. (2006). "Elastoplastic phenomena in multibody impact dynamics." *Comput. Methods Appl. Mech. Engrg.*, 195, p. 6874-6890.

44. Sherrit, S., Dolgin, B.P., and Bar-Cohen, Y., (1999) "Modeling of Horns for Sonic/Ultrasonic Applications, *Proc., IEEE Ultrasonics Symposium*, Caesars Tahoe, Nevada.

45. St. Venant, B.D., and Flamant (1889). "Courbes representatives des lois du choc longitudinal et du choc transversal d'une barre prismatique." *J. exole polytech.*, Paris, 59, 97.

46. Take, W., Valsangkar, A.J., and Randolph, M.F. (1999). "Analytical Solution of Pile Hammer Impact." *Computers and Geotechnics*, 25(2), 57-74.

47. Tavares, L.M. (1999). "Energy Absorbed in Breakage of Single Particles in Drop Weight Testing." *Minerals Engineering*, 12(1), 43-50.

48. Tedesco, J.W., McDougal, W.G., and Ross, C.S. (1999). *Structural Dynamics: Theory and Applications*. Addison Wesley Longman Inc., Menlo Park, CA.

49. Thornton, C., and Ning, Z. (1998). "A theoretical model for the stick/bounce behaviour of adhesive, elastic-plastic spheres." *Powder Technology*, 99, p. 154-162.

50. Timoshenko, S. (1913). "Zur Frage nach der Wirkung eines Stosses auf einen Balken" *Zeitschrift für Mathematik und Physik*, 62, 198.

51. Timoshenko, S., Young, D.H., and Weaver, Jr., W. (1974). *Vibration Problems in Engineering*. 4th Ed., John Wiley & Sons, Inc., Hoboken, NJ.

52. Udwadia, F.E. (2012). "On the longitudinal vibrations of a bar with viscous boundaries: Super-stability, super-instability and loss of damping." *Int. J. of Engineering Science*, 50, p. 79-100.

53. Valkering, T.P. (1994). "Non-Trivial Dynamics in a Driven String with Impact Non-Linearity." *J. of Sound and Vibration*, 175(3), 397-422.

54. Vila, L.J., and Malla, R.B. (2013). "Dynamic and Contact Analysis of a Special Percussive Mechanism for Planetary Subsurface Exploration," *Procs. of the* 54th *AIAA/ASME/ASCE/AHS/ASC Structures, Structural Dynamics, and Materials (SDM) Conference*, SDM, Boston, MA.

55. Vila, L.J., and Malla, R.B. (2014a). "Analysis of the Hammering Mechanism of a Special Percussive System for Space Exploration." *Proc., AAIA SciTech 2014/55th*

AIAA/ASME/ASCE/AHS/ASC Structures, Structural Dynamics, and Materials (SDM) Conference; AIAA, Reston, VA; 11 pages.

56. Vila, L.J., and Malla, R.B. (2014b). "Longitudinal Impact Force on a Special Drill for Planetary Exploration." *Proc., Earth & Space 2014 - Engineering, Science, Construction and Operations in Challenging Environments; ASCE, Reston, VA;* 10 pages.

57. Volterra, E. and Zachmanoglou, E.C. (1965). *Dynamics of Vibrations*, Charles E. Merrill Books, Inc., Columbus, Ohio.

58. Vu-Quoc, L., and Zhang, X. (1999). "An elastoplastic contact force-displacement model in the normal direction: displacement-driven version." *Proc. R. Soc. Lond.,* 455, 4013-4044.

59. Vu-Quoc, L., Zhang, X., and Lesburg, L., (2000). "A normal force-displacement model for contacting spheres, accounting for plastic deformation: Force-driven formulation." *ASME Journal of Applied Mechanics*, 67(2), 363-371.

60. Vu-Quoc, L., Zhang, X., Lesburg, L., (2001). "Normal and tangential force-displacement relations for frictional elasto-plastic contact of spheres." *International Journal of Solids and Structures*, 38(36-37), 6455-6489.

61. Weir, G. and Tallon, S. (2005). "The coefficient of restitution for normal incident, low velocity particle impacts." *Chemical Engineering Science*, 60, p. 3637-3647.

62. Wilcox, B. and Dankowicz, H. (2009). "Response of Electrostatically Actuated Flexible MEMS Structures to the Onset of Low-Velocity Contact." *Proc., ASME 2009 International Design Engrn. Technical Conerences & Computers and Information in Engrn. (IDETC/CIE) Conference*; ASME, San Diego, CA; 1777-1786

63. Wojtkowski, M., Pecen, J., Horabik, J., and Molenda, M. (2010). “Rapeseed impact against a flat surface: Physical testing and DEM simulation with two contact models.” *Powder Technology,* 198, p. 61-68.

64. Xing, Y.F., and Zhu, D.C. (1998). “Analytical solutions of impact problems of rod structures with springs.” *Comput. Meth. Appl. Mech. Engrg.*, 160(3-4), 315-323.

65. Yongqiang, Y., and Lili, X. (2011). “Comparison Research on Determination of Contact Loads with Finite Element Method and Mode Superposition Method.” *Advanced Materials Research,* 217-218, 62-65.

66. YuFeng, X., and DeChao, Z. (1998). “Analytical solutions of impact problems of rod structures with springs.” *Comput. Methods Appl. Mech. Engrg.*, 160(3-4), 315-323.